U.PORTO

FEUP FACULDADE DE ENGENHARIA UNIVERSIDADE DO PORTO

ANALYSIS OF SELF-ANCHORED AND GROUND-ANCHORED SUSPENSION BRIDGES

CATARINA DA CUNHA NUNES DE SÁ MACHADO

Dissertação submetida para satisfação parcial dos requisitos do grau de

MESTRE EM ENGENHARIA CIVIL — ESPECIALIZAÇÃO EM ESTRUTURAS

Orientador: Professor Doutor Rui Manuel Meneses Carneiro de Barros

Coorientador: Professor Doutor Abolhassan Astaneh-Asl

JULHO DE 2014

Mestrado Integrado em Engenharia Civil 2013/2014

DEPARTAMENTO DE ENGENHARIA CIVIL

Tel. +351-22-508 1901

Fax +351-22-508 1446

✉ miec@fe.up.pt

Editado por

FACULDADE DE ENGENHARIA DA UNIVERSIDADE DO PORTO

Rua Dr. Roberto Frias

4200-465 PORTO

Portugal

Tel. +351-22-508 1400

Fax +351-22-508 1440

✉ feup@fe.up.pt

http://www.fe.up.pt

Avô Joaquim, não te dei um último adeus,
mas dedico-te este meu trabalho, pelo qual eu sei que ficarias orgulhoso.
Também aos meus Pais, Irmã e António
por tornarem este sonho realidade.

Don't cry because it is over, smile because it hapenned.
Theodor Seuss Geisel

ACKNOWLEDGEMENTS

I would like to express my deepest gratitude to Professor Abolhassan Astaneh-Asl and the Civil and Environmental Engineering Department at University of California Berkeley. Firstly, for accepting my application and considering me worthy of working amongst the world's top civil engineering students, researchers and Professors. Secondly, for including me in such a relevant, interesting, stimulating and complex project. I am proud and delighted to leave my contribution for it. Moreover, I learned immensely under Professor Astaneh's supervision. The Professor is altogether one of the most proactive and hard-working Engineers. He is involved in a full agenda of many on-going projects, but he still finds the time to kindly teach and guide his student researchers. I will always keep in mind his wisdom, teachings and kindness as a role model for my future work.

I would also like to leave my sincere gratefulness to Professor Rui Carneiro de Barros, not only for his essential help during my initial application process, but also for always sparing his precious time for this research. Furthermore, I would like to thank him for always being so understanding and practical. It was fundamental for my work and well being to know I had encouragement and support back in Portugal.

In a more personal note, I would like to thank my parents and family who has supported me unconditionally at all times. Without them this opportunity would not have been possible.

Last but not least, I would like to thank my friends, all of them in different ways contributed for my happiness and personality, but also in my studies and learning:

- To António, best friend and supporter through better and harder times.

- M. João and Francisco P., for an unexpected but altogether brilliant and amazing friendship that will last way beyond the Structural Engineering intense semester. Not only are they among the most intelligent people I came to know, but also the funniest and generous.

- To both Pedro F. (Ferreira and Fonseca) who were always by my side on this 5-year journey. All the hours spent together were priceless.

- To Sérgio P. a patient friend and crisis manager that always has a kind and reassuring word.

- To all my new friends from all over the world, for the unforgettable, amazingly unbelievable moments they provided me during this semester abroad. Indeed, their support and motivation was fundamental in the hardest times.

ABSTRACT

The new self-anchored suspension span of the East San Francisco-Oakland Bay Bridge is the main subject of study of this research project. It was completed and opened to traffic on September 2013. It is an asymmetric single-tower self-anchored suspension bridge. Instead of the conventional ground-anchored system used for most suspension bridges, this design has the main cable anchorages on the deck.

The aim of this research is a comparative study between self-anchored and ground-anchored suspension bridge systems. This study focus mainly on Gravity analysis, but also partially in Dynamic analysis. For the comparison, different complex finite-element models were studied, developed and analyzed for global analysis. These models were studied during an initial stage of design and the next step of calculating and introducing prestressing in suspender cables is not taken into consideration. This last process was studied, but it is not so relevant for a comparative study, since the main purpose of cable prestress it to annul the effect of dead and live loads on the deck deformed shape, by introducing prestress force in the cables.

The new East Bay Bridge is currently the largest self-anchored suspension span of its kind in the world. Nonetheless, this ambitious design is controversial and faced innumerous design and construction issues. It was designed after a partial collapse of the upper-deck of the previous East Bay Bridge, which had a steel truss system. The location, design and structural elements are explained in detail. Moreover, a summary of the major construction issues is provided to contextualize this study and for a full understanding of the Bay Bridge project. Fractured rods, steel corrosion, weld quality among other construction issues resulted from the complex erection method that the self-anchored span required. As a matter of fact, a simpler erection method would not only have reduced the six and half billion dollar final cost, but also would have avoided many construction quality problems.

After a thorough study of the existing bridge, a finite-element model replicating the geometry, section, materials and other properties of the self-anchored span was analyzed under Dead and Live load combination. The model components and analysis parameters are fully described. The complex geometry is replicated by means of shell elements for deck, tower and foundation pile caps, frame elements for piers and truss elements for cables. Also, a highly nonlinear analysis is required due to the existence of suspension cables. The bridge displacement, force and stress calculations are performed at the end of a nonlinear load case, which includes P-Δ and large displacements effects. The deformed shape and tension of the cable needed to be taken as initial conditions for the structural calculation.

From the initial self-anchored model (SAS), three ground-anchored finite-element models (GAS) were created. It was a process of design optimization, derived from the results of analysis of each GAS model created. In the end, there were two GAS models that performed well.

The results for nonlinear Static analysis (Gravity) are then plotted and compared, as well as results of the modal and time-history analysis. Modal analysis results are presented for GAS models. Time-history analysis is performed with multi-support excitation for one set of ground-motion. At last, some conclusions are drawn, mainly based on the Gravity results.

KEYWORDS: Self-anchored Bay Bridge; Ground-anchored suspension bridge; Finite-element; Gravity analysis; Comparative study

RESUMO

A mais recente travessia entre São Francisco e Oakland - *East Bay Bridge* é a principal estrutura estudada nesta dissertação. Mais concretamente, o troço suspenso com ancoragem no próprio tabuleiro. A sua construção foi terminada em Setembro de 2013 e aberta ao tráfego automóvel. É uma ponte suspensa com uma torre apenas entre vãos assimétricos e cujas ancoragens do cabo principal estão localizadas no próprio tabuleiro da ponte. Este tipo de ancoragem difere totalmente do método de bloco no solo mais frequentemente usado.

O principal objectivo deste trabalho é um estudo comparativo entre pontes suspensas com ancoragem no próprio tabuleiro e pontes suspensas com bloco de ancoragem no solo. Este estudo será realizado principalmente para análise estática gravítica, mas também em parte para análise dinâmica. Para a comparação, modelos de elementos finitos foram estudados, desenvolvidos e analisados para análise global. Estes modelos foram calculados e analisados para uma fase inicial de dimensionamento, na qual não se considerou o pré-esforço a introduzir posteriormente nos cabos de suspensão. Esta última fase foi estudada e compreendida, mas não é relevante para o estudo. De facto, este pré-esforço é calculado e introduzido nos cabos de suspensão de modo a anular o efeito das cargas estáticas para a deformada do tabuleiro (de modo a colocar o tabuleiro praticamente na sua posição indeformada).

Esta recente *East Bay Bridge* é de momento a maior ponte suspensa ancorada no próprio tabuleiro, para o seu tipo (torre única) no Mundo. No entanto, este projeto tem tanto de ambicioso como de controverso e deparou-se com inúmeros problemas de construção. Esta ponte veio substituir a anterior *Bay Bridge*, ponte metálica treliçada, a qual sofreu um colapso parcial do tabuleiro superior durante o terramoto de 1989. Para melhor compreensão do projeto, a localização, condições e elementos estruturais são apresentados em detalhe. Igualmente, foi feita uma descrição dos problemas de construção (corrosão, rotura de parafusos, soldaduras) para contextualizar a relevância deste presente estudo. De facto, este problemas estão muito relacionados com o complexo método de construção necessário para uma ponte suspensa ancorada no próprio tabuleiro. Um método de construção mais simples poderia reduzir o custo final de seis biliões e meio de dólares, bem como evitar os problemas supramencionados.

Um modelo com a geometria, seções, materiais e outras propriedades do vão suspenso será analisado para combinação de cargas e totalmente descrito neste trabalho. São utilizados elementos de membrana para tabuleiro, torre e maciço de fundação; elementos coluna para os pilares, vigas de encabeçamento e estacas de fundação; e elementos treliçados para os cabos. A análise é altamente não linear devido ao elemento cabo. O cálculo de deslocamentos, forças e tensões na estrutura incluem efeitos de não-linearidade geométricas (P-Δ e grandes deslocamentos), pois a deformada e tensão dos cabos necessitam de ser consideradas a priori para o cálculo da estrutura.

Partindo de um modelo *SAS* inicial *(self-anchored span*), três modelos *GAS* com ancoragem exterior (*ground-anchored span*) serão desenvolvidos. Foi um processo de optimização, através dos resultados obtidos para cada modelo. Os resultados relevantes obtidos serão apresentados e comparados para análise estática, mas também para análise modal e dinâmica. A análise dinâmica tem diferentes funções para diferentes fundações, devido a condições geológicas. Por fim, algumas conclusões são apresentadas com base nos resultados da modelação efectuada.

PALAVRAS-CHAVE: East Bay Bridge; Ponte suspensa ancorada no tabuleiro; ancoragem exterior; Elementos finitos; estudo comparativo; Análise estática e dinâmica

TABLE OF CONTENTS

ACKNOWLEDGMENTS I

ABSTRACT III

RESUMO V

1. INTRODUCTION 1

1.1. PROJECT SCOPE 1

1.2. REPORT ORGANIZATION 2

2. LITERATURE SURVEY 3

3. EAST BAY BRIDGE: DEFINITION OF SELF-ANCHORED SPAN 13

3.1 INTRODUCTION 13

3.2 SOIL CONDITION 16

3.3 ALIGNMENT 17

3.4 FOUNDATIONS AND PILES 18

3.4.1 EAST FOUNDATIONS 18

3.4.2 WEST FOUNDATIONS 19

3.4.3 MAIN TOWER FOUNDATIONS 20

3.5. PIERS AND ANCHORAGES 22

3.5.1. E2 PIERS AND EAST ANCHORAGE 22

3.5.2. W2 PIERS AND WEST ANCHORAGE 24

3.5.3. BEARINGS AND SHEAR KEYS 27

3.6. SUPERSTRUCTURE 29

3.6.1. ELEVATION AND PLAN 29

3.6.2. DOUBLE-DECK 30

3.6.3. DETAILED CROSS SECTION 31

3.6.4. CROSS BEAMS AND FLOOORBEAMS 33

3.7. MAIN TOWER 33

3.7.1. SHAFTS AND SHEAR LINKS 35

3.7.2. TOWER SADDLE 39

3.8. CABLE 40

3.8.1. MAIN CABLE 40
3.8.2. HANGERS 42
3.9. SEISMIC DESIGN CRITERIA, ANALYSIS AND RESPONSE 43
3.10. ERECTION METHOD OF SELF-ANCHORED SPAN 44
3.11. RAINBOW BRIDGE AND SELF-ANCHORED SPAN OF SAN FRANCISCO-OAKLAND BAY BRIDGE: A COMPARATIVE STUDY 49
3.11.1. RAINBOW BRIDGE STRUCTURE 49
3.11.2. SOIL CONDITIONS 53
4. CONSTRUCTION ISSUES 61
4.1. STRUCTURAL AND CONSTRUCTION ISSUES 61
4.1.1 THREADED RODS AND BOLTS 62
4.1.1.1 Shear Keys S1 and S2 68
4.1.1.2. Other SAS locations with A354 Grade BD 75
4.1.2 CABLE 81
4.1.3 TOWER 82
4.1.3.1 Top Saddle 82
4.1.3.2. Base 83
4.1.3.3. Composite piles 84
4.1.4. SUPERSTRUCTURE 84
4.1.4.1. Steel Orthotropic Deck 84
4.1.4.2. Skyway 87
4.1.5. WEST SIDE (W2) 88
5. FINITE-ELEMENT MODELS 89
5.1 INTRODUCTION 89
5.2 GROUND MOTION AND MULTIPLE-SUPPORT EXCITATIONS 90
5.3 CALTRANS MODEL FOR SAS 93
5.4 SELF-ANCHORED MODEL 95
5.4.1 ELEMENTS 96
5.4.2 MATERIAL PROPERTIES 108
5.5 GROUND-ANCHORED MODEL WITH CABLE DISCONNECTED 112
5.6 GROUND-ANCHORED MODEL REDESIGNED 113
5.7 SYMMETRIC REDESIGNED GROUND-ANCHORED MODEL 114
5.8 ANALYSIS 115

5.8.1 GRAVITY (NONLINEAR STATIC) 116
5.8.2 MODAL 116
5.8.3 NONLINEAR TIME-HISTORY 118
5.9 LOAD CASES AND FUNCTIONS 118
5.9.1 DEAD LOAD 119
5.9.2 LIVE LOAD 121
5.9.3 P-DELTA 121
5.9.4. MODAL 122
5.9.5. NL TIME HISTORY 122
6. ANALYSIS RESULTS 123
6.1. STATIC GRAVITY ANALYSIS 123
6.1.1 SAS MODEL 123
6.1.1.1 Stresses 123
6.1.1.2 Forces 124
6.1.1.3 Displacements 127
6.1.2 GAS MODEL WITH CABLE DISCONNECTED 128
6.1.2.1. Stresses 128
6.1.2.2. Forces 129
6.1.2.3. Displacements 131
6.1.3. REDESIGNED GROUND-ANCHORED MODEL 132
6.1.3.1. Stresses 132
6.1.3.2. Forces 133
6.1.3.3. Displacements 135
6.1.4. SYMMETRIC GROUND-ANCHORED MODEL 136
6.1.4.1. Stresses 136
6.1.4.2. Forces 138
6.1.4.3. Displacements 139
6.2. MODAL ANALYSIS 140
6.2.1. GAS MODEL WITH CABLE DISCONNECTED 140
6.2.2. REDESIGNED GAS MODEL 147
6.2.3. SYMMETRIC GAS MODEL 153
6.3. TIME-HISTORY ANALYSIS 159

7. COMPARISON AND CONCLUSIONS 165

7.1 STATIC GRAVITY ANALYSIS 165

7.2 MODAL ANALYSIS 172

BIBLIOGRAPHY 174

LIST OF FIGURES

Fig. 2.1 - Self-anchored and ground-anchored suspension bridges force distribution. 11

Fig. 2.2 – Different types of sockets. 12

Fig. 3.1 –Project location and limits are between the arrows 13

Fig. 3.2 – East Bay Bridge partial collapse in 1989. 14

Fig. 3.3 – Earthquake accelerograms, including the 1989 Loma Prieta. 14

Fig. 3.4 – Self-anchored Bay Bridge span and Yerba Buena Island. 15

Fig. 3.5 – Entire East San Francisco-Oakland Bay Bridge structure and Self-anchored suspension span, respectively. 16

Fig. 3.6 – Contour of elevation of base of young bay mud spaced at 5m 17

Fig. 3.7 – Geotechnical conditions of the soil along the bridge longitudinal axis 17

Fig. 3.8 – Previous East Bay Bridge, possible and selected alignments 18

Fig. 3.9 – Plan and elevation sections of the East piers and pile cap 18

Fig. 3.10 – Cross Section of East piles inside Pile cap 19

Fig. 3.11 – Cross Section at mid height of East foundation piles 19

Fig. 3.12 – West footings of east and west lines respectively. 20

Fig. 3.13 – Plan view of pile cap for the Tower base with foundation piles and tower shafts. 21

Fig. 3.14 –Plan view of dowels and anchor bolts on the tower base. 21

Fig. 3.15 – Tower base during construction 22

Fig. 3.16 - East pier cross section with dimensions (mm) and with rebar's detail. 22

Fig. 3.17 - East pier transverse elevation with pile cap, piers, cap beam, deck anchorage. 23

Fig. 3.18 – Side view of the east deck cable anchorage. 23

Fig. 3.19 – Plan view of the east deck cable anchorage 24

Fig. 3.20 – Socket details for east deck cable anchorage 24

Fig. 3.21 – Cross section of the 4 separate columns for the west piers. 26

Fig. 3.22 – Half of Pier W2 plan view. 26

Fig. 3.23 – West transverse elevation with foundations, pier, cap beam and typical cross section 27

Fig. 3.24 – Shear Key for the east pier connection, with anchor rods visible 28

Fig. 3.25 – Plan and lateral view of shear key at Pier E2. 28

Fig. 3.26 – Lateral view of bearing at Pier E2. 28

Fig. 3.27 – Hinge pipes for SAS-YB and SAS-Skyway connection. 29

Fig. 3.28 – Elevation and plan of the Self-anchored span. 30

Fig. 3.29 – Typical Cross section of the deck 31

Fig. 3.30 – Typical Cross section of the Skyway's deck 31

Fig. 3.31 – Typical Cross section of one deck 32
Fig. 3.32 – Reduced-scale specimens of the upper and lower deck, respectively. 32
Fig. 3.33 – Typical crossbeam section. 33
Fig. 3.34 – Typical floorbeam section. 33
Fig. 3.35 – Tower longitudinal elevation and typical diaphragm sections 34
Fig. 3.36 – Tower transverse elevation 35
Fig. 3.37 – Shaft segments with shear link connections visible 36
Fig. 3.38 – Cross section, transverse and longitudinal tower elevation, respectively 36
Fig. 3.39 – Typical Pushover Analysis results (top load). 37
Fig. 3.40 – Type 1 (transverse) link deformation and detail on weld crack after a 345mm displacemen 37
Fig. 3.41 – Type 1 (transverse) and 3 (longitudinal) links respectively, with brittle fracture visible 38
Fig. 3.42 – Type 1 (transverse) and 3 (longitudinal) graphs, respectively 38
Fig. 3.43 – Saddle grillage being lifted to the top of the tower 39
Fig. 3.44 – Plan, longitudinal and lateral views of the tower saddle. 39
Fig. 3.45 – Final section of the main cable after compaction 40
Fig. 3.46 – Transverse and longitudinal Suspenders detail. 42
Fig. 3.47 – Elevation of the bridge, with plastic hinges marked 44
Fig. 3.48 – SAS span and skyway foundations, respectively 44
Fig. 3.49 – Pier E2 and W2 erection, respectively 45
Fig. 3.50 – Falsework 45
Fig. 3.51 – Crane barge lifting steel orthotropic deck segment 46
Fig. 3.52 – Tower shaft lift 46
Fig. 3.53 – Aerial view with catwalk for cable strands assembly and steel strands pulling the tower to the West side 47
Fig. 3.54 – Top of the tower with main cable strands assembled 47
Fig. 3.55 – Cost summary of San-Francisco Oakland East Bay Bridge by September 2012 49
Fig. 3.56 – Tokyo Rainbow Bridge. 50
Fig. 3.57 – Side and Plan view of the Tokyo Rainbow Bridge 50
Fig. 3.58– Shibaura side and Daiba side ground-anchorages. 50
Fig. 3.59– Shibaura side and Daiba side main towers, respectively 51
Fig. 3.60– Shibaura side and Daiba side towers, respectively. 51
Fig. 3.61– Tokyo Rainbow Bridge's typical double-deck section 52
Fig. 3.62– Tokyo Rainbow Bridge's wire, strand and bundle of strands 52

Fig. 3.63–North Tokyo Bay region with Rainbow Bridge specific location. 54
Fig. 3.64– Soil profiles for Ukita and Edogawa with SPT test results 54
Fig. 3.65– Takasago testing location and soil profile 55
Fig. 3.66 – Urayasu soil profile....56
Fig.3.67 – Tokyo Rainbow Bridge longitudinal geological profile....56
Fig.3.68 - Rainbow Bridge anchorage system and observatory platform 57
Fig. 3.69 – Map Contour with location of Pier W2, Tower T1 and Pier E2 for SAS 57
Fig. 3.70 –Longitudinal geological profile for the Self-anchored Span of the SFOBB....58
Fig. 3.71 – CPT results and scale for Pier E2 section....59
Fig. 4.1. – SAS bridge side view with ten highlighted locations. 62
Fig. 4.2. – Galvanization process for the East SAS Bay Bridge according to TBPOC.....66
Fig. 4.3. – Main causes for Hydrogen embrittlement (HE) or Stress Corrosion cracking (SCC).....67
Fig. 4.4. – Timeline for the anchor rods (2008) failure on Shear keys S1 and S2 68
Fig. 4.5. – Shear Keys and bearings at Pier E2 69
Fig. 4.6. – Shear Key S1 and S2 with L1 and L2 type of rods, as well as failed rods and samples extracted 69
Fig. 4.7. – Facture surface of Shear Key S1 rod after cleaning 71
Fig. 4.8. – Rockwell C hardness test results from Shear Key S1 and S2 two samples 71
Fig. 4.9. – Hardness testing comparison between 2008 and 2010 samples, respectively, from Pier E2 72
Fig. 4.10. – Reduced section tensile strength and Impact testing for 2008 and 2010 samples, respectively 73
Fig. 4.11. – Solution 1 and 2 respectively for the Pier E2 failed shear keys 74
Fig. 4.12. – Detailed steel saddle solution for Shear key replacement (Option 2) 74
Fig. 4.13. – Location #1 to #6 of the A354 Grade BD threaded rods and bolts 75
Fig. 4.14. – Location #7 to #12 of the A354 Grade BD threaded rods and bolts 76
Fig. 4.15. – Location #15 to #17 of the A354 Grade BD threaded rods and bolts 77
Fig. 4.16. –TBPOC KI-HRC graph from testing (left) and the same overlapped with a typical KI_{SCC}-HRC curve....78
Fig. 4.17. –KI_{SCC}-HRC curve from Townsend study....79
Fig. 4.18. –Comparison of HRC for cut and rolled threads and the scenario at the surface for cut and rolled threads, respectively 81
Fig. 4.19. –Average Rockwell hardness distribution for location #18, respectively....82
Fig. 4.20. –Average Rockwell hardness distribution for locations #12 and #13, respectively....83
Fig. 4.21 – Connection between guardrail and steel orthotropic deck top plate 86

Fig. 4.22. –Water leak inside the deck on the guardrail bolted connection. 86

Fig. 4.23 –Corrosion signs inside the deck. 86

Fig. 4.24 –Connection between bike path and steel orthotropic deck. 87

Fig. 5.1 – Set 1 of Ground motions from Caltrans (Rock motions for T1 and W2 foundations). 92

Fig. 5.2 –Soil motions from Caltrans for Pier E2 foundation 93

Fig. 5.3 – ADINA global model of the bridge 94

Fig. 5.4 – Hybrid and detailed models of the East piles 95

Fig. 5.5 – SAP2000 model of the SAS span used in this study. 96

Fig.5.6 – 3D view of the West side and cross section of one W2 column 99

Fig. 5.7 – 3D view of the East side and cross section of E2 pier 99

Fig. 5.8 – Hinge at the transition to Skyway and spring modeling at SAP2000. 99

Fig. 5.10 – Tower with detail of 1 of 4 tower shafts with plate labeling as in SAP2000 model. 102

Fig. 5.12 – Typical section of the Deck (“W” Line) with plate numeration. 106

Fig. 5.13 – Stiffeners type for typical section of the Deck (“W” Line). 106

Fig. 5.14 – Equivalent thickness of the steel orthotropic deck plate without ribs. 106

Fig. 5.16 – Results of boring test at Tower location with undrained soil shear strength until 60-meter deep 112

Fig. 5.17 – SAP2000 ground-anchored model views 113

Fig. 5.18 – SAP2000 redesigned ground-anchored model views. 114

Fig. 5.19 – SAP2000 symmetric design of ground-anchored bridge 115

Fig. 5.21 – XZ view of SAS model with span division. 121

Fig.6.1 – Longitudinal stresses on the **top plates of the SAS bridge deck** for Gravity Analysis. 123

Fig.6.2 – Longitudinal stresses on the **bottom plates of the SAS bridge deck** for Gravity analysis. 124

Fig.6.6 – Vertical and longitudinal displacements for **SAS bridge** for Gravity Analysis 127

Fig.6.7 – Longitudinal stresses on the **top plates of the GAS bridge deck** for Gravity Analysis 128

Fig.6.8 – Longitudinal stresses on the **bottom plates of the GAS bridge deck** for Gravity Analysis 129

Fig.6.9 – Vertical and longitudinal displacements for **GAS bridge** for Gravity Analysis, respectively. 131

Fig.6.10 – Longitudinal stresses on the **top plates of the redesigned GAS bridge deck** for Gravity Analysis. 132

Fig.6.11 – Longitudinal stresses on the **bottom plates of the redesigned GAS bridge deck** for Gravity Analysis. 134

Fig.6.12 – Vertical and longitudinal displacements for GAS bridge for Gravity Analysis, respectively 135

Fig.6.13 – Longitudinal stresses on the **top plates of the symmetric GAS bridge deck** for Gravity Analysis. 137

Fig. 6.14 – Longitudinal stresses on the **bottom plates of the symmetric GAS bridge deck** for Gravity Analysis. 137

Fig.6.15 – Vertical displacements for symmetric GAS bridge for Gravity Analysis. 139

Fig. 6.16 – 3D view of 1st mode for GAS model 141

Fig. 6.17 – XZ view of 1st mode for GAS model 141

Fig. 6.18 – XY view of 1st mode for GAS model 141

Fig. 6.19 – 3D view of 2nd mode for GAS model 142

Fig. 6.20 – XZ view of 2nd mode for GAS model 142

Fig. 6.21 – XY view of 2nd mode for GAS model 142

Fig. 6.22- 3D view of 3rd mode for GAS model 143

Fig. 6.23 – XZ view of 3rd mode for GAS model 143

Fig. 6.24 – XY view of 3rd mode for GAS model 143

Fig. 6.25– 3D view of 4th mode for GAS model 144

Fig. 6.26 – XZ view of 4th mode for GAS model 144

Fig. 6.27 – XY view of 4th mode for GAS model 144

Fig. 6.28 – 3D view of 5th mode for GAS model 145

Fig. 6.29 – XZ view of 5th mode for GAS model 145

Fig. 6.30 – XY view of 5th mode for GAS model 145

Fig.6.31 – 3D view of 6th mode for GAS model 146

Fig. 6.32 – XZ view of 6th mode for GAS model 146

Fig. 6.33 – XZ view of 6th mode for GAS model 146

Fig. 6.34 – 3D view of 1st mode for redesigned GAS model 147

Fig. 6.35 – XZ view of 1st mode for redesigned GAS model 147

Fig. 6.36 – XY view of 1st mode for redesigned GAS model 147

Fig. 6.37 – 3D view of 2nd mode for redesigned GAS model 148

Fig. 6.38 –XZ view of 2nd mode for redesigned GAS model 148

Fig. 6.39 – XY view of 2nd mode for redesigned GAS model 148

Fig. 6.40 – 3D view of 3rd mode for redesigned GAS model 149

Fig. 6.41 – XZ view of 3rd mode for redesigned GAS model 149

Fig. 6.42 – XY view of 3rd mode for redesigned GAS model 149

Fig. 6.43 – 3D view of 4th mode for redesigned GAS model 150

Fig. 6.44– XZ view of 4th mode for redesigned GAS model 150

Fig. 6.45 – XY view of 4th mode for redesigned GAS model 150
Fig. 6.46 – 3D view of 5th mode for redesigned GAS model 151
Fig. 6.47 – XZ view of 5th mode for redesigned GAS model 151
Fig. 6.48 – XY view of 5th mode for redesigned GAS model 151
Fig. 6.49 – 3D view of 6th mode for redesigned GAS model 152
Fig. 6.50 – XZ view of 6th mode for redesigned GAS model 152
Fig. 6.51 – XY view of 6th mode for redesigned GAS model 152
Fig. 6.52 – 3D view of 1st mode for symmetric GAS model 153
Fig. 6.53 – XZ view of 1st mode for symmetric GAS model 153
Fig. 6.54 – XY view of 1st mode for symmetric GAS model 153
Fig. 6.55 – 3D view of 2nd mode for symmetric GAS model 154
Fig. 6.56 – XZ view of 2nd mode for symmetric GAS model 154
Fig. 6.57 – XY view of 2nd mode for symmetric GAS model 154
Fig. 6.58 – 3D view of 3rd mode for symmetric GAS model 155
Fig. 6.59 – XZ view of 3rd mode for symmetric GAS model 155
Fig. 6.60 – XY view of 3rd mode for symmetric GAS model 155
Fig. 6.64 – 3D view of 7th mode for symmetric GAS model 156
Fig. 6.65 – XZ view of 7th mode for symmetric GAS model 156
Fig. 6.66 – XY view of 7th mode for symmetric GAS model 156
Fig. 6.67 – 3D view of 8th mode for symmetric GAS model 157
Fig. 6.68 – XZ view of 8th mode for symmetric GAS model 157
Fig. 6.69 – XY view of 8th mode for symmetric GAS model 157
Fig. 6.70 – 3D view of 9th mode for symmetric GAS model 158
Fig. 6.71 – XZ view of 9th mode for symmetric GAS model 158
Fig. 6.72 – XY view of 9th mode for symmetric GAS model 158
Fig.7.1 – **Von Mises stresses** on top deck plates of Original SAS model for Gravity analysis. 166
Fig.7.2 – **Von Mises stresses** on top deck plates of GAS model with cable disconnected for Gravity analysis. 166
Fig.7.3 – **Deck's displacement and stresses** comparison between the 3 models for Gravity analysis. 168
Fig.7.4 – **Forces** comparison between the 3 models for Gravity analysis. 169
Fig.7.5 – 1st Gravity and Modal analysis results for **symmetric GAS model** 170
Fig.7.6 – **Deck's displacement and stresses and forces** for the Symmetric GAS model for Gravity analysis. 171

LIST OF TABLES

Table 2.1 – ATC-32 Minimum required analysis 10

Table 3.1 – Comparison between two cable construction methods……41

Table 3.2 – Rainbow Bridge's main structural characteristics……..……..…52

Table 4.1. – TBPOC Committee comparison between steel rods types……....64

Table 4.2. – 17 Locations of the A354 BD rods at SAS span……..65

Table 4.3. – Rod-by-rod resolution according to TBPOC Committee…….....80

Table 5.1 – **West Side and Cable elements** and properties at the SAP2000 model for the Self-anchored span……..……..……..……96

Table 5.2 – **East Side** elements and properties at SAP2000 model for the Self-anchored span…..…97

Table 5.3 – **Tower elements properties** at the SAP2000 model for the Self-anchored span…….100

Table 5.4 – **Tower plate's properties** at the SAP2000 model for the Self-anchored span……..101

Table 5.5 – **Tower shear link and bracing's properties** at the SAP2000 model for the Self-anchored span ……..……..……..……103

Table 5.6 – **Tower elements and properties** at the SAP2000 model for the Self-anchored span ……..……..……..……103

Table 5.7 – **Tower elements and properties** at the SAP2000 model for the Self-anchored span ……..……..……..……104

Table 5.8 – **Steel orthotropic deck** plate's properties at the SAP2000 model for the Self-anchored span ……..……..……..……...105

Table 5.9 – **Steel orthotropic deck** diaphragms and cross beams at the SAP2000 model for the Self-anchored span……..……..……..……..……....107

Table 5.10 – **Materials** at SAP2000 model. ……..……..……108

Table 5.11 – **Restraints and releases** assigned for SAS model. ……..……..……..110

Table 5.12 – Load Combination……..……..……..……...119

Table 5.13 – **Dead load for counterweight/bike lane**……..……..……....119

Table 5.14 – Dead load for Overlay……..……..……..……119

Table 5.15 – Dead load for Guard Rails……..……..……..……..120

Table 6.1 – **Axial Force** at the cables for Gravity analysis……..……..……124

Table 6.2 – **Forces** at the Piers and piles for SAS Gravity analysis……..……...125

Table 6.3 – **Vertical and longitudinal displacements** for SAS Gravity analysis……....…….....128

Table 6.4 – **Axial Force** at the cables for Gravity analysis for GAS model. ……...129

Table 6.5 – **Forces** at the Piers and piles for Gravity analysis for GAS model. ……130

Table 6.6 – **Vertical and longitudinal displacements** for GAS with cable disconnected for Gravity analysis……..……132

Table 6.7 – **Axial Force** at the cables for Gravity analysis for redesigned GAS model. ……..…133

Table 6.8 – **Forces** at the Piers and piles for Gravity analysis for GAS model. ……..….134

Table 6.9 – **Vertical and longitudinal displacements** for redesigned GAS Gravity analysis……..128

Table 6.10 – **Axial Force** at the cables for Gravity analysis for symmetric GAS model. ……..…..138

Table 6.11 – **Forces** at the Piers and piles for Gravity analysis for symmetric GAS model. ……..….138

Table 6.12 – **Vertical and longitudinal displacements** for symmetric GAS Gravity analysis……...140

LIST OF GRAPHS

Graph 5.1–%Cumulative Mass participation ratio per mode for GAS model……117

Graph 5.2 – % Cumulative Mass participation ratio per mode for redesigned GAS model……..117

Graph 5.3 – % Cumulative Mass participation ratio per mode for new symmetric GAS design…...…118

Graph 6.1 – Interaction curve P-M for W2 columns with Gravity analysis maximum results…..……..126

Graph 6.2 – Interaction curve P-M for E2 piers with Gravity analysis maximum results……..127

Graph 6.3 – Displacement of main span as function of time for **SAS model**.....159

Graph6.4–Displacement of main span as function of time for **GAS with only cable** disconnected...160

Graph 6.5 – Displacement of main span as function of time for **symmetric GAS**.....160

Graph 6.6 – Main span von Mises stress at deck top plates for three models. 161

Graph 6.7– Deck (X=0m) von Mises stress for three models. 161

Graph 6.8 – SAS and GAS with cable disconnected P-M(longitudinal) for **time-history at Top of Pier W2**. 162

Graph 6.9 – SAS and GAS with cable disconnected P-M(longitudinal) for **time-history at Bottom of Pier W2**.....162

Graph 6.10 – SAS and GAS with cable disconnected P-M(longitudinal) for **time-history at Bottom of Pier E2**. 163

1
INTRODUCTION

1.1. PROJECT SCOPE

Bridge engineering is one of the oldest sciences in the history of humanity. The fundamental purpose of a bridge is to allow the crossing of watercourses and other major obstacles to society's expansion and development. It evolved from the simplest of shapes and materials to the most complex and indeterminate structures that stretch the limits of engineering and creativity. Longer distances needed to be crossed and a new system eventually arose: cable suspended and more specifically, ground-anchored suspension bridges. This system appeared later in time, due to the need of high strength materials and more advanced theories.

For the Bay area region, the San Francisco-Oakland Bay Bridge has been an essential connection even before the iconic Golden Gate Bridge. Located between active seismic faults such as San Andreas, Hayward, among others, the Bay Bridge requires high design standards. The Bay Bridge is part of the Interstate-80 route and registers a daily traffic of around 250000 people. It consists of two separate spans (East and West) divided by Yerba Buena Island. The 1989 Loma Prieta earthquake caused a 17-meter long upper-deck section of the old East Bay Bridge to collapse. Not only human lives were lost, but also the construction repairs and the delay in the re-opening of the crossing had very negative impacts on the Bay area community. After several years of study, the previous steel truss bridge replacement was decided and the new East self-anchored suspension span was the chosen design. The new East Bay Bridge opened to the public in September 2013.

This self-anchored suspension system derives from the conventional ground-anchored suspension system and its practice is not widely spread. Some of the reasons are its less redundant structure only feasible for shorter spans, which needs a more complex and expensive erection method when compared to a conventional ground-anchored suspension system. Specifically, as far as the new East Bay Bridge self-anchored span is concerned, several problems and controversies arose during the 15 years of design and construction. Indeed, many experts expressed their opinion against the design choice and question its safety in the long-term. Professor Astaneh-Asl is one of the most experienced voices questioning the Bridge design choice and safety. Therefore, Professor Astaneh-Asl supervised this MsC dissertation, which is a part of the main research project on the new Bay Bridge self-anchored span.

The main scope of this research is the study of the overall East Bay Bridge existing self-anchored span project and development of an altered design with a ground-anchored suspension system instead. The comparative analysis of these opposed designs was achieved by means of finite-element models. The final goal is to have a clear vision of the differences, advantages and disadvantages of each system - self and ground-anchored suspension span.

1.2. REPORT ORGANIZATION

This report is divided in seven chapters. Besides this explanatory introductory note, Chapter two summarizes all the scientific and technical literature found relevant by the author and studied for the development of this analysis. Besides the fact the self-anchored suspension system is not intuitive or commonly done, the new East Bay Bridge has even more complex characteristics such as asymmetric spans with single tower and 3D cable geometry. Therefore, literature survey was fundamental for further knowledge.

The third chapter dissects the Bridge self-anchored span structural elements and summarizes their characteristics and properties, as defined by the design team. The author was given access to the official project drawings from Caltrans, as well as to a complex finite-element model developed by Professor Astaneh and his research students that replicates the existent self-anchored span. A fully correct understanding of the structure is the first step towards an adequate and fair comparative study.

The fourth chapter includes a full description of the main issues and problems that arose during construction. As said before, the new East Bay Bridge self-anchored span is controversial. Indeed not only it was the most expensive project ever in the State of California, but also it faced various quality problems that might undermine the Bridge 150 service-life. This Chapter was found relevant to show some of the motives why different alternatives are being studied to compared with the existent SAS span.

As a matter of fact, Chapter three comes as an introduction to the fifth Chapter, which describes in detail the SAP2000 finite-element models, load definition and analysis parameters performed. The initial SAS model was previously developed and fully checked by the author. Furthermore, the author also did some improvements to the SAS model. After the SAS (self-anchored) model is set, the development of the GAS (ground-anchored) models started and in the end there were created three different GAS models. Firstly, it was analyzed a ground-anchored model with all the same characteristics of the initial SAS, but with the main cable disconnected at its extremities and pinned. This model intends to compare the differences that come from a simple change as the type of cable anchorage. Although presenting very good results, some elements are now overdesigned for a ground-anchored design and can use some developments. A second GAS model is created without some heavier structural elements, no longer needed in case of a ground-anchored suspension bridge. This redesigned GAS model kept the asymmetric spans but changed the cable sag slightly. Nevertheless, it was definitely not an optimized ground-anchored suspension, due to the asymmetry and cable sag to span ratio. Consequently, a last GAS model was designed keeping the single-tower, but with the tower location changed to have symmetric spans. The main models for comparison were the 1st and 3rd GAS models (with only cable disconnected and with symmetric spans) and the initial SAS model.

Last but not the least, Chapter six and seven present relevant plotting results for the models and some comparisons and conclusions, respectively.

2
LITERATURE SURVEY

Suspension Bridges have been studied and used for around 200 years now. Some important design advances have been made throughout the years, particularly after well-known failures and collapses of bridges such as Tacoma Narrows Bridge (1940). Advances in engineering are very much related to learning from past errors. This way, dynamic analysis of bridge structures has become a priority in the past decades. McCallen and Astaneh-Asl [1] state that both the 1989 Loma Prieta Earthquake and the 1994 Northridge California earthquakes brought awareness *to seismic vulnerabilities of transportation systems*, since many structures where built between 1930 and 1960 and lack modern seismic methodologies. McCallen and Astaneh-Asl [1] used the West San Francisco-Oakland Bay Bridge as object of study and investigated issues such as *spatially varying ground motions and nonlinear response simulations of the bridge system dynamic response.* Also it relates the wide range of frequencies of suspension bridges (modes of deck system with low frequency and tower with high frequency [2]) with the consideration of long period modes of vibration near active fault sites. For these cases, it is important to consider the possibility and consequences of large ground motion displacement pulses with around 5-second period. For short period structures (stiff), they would have minimal dynamic response to these long period motions and would move essentially as a rigid body with the ground motion. On the other hand, long period structures (flexible), would register a significant dynamic response to these long period pulses. For instance, the Bay Bridge west crossing has a transverse vibration of main span as fundamental vibration mode with about 9 to 10s. The ground motion pulse lasts around half of the fundamental period of the bridge. As a consequence, the pulse inputs tremendous energy to the Bay Bridge at the start of the earthquake motions, creating opposite displacements between towers and deck *(main deck span flung between the towers in sling slot fashion)* [2].

Also Astaneh, A. (1996) enumerated consequences of Loma Prieta earthquake and how it was a warning for seismic damage vulnerabilities of long span steel bridges. These type of bridges have complex seismic behavior due to: i) site condition varies significantly from bridge to bridge and also from pier to pier; ii) each long span bridge has unique structural configuration (suspension, cable-stayed, cantilever spans or simply supported trusses); iii) light or regular weight concrete as well as steel orthotropic decks have been used; iv) long spans bridges in the San Francisco Bay area have been built, using a variety of connectors (rivets, bolts and welds); v) Long span bridges have thousands of members and connections, which many of them are expected to experience inelasticity during major earthquakes. The analytical model should include material and kinematic nonlinearities; vi) Long span bridges have close modes of vibration with mass participation distributed over these modes and, as a result, response spectra analysis does not provide reliable results. Time history analysis with multiple support excitations is needed to understand seismic response properly. Furthermore, this paper

provides Seismic performance criteria as related to *bridge-priority ratings* and Structural analysis aspects such as Demand/Capacity ratios for inelastic and elastic analysis [3].

Nowadays, many scientific and technical papers and projects exist on conventional suspension bridges (McCallen and Astaneh-Asl, 2009; Shinozuka et al, 2009; Liu et al, 2000), which shows that the traditional suspension bridges anchored to the ground are widely used.

During early 1900's, a variation from the abovementioned structural system was developed: self-anchored suspension bridges. Over the last 30 years the self-anchored suspension bridge was brought to use again. Ochsendorf et al (1999) has a thorough characterization of this new type of bridge, its historical development, its possible analysis and design. Contrary to ground-anchored suspension bridges, which imply the use of large ground anchorage systems for the main cables, the self-anchored has the main cables secured to each end of the bridge deck. The deck now has two functions. First, it carries the horizontal component of the cable tension as a compression force, which is generally large and should be taken into consideration in the analysis. Secondly, the deck carries the vertical traffic loads and spreads it to the suspenders. Moreover, this paper refers examples of existing SAS bridges: Konohana (Japan) and Yong Jong (Korea). Konohana is a successful example because: i) used an efficient method of erection, which included tower construction, prefabricated deck sections and prefabricated parallel wire strands method for the cable; ii) inclined and prestressed hangers to avoid slacken under load condition; iii) inverted trapezoidal box girder designed to minimize falsework (closed box shape provides excellent aerodynamic and torsional performances). For both bridges a finite element model was created in order to obtain the following conclusions:

- Inclined hangers have beneficial effects on the bridge's behavior, because it reduces 34% of the maximum moment and 26% of the maximum deflections in the girder, for static loading. Also, they improve dynamic damping;

- A camber in the deck does not significantly influence the overall behavior of the bridge [4].

A more recent study by van Goolen (2006) has defined many other characteristics of SAS bridges and modeled this structural system in order to take some important conclusions. For the stiffening girder, an augment of the span length causes an increase of axial force and second order effects (geometric nonlinearities), which consequently increases the risk of global buckling instability, aerodynamic reactions and erection method. Also, adding weight distribution to the stiffening girder can decrease natural frequencies and increase the main cable tension force. Furthermore, for conventional suspension bridges, the slenderness of the girder is higher than on SAS bridges (more axial forces, more stiffness). The phenomenon of geometric nonlinearity is also presented in long span bridges as referred to before. For the towers, they have to support the main cable and transmit vertical forces to the foundations. Steel towers are more common and usually comprised of steel multi-cells or box single-cell sections. They must be stiffened with ribs to prevent local buckling [5].

Ochsendorf et al (1999) enumerates advantages and disadvantages of this new method and states that these disadvantages have prevented it from widespread acceptance. Nevertheless, many engineers in the United States, Korea and China have shown interest in self-anchored bridges, which must indicate it is not an inferior form and that is actually competitive for spans between 250-400m.

Advantages:

- elimination of large anchor blocks;

- relatively stiff superstructure;

- aesthetics benefits of traditional suspension bridges;

- end supports resist only vertical component of cable force , which is an advantage in case the soil conditions are not ideal;

- its economic benefits vary depending on the specific site conditions, but as the anchorage system is a great part of the cost, eliminating the external anchorages can provide a cheaper construction cost. Nevertheless, this will always depend on the erection method.

Disadvantages:

- complex construction resulting from erection of the stiffening girder prior to the installation of main cables;

- *lower degree of redundancy* than a conventional ground-anchored suspension bridge;

- the stiffening girder must be maintained and protected from damage, in order to prevent *catastrophic collapse*;

- unfamiliar form that can present analysis and design difficulties (e.g. second order effects are larger) [4].

Since the SAS structural system is still far from common, a list of the relevant self-anchored suspension bridges ever constructed and its key structural characteristics is given [5]. This list can be found in Annex A.2.1. It should be emphasized that the main boost in its construction was registered in China. Indeed, Zhang et al (2006) enumerates and describes techniques for three of these new SAS bridge examples in China [6].

As was mentioned earlier, in 1989, due to Loma Prieta earthquake, the east span of the San Francisco-Oakland Bay Bridge suffered a partial collapse of 17-meter long deck. A construction of a new east crossing was decided and the new self-anchored span alternative approved [7, 8, 9]. Since then, A. Astaneh-Asl is one of the experienced voices who has raised doubts and serious worries about the design of the new east span of San Francisco-Oakland Bay Bridge. The UCBerkeley Professor shared his concerns with MTC officials before the advisory panel approved the design in 1998. Also, he has publicly shared his opinion in several occasions: "*Think of a tower holding up a tray. Instead of being anchored in the ground, as is traditionally the case, the bridge is essentially holding itself up. That means if there is a sufficient rupture, all or part of the span could unravel (...) with a self-anchored suspension span, permanent displacement could cause a completely different story. Because the suspension cables are anchored into the deck, should the deck give way and lose compression, there's nothing to hold the cables. The entire [suspension] span could unravel".* That scenario has been discounted by Caltrans and Herb Rothman (bridge's chief design engineer): *"This bridge will be very well suited to a high seismic area. As far as we're concerned, the bridge has ideal earthquake characteristics, and meets all the standards that the state mandated for it."* [10]

The designing team of the new East San Francisco-Oakland Bay Bridge has published several papers about its design. Indeed, Manzanarez et al (2000) and Nader et al (2000) explain in more detail other design alternatives, how the soil conditions dictated the choice for the self-anchored signature span and its seismic design philosophy [7, 9]. Likewise, Sun et al (2002) justifies the project decision towards a looped cable anchorage system on the West bent and also explains the West bent composition: looped anchorage, cap beam, tie-down system and connectivity between the cap beams and piers [8]. As far as the suspension cable of the bridge is concerned, Sun et al (2004) published its design considerations. It is referred its layout, favored construction method, advantages and corrosion protection systems. Since the suspension cable is one of the main structural elements and has a unique 3D geometric configuration, its design was truly a challenge. Sun also explains why the modified octagonal strand layout was chosen [11]. Soon after the paper was published, it was brought to open

discussion by Knox, H. [12] who had concerns about the modified octagon strand arrangement and its future *difficulties in construction* as well as the overall construction method and cost. In response to the concerns raised, Sun et al (2004) provided additional information related to the suspension cable design and construction.

Still related with the new east Bay Bridge design, McDaniel and Seible (2005) studied the influence of inelastic tower links on the seismic response, more specifically the influence of ground motion intensity and tower links stiffness, location and hysteretic characteristics. These allowed them to conclude that the links addition improved the behavior of the structure. The most important conclusions were that inelastic links reduced the seismic displacement and moment demands through hysteretic response and coupling of the tower shafts, as well as the tower's middle region to be the most effective location for reducing demand/capacity ratios [13]. Also, the abovementioned authors, with Uang and Chou released another scientific paper related to the performance evaluation of the same tower shear links as well as the orthotropic steel deck panels. Cyclic tests on full-scale links proved these are able to reach inelastic rotation more than it would occur in a SEE seismic event, however brittle failure was registered and alterations were proposed in the welding details. Monotonic testing for two reduced scale deck panels (stiffened with closed ribs or open ribs) showed that they can develop a compression capacity greater than what would be produced by the design earthquake [14].

Later, Nader and Maroney (2007) published another paper related to the design of the new East Bay Bridge. It describes the bridge as a *one-of-a-kind design* and includes statistics and design details. It defines the 385-meter main span as record-setting and the Bay bridge itself as the first suspension bridge without connection between the tower and deck as well as a unique and first-time ever tower design. Furthermore, some important structural elements, such as Piers E2 and W2, tower, hinges and steel orthotropic deck are discussed [15].

It was mentioned before that there has been a boost of SAS bridges' construction in China in recent years. As a consequence, mainly in the past five years several papers with SAS-related studies have been published. Gao et al (2009) performed seismic analysis and optimization design for an approved SAS bridge design over Huangshuihe River. They performed modal analysis and nonlinear time history analysis with a SAP2000 model. Girder, towers, piers, piles, main cables and suspenders were modeled with frame elements and a compression limit of zero was imposed to the cable and suspenders. They studied an optimization for the bridge seismic response and for that they analyzed the discontinuity in the towers (architectural configuration) and the possible use of nonlinear fluid viscous dampers [16]. Li et al (2009) studied the pile-soil-structure interaction on seismic response of a SAS bridge, using the Dalian Jinzhou Bridge as the subject of the study. They used three different models, one for SAS bridge without pile-soil-structure interaction, one for SAS bridge with pile-soil-structure interaction and another for a ground-anchored suspension bridge (with same parameters) with pile-soil-structure interaction. From these models, several conclusions were drawn about the consequences of the abovementioned interaction. They concluded that pile-soil-structure interaction makes the structure of SAS bridge more flexible and, therefore reduces the first order frequency. Also, under the effect of seismic ground motion, this interaction increases significantly the longitudinal displacement, the axial force at the bottom of the tower and the moment at the main span of the stiffening girder for the SAS bridge. Nevertheless, the authors concluded that the *vertical displacement and moment of the stiffening girder for the self-anchored is significantly less* then for the ground-anchored suspension bridge, but the *moment and longitudinal displacement at the top of main tower are significantly greater for the self-anchored bridge* then the ground-anchored suspension bridge. They used a merging pile model of equivalent embedded fixation to simulate the interaction [17]. Mu et al (2009) studied a design for a self-anchored cable-stayed suspension bridge (Zhuanghe

bridge), by establishing a finite element model of the bridge and conducting its dynamic analysis. The main difficulty was to simulate the stiffness of main beam, tower, cable, pier and foundation of the bridge, as well as the boundary conditions. For the dynamic analysis, the input for the time-history analysis was an artificial seismic wave. Since it was a very flexible structure, the load-deformation relationship was nonlinear and the non-linearity becomes more relevant as we increase the span of the bridge. Besides the analysis of the seismic response of the bridge structural elements, they studied the impact of changes in structural parameters, more specifically changes in the restriction of the main beam. From this analysis, it was concluded that increasing the longitudinal restrains gradually decreases the bending moment at the bottom of the tower, as well as the displacement at the top of the tower and beam end. Nevertheless, this reduction is minor and *so other measures can be tried to reduce earthquake impact on the Zhuanghe Bridge* [18]. Jiang et al (2009) discussed the possible reduction of seismic response in self-anchored bridges, for instance between the tower and stiffening girder connection. Using time-history analysis, the pounding of the deck against the tower is studied for different case scenarios: different stiffness, free gap, damping coefficient of the device and different seismic waves. The frequency spectrum characteristics of the seismic wave alter significantly the pounding characteristics. Firstly, the authors discuss the most common measures to dissipate seismic energy, which are elastic restraint, pounding bearings and dampers between the girder and piers. Nevertheless, a SAS bridge works differently and devices are installed between the tower and girder in order to reduce the displacements/forces caused by a longitudinal seismic wave. For a more detailed study, the Chaoyang Huanghelu Bridge was used as the subject of study. For the modeling, beam elements were used for girder, pylons, piers and pile foundations, while the main cable and hangers were simulated as cable elements, including the influence of the initial internal stresses of the main cables in the main cable stiffness. The influence of the pounding among bridge members was studied and the following conclusion were drawn: i) for SAS bridge the girder-pylon effect can be favorable or unfavorable for the stress in the pylon. With the increase of the initial gap between elements, the seismic performance reduces and both the displacement of girder and moment in the tower rise. However, a small gap can also cause local damage; ii) viscous dampers consume large amounts of energy without causing extra static stiffness to the structure and its use reduces very much the moment and pounding force in the pylon significantly [19].

More recently in 2011, Nie et al researched on a new cable anchorage system for self-anchored suspension bridges with steel box girders, because *an optimized design of the cable anchorage is very important for the rational design of the whole bridge*. The main goal was the optimization of the mechanical behavior of the common cable deck anchorage systems. The studied composite anchorage, due to the composite effect between steel and concrete, reduced significantly the stress levels in the plates (around 40%). Also, the stresses were much more uniformly distributed. Both a finite element model (ANSYS) and a scale model testing were used to obtain these results. After discussing various types of anchorage: traditional concrete; looped concrete; pure steel; steel-concrete composite; the authors analyzed the advantages of the composite anchorage system. The most relevant advantages according to them were the reduction of stress levels on the steel plates and, consequently the thickness of the plates, improving the reliability of the steel plates welding and the reduction of the number of stiffeners and their thickness. Nevertheless, the authors state that this system still requires further studies in order to be accepted as a practical solution. For that reason, it was not used in the Qingdao bridge project. As far as the looped cable anchorage system is concerned, the authors state that it provides *structural compactness and excellent seismic performance*, but requires more strands and both the mechanical behavior and site construction of the prestressed cap beam become complex. The new San Francisco-Oakland SAS span is the only reference given by the authors as an existing example of this kind of system [20]. Most of the previous authors published another very recent paper

continuing the research on cable anchorage systems for SAS bridges (Nie et al, 2014). The Taohuayu Bridge (THY) the largest three-span double-tower SAS bridge is the case study. This paper focuses on a new *multi-scale modeling method*, in order to improve the reliability of conventional modeling methods. These traditional modeling methods are presented and their characteristics enumerated: Structural, Traditional scale and Full-scale (local and global). Although the full-scale method already reduces the influence of the fuzzy region and is very common, the authors decided to go further and model different parts of the structure in different appropriate scales. This resulted in accurate analysis for each part. This approach was made possible by adopting flexible boundary conditions (BC), which eliminates the influence of the fuzzy region and by validating results with a scale model test. The flexible BC's are like generalized BC's that represent the real loads, supports and calculates the comprehensive strain and stress distribution efficiently. Moreover, it was also concluded in this paper that the full-scale method is inefficient to model the entire bridge and that the structural method cannot analyze the stress distribution of the cable anchorage system. On the other hand, the scale model can complement and partially validate the multi-scale method and vice-versa [21].

Lianzhen and Tianliang (2012) studied the dynamic characteristics and seismic response of a self-anchored bridge across the Hunhe River in China. For that purpose, they used an artificial seismic wave for the ground motion input. Regarding the self-anchored suspension bridges in China, it is said that the first of this type was built in 2000 and that around year 2012 *thirty self-anchored suspension bridges have been finished in China* (See Annex A2.1.). The authors consider SAS bridges as *self-balance structures*, meaning that the girder has weaker boundary constrains, in order to satisfy longitudinal movement. This way, during a seismic event the girder will create longitudinal floating movement and *the tower will bear huge horizontal earthquake forces.* A SAP2000 model was created, using frame elements to model the girder and pylons and cable elements. In this model, for time-history analysis *Rayleigh damping* was used to model the damping of the structure. The following conclusions were drawn: for longitudinal seismic excitation, the longitudinal displacement of the tower is under control and its bottom section is critical since it has high bending moment (as expected); for transverse seismic excitation the lateral displacement of the tower is controlled and the bottom of the tower and midpoint of the main span are critical sections for bending moment; the vertical seismic excitation can not be ignored when considering the three directions of excitation, because it has an evident impact on the girder [22]. Furthermore, other scientific papers related to seismic analysis of SAS bridges were written. Among them, Qiu et al (2012) states that SAS system can save on construction costs and time incurred on the construction of the anchorage system. However, it also mentions that *the feasibility of a self-anchored suspension bridge in a strong earthquake zone and the use of dampers to reduce seismic response have yet to be fully investigated.* The authors used the Yellow River Road Bridge in Mainland as object of their study. A finite element model was created in ANSYS, using beam element for tower, piers, piles, main girders and cross beams, while the main cables and suspenders used truss elements. Springs were used to model the foundations. The seismic response of the bridge was obtained by a nonlinear time-history analysis, considering the geometric nonlinearity of the structure and the material nonlinearity of the tower. It becomes clear after running the model that the first mode of vibration is a longitudinal floating mode with longer period. This is typical of the SAS bridges, according to the authors. After performing seismic analysis it was concluded that the longitudinal displacements in the girder were excessive (0,5 to 0,6m depending on elastic or ductility analysis) and that it proved necessary to install metal dampers in the connections between the tower and the girder. The main conclusions were: for dynamic analysis the SAS bridge still has longer period of the first mode and concentration of vibration modes, which matches the ground-anchored suspension bridges characteristics; due to free movement of the main girder longitudinally, this represents the 1st vibration mode and results in too large longitudinal

displacements thus r*esulting in a seismic disaster of dropping girder or damaging expansion joints*; the ductility analysis clearly reduced the moment of the tower's bottom section but increased the displacements of the main girder and top of the tower; the installment of the metal dampers controlled the excessive displacements as well as the bending moment at the bottom of the tower, and also protected the expansion joints against damage and the dropping of the girder [23].

During the present year (2014), Lu et al studied the optimization of a model for SAS bridges. Since the suspenders of the bridge need to be tensioned adequately during construction, a simplified optimization calculation method of cable force has been developed based on optimization theories for cable-stayed bridges (minimum bending energy method; internal force balanced method; influence matrix method), which are optimization analytical methods. The indeterminate mechanical behavior of the SAS type of bridge makes it complex to solve this optimization question and, consequently there are still many other theories/studies needed to make the mechanical behavior clearer both in construction and completed stage. On the other hand, for comparison, an ANSYS finite element model was analyzed and the conclusion was that the cable force computed and the cable force from the optimization method are similar. This way, this proves the accuracy with which the completion stage cable force can be obtained with the optimization method. From that, the authors developed an optimized tension method through the analysis of tension order of the suspension bridge (from actual construction data) [24]. Very recently, Yuanming et al (2014) also studied the dynamic characteristics of a large self-anchored suspension bridge. According to the authors, *anti-seismic capacity, wind resistance capacity and vehicle-bridge vibration problems are usually the main controlling factors when designing suspension bridge.* For these kind of bridges their geometry, load conditions, boundary conditions and material properties are complex and very inaccurate results may result from simplified dynamic analysis. Therefore, the Taohuayu Yellow River Bridge was modeled using MIDAS finite element analysis program, with beam element for pylon, saddle, stiffening transverse girder and truss element for the main cable and suspenders. The initial forces of main cable increased significantly and, consequently the stiffness of it increased too (gravity stiffness). Therefore, static calculation should be done before dynamic analysis, in order to use its results as initial conditions for the dynamic analysis. For this long span SAS bridge with double tower and middle span, the vertical bending of the deck is the first vibration mode because the stiffness of the girder is small. To make a modal analysis, it is chosen a subspace iteration method and the first 10 modes are analyzed. This paper also includes a comparison between self-anchored and ground-anchored suspension bridges. It states that their major difference in dynamic properties is the modal shape decided by the tower. The top of the tower has different restrictions in both cases and the frequency is lower for the SAS bridge. The calculation was made for both cases and the difference in the frequency values was of hundredth decimal. Also, for the mode decided by the girder vibration the frequency is lower in the SAS bridge (more axial force, weaker geometric stiffness) [25].

Furthermore, some other literature related with bridge design in general, as well as cable supported bridges has been published throughout the years. For this study, the Bridge Engineering Handbook (2000) it was specifically studied. As far as structural modeling is concerned, the book states that the computer software ADINA is among the most popular, but also more powerful and complex computer analysis programs. Also, it states that a **nonlinear analysis is usually preceded by a linear analysis** as part of the procedure to capture the physical and mechanical interactions of seismic input in structural response. The output from the linear analysis is used to predict which nonlinearities are going to affect the response significantly (engineers can justify the effect of each nonlinear element introduced at the adequate locations and have a reliable nonlinear analysis). The book gives examples of the benefits of orthotropic steel box girders in suspension bridges and makes reference to the deck for the new East Bay Bridge. It also states that *the cost can be increased, sometimes significantly, by a*

concept that is difficult to erect (it is all about cost, appearance, reliability and serviceability). Additionally, it confirms that the most critical area of the tower design is the **tower-to-foundation connection,** since both shear forces and bending moments are maximum on this section. Anchor bolts are usually used at the base of the steel towers and must be deeply embedded in the concrete footing in order to transfer the loads to the footing reinforcement. For suspension bridges, it refers to various systems that can be used.

Furthermore, various examples of earthquake damage to bridges are documented in chapter thirty-four of this book, more specifically the partial collapse of the previous East Bay Bridge in 1989. Indeed, one of the main causes of damage is the spatial and temporal variation in the ground motions on the bridge's foundations (different piers are subjected to different ground motions at any one time, because seismic waves take time to travel from one bridge pier to another). This effect can cause one pier to be pulled in one direction and other in the opposite. Another very important and useful topic is addressed in chapter thirty-seven: Seismic Design Philosophies. It discusses both criteria, No-collapse design and Performance-based criteria. The first one is used for *ordinary bridges* and can have two approaches: i) conventional force-based; ii) recent displacement-based. The second one was developed more recently (after some major earthquake damage to structures) and consists of establishing performance requirements first and afterwards defining loads, materials, analysis, methods or acceptance criteria that allow achieving the pre-defined performance. These requirements can include brittle failure modes, joint shear design and limit state definition. For the No-Collapse design, the book makes reference to both AASHTO and Caltrans Bridge seismic design specifications. For the Performance-based criteria design, it makes reference to the Caltrans practice and its improvements throughout the years, mainly after ATC-32 recommendations.

Table 2.1 – ATC-32 Minimum required analysis

Bridge Type		Functional Evaluation (FEE)	Safety Evaluation (SEE)
Ordinary	Type I	None required	- Equivalent static analysis - Elastic dynamic analysis
	Type II	None required	Elastic dynamic analysis
Important	Type I	- Equivalent static analysis - Elastic dynamic analysis	- Equivalent static analysis - Elastic dynamic analysis
	Type II	Elastic dynamic analysis	Inelastic dynamic analysis

This way, first a category is assigned to the bridge (Table 1) and its equivalent design *damage levels* and required analysis. Then, the ductility of the structure is taken into consideration, because *it is the predominant measure of structural ability to dissipate energy.* Also, displacements demands are used instead of forces to measure the earthquake damage, since by using displacements we can ensure that the structure and its individual components can withstand the deformation imposed by the design earthquake. The seismic demand of displacements for long period bridges (T>3s), as is the case of the self-anchored span being studied, is overestimated with a linear elastic analysis and so a linear elastic displacement response spectra analysis with effective component stiffness can/should be used. The following analysis are made for the determination of demands in important bridges: i) Static linear analysis (forces due to self-weight, wind, water, temperature and live load); ii) Dynamic response spectrum (used on the simplified global model to determine mode shapes, periods and initial estimates

of seismic forces and displacements, in order to verify the model and eliminate modeling errors); iii) Dynamic time history analysis (linear elastic, nonlinear elastic and nonlinear inelastic). As far as capacities are concerned, for strength and deformation capacity of a flexural element it can be evaluated by moment-curvature analysis considering P-Δ and P-δ effects (combined axial and bending). Displacement capacity should be evaluated with a static pushover analysis. The *nominal strength of structural components* can be determined in accordance with the code formula or verified with experimental/analytical models or project-specific criteria. *The structural deformation capacity* should be determined by a nonlinear inelastic analysis and based on accepted damage levels, considering material and geometric nonlinearities. After measuring demands and capacities of elements, to achieve performance goals they must satisfy certain demand/capacity ratios. As discussed before, demands in terms of factored moment, shear, axial and displacement/rotation deformations should be determined with dynamic response spectrum analysis for ordinary bridges and with nonlinear inelastic dynamic time history analysis for important bridges. Afterwards, structural elements are divided into two categories: *critical or other.* Other components protect the critical elements from seismic damage of a FEE or SEE seismic events. It is not possible for a bridge to remain elastic during major earthquakes and so a nonlinear inelastic response is expected, but the designer usually uses the other components (and not the critical ones) to have seismic damage and allow the global structure to stay mainly elastic and functional after FEE or SEE. Indeed, inelastic behavior (controlled damage) is permitted for some *other components* such as cross frames, end diaphragms, shear keys and bearings. For these, acceptable demand/capacity ratios vary from 1 to 2.5 (when moment is dominant) or from 1 to 2.0 (when axial force is dominant).

Another example of a book that emphasizes bridge design, more specifically cable-supported bridges, is by Gimsing, N. (1983) [26]. It compares and distinguishes different existing structural systems for suspension systems and cable stayed systems, as well as theirs variations. The suspension one is comprised of parabolic cable (catenary) and vertical or inclined hangers that connect it to the stiffening girder. The *cable stayed system contains straight cables connecting the stiffening girder to the pylons.* The cables can radiate from the top of the pylon or they can be parallel cables (or a mixed system). They can be characterized also by the cable anchorage system as *earth anchored* or *self-anchored* (as referred previously).

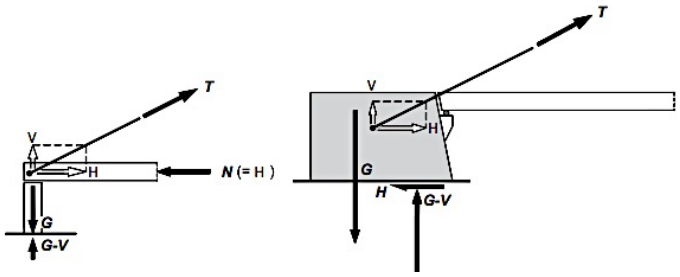

Fig. 0.1 - Self-anchored and ground-anchored suspension bridges force distribution, respectively [26].

The author states that self-anchored system can be used for both cable-stayed and suspension bridges, but that in practice the ground-anchored system is mainly used for suspension bridges and the self-anchored for cable-stayed bridges. More importantly, the author states that *in some smaller suspension bridges the self-anchored system can be applied. At first glance it might look very promising to avoid the large horizontal forces on the anchor blocks, but taking into account that the compression in the*

stiffening girder requires a larger cross section leading to increasing dead load and that during erection the main cable cannot be subjected to loading until the stiffening girder is in place, makes the self-anchored system less attractive. Adding to this that the self-anchored suspension system is inferior to the self-anchored cable-stayed system in almost any respect makes it probable that a very limited number of self-anchored suspension bridges will be built in the future.

As far as cables are concerned, the author states that the reeling problem associated for many years to the parallel-wire strand has been tested and excluded. Therefore, that method has become common and it uses usually 5mm wires for suspension bridges main cables and a regular, deformed or quasi-hexagonal pattern. Also, for the erection methods air-spinning and prefabricated parallel-wire strand are the two methods for long cables. PWS accelerates erection and, due to its higher weight per unit length it becomes more stable (less affected by wind). For cable anchorage and connections, it is stated that the most common method of anchoring single prefabricated strands is by socketing its ends. It consists of a steel cylinder that is filled with a metallic alloy (e.g. zinc).

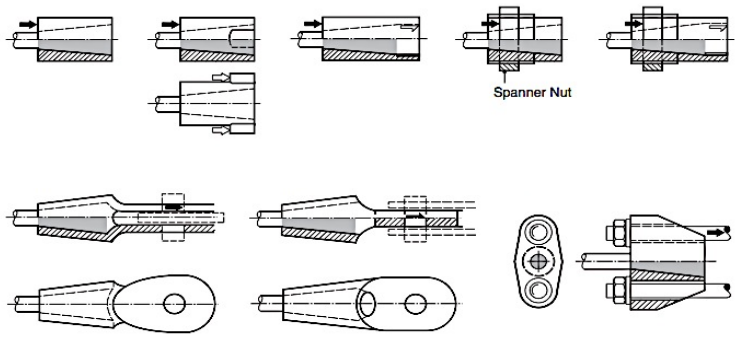

Fig. 0.2 – Different types of sockets [26].

There can be some problems related to the symmetrical spreading of multi-strand cable with more than three layers of strands. Consequently it is used a splay saddle supported to the adjoining structure so that the transversal force component can be transferred.

For the connection between the main cable and the main tower, the author refers three different types, but only one that is usual for suspension bridges: fixed saddle with the cable being led continuously over it. Also, for parallel-wire strands a compaction of the main cable is essential after the erection of all strands. For that, a compacting machine pulls the strands together and changes the hexagonal initial shape to a *nearly circular configuration*. The percentage of voids in the cable measures the efficiency of this process and 9.3% is stated as the percentage for the theoretically perfect compacted cable. In reality, this percentage varies from 17 to 23% [26].

3

EAST BAY BRIDGE: DEFINITION OF SELF-ANCHORED SPAN

3.1 INTRODUCTION

The new East San Francisco-Oakland Bay Bridge is the main object of study of this thesis, particularly the self-Anchored signature span. It is located in the United States of America, State of California, on the San Francisco Bay area (Fig.3.1). The previous East Bay Bridge was constructed in 1936, accordingly to the 1930 Uniform Building Code for only 10% gravity earthquake accelerations. It suffered a 15-meter collapse of the upper deck, due to Loma Prieta earthquake in 1989 (Fig. 3.2), which was a 7,1M Ritcher scale earthquake caused by a rupture in San Andreas Fault with epicenter around 100 km south of San Francisco (Fig. 3.3) [9].

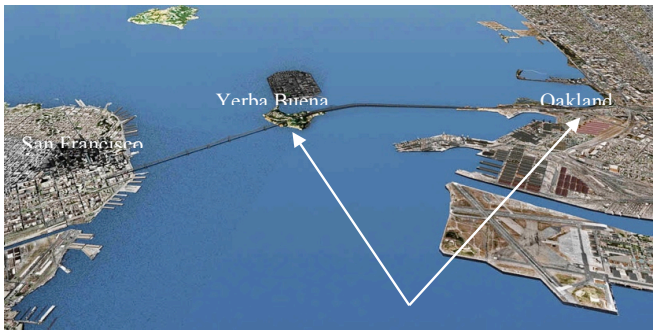

Fig. 3.1 –Project location and limits are between the arrows [Ref.: Caltrans presentation by Amer Bata, P.E.]

This collapse occurred over Pier E9, which connects the 154m-west truss spans and the 88m-east truss spans. This transitional span was supposed to transmit longitudinal forces between adjacent spans and Pier E9. The failure of a bolted connection resulted in a sliding and unseating of this transition span. This failure mode was due to spatial and temporal variations in the ground motions on the Bridge's foundations, meaning that different piers are subjected to different ground motions at any one time, because seismic waves take time to travel from one bridge pier to another. The aforementioned effect causes one pier to be pulled in one direction and other pier in the opposite. Since the Bay Bridge had a variety of different superstructure and substructure configurations, variable soil condition and is long enough for spatial/temporal variations in ground motions to induce large relative displacements between adjacent bridge segments, this effects occurred. It took more than a month to reopen this critical traffic line that connects Oakland to San Francisco [27].

Fig. 3.2 – East Bay Bridge partial collapse in 1989 [Ref.: http://baybridgeinfo.org/timeline#c1989].

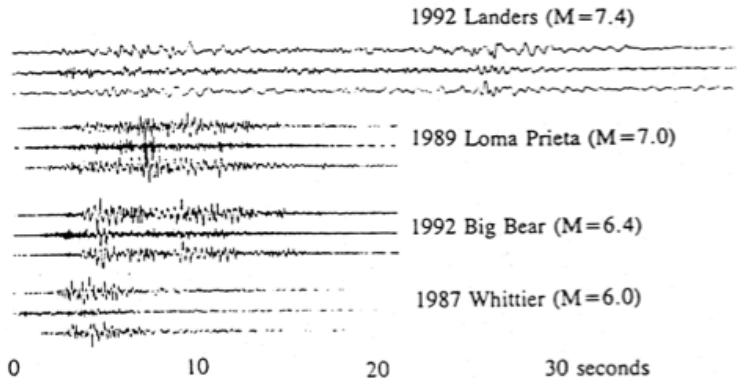

Fig. 3.3 – Earthquake accelerograms, including the 1989 Loma Prieta *[Ref.: Bridge Engineering handbook, 2000].*

After this collapse, California Department of Transportation (Caltrans) decided it would be more cost effective to design a new East Bay Bridge rather then just retrofitting the existing bridge for a major seismic event predicted for the next 50 years [7]. After a design workshop held by EDAP (Engineering and Design Advisory Panel), 16 designs were presented to the jury panel and in the end T.Y. Lin International and Moffat & Nichol (join venture) design of the new signature project was chosen. The signature span was selected from four final alternatives and it consists of a single-tower asymmetric self-anchored suspension bridge. According to the designing team, the choice for a self-anchored bridge was mostly due to detrimental soil conditions and aesthetics. The asymmetry is recommended mainly due to soil conditions (Fig. 3.6 and 3.7), but also to accommodate the main span navigation clearance and to highlight the grace of the catenary curve of the main cable. The main span length to side span length ratio is of 4 to 3, when compared to a conventional symmetrical suspension span [8].

The complete bridge project consists of four different structures: i) a low rise post-tensioned concrete box girder, connecting the toll plaza at Oakland Mole to the skyway (*Oakland approach*); ii) 2.4 km

long segmental concrete box girders, consisting of two parallel structures to carry the traffic in opposite directions separately (*Skyway*); iii) self-anchored suspension span (*SAS*) and iv) post-tensioned concrete box girder that makes the transition with the Yerba Buena Island tunnel (*transition structure*).

The skyway is comprised of segmental concrete box girders with varying span lengths from 120 to 160m and it was constructed using a balanced cantilever precast segmental construction method. The piers are box reinforced concrete and the skyway is founded on large diameter steel piles (battered), 90 m to 100 m long, arranged in groups of 6 and 4, and partially filled with reinforced concrete. During the construction of the Yerba Buena transition structure, it was necessary to built two temporary detour structures for traffic routing [7, 9]. The new design was completed in 2001 and the construction of the SAS span started on 2005. The new East Bay Bridge was opened to the public on Labor Day 2013 (September 2) after several years of delays and a final budget of approximately 6.5 billion US dollar (see fig.3.55). The demolition of the previous East Bay Bridge started in November 2013 and it is scheduled to end by 2016.

In order to provide a general idea of the volume of work on the Self-anchored part of the project, approximately 25 000 m^3 of structural concrete, 5 200 000 Kg of bar reinforcement steel and 52000000 Kg of structural steel were used. Shangai Zhenhua Heavy Industry (ZPMC) was the main steel fabricator (deck and tower sections, as well as temporary supports). This company is one of the largest heavy-duty equipment manufacturers in the world. The SAS sections were fabricated at ZPMC's facility on Changxing Island [28].

Fig. 3.4 – Self-anchored Bay Bridge span and Yerba Buena Island *[Ref.: baybridgeinfo.org].*

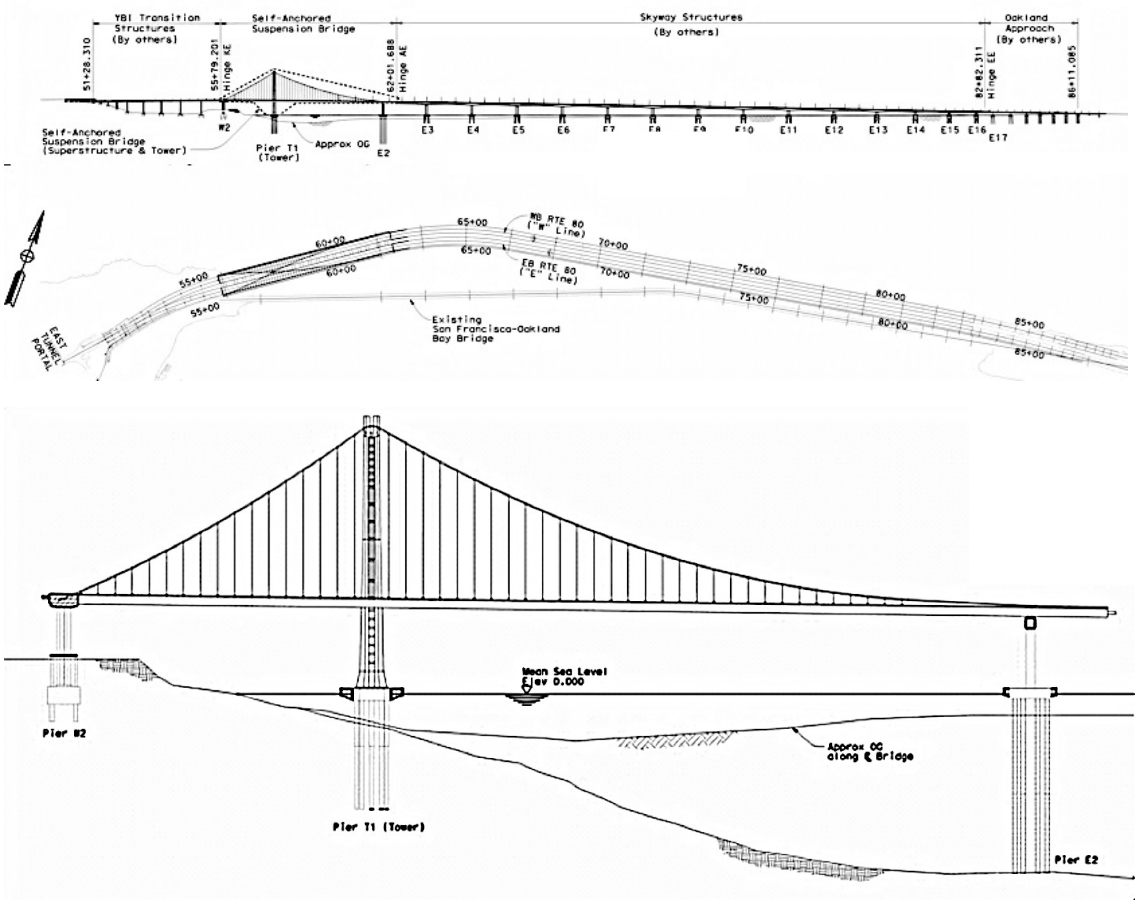

Fig. 3.5 – Entire East San Francisco-Oakland Bay Bridge structure and Self-anchored suspension span, respectively *[Ref.: Caltrans drawings 418/1204].*

3.2 SOIL CONDITION

From West to East, the longitudinal soil conditions vary significantly with the bedrock (San Franciscan formation) steep slope to bigger depths. According to Caltrans, the main reasons for the design choice of a self-anchored suspension bridge were the unfavorable soil conditions, as well as aesthetics. In fact, not only these conditions are unfavorable, but also they change very much along the longitudinal direction of the bridge (Fig. 3.6 and 3.7). Starting nearer to the Yerba Buena transition, the west piers are founded on rock. On the other hand, at the east piers the Franciscan Formation (bedrock) reaches more than 100 m depth. The soil consists primarily of young bay mud, interlayered clays and sands from the Alameda formation [9]. A correct and detailed profile of the soil is essential since this great heterogeneity will cause the east and west foundations of the bridge to experience different displacements during a seismic event.

More detailed information such as the longitudinal soil profile and testing results for the SAS span are presented in Subchapter 3.11.2, in order to establish comparison with other suspension bridges around the world supported on unfavorable soil conditions.

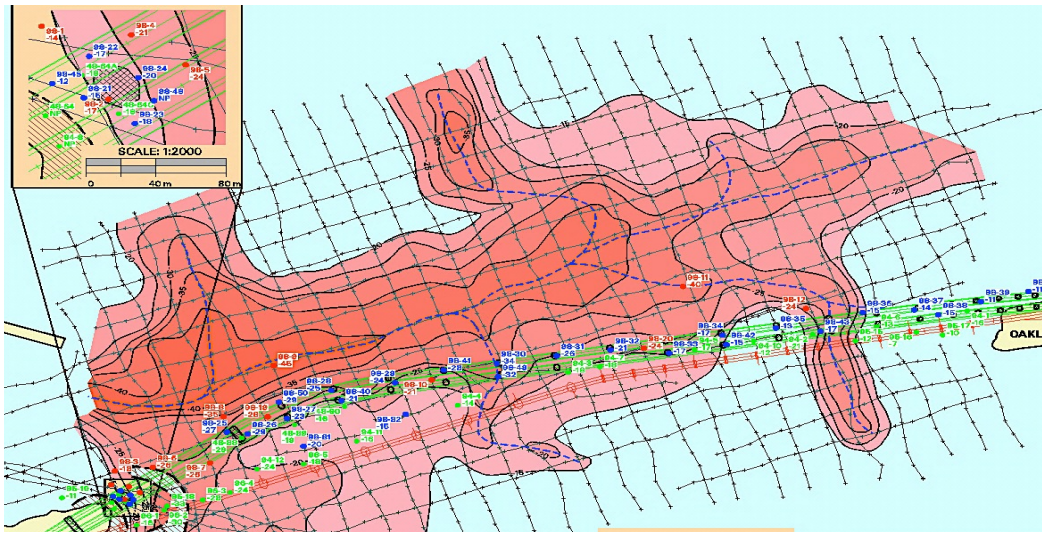

Fig. 3.6 – Contour of elevation of base of young bay mud spaced at 5m *(*Ref.: *Caltrans presentation by Anthony Dover, P.E. and G.E.)*

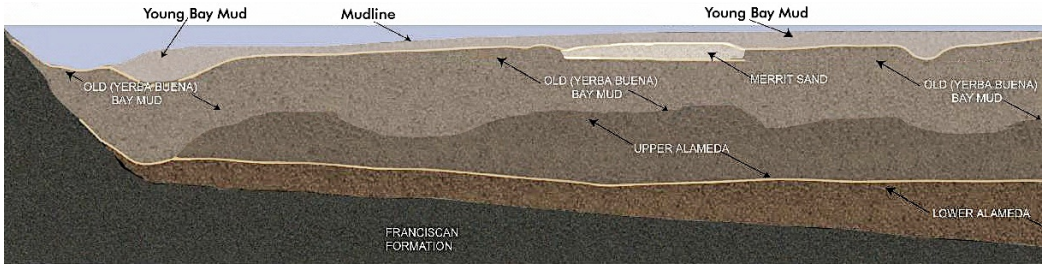

Fig. 3.7 – Geotechnical conditions of the soil along the bridge longitudinal axis [9].

3.3 ALIGNMENT

The previous Bay Bridge has the alignment represented by the black line (Fig. 3.8). The limits for the potential new bridge locations were defined by the alignments designated as N1 (north) and N2 (south). Alignment N2 was designed to minimize the bridge length, by following closely the previous East Bay Bridge, and has a 3479-meter total length. The N1 alignment was designed to avoid conflicts with the EBMUD[1] sewer outfall. This alignment was chosen in order to maximize the views to San Francisco skyline, while minimizing construction in parts of the Bay where the geological conditions could increase complexity and cost of the project. The total length for this alternative is 3514m and approximately 600m east of the Yerba Buena Tunnel it would transition from a double-deck structure to two parallel bounds. Also, 1300m after the Oakland Touchdown it transitions and adapts to the double deck skyway [29].

[1] East Bay Municipal Utility District

[2] Cutting the sound rock and socketing for a depth (at minimum) of one diameter. Piles on rock carry the load by point

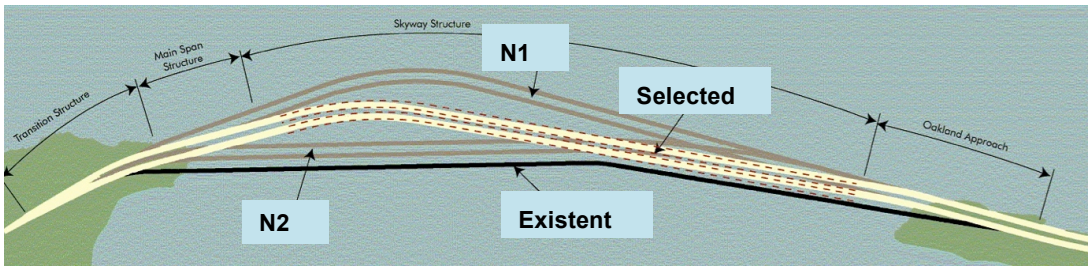

Fig. 3.8 – Previous East Bay Bridge, possible and selected alignments [9].

3.4 FOUNDATIONS AND PILES

3.4.1 EAST FOUNDATIONS

The variation of soil conditions longitudinally can be observed in Figure 3.6 and 3.7. It is also obvious that the east foundation of the Self-anchored has to solve the problem of the 100-meter deep layers of mud and sand above the bedrock. According to the project drawings, this foundation consists on 16 piles (2500 Dia CISS Concrete Piling) that are 105m long. These piles are filled with concrete on their top 55m [7, 15].

Annex A3.1 and Annex A3.2 contains detailed AutoCAD drawings by the author of the longitudinal view of the east piles.

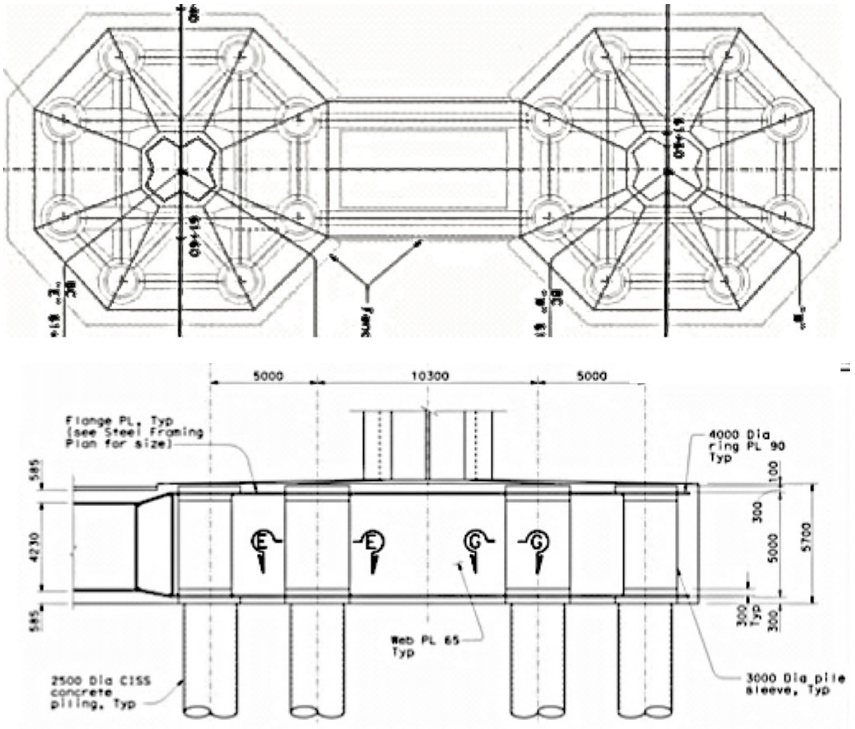

Fig. 3.9 – Plan and elevation sections of the East piers and pile cap (Ref.: Caltrans drawings 46/118).

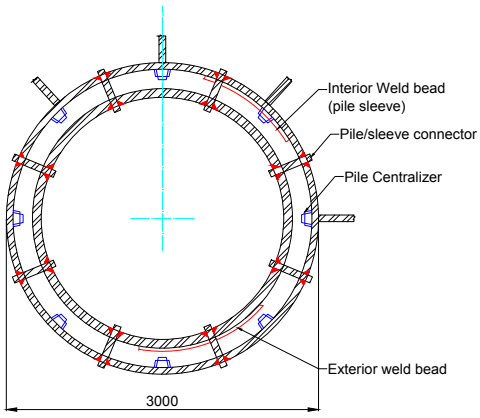

Fig. 3.10 – Cross Section of East piles inside Pile cap [Ref.: AutoCAD made by the author].

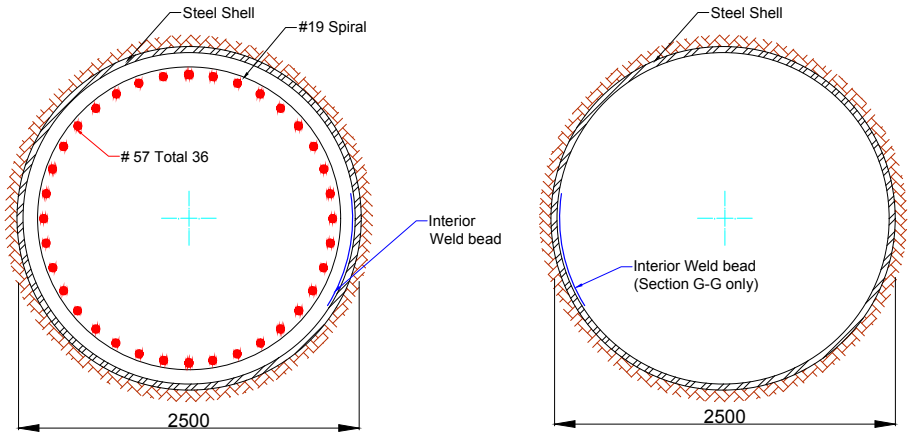

Fig. 3.11 – Cross Section at mid height of East foundation piles (Ref.: AutoCAD made by the author).

3.4.2 WEST FOUNDATIONS

This foundation is supporting one of the most structurally important elements of the Self-anchored span, the west bent. It is supported on gravity footings (cast into rock) with 10-meter long corner piles. There are 4 piles with 2,5-meter diameter, which are CIDH (Cast in Drilled Holes) [7,15]. The gravity footings are connected to the cap beam by means of a cable tie-down system, designed to keep the west piers in compression in case of a seismic event. This tie-down consists of 28 stay cables, which are anchored into the rock through 4 additional CIDH 2,5-m diameter piles [7]. The choice for CIDH piles may rely on various aspects. One fact is that it is easier to penetrate deep into bedrock using that system, rather then driven piles [30].

To build the western supports it was required 2000 tons of steel reinforcement and more than 12000 m^3 of concrete [28].

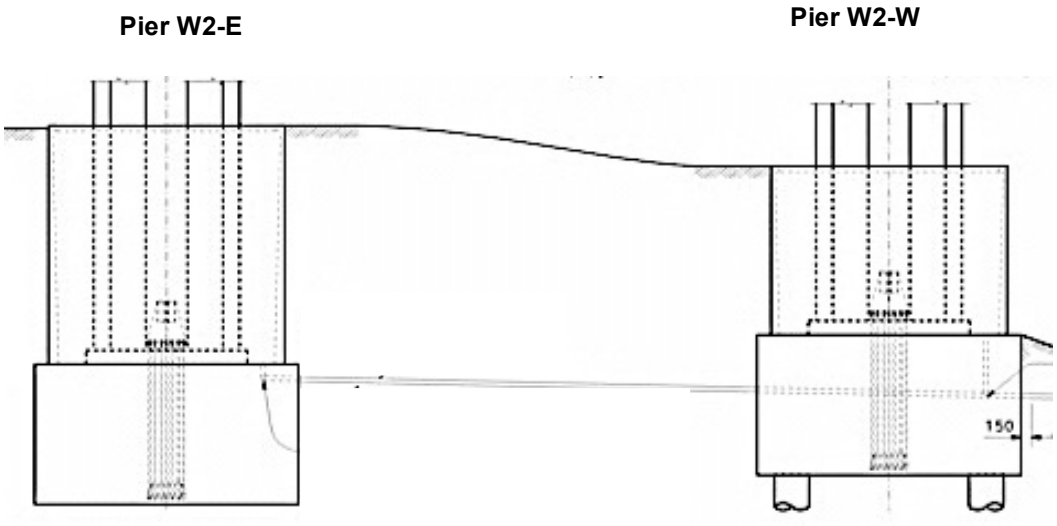

Fig. 3.12 – West footings of east and west lines respectively [*Ref.: Caltrans].*

3.4.3 MAIN TOWER FOUNDATIONS

The tower foundation consists of a 6,5-meter height pile cap (steel moment frame encased with concrete) welded to steel shells surrounding each of the 13 piles. These piles are 60-meter long and 2,5m-diameter steel shell pipes. They are fixed on the bedrock. The embedding of the piles on the rock was not an easy task and was only possible due to a process called *rock socketing*[2] [15, 28]. Two parts comprise these piles: a lower portion made of heavily reinforced concrete and placed within shafts/rock sockets drilled into bedrock (2200 Dia CIDH Concrete Piling) and an upper portion, which is a permanent steel shell filled with heavily reinforced concrete (2500 Dia CIDH Concrete Piling). This upper shell is welded to the pile cap [28]. The connection between the pile cap and the tower shafts first segment was made using dowels, anchor rods, bolts and welds. There are 150 dowels, sticking out of the foundation and 424 large anchor rods to fasten these sections (Fig. 3.13 to 3.15). For more information on these fasteners, see Chapter 4.

As it can be noticed on Figure 3.28 the rock slope is benched in order to give the piles the same lateral stiffness and to avoid torsional response [9].

The 6,5-meter pile cap or steel footing box was made in Texas and shipped to the construction site through the Panama Canal.

[2] Cutting the sound rock and socketing for a depth (at minimum) of one diameter. Piles on rock carry the load by point bearing. To ensure proper contact between base of pile and rock surface, it is needed to socket the pile into hard rock. This is achieved by means of cutting out weathered and soft rock, cutting hard rock for a reasonable depth (1D) and introducing the piles [8].

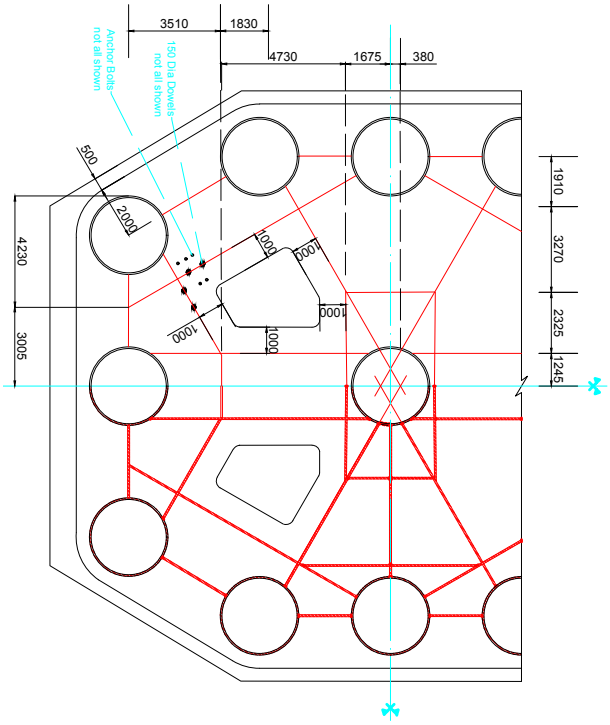

Fig. 3.13 – Plan view of pile cap for the Tower base with foundation piles and tower shafts *[Ref.: AutoCAD made by the author]*.

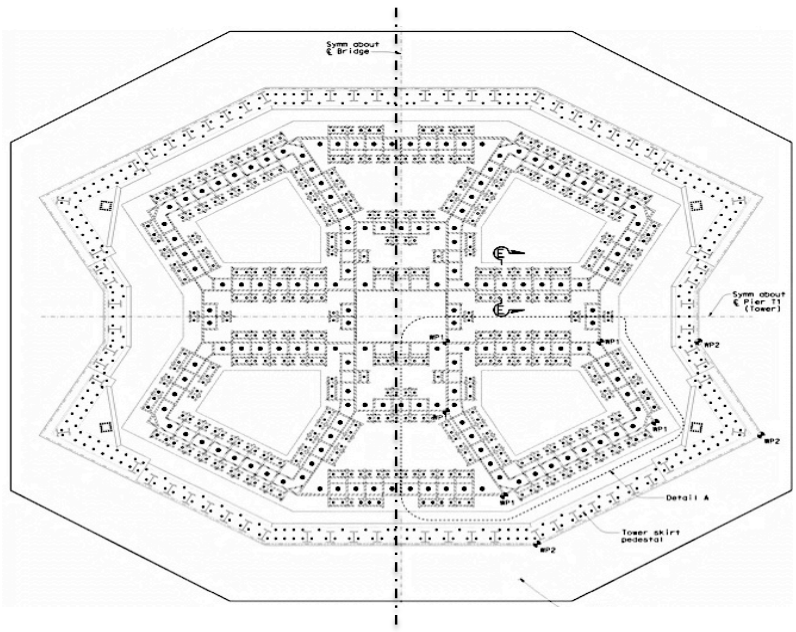

Fig. 3.14 –Plan view of dowels and anchor bolts on the tower base *[Ref.: Caltrans]*.

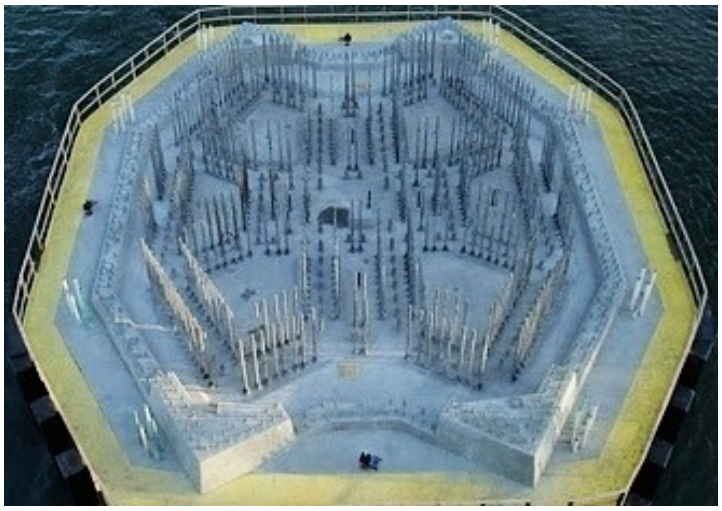

Fig. 3.15 – Tower base during construction *[Ref.: Mason Construction Ltd.].*

3.5. PIERS AND ANCHORAGES

3.5.1. E2 PIERS AND EAST ANCHORAGE

The east bent was named Pier E2 and consists of two reinforced concrete piers and a prestressed concrete cap beam. The steel box girders are supported on bearings and shear keys, which in turn are supported on the cap beam. The two piers are supported on pile caps and rise independently around 37m above the average sea level. On top they are linked by the cap beam (below the decks). These separate columns intended to support both the east and westbound decks [28].

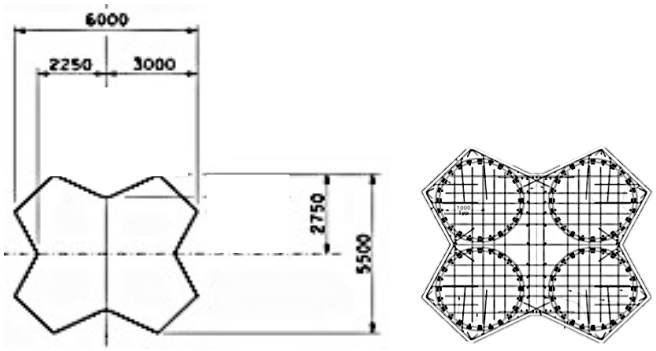

Fig. 3.16 - East pier cross section with dimensions (mm) and with rebar's detail (Ref.: *Caltrans)*.

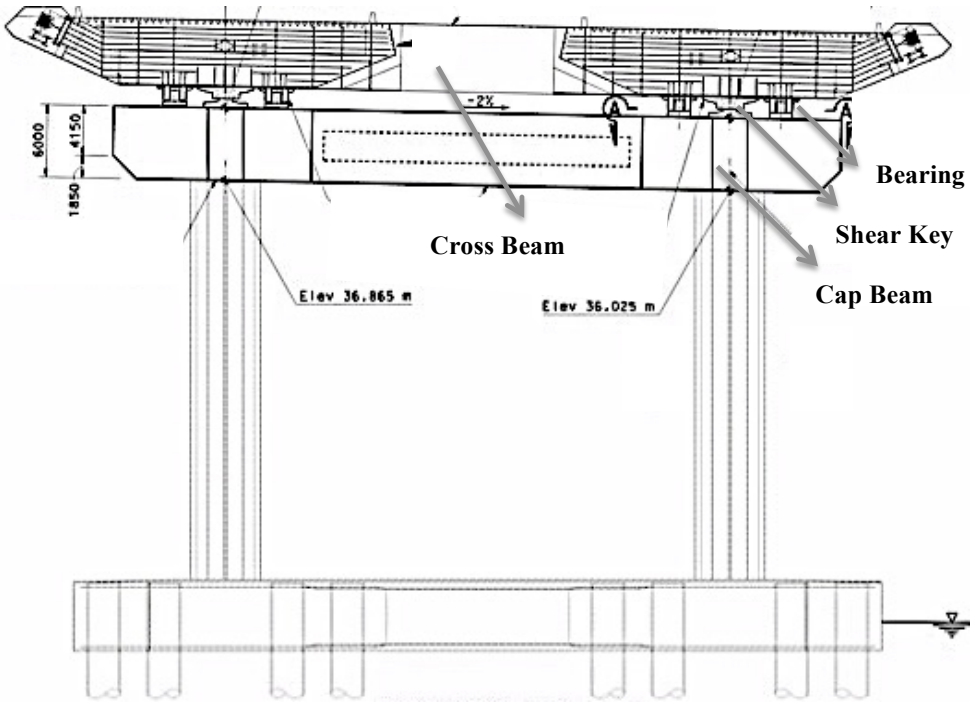

Fig. 3.17 - East pier transverse elevation with pile cap, piers, cap beam, double deck and deck anchorage [Ref.: *Caltrans]*.

The main cable anchorage on the east side is a deck anchorage where the main cable is splayed and anchored, for both deck girder. The 137 strands that comprise the main cable are separated individually as shown in Figure 3.18 and 3.19. The cables are splayed over 65 m. A portion of deck was added for westbound and eastbound on the outside of the deck box girders to create extra space for the cable splaying (Figure 3.19). Sockets and A354 BD anchor rods are used to fix each strand at their end (Fig. 3.20).

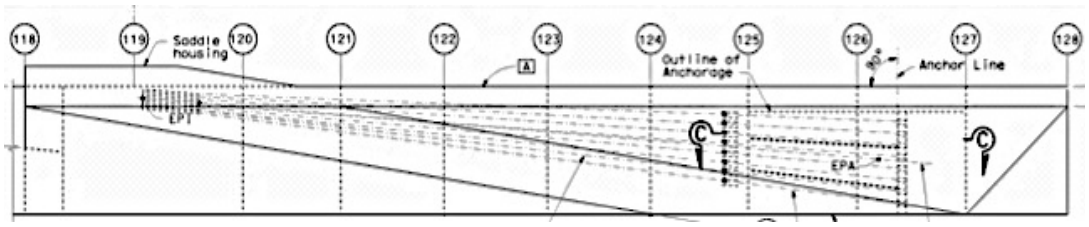

Fig. 3.18 – Side view of the east deck cable anchorage (Ref.: *Caltrans drawings 731/1204)*.

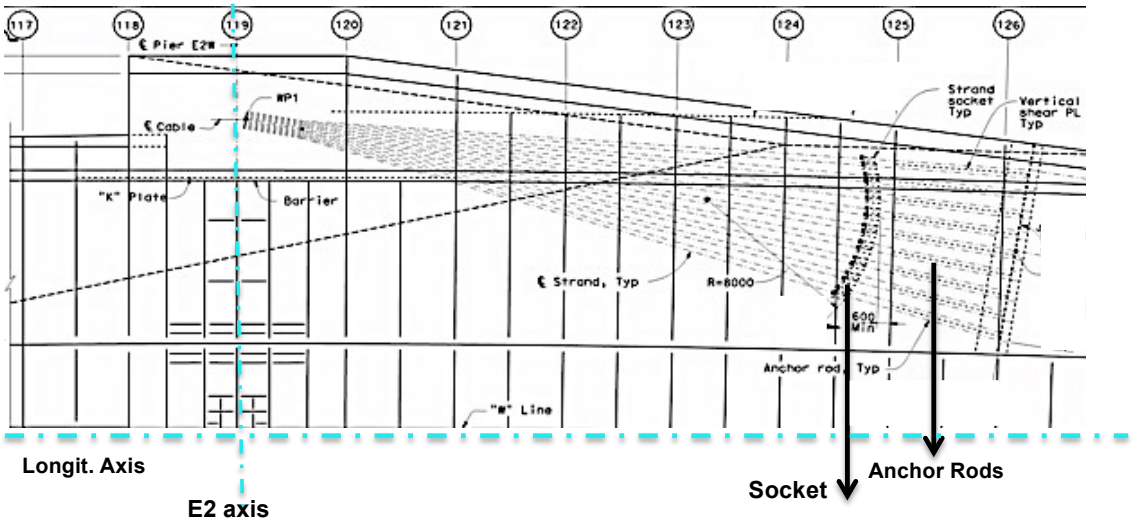

Fig. 3.19 – Plan view of the east deck cable anchorage (Ref.: *Caltrans drawings 734/1204)*.

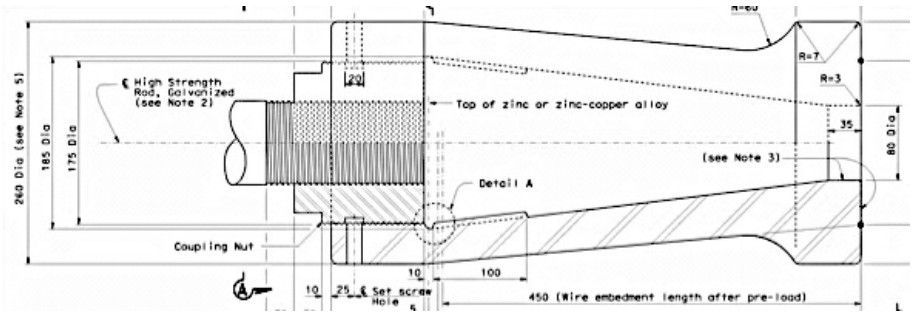

Fig. 3.20 – Socket details for east deck cable anchorage (Ref.: *Caltrans drawings 737/1204)*.

3.5.2. W2 PIERS AND WEST ANCHORAGE

Since the soil conditions require a deck anchorage for Pier E2, this implies that compression delivered to the deck box girders be countered by the west anchorage at the elevation of the main box girder centroid. Therefore, the main cables should be anchored on the deck as well, since the traditional ground-anchorage system is not used. After analyzing various possibilities for deck anchoring, the loop cable anchorage (Fig. 3.22) was considered the most structural efficient, reliable, compact and cost-effective alternative [8, 11]. The loop cable anchorage consists of several key structural elements: prestressed cap beam, multicolumn piers, loop anchorage cable and anchorage saddles, as well as an independent cable tie-down system.

This way, the west bent consists not only of two massive reinforced concrete piers; each one of them comprised of 4 separate columns connected by concrete closure walls, but also on all the aforementioned anchorage system elements. These piers are monolithically connected to the prestressed cap beam and contain the **tie-down system** to resist seismic uplift, which consists of 28

stay cables with 61 strands of 15mm each. The stay cables are anchored into rock through 4 additional CIDH 2,5m-diameter piles, but are not attached to the pier columns, so that these cables are kept from being damaged when the pier columns experience large lateral displacement, or even failure [7,8]. Uplift under seismic loads or pier failure under unexpected overloads, if not balanced, could lead to an unstable vertical load carrying system, which consequently will lead to collapse of the suspension span. The tie-down system is designed as a 'second line of defense' to address these concerns. Moreover, this tie-down system was design with a safety factor of two [15].

The longitudinal asymmetry of the bridge span causes a vertical uplift on piers W2, which is totally counterbalanced by the prestressed concrete cap beam. In fact, the **cap beam** has several structural functions: i) together with the deviation saddles and the jacking saddle, it anchors the main cable. The massive cable is then redistributed in the transverse, longitudinal and vertical directions through the cap beam; ii) as the most important "joint of the bridge", it connects the main cable, the W2 pier, the main span box girders, the west approach span hinges and the expansion joint; iii) serves as counterweight for the main span for design service loads. Furthermore, it has three types of prestressing tendons: longitudinal, transverse and vertical tendons (bars). Longitudinal tendons (parallel to bridge axis) are 'continuity tendons' connecting the main steel girders to cap beam. The transverse tendons (parallel to the cap beam axis) are designed to counter the moment induced by vertical load and the in-plane bending induced by the eccentricity between the cable force transverse thrust and the centroid of cap beam. Vertical tendons (bars) are used to resist local tension induced by actions such as bursting [8].

Since the east pier is on a flexible foundation (100-meter long piles), the overall structural stiffness (mainly in longitudinal direction) is dictated by that of the **west piers**. Also, vertical and lateral stiffness of W2 piers may affect the global response.

Indeed, the west anchorage piers can take almost 70% of the base shear in longitudinal direction in case of a seismic event. As mentioned earlier, this requirement is the result of the limited capacity of a flexible tower and a flexible foundation system on the east side.

The alternatives for the west piers' geometry were: i) single hollow rectangle with four corner columns; ii) a twin column and iii) a 4-column pier section. The last alternative was chosen for the following reasons:

- The lateral flexibility of the four-column piers increases the fundamental period of the bridge to more than 3,5 s;
- Reinforced concrete column has adequate vertical stiffness to limit the first vertical mode period to less than 0.1 s, which is different from the peak vertical response period of 0.15 s.

Additionally, two performance requirements were taken into consideration for the piers seismic design: i) minimal damage for a functional evaluation earthquake (FEE) and ii) repairable damage[3] for a safety evaluation earthquake (SEE).

For the **connectivity between the cap beam and the piers**, theoretically there can be 3 types: i) bearing connection; ii) monolithic connection (full moment transfer); iii) monolithic connection (partial moment transfer).

A 'pin' seems attractive, since it eliminates the bending moment transfer to the deck girder from the piers, however it proved to be difficult to achieve due to the large vertical force (dead and seismic

[3] Repairable damage: yielding of reinforcement, spalling of concrete or small permanent deformation.

loads). Also, 'pinned bearings' are undesirable for erection loading conditions (considering flexible tower and sliding bearing at east piers) and its condition would be questionable for the 150-year of the bridge's service life.

The idea of a partially fixed connection is to design a pier column section so that it works as the fixed joint during erection, service, and functional earthquake loads, and also works as a hinge (on top) when designed moment capacities are exceeded under SEEs. A concern about the partially fixed concept is that it will experience more frequent damage and will need more repairs than that of a fully fixed connection. The final design has the deck monolithically connected to the west anchorage pier W2 and supported on sliding bearings for service load conditions and effectively pinned for SEE earthquake loads at the east pier E2 [8].

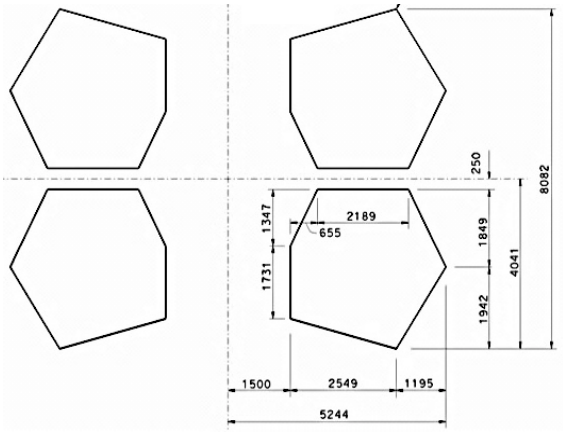

Fig. 3.21 – Cross section of the 4 separate columns for the west piers *(*Ref.: *Caltrans)*.

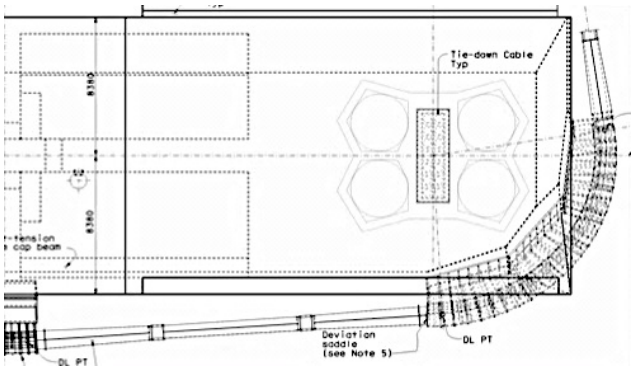

Fig. 3.22 – Half of Pier W2 plan view *(*Ref.: *Caltrans drawings 728/1204)*.

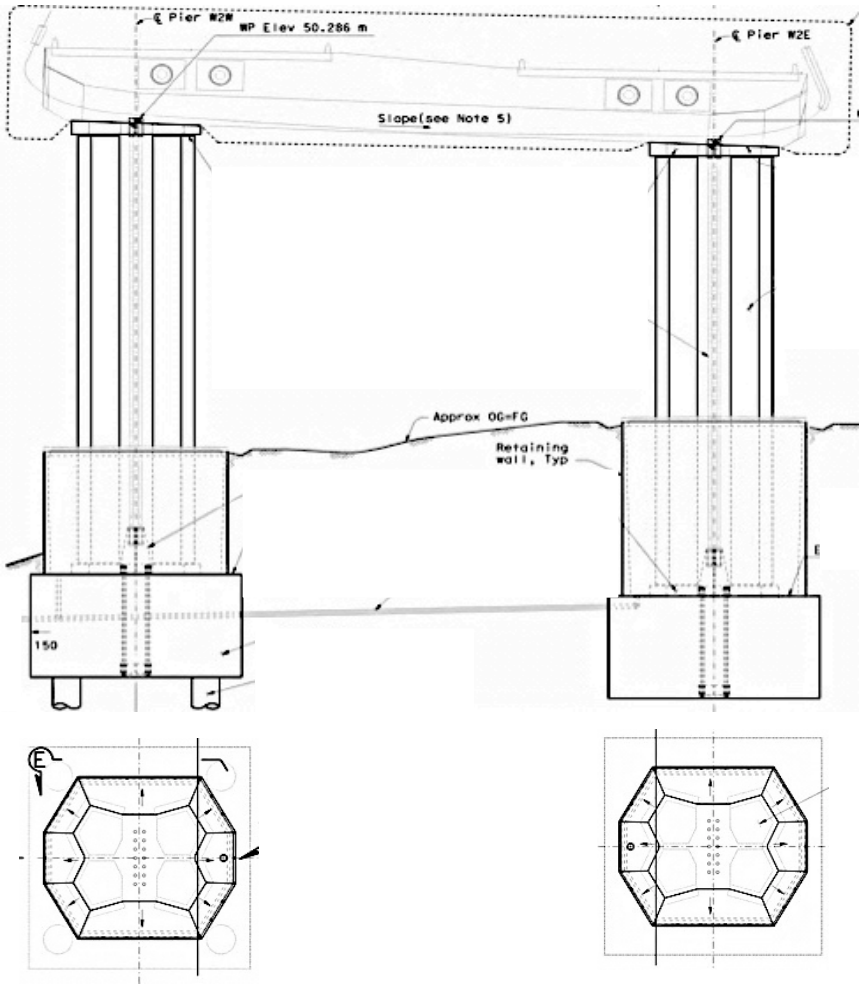

Fig. 3.23 – West transverse elevation with foundations, pier, cap beam and typical cross section *(*Ref.: *Caltrans)*

3.5.3. BEARINGS AND SHEAR KEYS

The **vertical bearing system** consists of the girder being supported only on bearings at the west and east piers and totally unsupported at the tower (no connection). The bearings and shear keys, which connect the box girder to the east bent are supported on the prestressed cap beam. The bearings are designed to support the vertical loads (with the capacity to resist lateral loads), whereas the shear keys are designed to resist all the lateral loads. Also, tie rods are provided to carry uplifts. The bearings are made of a spherical bushing assembly capable of relatively large rotations about the transverse axis of the bridge, thus providing an almost true pin connection [15].

Fig. 3.24 – Shear Key for the east pier connection, with anchor rods visible (*Ref.: SFGate, 2013*)

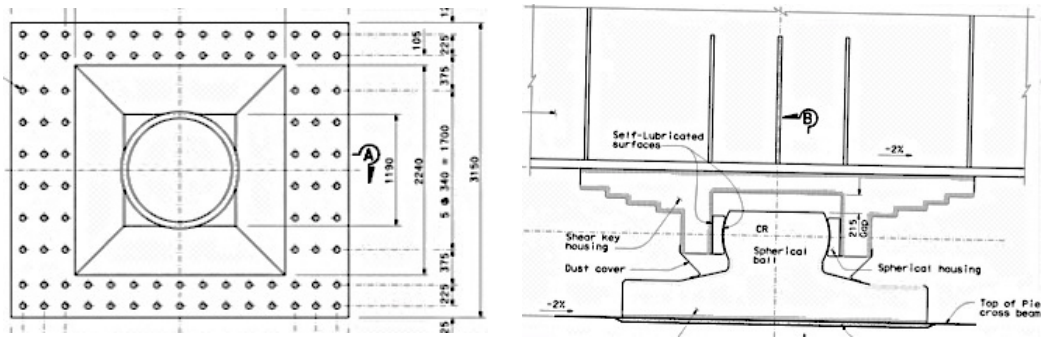

Fig. 3.25 – Plan and lateral view of shear key at Pier E2 *[*Ref.: *Caltrans drawings 888/1204].*

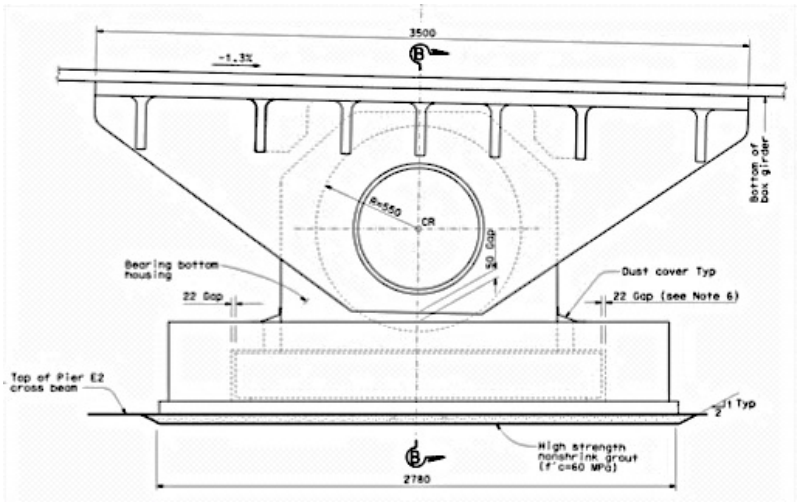

Fig. 3.26 – Lateral view of bearing at Pier E2 *[*Ref.: *Caltrans drawings 883/1204].*

3.6. SUPERSTRUCTURE

The superstructure consists of an orthotropic steel box girder double-deck connected by cross beams. There is no connection between the deck and the tower shafts. According to the design team, this self-anchored span will be the first worldwide to be constructed without this connection. As a matter of fact, the suspenders will be the only element providing connection between the box girder and the tower. The gap between the tower and the deck is designed to be sufficiently large to avoid impact during a SEE earthquake (safety evaluation earthquake). Moreover, the connections between the Self-anchored span and Skyway and also YB approach each have a hinge. These hinges allow the structure to move relative to each other in the longitudinal direction only. These hinges are steel beam pipes capable of transferring dead and live loads with elastic behavior and transmit design level seismic loadings by yielding, in order to protect major structural elements [15].

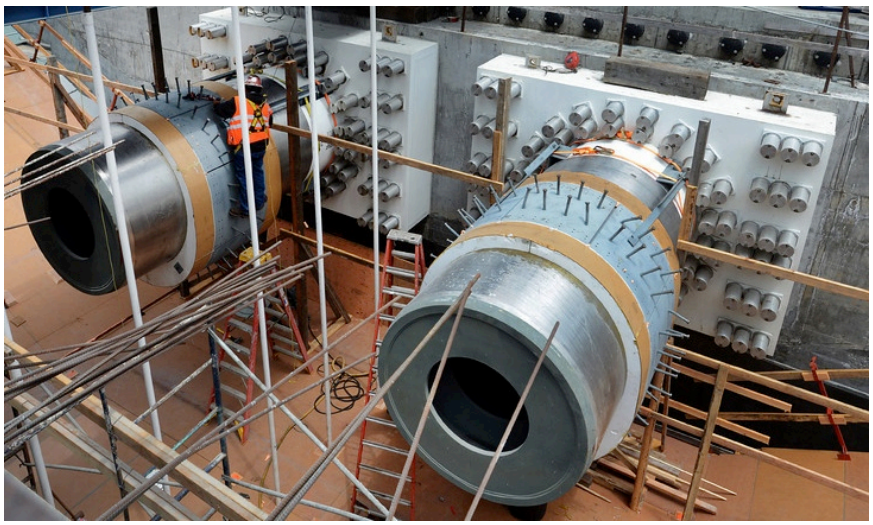

Fig. 3.27 – Hinge pipes for SAS-YB and SAS-Skyway connection (*Ref.: Mercury News, 2013*)

3.6.1. ELEVATION AND PLAN

The SAS bridge has asymmetrical spans; the main one with 385 m and the back span measuring 180 m. This makes the new Bay Bridge the world largest of its kind. In fact, the new Bridge project has been characterized by the design team as *one-of-a-kind Design* [15]. It is a single-tower project that elevates itself 160-meter above the average sea level and that has shear links spaced along its height. There is only one main cable that starts at the east piers anchorage, goes through the tower saddle and loops around the west bent. Due to its uniquely rare characteristics, the erection process of the bridge was opposite to conventional ground-anchorage suspension bridges, where the tower is the first element to be constructed. In this case, the deck was erected first and required falsework. In the end, this meant there was a needed to "build two bridges" [31]. It has an approximately 49m cantilever at the east anchorage and in order to balance moments around the E2 pier in the box girder, the suspenders do not support a 35m segment of the eastern end of the main span [15]. See Annex A3.3 for a complete scaled drawing of the elevation and plan of the SAS Bay Bridge.

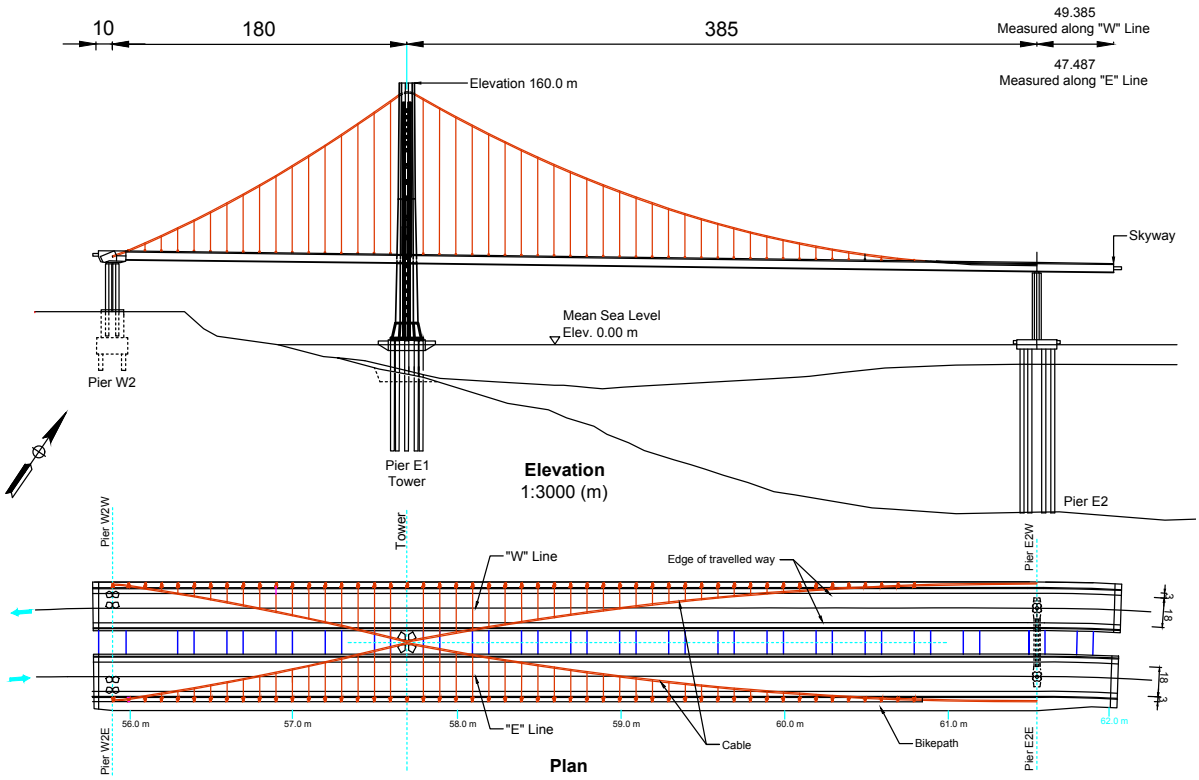

Fig. 3.28 – Elevation and plan of the Self-anchored span *(Ref.: AutoCAD made by the author)*.

3.6.2. DOUBLE-DECK

The superstructure consists of dual hollow ASTM Grade 50 orthotropic steel boxes (Fig. 3.29), with 5 lanes of traffic in each direction. See Annex A3.4 for detailed and scaled AutoCAD drawings of the deck. The deck consists of 14 segments in each direction (28 in total), which were lifted into place and welded to each other. These boxes are in compression (resisting the cable tension forces) and are part of the gravity load system. Diaphragms spaced at 5 m support the orthotropic deck and distribute the suspender loads to the box. The two separate box girders are connected to each other by crossbeams. It was recommended by the EDAP and MTC to include a pedestrian/bike path and a light rail (Fig. 3.29 and 3.30). The southern box girder ("E" line) has the bike path and this eccentric load is balanced by a counterweight on the other side [7, 9].

According to the Bridge Engineering Handbook, the new East span of San Francisco-Oakland Bay Bridge uses two separate orthotropic decks as superstructure, where each half is actually a separated superstructure, which is a solution based on the British Severn Bridge completed in 1966. The open-spaces, while strongly increasing the aero-elastic stability (flutter), reduce wind loading and has a grillage that allows lanes for emergency stop and maintenance vehicle traffic. The orthotropic deck is stiffened with close-ribs in the top of the deck and with open-ribs on the other sides [32].

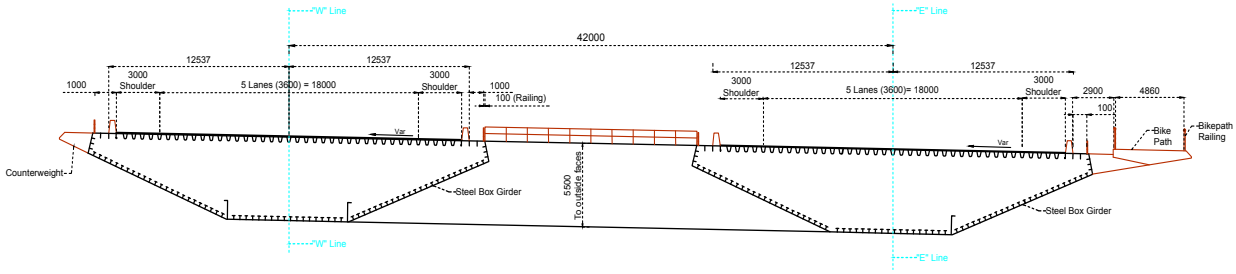

Fig. 3.29 – Typical Cross section of the deck *(Ref.: AutoCAD made by the author)*

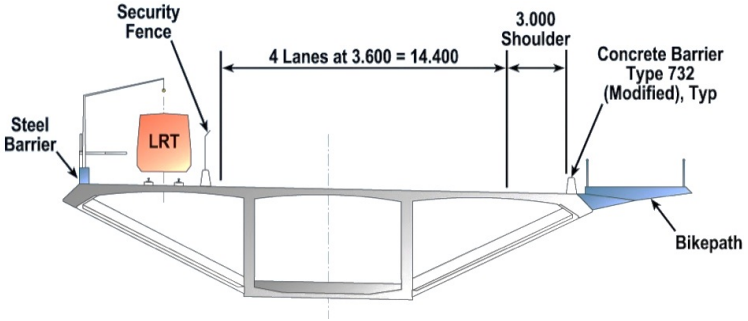

Fig. 3.30 – Typical Cross section of the Skyway's deck (Ref.: Caltrans presentation by Rafael Manzanarez, P.E. and Sajid Abbas, P.E.)

3.6.3. DETAILED CROSS SECTION

Each deck of the Self-anchored span is an orthotropic[4] steel girder. The choice for orthotropic box girder has been one of the most recurrent choices for suspension bridges. That is justified by the advantages it can bring: the deck plate is stiffened with longitudinal ribs, closed in this case and with great torsional resistance. Also, transverse floor beams (diaphragms) directly supporting live loads. Ribs are placed only on the inside face of the girder for aesthetics reasons and to minimize the corrosion [32]. Closed rib is torsionally stiff and is essentially a miniature box girder. It is apparent that a series of closed-ribs side by side is more efficient than a series of T-ribs.

As far as economy is concerned, this system becomes an alternative when lower mass, ductility, thinner/shallower sections or quick installation are important factors. The mass reduction achieved by using orthotropic decks was 18-25% for long-span suspension bridges. This is extremely important since dead load is responsible for 60-70% of the stresses in the cables and towers. Also, this way the bridge response to seismic event can be reduced (greater mass, greater the seismic forces). A good example is Golden Gate Bridge that had its concrete slab deck changed to an orthotropic deck in 1985 [32].

[4] Orthotropic: derivation of the word comes from two terms. The system of ribs and floor beams are orthogonal and their elastic properties are different or anisotropic with respect to the deck: thus orthogonal-anisotropic becomes orthotropic.

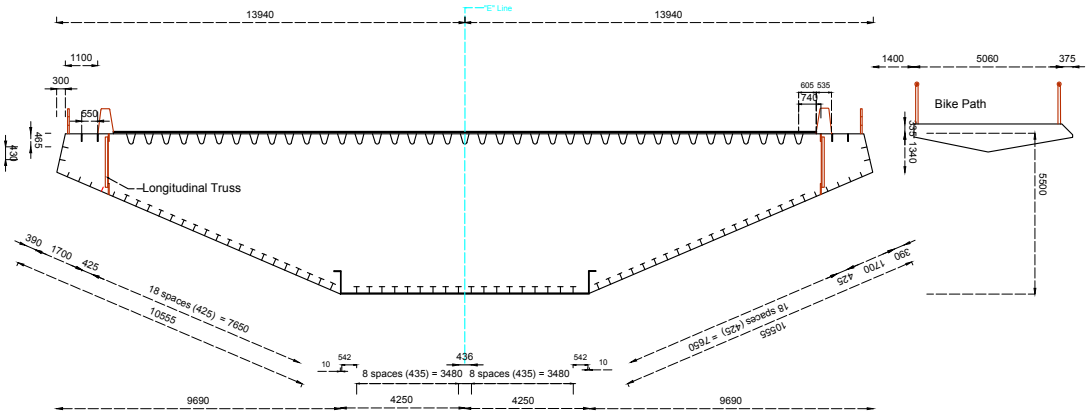

Fig. 3.31 – Typical Cross section of one deck (Ref.: AutoCAD made by the author, based on Caltrans' official project drawings).

These box girders have three different types of longitudinal ribs (Fig. 3.32): i) closed ribs; ii) structural tees; iii) flat plates. The ribs are used to stiffen the girder plates such that the yield strength of the girder section can be developed prior to local buckling of the plates. Also, inside the box girders there are floor beams spaced every 5m.The box girders are designed to remain elastic under a Safety Evaluation Earthquake (SEE) with a 1500-year return period [14].

For the new San Francisco-Oakland bay Bridge design, some relevant testing was done in order to validate the use of the steel orthotropic deck. These tests were performed at University of California, San Diego. The objective was to evaluate the *ultimate compression strength and post-buckling behavior* for the deck panels. A monotonic test procedure was used for top and bottom parts of the box girder, because the box girders were designed to remain elastic in a SEE event (cyclic testing intended to yield and dissipate energy). Figure 32 shows the reduced-scale specimens used in the testing, which represent portions of the top and bottom of a box girder. Since floor beams are spaced at 5m inside the deck, the girder can buckle longitudinally in S-shape. This way, 2 spans were used for each specimen to verify both positive and negative bending directions.

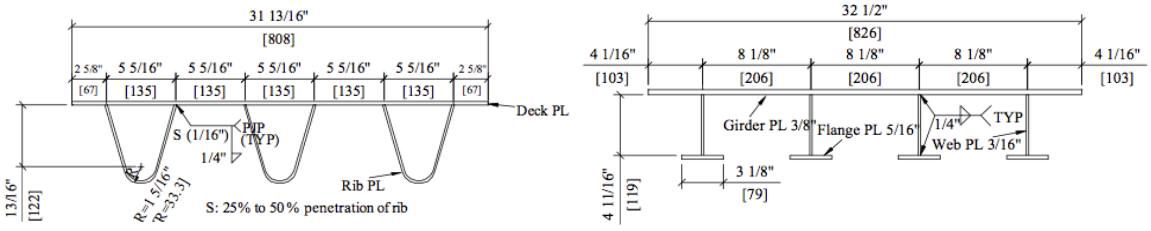

Fig. 3.32 – Reduced-scale specimens of the upper and lower deck, respectively *[15]*.

Both models *reached yielding before local buckling of the plate occurred* and reached a *compression capacity greater than the one expected in a SEE event.* A finite element analysis was made using ABAQUS and the numerical simulation showed the residual stresses influence more the ultimate strength and post-buckling behavior than the geometric imperfections (both effects considered in the FE analysis) [14].

3.6.4. CROSS BEAMS AND FLOOORBEAMS

These elements make the connection between the double-deck (two box girders). Their dimensions are 10m (wide) x 5,5m (deep) with 30-meter spacing between adjacent crossbeams. The purpose of these connectors is to carry the transverse loads between the suspenders, which are connected to the exterior sides of the box girders and are spaced at 10m. Also, the crossbeams ensure that the box girders act together under wind and seismic loads.

On Fig. 3.28, the cross beams are visible (plan view of SAS span). Also, Fig. 3.29 (typical cross section of superstructure) shows the dimensions of these connecting beams.

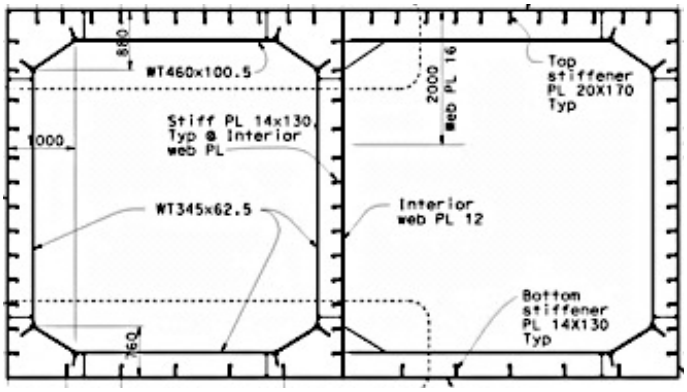

Fig. 3.33 – Typical crossbeam section (Ref.: Caltrans drawings 656/1204).

Furthermore, there are *floorbeams* (transverse and longitudinal diaphragms) along the length of the deck. They consist of plates with vertical and horizontal stiffeners and their characteristics vary along the length.

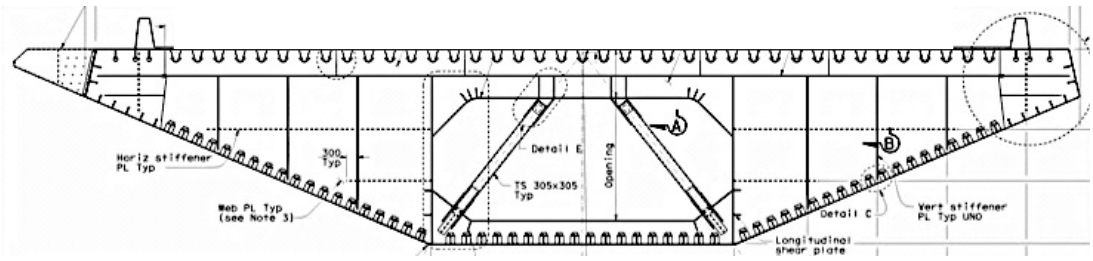

Fig. 3.34 – Typical floorbeam section (Ref.: Caltrans drawings 646/1204).

3.7. MAIN TOWER

There is only one tower, contrary to other conventional self or ground-anchored suspension bridges, which have two towers. The tower rises to a height of 160m and is the most unique design element. It is composed of four shafts interconnected by shear links along its elevation. At its bottom the tower is fixed to a 6,5-meter deep pile cap. At the top the tower is fixed to the saddle grillage. These top and bottom rigid connections imply that the tower is not the primary element resisting the box girder's lateral seismic loads. In fact, the tower seismic response is mainly governed by its own mass and stiffness. Also, as the asymmetry of the spans causes a vertical uplift in pier W2 (as discussed before)

and the bridge is not monolithically connected at pier E2, the main tower is supporting most of the bridge dead load [15]. It has horizontal diaphragm plates along its height, in order to improve its buckling resistance (Fig. 3.35).

The design of the tower in a suspension bridge is very important because, for instance, the total cost can be increased (significantly) by a conceptual design that is difficult to erect. Moreover, its most critical section is the tower-foundation connection, where both shear force and bending moment are maximum (see subchapter 3.4.3). Fasteners must be proportioned to transfer the loads between tower and the foundations and they must be deeply embedded in the concrete footing [33].

See Annex A3.5 for detailed and scaled AutoCAD drawings of the Tower.

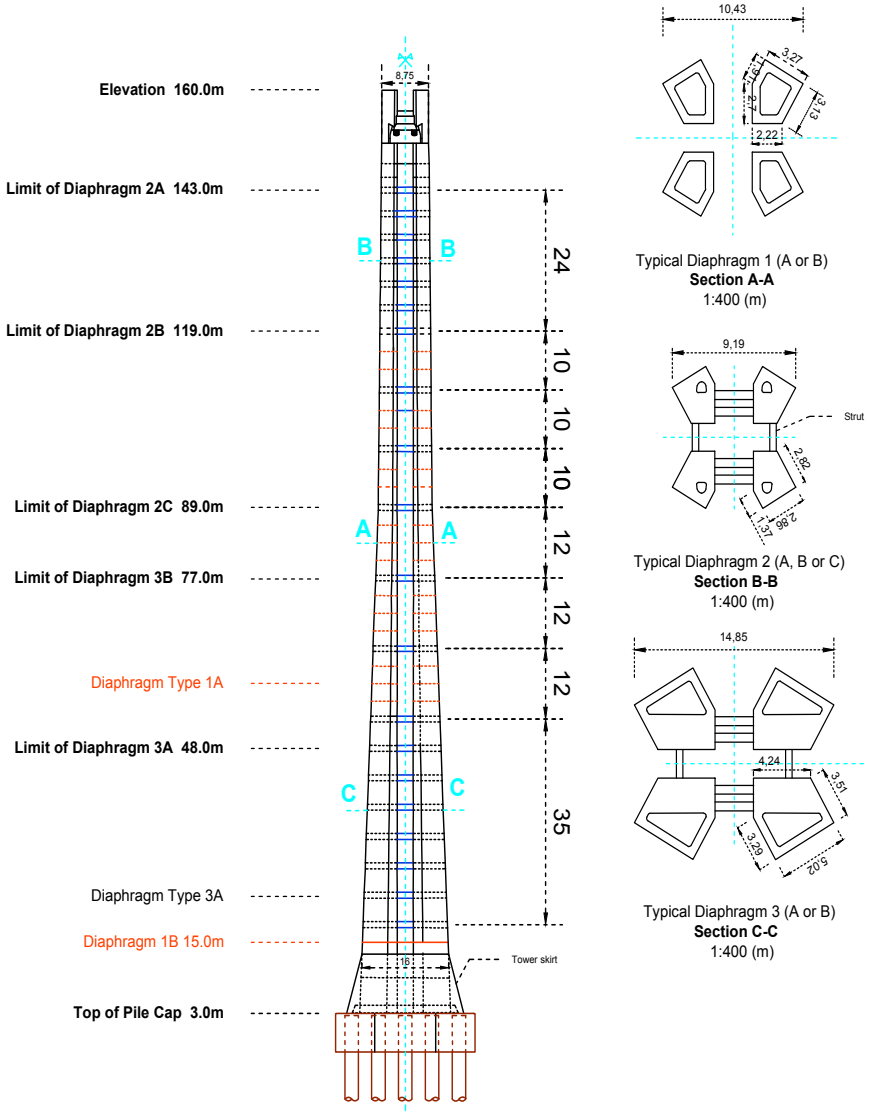

Fig. 3.35 – Tower longitudinal elevation and typical diaphragm sections (Ref.: AutoCAD made by the author).

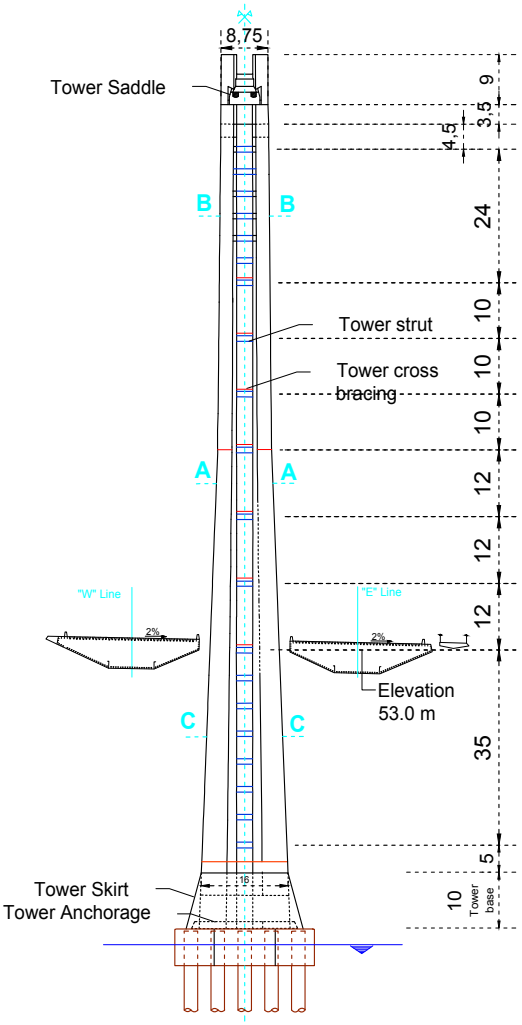

Fig. 3.36 – Tower transverse elevation (Ref.: AutoCAD made by the author).

3.7.1. SHAFTS AND SHEAR LINKS

The four shafts that constitute the main tower use box members made of tapered stiffened steel (ASTM A709 Grade 50). Its cross section reduces from bottom to top of the tower. These shafts are vertically stiffened pentagonal steel box sections and are provided with horizontal diaphragms, whose spacing and section can be observed on Figure 3.35 [9]. They are designed following ATC-32[5], which ensures that they remain elastic, but that can suffer large inelastic compressive strains without buckling. The shafts are expected to remain elastic during a SEE (safety evaluation earthquake). When shaft sections are stacked on top of each other, they are bolted together using splice plates. There are cross bracings along the height of the tower connecting the shafts (Fig. 3.36). They have X-shape in the plan view (Fig. 3.38).

[5] ATC-32: Improved Seismic Design Criteria for California Bridges: Provisional Recommendations (1996). See Chapter 37, Bridge Engineering Handbook, 2000.

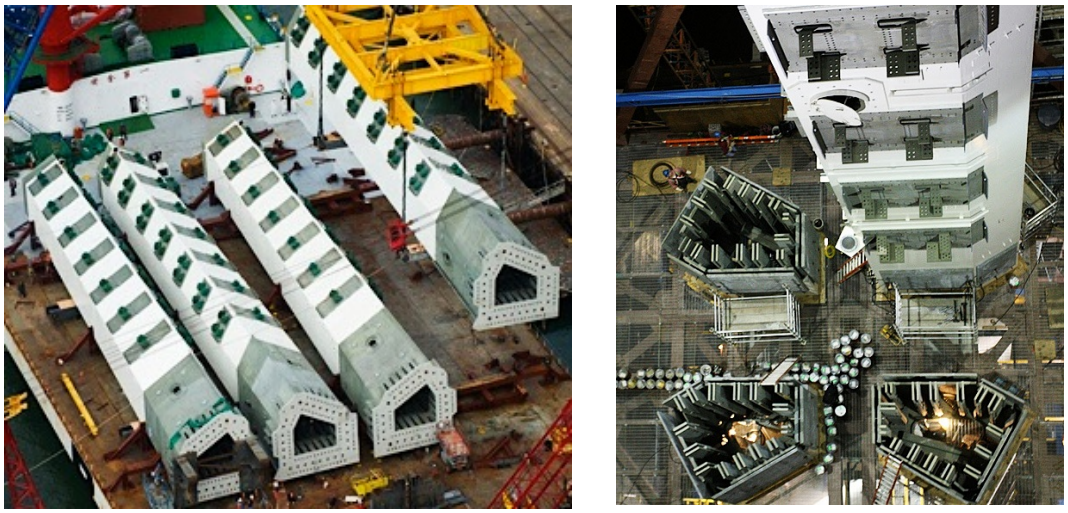

Fig. 3.37 – Shaft segments with shear link connections visible (*Ref.: bay Crossings 2010; www.mtc.ca.gov, 2011*).

Furthermore, the four shafts are interconnected with replaceable shear links both in longitudinal and transverse directions (Figure 3.35 and 3.36). According to the design team, the shear links are designed to deform inelastically, in order to protect the tower shafts from damage during a SEE. There are three different types of shear links along the tower's height, as shown on Figure 3.38.

These links were designed to:

- give the tower proper stiffness to resist service loads;

- remain almost elastic during a FEE (functional evaluation earthquake);

- yield and create plastic shear hinges during a SEE (safety evaluation earthquake) and consequently dissipating energy and protecting the tower shafts from damage with maximum and ultimate rotation demand of 0,04 and 0,09 radians, respectively;

- to be replaced after a SEE, if needed.

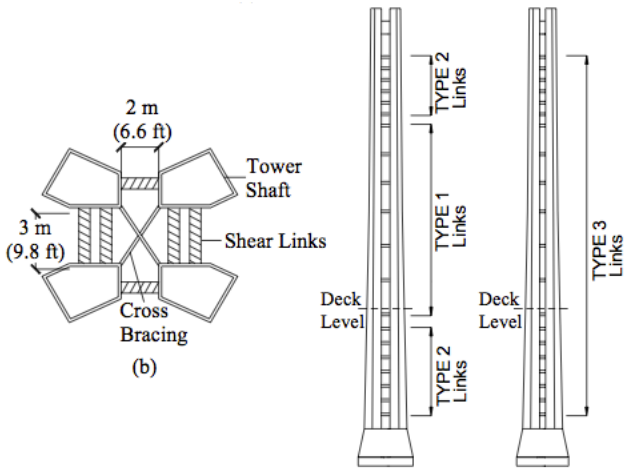

Fig. 3.38 – Cross section, transverse and longitudinal tower elevation, respectively [14].

To satisfy the abovementioned parameters, designers evaluated various configurations for the tower, such as strength/stiffness of shear links and their location. For that, they performed static pushover analysis and determined the optimal layout of these shear links, for a certain response of the tower to service loads, wind loads and FEE and SEE loads. Figure 39 shows the results of a typical pushover analysis and the advantages on the use of these links (reduces both displacements and base shear).

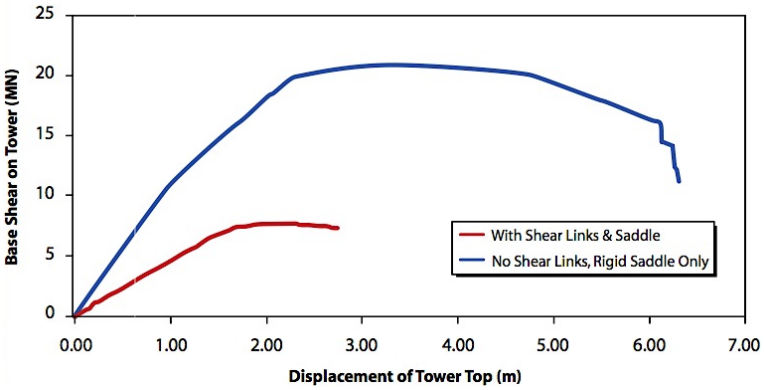

Fig. 3.39 – Typical Pushover Analysis results (top load) [15].

Additionally, University of California San Diego performed full-scale tests of 2 built-up shear links with the following goals: i) evaluate the cyclic force and deformation characteristics of the full-scale links and ii) evaluate the cyclic overstrength of the links, that is needed for the capacity design of the towers and link connection to the tower shafts. The two tested samples were a Type 1 transverse link and a Type 3 longitudinal link (Figure 3.40 and 3.41). The built-up shear links had a "deformable region" in the middle and a "connection region" on the extremities. The plates on the deformable region were A709 Grade 50 with real yield strength not exceeding 379 MPa, so that the ultimate shear force in the links did no exceed the design capacity of the connection regions (This was one of the SFOBB design specifications, established by the design team). Moreover, the links were designed according to AISC Seismic provisions, which means their length was less than 1,6 Mp/Vp (Vp nominal shear strength and Mp nominal plastic flexural strength). This way, shear behavior dominates the response. To delay buckling of the shear links' web, there were added vertical stiffeners in the middle region. After a quasi-static cyclic displacement-controlled loading, cracks were clearly visible at the ends of the vertical fillet welds connecting the intermediate stiffeners to the link web. As the lateral displacement increased, those cracks propagated into the web creating a brittle fracture of the web [14].

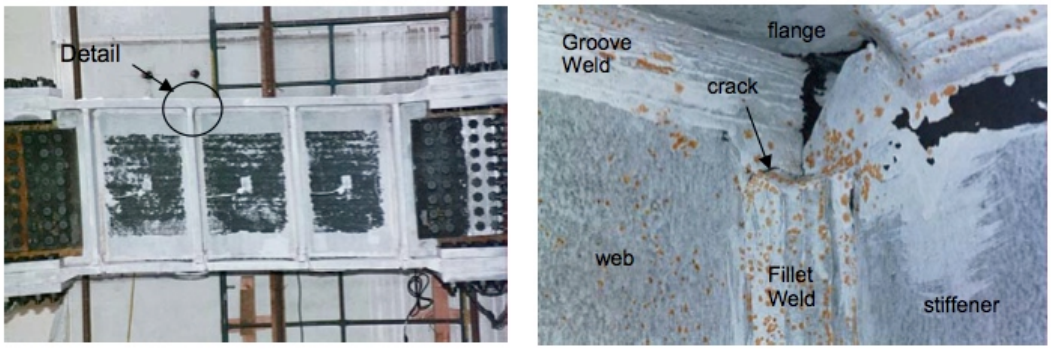

Fig. 3.40 – Type 1 (transverse) link deformation and detail on weld crack after a 345mm displacement [14].

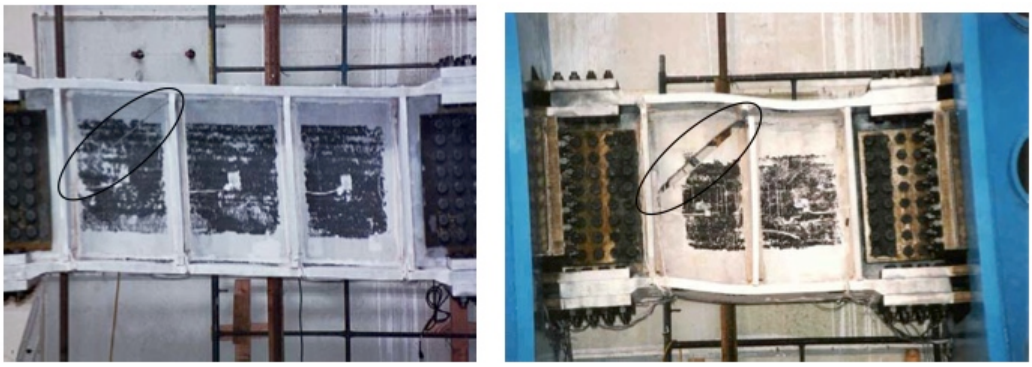

Fig. 3.41 – Type 1 (transverse) and 3 (longitudinal) links respectively, with brittle fracture visible [14].

Figure 3.42 shows the relationship between shear force and average shear deformation (deformable region). The inelastic rotation reached 0.06 and 0.066 radians for Type 1 and 3, respectively. On the connection region the shear deformation was low with the response remaining always elastic. The overstrength factor for both specimens was calculated with the quotient between maximum and plastic shear strength (based on the measured yield strength of the web material). They were 1.83 and 1.94 for type 1 and 3, with 1.25 being the overstrength value recommended by the AISC (non-conservative).

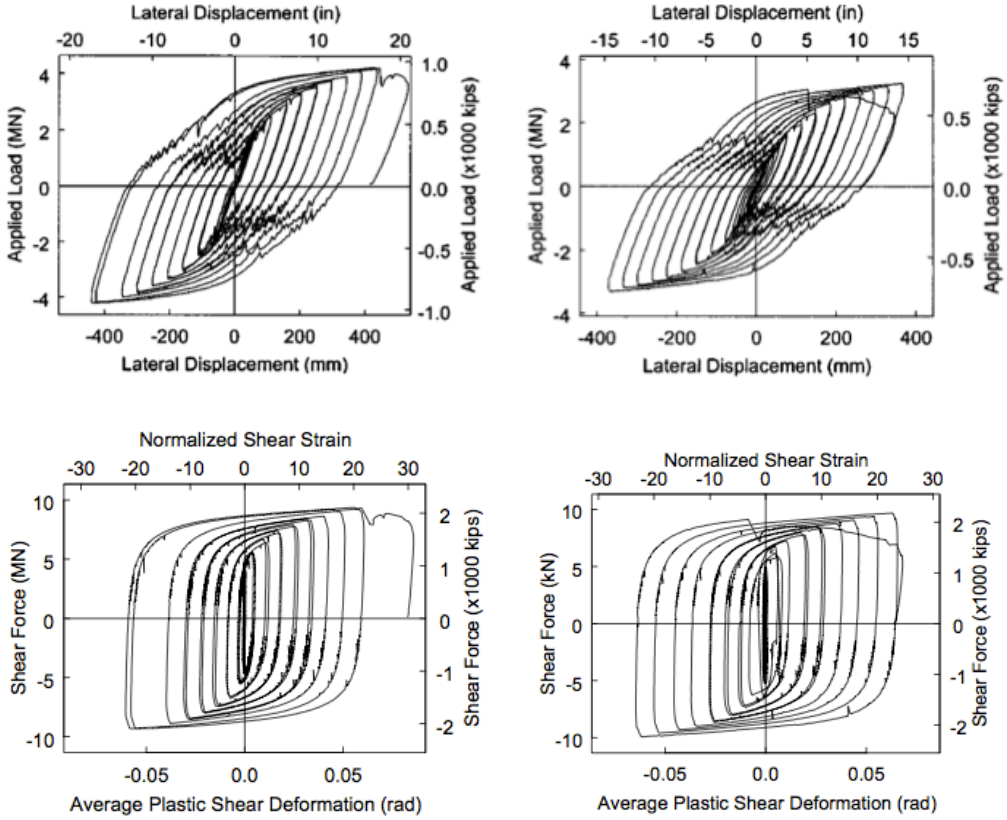

Fig. 3.42 – Type 1 (transverse) and 3 (longitudinal) graphs, respectively [14].

The brittle fracture failure that occurred in this large-sized links had not been reported previously. This testing showed that the specimens were able to reach inelastic rotation more than twice what would be produced in a SEE. Nevertheless, brittle fracture occurs before inelastic design rotation capacity

required by the AISC Seismic Provisions is developed. The fracture occurred at the ends of the vertical welds of the intermediate stiffeners, near the highly restrained location (see Figure 3.41). To mitigate the cracking at the fillet welds, it was suggested that the fillet welds be terminated further from the web-flange-stiffener intersection. Therefore, by augmenting the distance *c* to about 5 times the web thickness the results showed that stress and effective plastic strain were reduced significantly. With the welding changes proposed above, it would be possible to avoid brittle fracture in future tests. This recommendation was used on the link fabrication for links on SFOBB, which were tested at University of Nevada, Reno [14].

3.7.2. TOWER SADDLE

The tower shafts are fixed at the top to a saddle grillage. The grillage weights 456 tons. It measures 30x30ft (9,15m approximately) and 15ft (4,6m) of height. It is the largest for a suspension bridge.

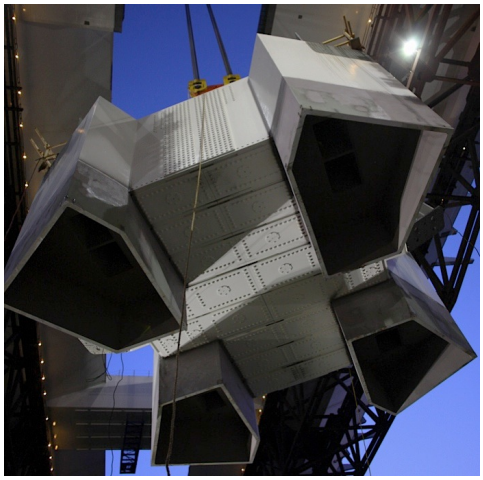

Fig. 3.43 – Saddle grillage being lifted to the top of the tower (*Ref.: www.baybridgeinfo.org*).

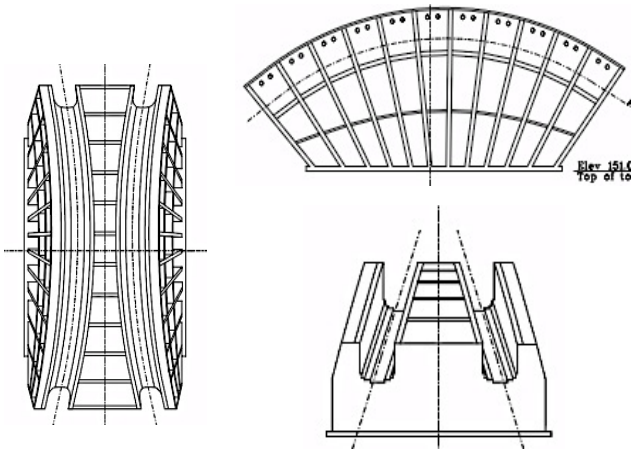

Fig. 3.44 – Plan, longitudinal and lateral views of the tower saddle (*Ref.: Caltrans)*.

3.8. CABLE

The unique configuration of this bridge and the 150-year requirement for design service life required that some special considerations be given to the main cable design. Therefore, the main cable was designed as a continuous cable with a 3-dimensionally geometric profile in space. It consists of 137 strands, each strand having 127 wires. For the process of lifting the superstructure off the falsework and activating the cable, each strand was individually anchored within the deck itself at the east flanking pier E2. The main cable passed through the top supported by a twin-trough tower saddle, looped around the cap beam (two deviation saddles and a jacking saddle) at pier W2 and returned to the other side of the east pier to be anchored on the deck again. The choice for a looped cable anchorage on the west bent was discussed on chapter 3.5.2.

3.8.1. MAIN CABLE

The 0,78m- diameter main cable is composed of 137x127 wires, in total 17399 high strength 5,4mm-diameter galvanized parallel wires. The specified minimum wire strength for the cable wire is 1,800 MPa. The total weight of the cable is approximately 5291 tons.

The tower saddle trough faces nearly upward, while the west and east deviation saddles trough face sideway. That causes the cable to twist nearly 100°. This will be an almost certain consequence if a conventional hexagon cable strand layout is adopted for this cable design. The twist of about 100º could cause tangling of strands during cable construction. In this case, it was adopted a modified octagon strand layout was adopted to alleviate the problems derived from cable twist between Tower saddle and the West saddle [11]. The modified octagon strand layout basically means the cable strands are symmetrical about both principal axes of the saddle trough. This innovative strand layout essentially eliminates the twist of the main cable by cutting 90° off the total twist.

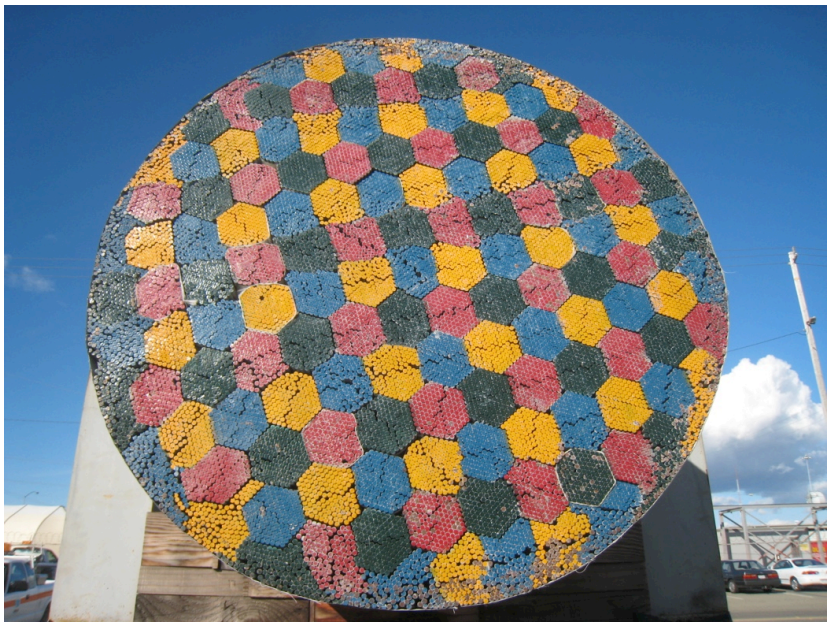

Fig. 3.45 – Final section of the main cable after compaction *(Ref.: Diana Tsuizaki photography, 2012)*

For the Cable Construction Method, two construction methods were taken into consideration: AS and PWS (aerial-spun method and prefabricated parallel wire strand methods, respectively).

Table 3.1 – Comparison between two cable construction methods [11].

Characteristic	PWS	AS
Quality of cable	No wire splice	Wire splice required
	Less crossing of wires	Crossing of wires probable
	Small void ratio (17-18%)	Slightly higher void ratio (20-23%)
	Superior uniformity	High wire stress concentration at strand shoe
Erection	Shorter erection period	Longer erection period
	Less vulnerable to weather	Vulnerable to weather
	Larger anchorage size when conventional anchorage is used	Smaller anchorage size when conventional anchorage is used
Economy	Higher base material cost	Lower base material cost
	-	More erection labor and equipment cost

The main difference between AS and PSW methods is that in the aerial spun method (AS) the cable is built by pulling single wires across individually, in situ, while in prefabricated parallel wire strand method (PWS) the cable is constructed by strands or bundles of wires prefabricated to the correct length.

The prefabricated parallel wire strands method was the preferred one, considering that the strands are better fabricated and that is eases and fastens the construction and makes it faster for the 3D cable geometry of this bridge.

As far as corrosion of the cable is concerned, it is known that corrosion can compromise safety, since corrosion reduces the effective cable area and thus the strength of the cable. So, for the cable Corrosion Protection System four methods more or less common around the world for parallel wire cables of suspension bridges were used [11]: i) painted-wire wrapping (very much used); ii) composite cover (no general acceptance); iii) S-wire wrapping and iv) cable dehumidification systems (both used for the past two decades).

The first system (painted-wire) consists of soft annealed wire wrapping over a corrosion protection paste/coating and a top paint coating. This wire wrapping has usually a 3.5mm diameter and is wrapped under an approximately 150 MPa tension stress by means of a wrapping machine moving along the cable. The aim of this system, as many others, is to minimize moisture penetration into the cable. The composite cover system has successive layers of material (elastomeric neoprene wraps and acrylic resin coatings). The elastomeric neoprene wraps were used on Rainbow Bridge (1994) in Japan. It is highly laborious so it has not been widely used in suspension bridges. The S-wire wrapping consists of a “flat” interlocking wire for the outer wrapping of the cable. This interlocking mechanism minimizes gaps and therefore paint coatings applied to it crack less often than coatings applied to round wrapping wire under similar load/temperature changes. The cable dehumidification system aims to solve the moisture penetration problem during construction (for instance) before wrapping. It consists on blowing dry air into the void spaces on the assembled main cable. It should be highlighted

that S-wire wrapping and cable dehumidification measures could be applied independently and separately.

For the Bay bridge design, it was recommended by the design team that the multi-layer corrosion systems all be used, which were:

- Zinc galvanization of each steel wire;

- Grease application to each individual cable wire during PWS;

- A paste composed of a blend of zinc oxide with zinc dust and a non-dry thermoplastic polymer base;

- S-wire wrapping;

- Elastic noxide primer and paint;

- Dehumidification of the cable sections at locations of the east anchorage, west loop cable anchorage, and tower saddle.

3.8.2. HANGERS

The hangers for the main cable are spaced at approximately 10m from each other. These are inclined due to the 3D geometry of the main cable, which starts at the tower saddle and opens until it reaches the external side of the deck.

One of the main construction phases was the load transfer from the temporary supports to the cable, making the bridge self-supported and self-anchored. After the main cable and 200 suspender ropes where in place, the operation began with hydraulic jacks to gradually tension the 200 suspenders that connect the main cable to the deck. As soon as 104 suspender ropes where tensioned the temporary supports were no longer needed. The tensioning of the suspenders caused the main cable to move down 4,88m and out 9m. Also, the deck uplift from the temporary supports was around 0,5m. Also, the jacking saddle at the west looping anchorage was used to maintain balance [28].

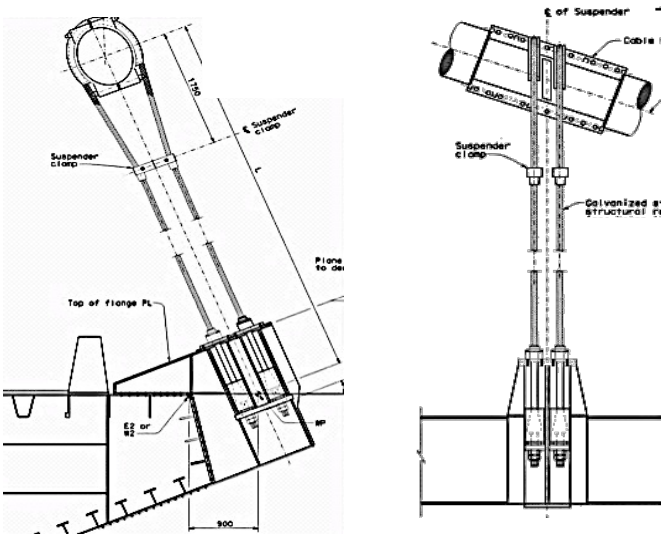

Fig. 3.46 – Transverse and longitudinal Suspenders detail [*Ref.: Caltrans official project drawings 742/1204].*

3.9. SEISMIC DESIGN CRITERIA, ANALYSIS AND RESPONSE

The bridge was designed as a limited-ductility structure: i) clearly defined plastic mechanism sequence for response to lateral loads; ii) inelastic behavior limited to tower shear links, piers and piles and iii) detailing and proportioning requirements for full-ductility structures were met.

In 1997, the EDAP and MTC[6] Bay Bridge Design Task Force made 17 recommendations for the bridge design, such that two cable-supported design alternatives are taken to 30 percent design completion before a final selection is made, the possibility of incorporating a bicycle and pedestrian path, provide post-earthquake "lifeline" service, 10 traffic lanes (five in each direction), accommodate the possibility of future light rail service, no double deck (either parallel separated decks or a single deck on the cable-supported span), the cable or suspension tower on the eastern bridge should not be taller than the suspension towers on the existing western span, or minimum horizontal clearance of 152 m and vertical clearance above mean sea level of 42 m [9].

For the **seismic analysis**, three methodologies were used: i) time history analysis (global model); ii) push-over analysis and iii) local detailed analysis. As discussed before, since the different foundations of the bridge have different soil conditions and ground motions, time history analysis was the main methodology. It allowed applying different time histories of ground displacement at the supports. Time history analysis was done as the restart analysis from the dead load deformed state. Pushover analysis was primarily used to evaluate ductility of critical elements and to establish failure mode sequence. Local detailed analysis was used to establish local strain/stress demands and to evaluate the modeling used for the global model. A large displacement analysis and the use of nonlinear material where necessary, in order to capture the true behavior of the bridge (geometric stiffness of bridge, P-delta effects, slacking of suspenders, plastic hinging of piers, tower shear links, etc.).

The **response** of the structure, since it has limited-ductility, has clearly defined and predetermined plastic hinging formation (Figure 3.47). The bridge structure is supposed to remain mostly elastic, with exception of east and west piers and tower shear links. For the piers, the plastic strain is 2/3 of the Mander equation for confined concrete columns. For the shear links, they are expected to yield with a SEE earthquake and also their maximum rotation demand is 0.03 radians compared with an ultimate rotation of 0.09 radians. The piles were designed to sustain minimal damage (strains less than 0.01% for concrete and 0.02% for steel) when subjected to the SEE displacement demands. The cable tie down at the west pier was designed with a factor of safety of two. The bridge is a long period structure and is mainly in the region of constant displacement demand. This improves the reliability of the structural response [7].

[6] Metropolitan Transportation Commission is a regional government agency that provides regional transportation planning and coordination of transportation activities for the Bay Area. It had an important role on the East Bay Bridge project, specifically on the signature span. It organized the Bay Bridge Design Task Force to consider replacement bridge alternatives. Afterwards, this Task Force formed EDAP to advise them on cost, engineering feasibility, and seismic safety among other issues.

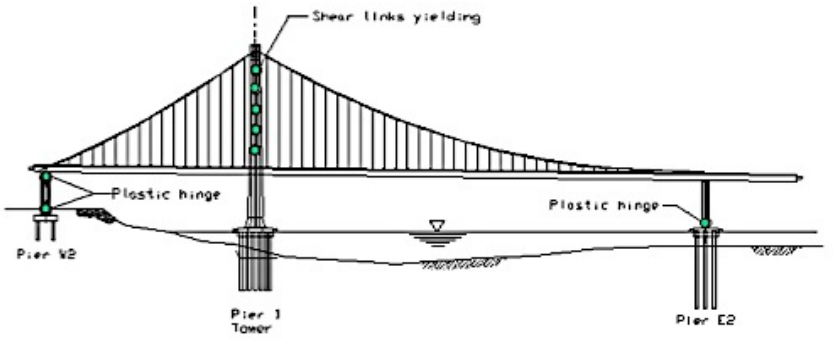

Fig. 3.47 – Elevation of the bridge, with plastic hinges marked [7].

3.10. ERECTION METHOD OF SELF-ANCHORED SPAN

As referred before, the erection of a self-anchored suspension is different from a ground-anchored suspension bridge. The East Bay Bridge span is an even more particular case with a single-tower and asymmetric spans, which requires a special construction strategy. Not only the deck segments cannot be hanged from the main cable (traditional ground-anchored), but also it has to be anchored on the deck itself. This way, the deck roadways and tower have to be built first [28; 41]. The Piers W2 and E2 are set into place previously to the steel deck. This support structure is afterwards removed and the loads transferred to the cables. Due to this erection method, it can be adequately assumed in modeling for Gravity analysis that Dead load is applied instantaneously.

1 Foundations

Fig. 3.48 – SAS span and skyway foundations, respectively *[Ref.:* http://www.pbase.com/donphotos/new_bay_bridge*]*

2 Erection of Piers E2 and W2

Fig. 3.49 – Pier E2 and W2 erection, respectively *[Ref.:* http://en.wikipedia.org*]*

3 Construct temporary supports (framework)

Fig. 3.50 – Falsework *[Ref.:* http://en.wikipedia.org*]*

4 Erect Deck Segments

Fig. 3.51 – Crane barge lifting steel orthotropic deck segment *[Ref.:* mtc.ca.gov*]*

5 Tower shafts lifting

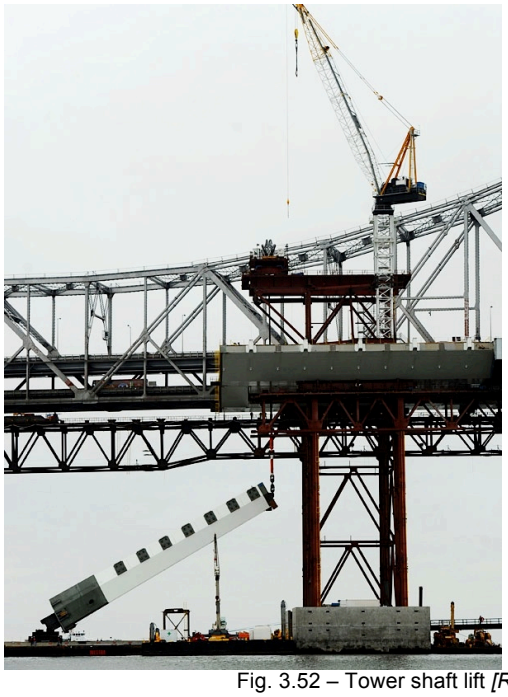

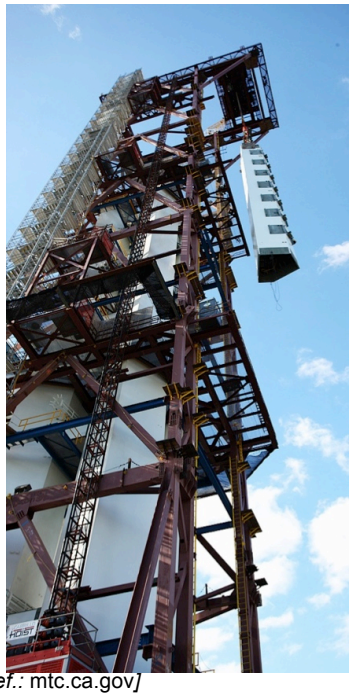

Fig. 3.52 – Tower shaft lift *[Ref.:* mtc.ca.gov*]*

6	Main cable assembly and compaction	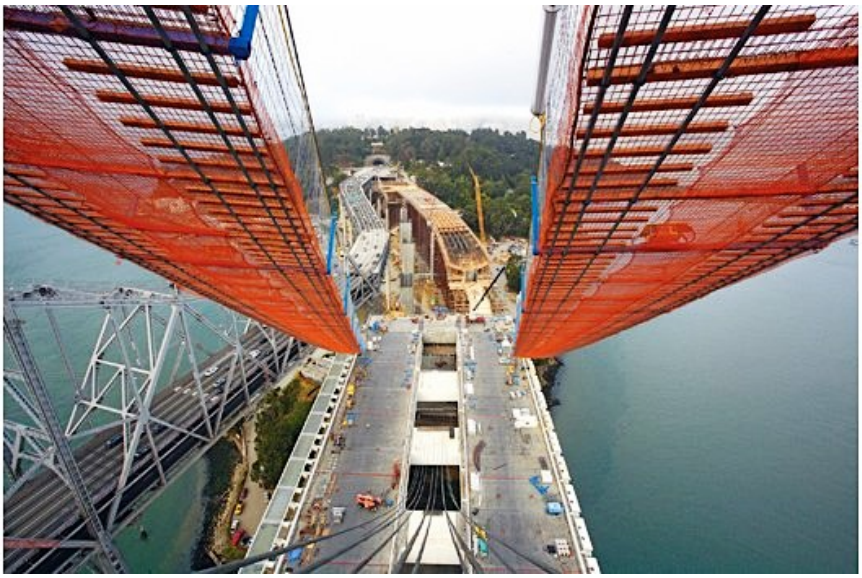 Fig. 3.53 – Aerial view with catwalk for cable strands assembly and steel strands pulling the tower to the West side *[Ref.:* popsci.com*]*
7	Suspender ropes and Load transfer	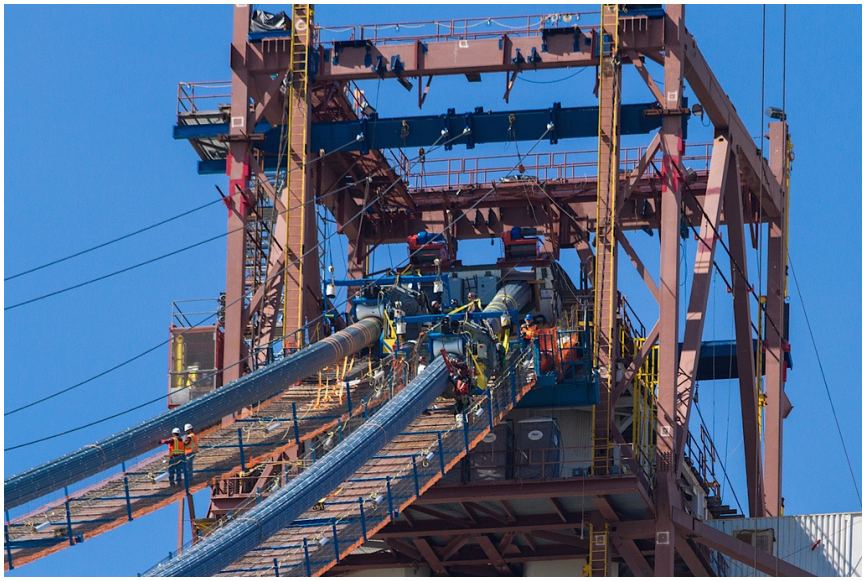 Fig. 3.54 – Top of the tower with main cable strands assembled *[Ref.:* mtc.ca.gov*]*

However, it is necessary a temporary support structure to hold the deck while it is being assembled, which is basically a 20000 ton steel falsework structure. Fig. 3.50 shows the framework in place. Both roadways are comprised of 14 segments (560-1700 ton each) and connected by 19 crossbeams. The lifting was done by means of a 400x100 ft barge equipped with a 1900 ton shear leg crane (1929 ton maximum lift weight). The crane barge was custom made for this project and it's the largest on the West Coast. The west side span had its deck sections lifted onto a cradle on the temporary support that slowly carries the section into place, because the water level is not deep enough for the barge.

For the tower construction, the leg sections were floated on barges to the open east side and erected one at a time. Each one of the 4 pentagonal legs is divided in 5 sections to lift. The top of these sections is lifted and a tipping-cart ensures the stability of the bottom. After lifting the section off the barge, thousands of liters of water are pumped from one side of the barge to the other to stabilize and steady it. The first sections are placed on top of 150 dowels sticking from the foundation pile cap and fastened with anchor rods. Splice plates are used to connect the sections and the shear link beams and cross bracings are attached after the section is in place.

For the SAS single main cable, a temporary catwalk was erected along the path of the main cable, so that ironworkers could access the cable. The cable erection method is fully described in Chapter 3.8. and consists on installing each strand individually by means of a hauling system that brings the cable around East anchorage splay chamber, tower saddle, West loop and East deck again. After the 137 strands were put into place, compaction of cable took place with 4 hexagon-shape compactor machines (max 9350 psi pressure). Once the diameter is achieved, temporary steel bands are placed around the cable. The process started at the top of tower and went 1,5m down at a time. Finally, 114 cable bands are bolted into place on the main cable and suspender cables start to be placed [11].

Once the main cable and suspenders were in place, the load transfer took place. It is a very complex process, for which hydraulic jacks were used. The 200-suspender ropes were gradually tensioned and after the 104 suspender the bridge was self-suspended. This tensioning caused the main cable to move down about 5 m and to the outside 9 m. Also, it caused a 0,5-meter uplift of the deck from temporary supports. Since the cable is splayed and anchored at the East side of deck, it will logically pull the tower to the East once is activated. That way, a 0,45m maximum west-side displacement was implemented at the tower by means of steel strands connected to Yerba Buena rock. Consequently, a jacking saddle between deviation saddles on the West anchorage was used to balance that side and return the tower to vertical position. After the initial phase of tensioning, connections between deck and cable, corrosion protection among others were performed [28].

On Fig. 3.55 it is shown the Cost Summary presented in 2012 by Bay Area Toll authority (BATA). The self-anchored span had a total cost of more than two billion US dollar. The complex erection method required very much contributed for this high cost. Indeed, the framework (temporary structure) cost around 350 million [41].

The comparative study done in this report is also based on the fact that a more conventional ground-anchored suspension bridge could have reduced the final cost of construction. Although the ground-anchorages would be complex and expensive, they would have simplified the erection process, as well as reduce the weight of some other structural elements as it will be discussed in following Chapters.

SFOBB East Span Seismic Replacement								
Capital Outlay Construction								
Skyway	Completed	1,293.0	(47.8)	1,245.2	1,237.2	1,245.2	-	
SAS Marine Foundations	Completed	313.5	(34.9)	278.6	274.8	278.6	-	
SAS Superstructure	Construction	1,753.7	293.1	2,046.8	1,705.4	2,058.0	11.2	
YBI Detour	Completed	131.9	360.9	492.8	466.1	[illegible]	(10.0)	
YBI Transition Structures (YBITS)		299.3	(37.3)	262.0	151.4	324.2	62.2	
YBITS 1	Construction			199.7	151.4	240.4	40.7	
YBITS 2 Cantilever and Demo	Advertised			59.0	-	80.5	21.5	
YBITS Landscaping	Design			3.3	-	3.3	-	
Oakland Touchdown (OTD)		283.8	50.8	334.6	213.7	325.4	(9.2)	
OTD 1	Completed			212.0	203.0	203.3	(8.7)	
OTD 2	Construction			62.0	5.0	56.3	(5.7)	
Detour	Completed			51.0	-	51.8	0.8	
OTD Electrical Systems	Design			-	-	4.4	4.4	
Submerged Electric Cable	Completed			9.6	5.7	9.6	-	
Existing Bridge Demolition	Design	239.2	(0.1)	239.1	-	237.4	(1.7)	
*Cantilever Section	Advertised			-	-	60.5		
*504/288 Sections	Design			-	-	70.2		
*Marine Foundations	Design			-	-	106.7		
Stormwater Treatment Measures	Completed	15.0	3.3	18.3	16.8	18.3	-	
Other Completed Contracts	Completed	90.4	-	90.4	90.0	90.4	-	
Capital Outlay Support		959.3	261.5	1,220.8	1,080.5	1,268.9	48.1	
Right-of-Way and Environmental Mitigation		72.4	-	72.4	51.7	80.4	8.0	
Other Budgeted Capital		35.1	(3.3)	31.8	0.7	[illegible]	(24.1)	
Total SFOBB East Span Replacement		5,486.6	846.2	6,332.8	5,288.3	6,417.3	84.5	

Fig. 3.55 – Cost summary of San-Francisco Oakland East Bay Bridge by September 2012 *[42]*.

3.11. RAINBOW BRIDGE AND SELF-ANCHORED SPAN OF SAN FRANCISCO-OAKLAND BAY BRIDGE: A COMPARATIVE STUDY

Due to some similarities in matters of structural system, soil conditions and seismicity level between the Tokyo Rainbow Bay Bridge and the new self-anchored span of the San Francisco-Oakland Bay Bridge, a brief summary of the Tokyo Bridge characteristics was found relevant and explanatory. This study aims to understand and evaluate the reasonability of the self-anchored system chosen for the new SFOBB in comparison to other structural options taken in similar scenarios.

3.11.1. RAINBOW BRIDGE STRUCTURE

Shuto Expressway n.º11 Daiba Route-Port of Tokyo Connector Bridge (more often called *Rainbow Bay Bridge)* constructed between 1987 and August 1993 and it consists of a ground-anchored suspension bridge with a total length of 798m and main span of 580m. It has two towers with a height of 126m above the sea level. This bridge makes the crossing on the north of Tokyo Bay between Shibaura pier and Daiba. Its double deck has an upper deck for Daiba Line Route 11 (main urban highway network) and a lower deck for Port Road, a walkway and New Transit *Yurikamome* (the first completely computer-automated rapid transit system) [34]. Due to its abovementioned capabilities, it is a key transportation line that connects the city center and suburban centers. The Yurikamome transit alone accounts for approximately 160 000 passengers per day. It was intended as an aesthetic bridge *oriented towards the future.* It has a long-life, power-saving and high brightness illumination system. The complex illumination of the bridge changes between 3 colors for each day of the week and weekend, which was a first-time innovation for a bridge. In fact, the popular name given to this bridge (Rainbow) derives from its illumination system [35].

Fig. 3.56 – Tokyo Rainbow Bridge *(Ref.: www.flickr.com, 2007).*

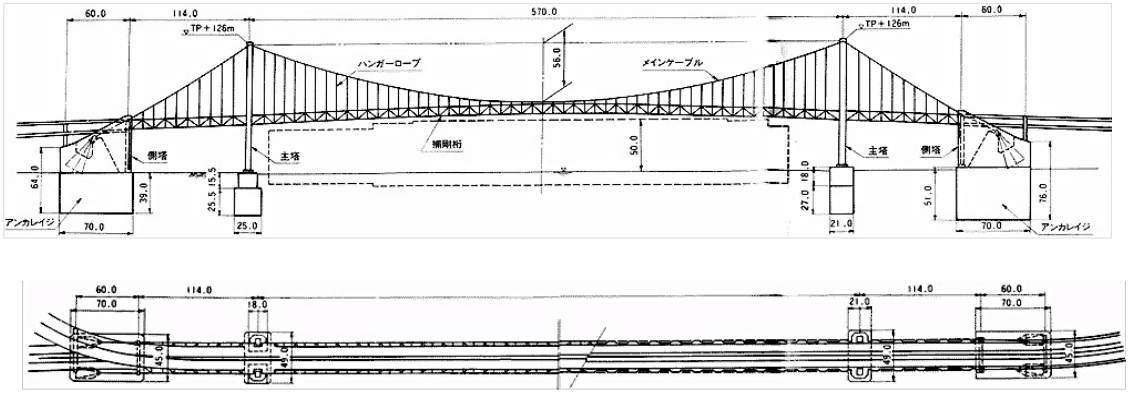

Fig. 3.57 – Side and Plan view of the Tokyo Rainbow Bridge [39].

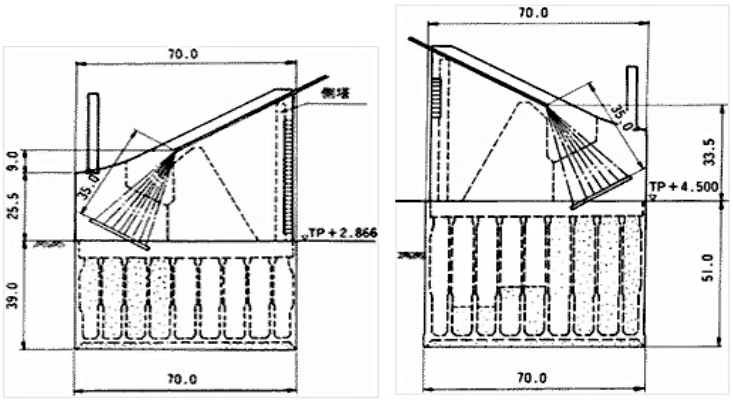

Fig. 3.58– Shibaura side and Daiba side ground-anchorages [39].

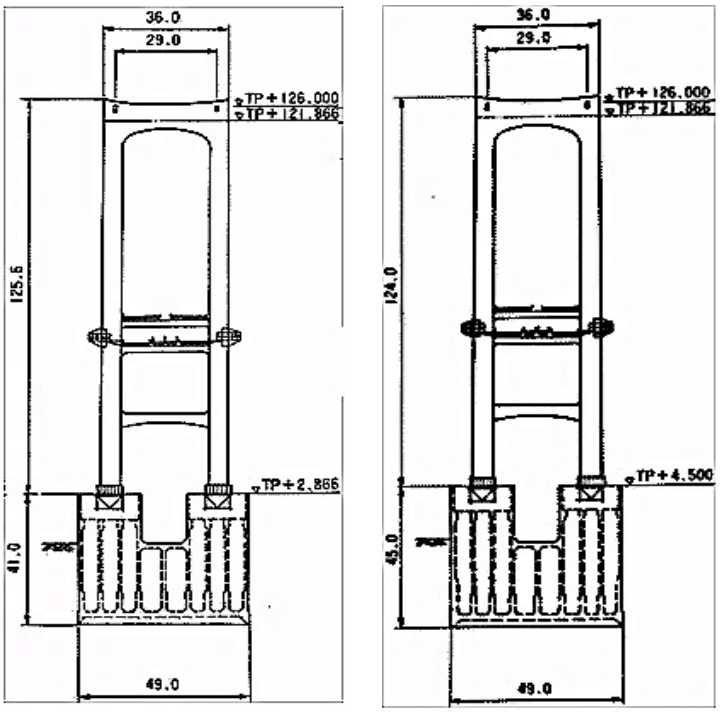

Fig. 3.59– Shibaura side and Daiba side main towers, respectively [39].

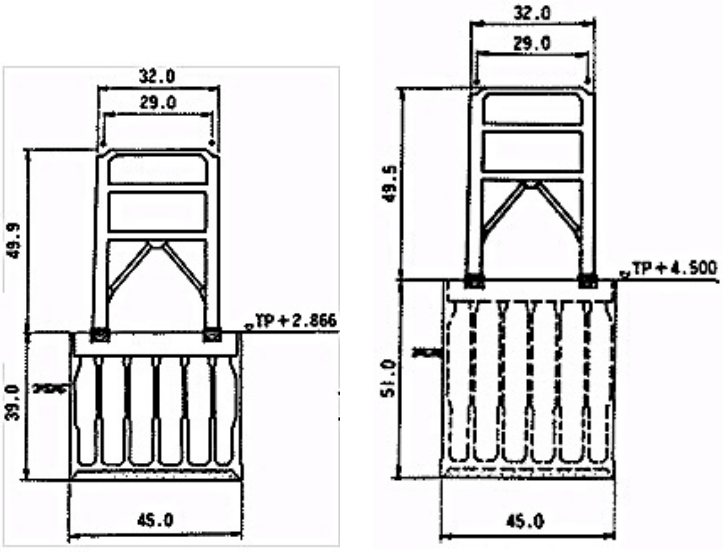

Fig. 3.60– Shibaura side and Daiba side towers, respectively [39].

The foundation system for this bridge is **caisson**, as shown in Fig. 3.57 to 3.60. This system is **very common for conventional ground-anchored suspension bridges.** As a matter of fact, it was used on the West San Francisco-Oakland Bay Bridge, which is a traditional symmetrical ground-anchored suspension bridge. The West Bay Bridge as one of its ground-anchorages in Yerba Buena Island bedrock. That would also have been a possibility for the new East Bay Bridge suspension span being studied. Furthermore, a ground-anchored suspension bridge design for the new East Bay Bridge would

require an offshore anchorage. That is not as common as a ground-anchorage inland, but as been done and studied before [40].

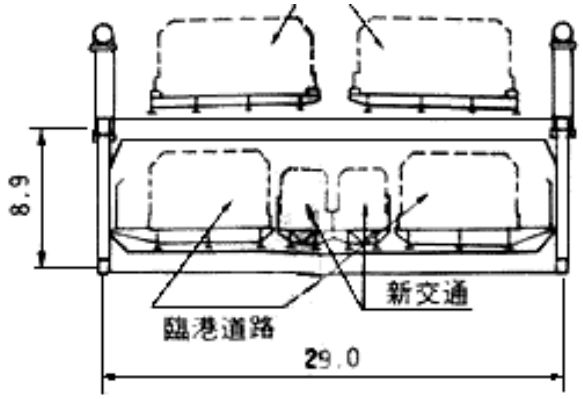

Fig. 3.61– Tokyo Rainbow Bridge's typical double-deck section [39].

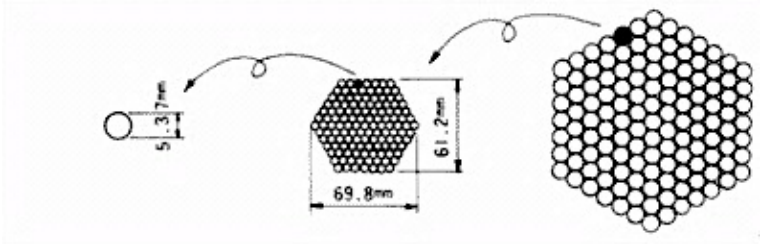

Fig. 3.62– Tokyo Rainbow Bridge's wire, strand and bundle of strands [39].

Table 3.2 – Rainbow Bridge's main structural characteristics [35].

Structural Element		Characteristics
Span	Stiffening girder	107.5m +562.0 m +107.5 m
	Cable	147.5m +570.0 m +147.0 m
Tower	Height	126m
Cable	System	PWS (parallel wire cable)
	Strands	127 wires each
	Center span	φ = 762mm (bundles of 127 strands)
	Side span	φ = 771mm (bundles of 130 strands)
	Center sag	57.594m
	Sag ratio	1/9.9

Structural Element		Characteristics
Deck	Stiffening girder	Parallel chord: Warren truss Horizontal: K truss
	Height and width	8.9m and 29m (Figure 3.61)
Anchorage	Type	Ground-anchored
	Dimension in plan view	70m x 45m (Figure 3.58 to 3.60)
Earthquake and wind resistance	Wind	Designed for 67 m/s wind
	Seismic	Withstand Kobe and Kanto earthquakes
Erection process	(with barge and crane)	1) Cable anchorages 2) Side towers 3) Main towers 4) Erection of the catwalk 5) Erection of the strands (PWS) 6) Erection of the hanger rope 7) Center span stiffening girder 8) Side span stiffening girder 9) Stiffening girder closure 10) Wrapping painting of main cable 11) Dismantling catwalk 12) Paint hanger ropes

The erection method for the Rainbow Bridge is typical of conventional ground-anchored suspension bridges.

3.11.2. SOIL CONDITIONS

The Rainbow Bridge is located north of the Tokyo Bay (see Fig. 3.63). The soil conditions there have been fully studied, tested and reported both as liquefaction prone and of dubious quality. The north Tokyo Bay is the delta of several watercourses and rivers such as Sumida, Arakawa, Edogawa and Old Edogawa among others.

Indeed, various papers have been published about the soil conditions and liquefaction that have occurred in that region. Ishihara (2006) studied the 1923 Kanto earthquake effects on the Tokyo area. The delta region seen in Fig. 3.64 was identified by the author as one of the areas most affected by liquefaction after the Great Kanto eartquake. For further investigation, soil testing has been conducted recently and soil profiles at Ukita and Edogawa are shown in Figure 56 [36]. The profiles match those *typical of alluvial deposits in the downstream delta area of big rivers.*

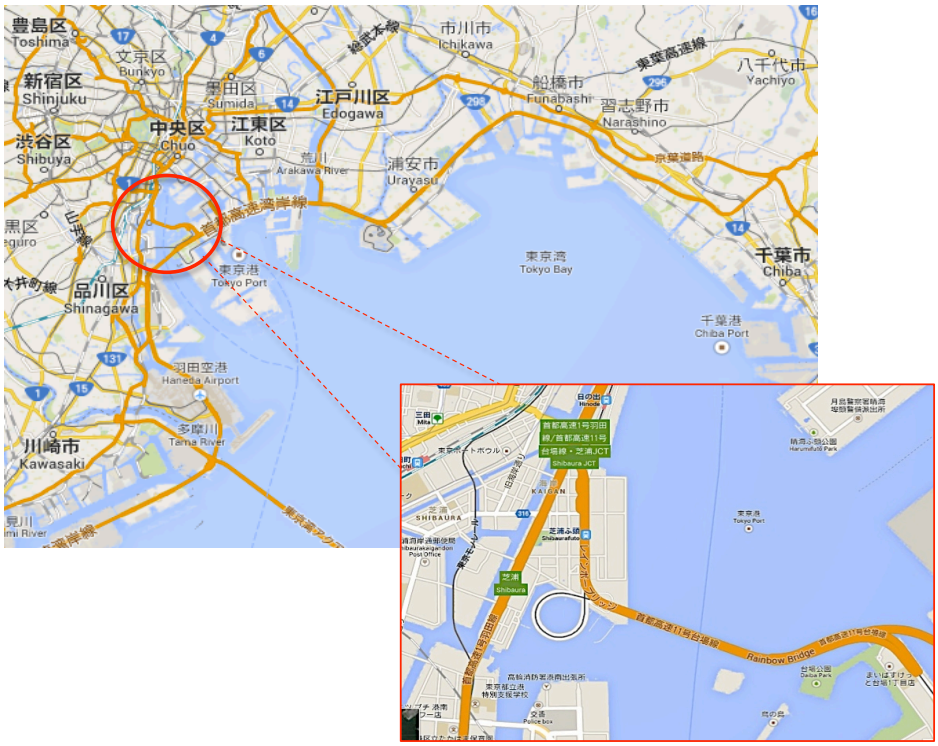

Fig. 3.63–North Tokyo Bay region with Rainbow Bridge specific location *(Ref.: www.maps.google.com).*

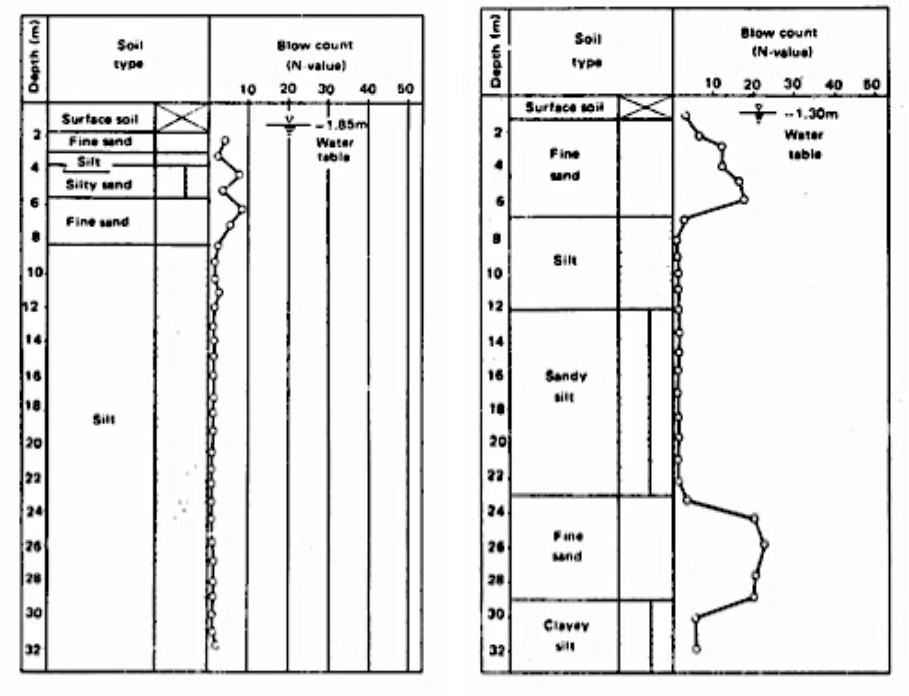

Fig. 3.64– Soil profiles for Ukita and Edogawa with SPT test results [36].

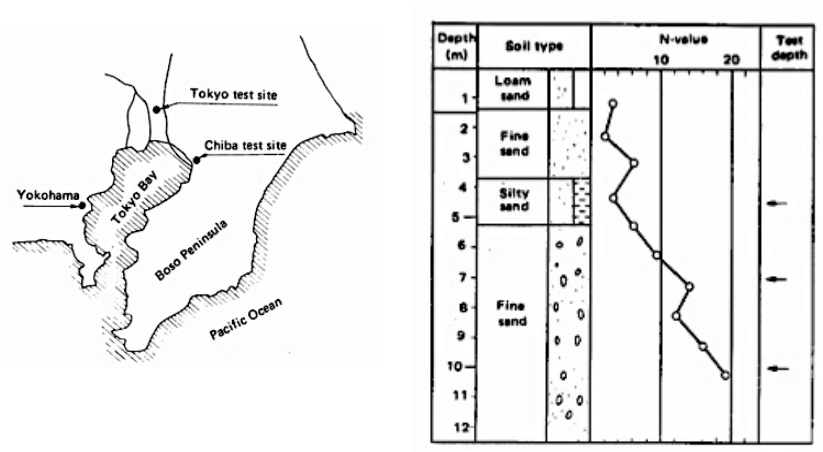

Fig. 3.65– Takasago testing location and soil profile [36].

Moreover, a soil profile was also obtained in a Takasago Middle school, in Tokyo, which consists of a natural levee deposit composed of fine sands, with similar distribution to those found in Chiba (Figure 3.65). Additionally, the author enumerates the three types of soils where liquefaction is more likely to occur: i) *sand deposits* with different grain composition with a depth of at least 20m; ii) *sandwiched sand deposits* 3-10 meter deep at shallow depths intercalated with silt or clay layers and iii) *thin sand layers on gravelly sand.*

Other authors have also studied the soils characteristics and damage caused by more recent earthquakes such as the 2011 Tohoku-Pacific Ocean earthquake [37]. It had a 9.0 magnitude (largest during the last 150 years of seismic observation in Japan) and it was the first to be recorded that caused such a widespread liquefaction and damage. Other earthquakes such as Kanto (1923) and Chibaken-toho-oki (1987) are also known to have induced liquefaction.

More recently in Japan, JGS, Chiba Prefecture and Tokyo Metropolitan have published new geotechnical databases. With that information, the authors [37] have estimated soil profiles, specifically in Urayasu (near the actual Rainbow Bridge) that is shown in Figure 3.66. Once again, as Ishihara (2006) had also showed, the soils in this region consist of "weak" soils such as *hill sand, dredged sand, alluvial sand and soft alluvial clay.* Also, another reason for the liquefaction is the long duration of the main and after shocks, since the seismic intensity in the liquefied zones was not high.

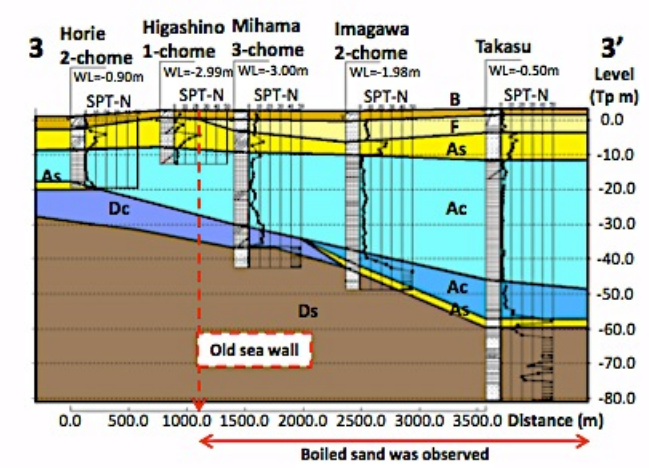

Fig. 3.66 – Urayasu soil profile [37].

Ishihara (2012) more recently published a new paper also related to the soil condition in Tokyo Bay, due to the major 2011 earthquake [38]. The earthquake shaking lasted approximately 150s, possibly the longest ever recorded and that was the main cause of the widespread soil liquefaction. In fact, liquefaction was induced in bay shore areas of Kanto Region, with approximately 70km^2 affected. This phenomenon was stated by the author as *unprecedented and truly record-breaking* due to the distance to epicenter and size of the affected areas.

After the abovementioned **general profile of the soil conditions around Rainbow Bridge**, it can be concluded that they are unfavorable. For the design of the bridge they were studied and tested. Figure 59 shows a **Rainbow Bridge longitudinal geological profile**. As expected, the profile is comprised of silty-clay and sands, as well as mudstone where the structure is founded.

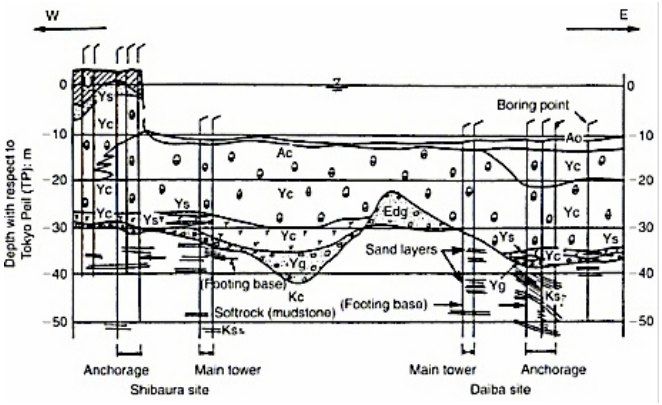

Geological age	Strata	Soil Types	Symbols
Holocene	Recent	Artificial Soil	
		Floating Mud	Ao
	Yurakucho formation	Silt–clay	Yc
		Sand	Ys
		Gravel	Yg
Pleistocene	Edogawa formation	Gravel	Edg
Pleistocene–Tertiary	Kazusa group	Softrock (mudstone)	Kc
		Uncemented fine sand	Ks

Fig.3.67 – Tokyo Rainbow Bridge longitudinal geological profile [39].

Because of the *weak* soil condition under the Rainbow Bridge, the cable anchorage system is massive and does not go unnoticed, but nevertheless it is iconic and was used as an advantage to captivate public attention. The massive anchorage structure includes elevators to the walkway and contains Observation Platforms to the Tokyo Bay, a unique characteristic in the world (Fig. 3.68).

Fig.3.68 - Rainbow Bridge anchorage system and observatory platform (*Ref.: https://www.google.com/maps*).

The new East San Francisco-Oakland Bay Bridge is also situated on an unfavorable geotechnical condition. Fig. 3.69 to 3.71 contain relevant soil-related information.

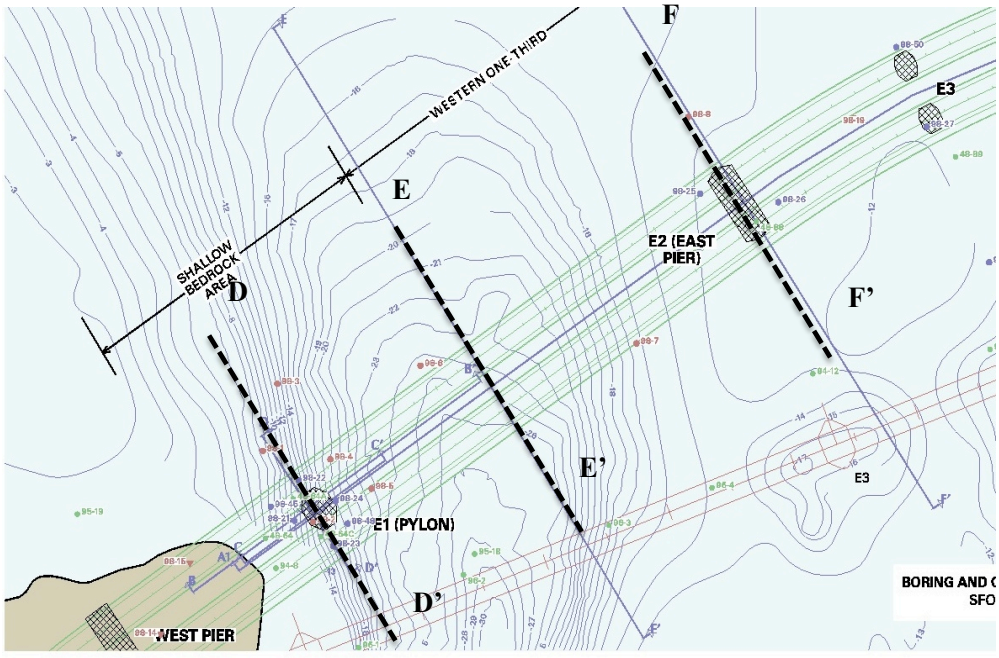

Fig. 3.69 – Map Contour with location of Pier W2, Tower T1 and Pier E2 for SAS (*Ref.: Caltrans presentation, by Anthony Dover, P.E., G.E.)*

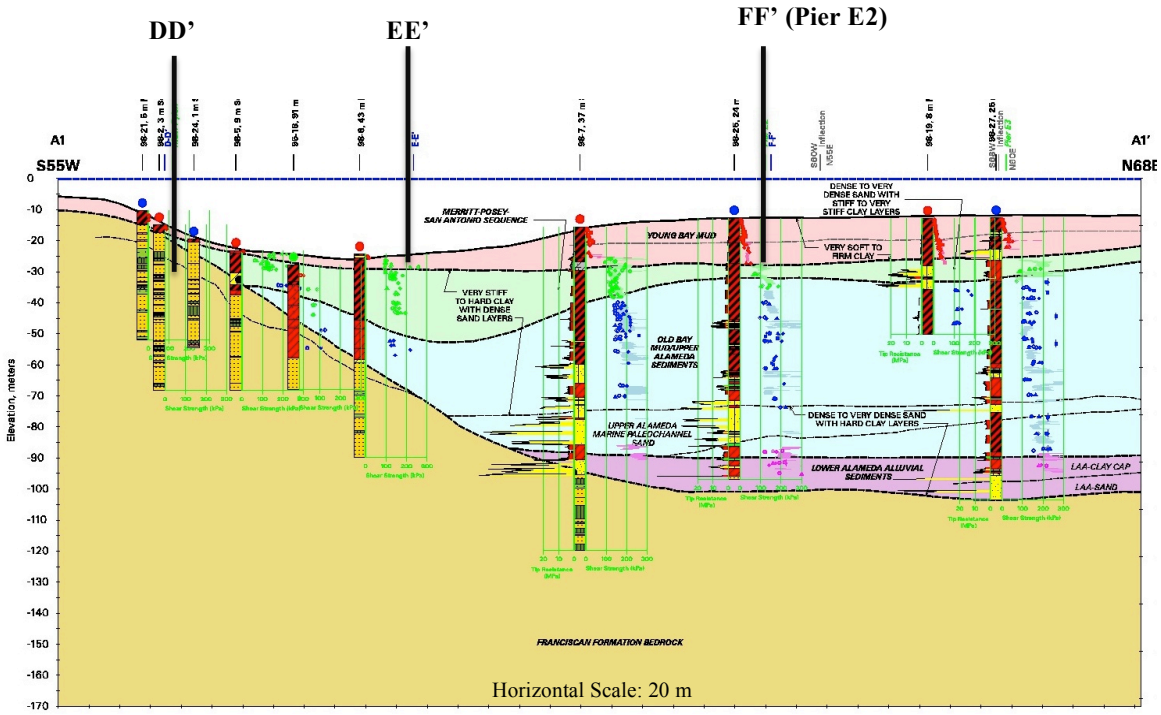

Fig. 3.70 –Longitudinal geological profile for the Self-anchored Span of the SFOBB (*Ref.: Caltrans presentation, by Anthony Dover, P.E., G.E.)*

There are some conclusions one can make when studying this soil conditions: i) the west piers can be built on top of the Franciscan formation (bedrock) and therefore shallow foundation were used; ii) the tower is located where the younger bay sediments layers begin to appear, but still presents satisfactory soil conditions. Indeed, the 60-meter deep piles are embedded on the San Franciscan formation bedrock; iii) between section D and F the soil profile changes abruptly to include new strata like young bay mud, hard clay, old bay mud, upper alameda sand and lower alameda sediments (top to bottom, respectively). This conditions are very unfavorable and one of the reasons given by the design team for the selection of the self-anchored system; iv) Pier E2 soil profile (FF') has the San Franciscan formation at around 100-meter depth. Nevertheless, around 70-meter depth the results of boring tests such as CPT reveal admissible undrained shear strength, with more than 200 kPa (see Figure 58 and 59) and Tip resistance of 10 MPa or more.

Comparing these values with the Rainbow Bridge ones, one realizes the Pleistocene-mudstone in which the Tokyo Bridge is based can present undrained shear strength of less than 200MPa, as well as for Tip resistance that has similar values to the San Francisco Bay soils.

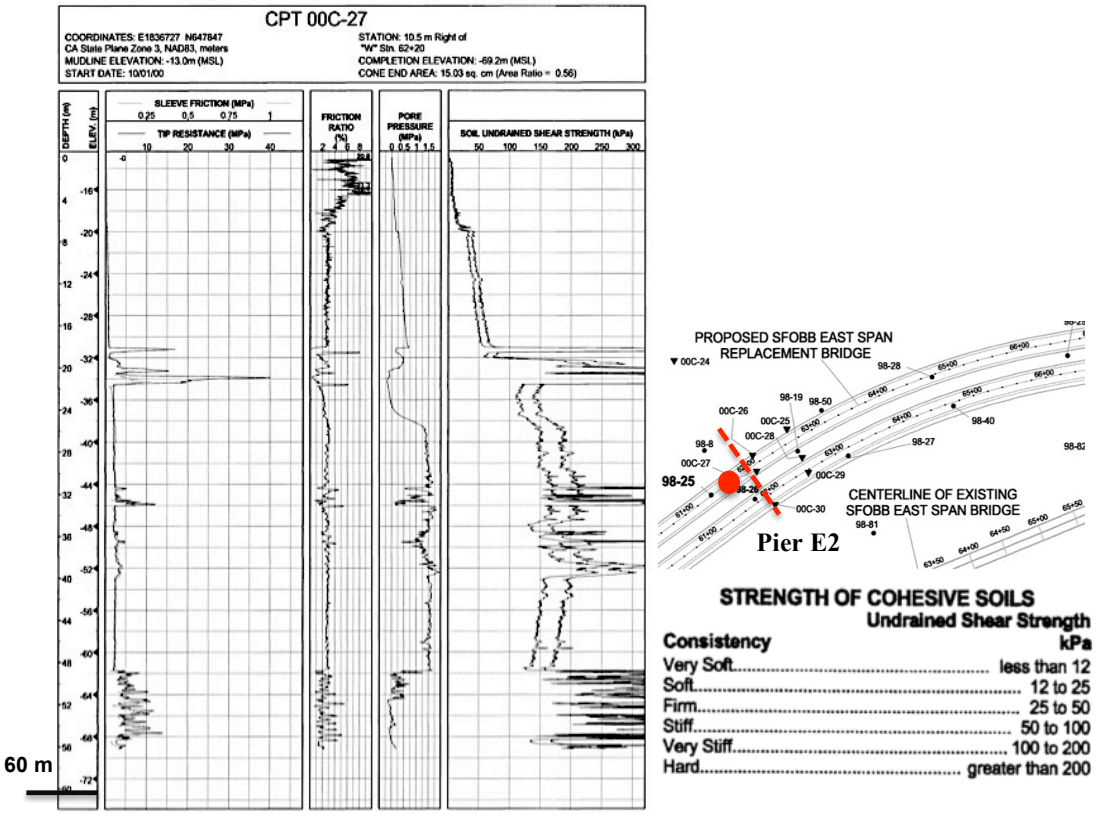

Fig. 3.71 – CPT results and scale for Pier E2 section (*Ref.: Caltrans drawings)*.

A successful example of ground-anchorage in unusually soft soils has been presented and the comparison with the SFO Bay Bridge aims to show the possibility of other structural alternatives. A different structural system might have been more economical and faster to erect than the selected self-anchored bridge. Taking into account the preference for a cable-supported bridge, other systems could have been Ground-anchored cable or Cable-stayed, for instance.

4
CONSTRUCTION ISSUES

4.1 STRUCTURAL AND CONSTRUCTION ISSUES

The design, construction and cost of the new East San Francisco Oakland Bay Bridge have not been lacking controversy. As a matter of fact, from the starting point voices have been raised against a structural system that has not been studied and analyzed as deeply as others to be used in such a critical seismic scenario with several active faults near the bridge. The question remains if aesthetics wasn't taken into consideration more than economical feasibility and safety. Indeed, the structural system implies an erection method, which is very complex, time-consuming and expensive, since it requires basically building "two bridges", one a temporary framework to support the final structure and then the final structure (see Section 3.10). Moreover, construction took more than a decade and faced several problems, which will be explained in more detail in the following subchapters. Figure 4.1. shows ten locations where problems have already arose or might arise in the future, due to uncertainty in materials or damage. The following subchapters enumerate and explain those problems. This chapter was found relevant and explanatory of the main goal of this study - viability of the self-anchored span and its comparison to a ground-anchored system of similar architure.

Issue #1 – Tensioned Pier W2

Issue #2 – A354BD bolts/rods at top of the tower (saddle)

Issue #3 – A354BD anchor bolts at the bottom of the tower and quality of welds

Issue #4 – Quality of concrete on composite piles

Issue #5 and #6 – A354BD threaded rods connecting suspenders to main cable and deck

Issue #7 – A354BD rods/bolts and corrosion at the strands on the east cable deck anchorage

Issue #8 – Quality of welds in the deck and mismatch of deck splice plates

Issue #9 – A354BD threaded rods at shear keys and bearings at Pier E2 that suffered brittle failure prior to the bridge opening

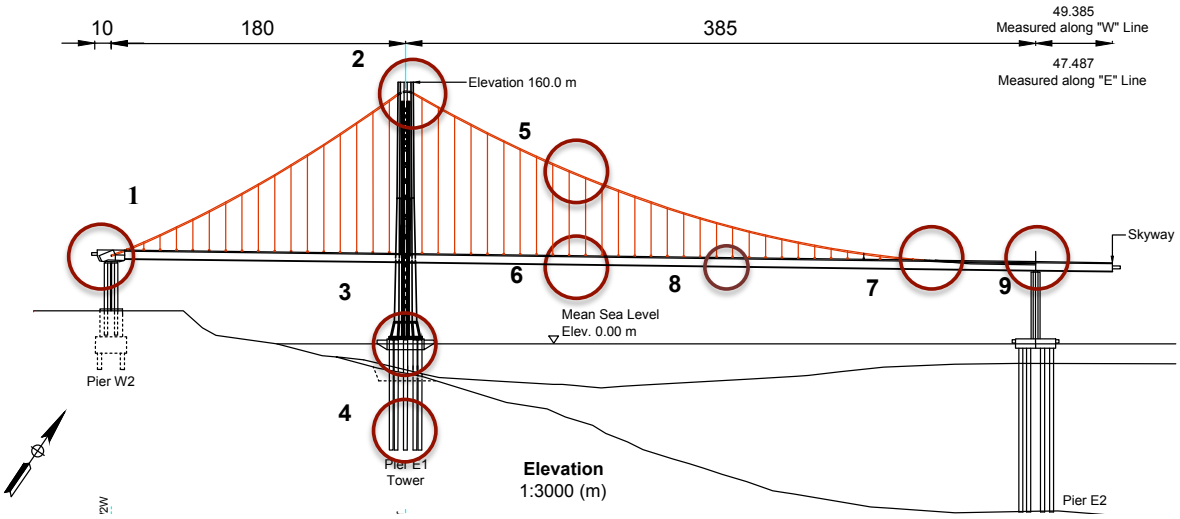

Fig. 4.1. – SAS bridge side view with ten highlighted locations (Ref.: AutoCAD made by the author).

4.1.1 THREADED RODS AND BOLTS

There were used high-strength bolts on the bridge because Caltrans defined Bay Bridge as a *Lifeline structure* (the economic consequences of failure are great and/or it provides a secondary life safety and/or are designated important by local emergency officials). Its location and crucial transportation route were the reasons for this decision. The important role of this bridge implies the earthquake design criteria to be very high standard. Indeed, according to the Chief Bridge Designer at Caltrans the self-anchored span has been designed to 40% more than the worst of six different 1500-year return period earthquake time history-generated loads. Also, due to the geological and geotechnical conditions the Pier E2 (with more flexible foundations) will behave differently from Pier W2 and Tower T1. To harmonize movements during a seismic event, the designers determined a strong connection to the east pier was necessary. Not only on this pier these high-strength connections were necessary, but at other high-load locations of the bridge.

According to ASTM[7], there are several high-strength steel rods available. More specifically, the ASTM A354 standard refers to A354 grade BD (high-strength) and BC (low-strength) rods. Grade BD have minimum tensile strength of 150 ksi (1034MPa) for 1/4 to 2-1/2inch diameters and 140 ksi for 2-3/4 to 4 inch diameters. These Grade BD threaded rods are equal in strength to ASTM A490 bolts, but the A490 are heavy hex structural rods/bolts and do not exceed 1-1/2inch diameter, while the A354BD specifications are unrestricted. Grade BC has minimum tensile strength of 115 ksi (793 MPa) and F1554 grade105 rods have minimum tensile strength of 125 ksi (862 MPa) for diameters greater than 1-1/2inch. Also, there are other alternatives according to ASTM, such as A722 rods. For the

[7] American Society for Testing and Materials (ASTM) is an international standard for defining chemical and mechanical properties to specific alloys for steel bolts and other threaded rods. The A354 specifications cover BC and BD anchor bolts, threaded rods and headed bolts for sizes 4inch and under diameter.

SFOBB, the TBPOC[8] Committee considered each rod type advantages and disadvantages, which are summarized in Table 4.1. Subsequently, the same Committee presented the following **reasons for choosing the A354 BD** steel rods for the structural steel connections on the self-anchored span:

- Low number of rod locations within the concrete pier cap and Pier E2 (higher strength required), or otherwise it would mean bigger pier cap and cross beam and consequently more mass, which increases seismic forces;

- Ungalvanized A354 BD are used on major bridge projects such as Golden Gate retrofit, when high loads are expected;

- Sole-source restrictions[9] that discouraged use of proprietary rods, unless it could be established that there was no alternative. For other materials, the designers would have to sole-source a vendor.

Therefore, many of the rods used on the self-anchored span are type A354 BD hot-dip galvanized bolts, more specifically 2306 in total at 17 different locations (see Table 4.2).

Nevertheless, this **choice and its main reasons are not all considered valid** by the metallurgical and materials engineers Chung and Thomas in a report issued by these experts to Caltrans and the California State Senate Transportation committee, pointing out several technical errors in the TBPOC official report [43]. As a matter of fact, the authors state that the shear keys are large steel casing with a 2,74m (9ft) square and 27,4cm (10,8in) thick base plate. Each of them has 48 anchor rods spaced 25,4 to 35,56cm (10-14in) apart and that each rod has a spherical washer (17,8cm or 7in). Therefore, it can accommodate 3-1/4in diameter BC as well as 3in diameter Grade BD rods, with no need to redesign the shear keys, pier cap or Pier E2. Indeed, the choice of Grade BC would have spared numerous problems such as a major rod failure on Pier E2 Shear Keys (see next subchapter 4.1.1.1). Following this failure, the authors state that *Grade BC being a lower strength material is not susceptible to Hydrogen Embrittlement (or Stress corrosion cracking) (...) if grade BC had been selected instead of Grade BD, there would have been no S1 and S2 failures (...) even when their bottom threads were exposed to pools of stagnant water for an extended period".* This issue is going to be fully reviewed on Subchapter 4.1.1.1.

The authors go even further in stating that the sole-source options of the design team would also not be a good option, since they would have faced the exact same issues as the Grade BD [43].

The TBPOC report states that the SAS Design Criteria established on July 15, 2002 does not mention **corrosion protection** for the fasteners listed on the design criteria report. Nevertheless, this protection must exist and some of the options are: hot-dip or mechanical galvanization (zinc coating), electroplating, "Dacromet" (zinc/aluminum coating) or "Magni 565" (organic/inorganic aluminum). The recommended procedures by ASTM for high-strength bolts are "Dacromet" and "Magni 565". However, the most common coating is by galvanization and there are two types: **hot-dip and mechanical.** Both apply a coating of zinc, which provides sacrificial or cathodic protection to the iron (since it corrodes first and protects the steel substrate). Additionally, hot-dip galvanization requires the use of heat (≈454ºC) and might be more cost-effective, but the usage of heat should be well defined

[8] The Toll Bridge Program Oversight Committee is composed of director of Caltrans, California Transportation Commission and the Bay Area Toll Authority and has managed the construction of the SFOBB since 2005. It was also charged with investigating and solving the problem of the fractured A354 BD hot-dipped galvanized steel rods that occurred in 2013.

[9] Cannot make project choices that limits the bidding to any specific concern or calling for a designated material by specific brand/trade name, unless is followed by the words "or equal" so that the bidders may furnish any equal material. Otherwise, it is necessary approval from Chief of Structure Division and FHWA.

because its excess releases internal hydrogen and might increase the odds for Hydrogen Embrittlement. Also, hot-dipped galvanization results in thicker and less aesthetical coating. Mechanical galvanization results in a uniform coating and reduces thread fit issues at assembly and is preferred for structural applications. It is performed at room temperature in order to apply the zinc coating to the surface without electricity (electroplating) or without heat (hot-dipped).

Moreover, before the galvanization processes a cleaning process of the surface (acid pickling and/or blasting) is needed. Figure 4.2. shows a chart with the processes applied to each steel rod location for the self-anchored span of the Bay Bridge [45].

Table 4.1. – TBPOC Committee comparison between steel rods types [45].

Rod Materials Type	Minimum Tensile Strength (MPa)	Equivalent Diameter (cm)	Pros	Cons
A354 Grade BD	965 (140 ksi)	7,62 (3 in)	- High strength - Generally available - Has a minimum specified tensile strength between 965-1034 MPa	- Susceptible to hydrogen Embrittlement without due care when galvanizing
A354 Grade BC	862 (125 ksi)	8,89 (3,5 in)	- Generally available - Less susceptible to Hydrogen Embrittlement - Can be galvanized without cautions - Minimum specified tensile strength between 793-862 MPa.	- Lower strength (than BD) - Requires more rods and larger connecting surfaces (than BD)*.
F1554	862 (125 ksi)	7,62 (3 in)	- Generally available - Less susceptible to Hydrogen Embrittlement - Can be galvanized without cautions - Minimum specified tensile strength between 862-1034 MPa.	- Lower strength (than BD) - Requires more rods and larger connecting surfaces (than BD)*.
A722	1034 (150 ksi)	7,62 (3 in)	- High strength - Minimum specified tensile strength of 1034 MPa.	- Proprietary connectors might require waiver from sole-source restrictions - No domestic suppliers produce 3-inch of these - Only available through certain suppliers.

*See Chung and Thomas [43].

Table 4.2. – 17 Locations of the A354 BD rods at SAS span [45].

N.º	Location	Component	Quantity installed	Diameter (cm)	Length (m)	Initial Tension (% of specified minimum ultimate tensile strength (140 ksi))
1	**Pier E2 (TOP)**	Shear Key Anchor Rods (2008)	96	7,62	3,05-5,2	0,70
2		Bearing & Shear keys Anchor rods (2010)	192	7,62	6,7-7	0,70
3		Shear Keys Rods (with orthotropic deck)	320	7,62	0,61-1,4	0,70
4		Bearing Rods (with orthotropic deck)	224	5,08	1,2	0,70
5		Bearing assembly	96	2,54	0,76	0,61
6		Bearing retainer ring plate assembly	336	2,54	0,06	0,40
7	**Anchorage**	Parallel wire strand (PWS) Anchor Rods*	274	8,89	8,53-9,75	0,32
8	**Tower (TOP)**	Saddle Tie Rods*	25	10,16	1,83-5,5	0,68
9		Saddle Turned Rods*	108	7,62	0,46-0,61	0,45
10		Saddle Grillage	90	7,62	0,305	0,10
11		Outrigger Boom	4	7,62	0,61	0,10
12	**Tower (BOTTOM)**	Anchor Rods Type 1*	388	7,62	6,1	0,48
13		Anchor Rods Type 2*	36	10,2	6,1	0,37
14	**Saddles (EAST)**	Anchor Rods	32	5,08	0,915	0,10
15		Tie Rods	18	7,62	1,52	0,20
16	**Cable (EAST)**	Cable band Anchor Rods	24	7,62	3,05-3,35	0,16
17	**Pier W2 (TOP)**	Bike path anchor Rods	43	3,7	0,46	0,10

* The indicated rod locations are dehumidified.

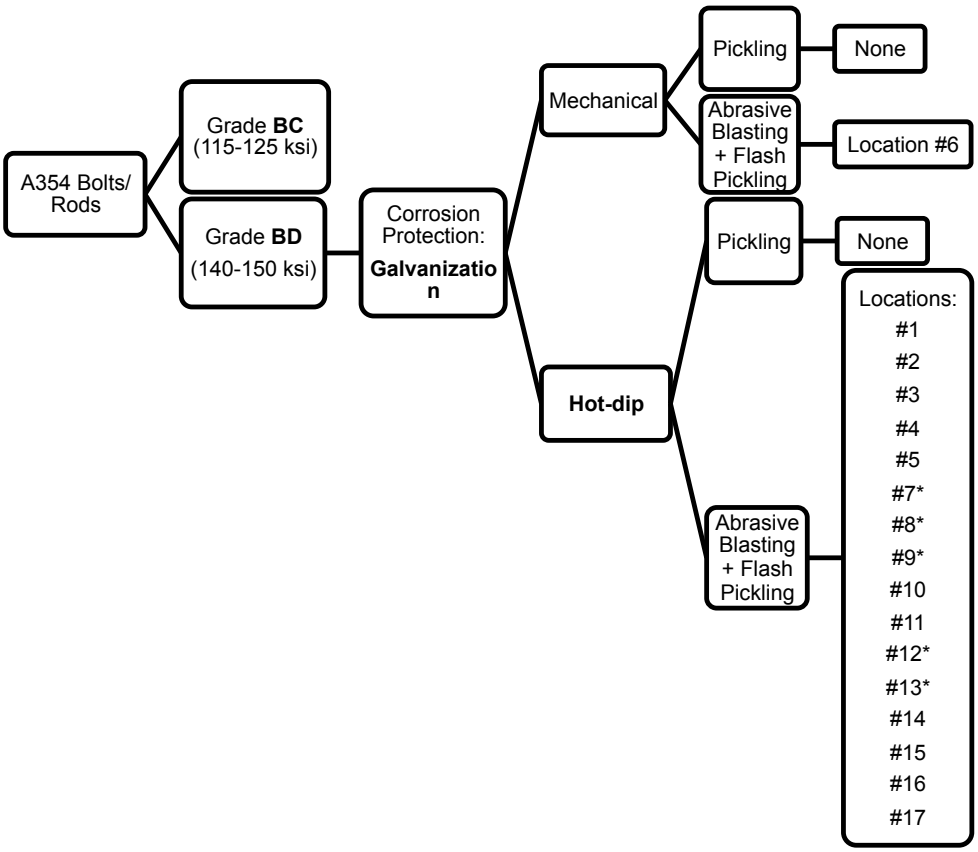

Fig. 4.2. – Galvanization process for the East SAS Bay Bridge according to TBPOC [45].

From the analysis of Figure 4.2, it can be concluded that only on a small percentage of A354 BD bolts/rods the Hot-dipping with abrasive blasting and flash-pickling was not used. Indeed, only Location 6 (Bearing Retainer Ring Plate assembly) received a different corrosion treatment.

The design team (supported by Caltrans) **chose hot-dip galvanization** for long-term corrosion protection and the reasons for this choice compared to other methods **were not documented.**

According to **ASTM A143** (Safeguarding against Embrittlement of hot-dip galvanized structural steel products and procedure for detecting Embrittlement): *"In practice hydrogen embrittlement of galvanized steel is usually of concern only if the steel exceeds approximately 150 ksi in ultimate tensile strength"*. Also, **ASTM F2329** (7.2.2) states that *"For high strength fasteners (having a specified minimum product hardness of 33 HRC), there is a risk of internal hydrogen embrittlement"*. For A354 BD bolts/rods, the minimum core hardness is usually C31 or C33 depending on the diameters and might vary between C31 to C39. Moreover, **ASTM A490** states that *"The bolts shall not be coated by hot-dip zinc coating, mechanical deposition, or electroplating with zinc or other metallic coatings"* and **ASTM A354** (Note 4, section 4) states that *"Research conducted on bolts of similar material and manufacture indicates that hydrogen-stress cracking or stress corrosion cracking may occur on hot-dip galvanized Grade BD bolts."*

As a matter of fact, all ASTM specifications stipulate that **hot-dip galvanization of ASTM A490 and A354 grade BD should be avoided,** due to the risk of internal hydrogen embrittlement. Also, industry standards and practice do not recommend it [46].

So, **what is the hydrogen embrittlement** phenomenon? High strength steels may fail under static loads when three conditions are simultaneously satisfied: hydrogen presence above a threshold level, stress above a threshold level and material susceptibility above a threshold level (Fig. 4.3). When these conditions are satisfied, micro-cracks start forming in high stress concentration sections, such as the root of a thread and grow with time until it causes instant failure under static load well below the yield strength of the metal.

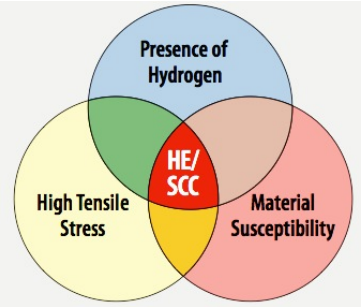

Fig. 4.3. – Main causes for Hydrogen embrittlement (HE) or Stress Corrosion cracking (SCC) [45].

The source of hydrogen determines the type of embrittlement: internal hydrogen embrittlement (IHE) or environmental hydrogen embrittlement (EHE). ASTM has a definition for both types: **IHE** is *caused by absorbed atomic hydrogen into the steel from an **industrial hydrogen emitting process** coupled with stress (residual or external)* and **EHE** is *caused by hydrogen introduced into steel from an **environmental source** coupled with stress (residual or external).*

The **time to failure does not influence the distinction between IHE and EHE**. On the other hand, if the failure can be related to hydrogen that was already present at the end of the manufacturing process (after acid pickling cleaning for hot-dip galvanization), the cause of failure is IHE. In contrary, if the source is a corrosion reaction after the manufacturing, the cause of failure is EHE. Nevertheless, it is common that EHE failures occur after a longer period (years or decades) particularly in atmospheric services, because it may take time for the corrosion to produce hydrogen and for it to accumulate to the threshold level, but there is no accurate predicting model to know exactly when this failure will happen. Also, **stress is a prerequisite for hydrogen embrittlement cracking to occur, but not for the hydrogen charging.** For IHE and EHE, either in the cleaning process or during corrosion, hydrogen is generated and its diffusion process into the steel occurs either under stress or not. Stress only helps to mobilize hydrogen to stress concentrated areas [43].

ASTM defines **Stress Corrosion cracking (SCC)** as a *cracking process that requires the simultaneous action of a corrodent and sustained tensile stress.* Therefore, SCC can be seen as a type of Environmental hydrogen embrittlement (EHE). The initial corrosion may occur at a point of high stress causing micro-cracks (inter or transgranular) and the long exposure to corrosion conditions grows the cracks until failure. This failure occurs after installation, since hydrogen is introduced by corrosion due to environmental causes [46]. Copson (1953) stated that **SCC failures might vary in time from *minutes to many years*** depending on the environment, which reinforces the idea that these phenomena are not distinguished by time. Moreover, SCC involves *electrochemical dissolution of metal along active sites* (intergranular stress corrosion cracking), but IHE and EHE do not require it (Fisher et al. 2001). Also, according to Eliaz et al. (2002) two of the main differences between hydrogen embrittlement (HE) and SCC are the effects of cathodic protection and temperature. Temperature increase accelerates SCC, contrary to HE where cathodic protection accelerates HE [43].

4.1.1.1 Shear Keys S1 and S2

Based on the information provided in previous sections, a **major bolt failure** occurred on the east pier (E2) on Shear Keys S1 and S2. On March 1, 2013 the joint venture between American Bridge and Fluor, proceeded to the load transfer of the roadway decks from the temporary framework onto the main cable. After this procedure, the A354 BD anchor rods fabricated in 2008 were tensioned at Shear Key S2. From March 2 to March 5, 2013 the anchor rods were tensioned at Shear Key S1 as well (96 rods in total). According to contract, the bolts were initially tensioned to 75% of the specified minimum ultimate tensile strength, but in the end the prestressing was only 68% due to seating losses. From March 8 to March 14, 2013, **32 out of 96 rods were discovered completely fractured under prestressing static load**. Caltrans then decided to lower the tension on the remaining unbroken bolts to 45% to avoid further fractures. The design specification requires that the rods be tightened to 70% of their ultimate strength. Figure 4.4 shows a histogram of the failed anchor rods, which occurred 14 days after tensioning [45]. ***All 32 failures occurred in the bottom threads***. Moreover, due to construction delays the anchor rods were placed into grout pipes while the reinforced concrete cap beam was built and remained there for 5 years, exposed to the environment [43].

The shear keys are supposed to transfer forces from the superstructure (Skyway and Steel Orthotropic Deck) to Pier E2 during a seismic event. Shear Keys S1 and S2 are located on the centerlines of the decks and above the columns. Shear Keys S3 and S4 are located on the pier cap under the crossbeam. The four bearings should provide fixity, accommodate thermal expansion and work as backup systems to transmit loads in case shear keys fail during a seismic event (Figure 4.5) [45].

Another distinction is that 60 out of the 96 rods in Shear Keys S1 and S2 are **17ft-long (L1)** and 36 out 96 are **10ft-long (L2).** Also, each shear key is anchored to the pile cap with 48 anchor rods and each bearing with 24 anchor rods. Moreover, 45% of the L1 rods and 14% of the L2 rods failed after tensioning [43].

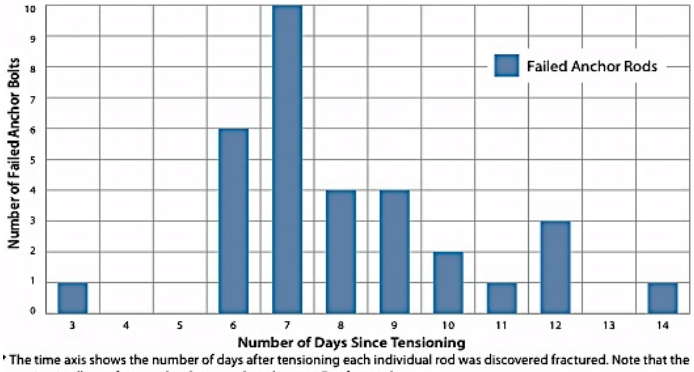

Fig. 4.4. – Timeline for the anchor rods (2008) failure on Shear keys S1 and S2 [45].

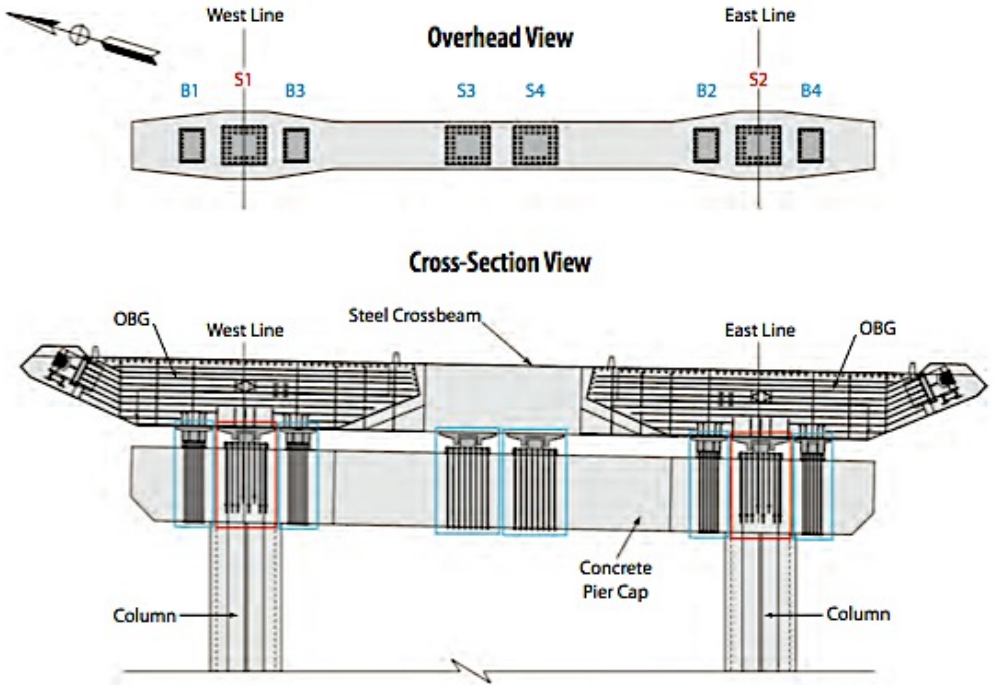

Fig. 4.5. – Shear Keys and bearings at Pier E2 [45].

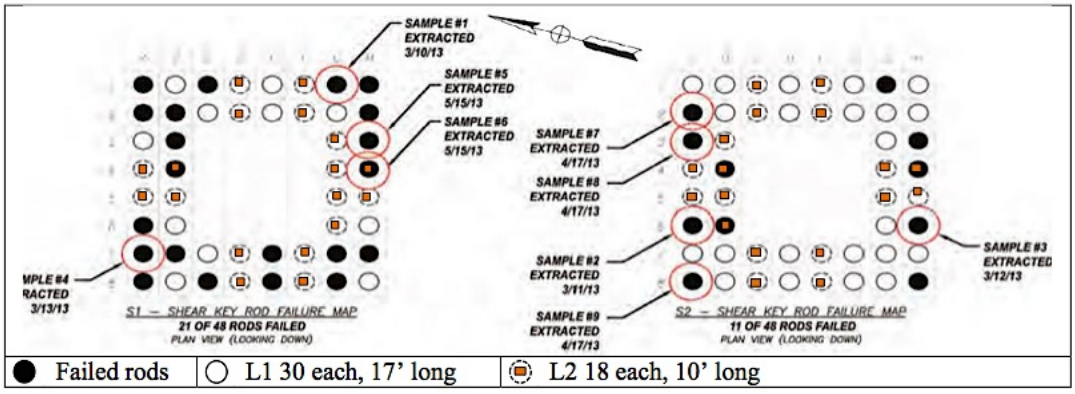

Fig. 4.6. – Shear Key S1 and S2 with L1 and L2 type of rods, as well as failed rods and samples extracted [43].

According to TBPOC, a metallurgical investigation team of experts from the Joint Venture and Caltrans gathered in order to understand the failure and test nine extracted samples of the broken steel bolts (see Figure 4.6). **Hydrogen embrittlement was considered the cause of the failure. Indeed, the 3 conditions were present** (Figure 4.3)**:** Material susceptibility, high tensile stress and presence of hydrogen.

However, the **Committee did not clarify whether the failures were due to Internal hydrogen embrittlement (IHE) or Environmental Hydrogen embrittlement (EHE).** As a matter of fact, they

stated that hydrogen embrittlement (HE) is a short-term phenomenon (*near-term*) and stated that EHE is a *long-term stress corrosion cracking.* This way, **one can only conclude *short term hydrogen embrittlement (*or *near-term)* is IHE in the TBPOC report.** Nevertheless, as discussed before in Chapter 4.1.1 time is not a scientific accurate differentiating factor between types of hydrogen embrittlement. This inconsistent use of terminology and nomenclature is considered *unscientific, confusing and unproductive* in understanding the rod failures by the independent team of experts Chung and Thomas [43].

The metallurgical team of experts took several conclusions from the **observation and testing of only 2 out of the 9 samples** retrieved from Pier E2 shear keys (see Figure 4.5):

- Visual observation: brittle appearance and evidence of hydrogen-assisted cracks (Figure 4.7);

- Scanning Electron Microscopy: intergranular cracking, which is a characteristic of brittle fracture mechanisms, including hydrogen-assisted cracking;

- Microstructural exam: non-homogenous material, with layers of ferrite and pearlite between martensite;

- Hardness testing (Rockwell C hardness test): large disparity in hardness from center to edge indicates that the material did not have *optimal through-tickness hardenability or was improperly heat-treated* (Figure 4.8);

- Tensile testing: the material meets yield strength, tensile strength and slightly above minimum elongation;

- Charpy V-Notch Impact testing: Low results, meaning lack of toughness;

- Chemical analysis: it meets the ASTM A354 BD requirements [45].

Despite the differences in failure rates on L1 and L2 rods, **only two samples of broken L1 rods were tested**, one each from Shear keys S1 and S2. Also, S1 had a 44% failure rate compared to the 23% rate of S2. Moreover, none of the unbroken 64 rods in Pier E2 shear keys were included in the samples for testing, which is a neglectful attitude since it is fairly simple to obtain samples from the top ends of these unbroken rods [43].

Furthermore, the TBPOC Committee enumerated some of the factors considered to be responsible for the shear keys failures:

- High hardness: values greater than 35 HRC;

- High ultimate strength: between 159-170 ksi, which is 20% greater than the 140 ksi minimum required strength;

- High tension levels: 70% minimum required ultimate tensile strength;

- Hot-dip galvanization;

- Additional heat treatment;

- Embedded rod detail exposure to environment: fabrication between June and September 2008 by Dyson and installation before the concrete pouring on December 5, 2008. They were embedded in the pier and **sitting in pipes for 5 years before they were tensioned, subjected to the environment and stagnant water.** During the 5 years, water was pumped out of the pipes.

Chung and Thomas (2013) highlight however that the Committee did not perform any testing to evaluate whether improper heat treatment was indeed the cause of heterogeneity in metallurgical

structure and lack of proper material properties. Indeed, this kind of rods (3in 4140 steel) cannot achieve uniformity on its cross section, because its *mass and chemical composition are not amenable for through-hardening*. Moreover, for the authors the 2nd heat treatment cannot *further harden* and strengthen the material any more than the 1st heat treatment that was done properly. In case the 1st was not done correctly and that is the cause for the 2nd treatment, the rod would have attained the right microstructure and hardness appropriate for the final tempering temperature used (would not have further hardened and strengthened the material) [43].

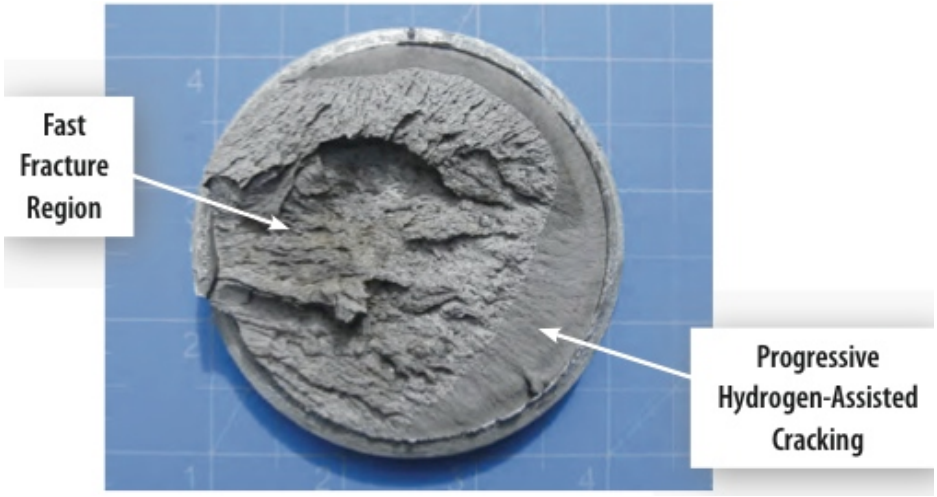

Fig. 4.7. – Facture surface of Shear Key S1 rod after cleaning [45].

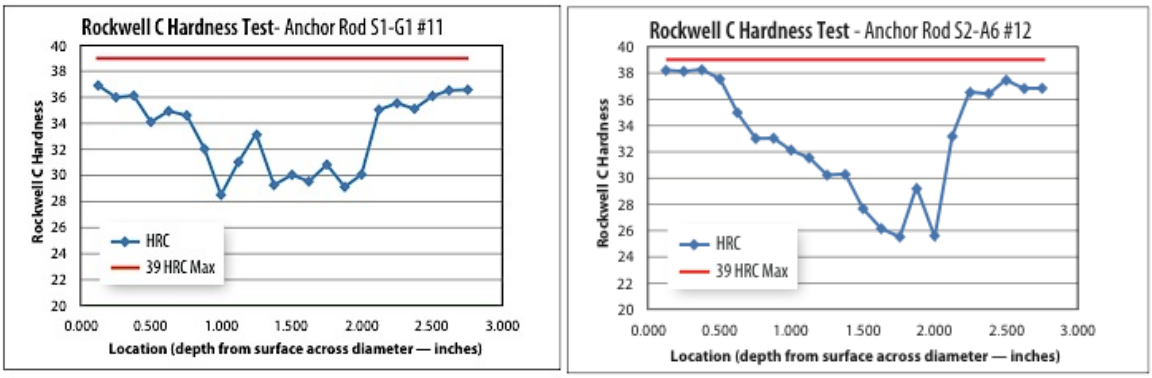

Fig. 4.8. – Rockwell C hardness test results from Shear Key S1 and S2 two samples [45].

Although, the TBPOC Committee concluded IHE (Internal Environmental Embrittlement) was the cause of the failure, the experts Chun and Thomas have a very different point of view. In their perspective, it is true the failures were a *short-term phenomenon* because they occurred within two weeks after tensioning (Figure 4.4). But nevertheless, it does not mean the hydrogen responsible for the cracks initiation and growth during those 2 weeks come from the rod manufacturing process. Indeed, **for the expert authors the cause of failure was EHE** (environmental hydrogen embrittlement) **and not IHE**. They give several main reasons:

- An IHE failure is not consistent with the fact all the 32 failures occurred on the bottom threads;

- The five years of environment exposure allowed *the bottom threads to be charged with hydrogen* [43];

- According to Brahimi et al (2009), lower hardness specimens in the range of 37 HRC are not embrittled by the galvanizing process. And since the surface hardness of the failed rods varies between 25 and 38 HRC, these rods are unlikely to have failed due to IHE [43];

- It is reasonable to expect more hydrogen can enter the steel from environments than from rod manufacturing processes [43].

Indeed, **the most important fact is the uniformity of the failures on the bottom threads**. IHE assumes the anchor rods were charged with hydrogen above a threshold during manufacturing processes such as acid pickling. And if so, the hydrogen concentration would have to be uniform throughout the rod length. Therefore, theoretically the probability of IHE failure occurring on top or bottom threads is 50%. Since this is an independent event, *the probability of the 32 anchor rods all failing in the bottom threads is less than one in four billion.* Lastly, it is possible that the bottom threads experienced longer periods of water exposure than the top ones, since they were enclosed inside the grout pipes for 5 years without protection, subjected to *stagnant water*. This way, the authors conclude that the hydrogen responsible for the failure had to have been introduced *after manufacturing or while* the rods were *inside the grout pipes* (unprotected) [43]

After the study of the failed 2008 rods in Pier E2, the TBPOC Committee report explored the **risk on the other 192 A354 grade BD anchor rods at Pier E2** fabricated in 2010 (Table 4.2 location #2). Testing was established in order to compare the 2008 failed rods to the 2010 ones. Monitored, time-dependent, in-situ tensioning test on the remaining 192 rods over a 30-day period was done, in order *to determine their susceptibility to hydrogen embrittlement*. The 2010 rods presented homogenous microstructure, improved toughness and more uniform hardness.

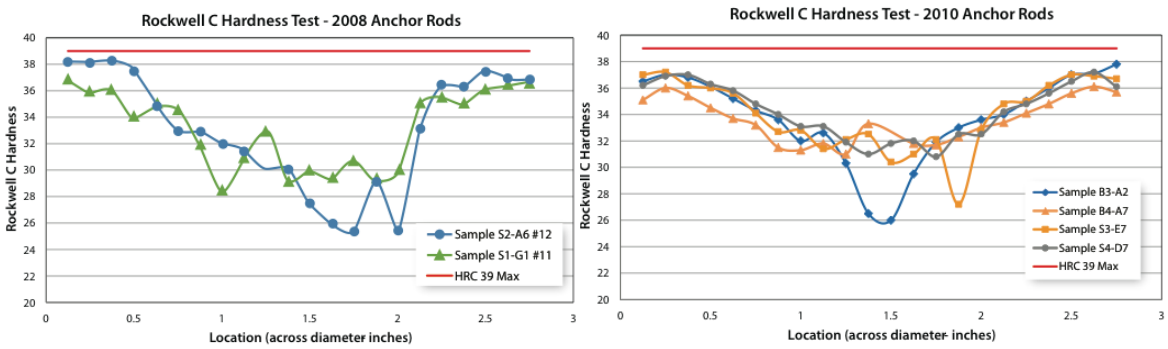

Fig. 4.9. – Hardness testing comparison between 2008 and 2010 samples, respectively, from Pier E2 [45].

505 Sample Tensile Test Results								
	2010 Samples				2008 Samples			
Identification	B3-A2	S4-D7	S3-E7	B4-A7	S2-A6 #12	S2-A6 #2	S1-G1 #11	Requirement
Yield Strength (ksi)	143	138	139	143.1	149	146	136	115 min.
Tensile Strength (ksi)	160	157	157	160.2	170	168	159	140 min.
Elongation in 2" Gage %	17.0	19.0	17.5	16.8	15.5	14.0	15.0	14 min.
Reduction of Area (%)	53.5	53.4	54.0	42.7	46.0	48.0	48.4	40 min.

Charpy V-Notch Impact Energy Test Results (ft-lb)											
	2010 Samples								2008 Samples		
Identification	B3-A2		S4-D7		S3-E7		B4-A7		S2-A6 #12	S2-A6 #2	S1-G1 #11
Temperature	40°F	70°F	40°F	70°F	40°F	70°F	40°F	70°F	70°F	70°F	70°F
Sample 1	35.5	37	37	37	38	38	39.5	39	18	15	13.5
Sample 2	38	38	37	38	37	37	36	39	18	14	13
Sample 3	37.0	38.0	37.5	37.0	37.0	37.0	37.5	37.0	17.0	15.0	14.0
Average	36.8	37.7	37.2	37.3	37.3	37.3	37.7	38.3	17.7	14.7	13.5

Fig. 4.10. – Reduced section tensile strength and Impact testing for 2008 and 2010 samples, respectively [45].

The material differences and the time that passed by since their tensioning were enough so that the TBPOC Committee decided the ***near-term risk of further hydrogen embrittlement in the rods of Pier E2 is low*** [45]. Nevertheless, the replacement after bridge opening was recommended for all the 2010 rods (740 of them in 4 different locations) even when considered far better than the 2008 rods. This decision derived from the FHWA review report and will be discussed later in this chapter.

After this failure, **the shear force strength of the shear keys needed to be restored**. The anchor rods installed could hardly be replaced, since they have been fully installed and embedded in the pier cap concrete and were aligned with the vertical columns. Also, the deck had been installed on top of the shear keys, limiting the access since the pier cap is heavily reinforced. Therefore, the resisting force must be restored in a different way that does not need the removal of the 2008 anchor rods.

Three potential options were taken into consideration by TBPOC: i) steel collar; ii) steel saddle and iii) removal and replacement of the anchor rods. The first option secures the plate of the shear key by using a steel brace that is anchored to the pier cap with anchor rods. These would be installed on either side of the cap. The second option secures the plate of the shear key with post-tensioning cables that extend to the sides of the pier cap. These cables would be enclosed in additional concrete casings on the sides of the pier cap (with minimal damage to the pier cap). The third option includes removing the shear keys so that broken and unbroken rods are replaced by post-tensioned cable anchors.

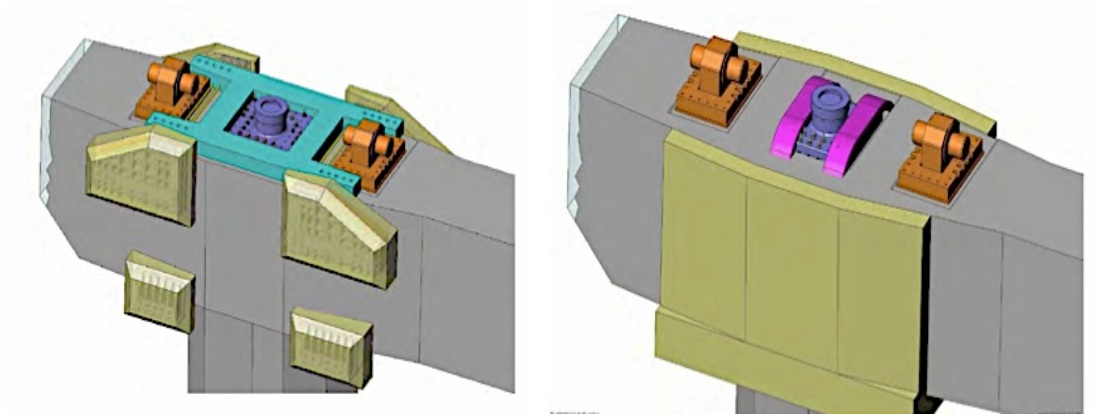

Fig. 4.11. – Solution 1 and 2 respectively for the Pier E2 failed shear keys [45].

Only option 1 and 2 presented by Caltrans bridge engineers were considered by TBPOC. Both options did not require removal of the Shear Keys S1 and S2. Nevertheless, option 2 would be less costly (10 million compared with 15 to 20 million dollars of Option 2), potentially easier to install and only requires a unique saddle system. The TBPOC chose **Option 2 as replacement** (Fig. 4.12). After its construction, this steel saddle solution ended up costing around 25 million dollars [45; 47].

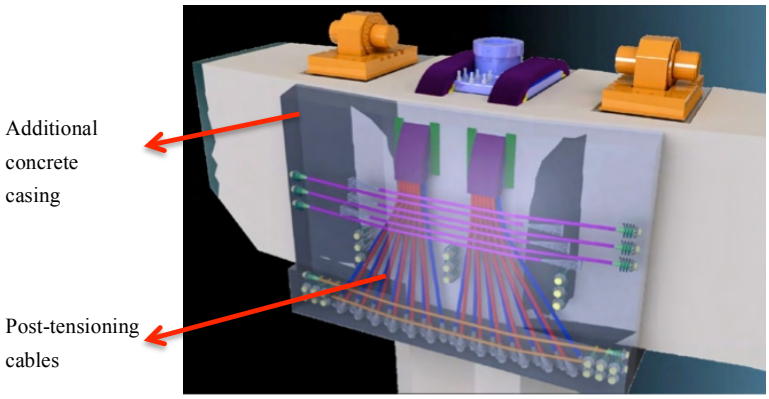

Fig. 4.12. – Detailed steel saddle solution for Shear key replacement (Option 2) [45].

4.1.1.2 Other SAS locations with A354 Grade BD

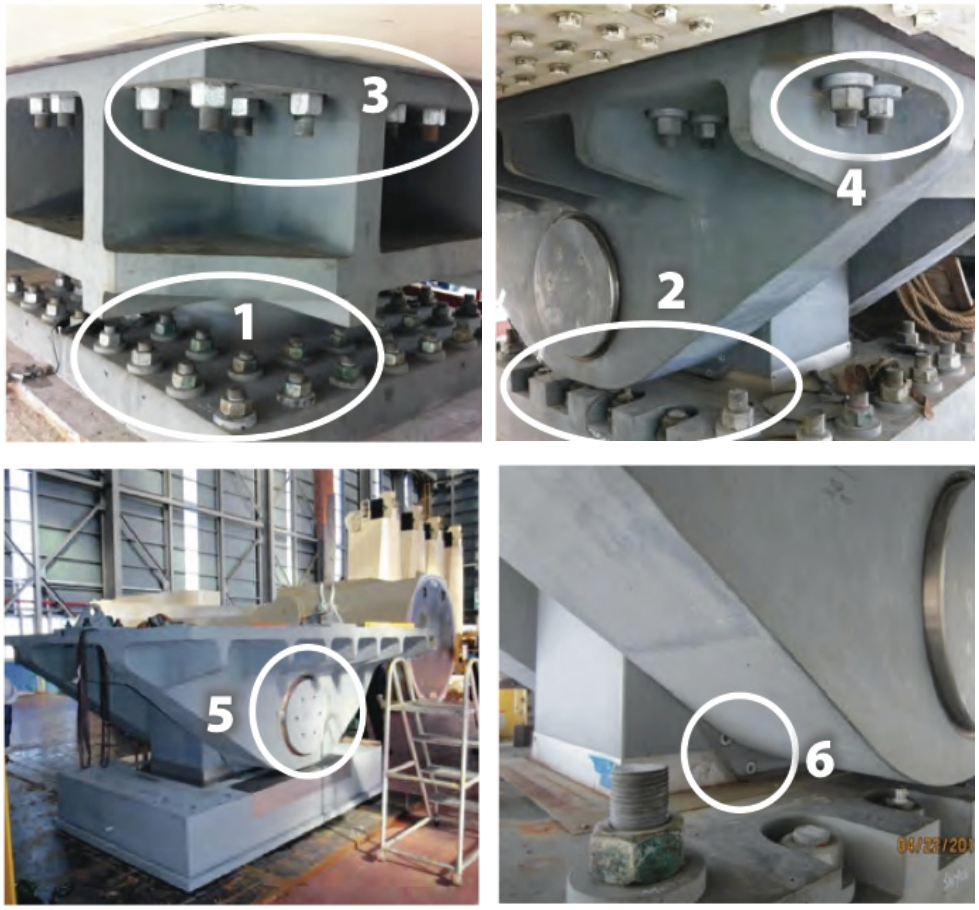

Fig. 4.13. – Location #1 to #6 of the A354 Grade BD threaded rods and bolts [45].

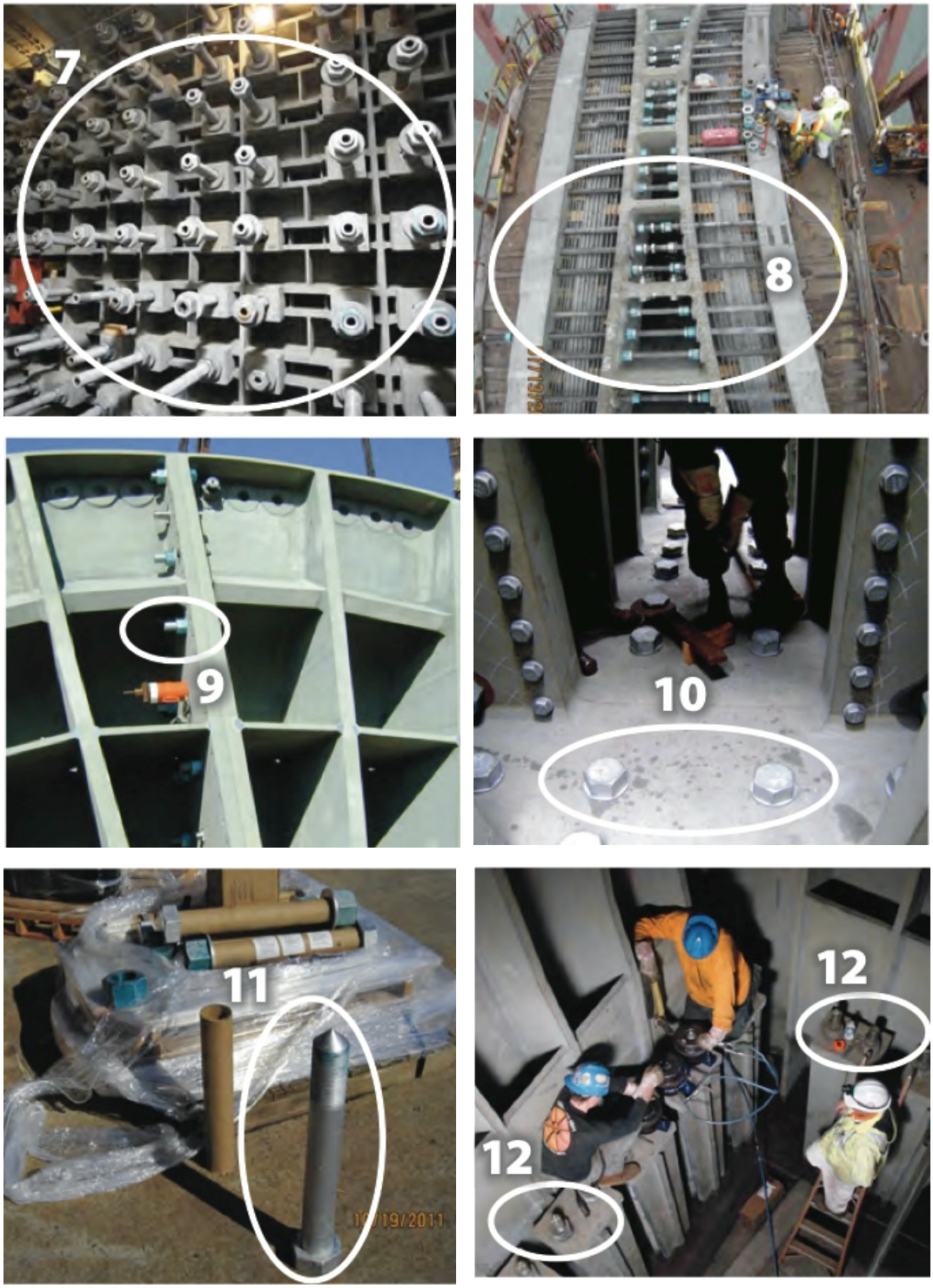

Fig. 4.14. – Location #7 to #12 of the A354 Grade BD threaded rods and bolts [45].

Fig. 4.15. – Location #15 to #17 of the A354 Grade BD threaded rods and bolts [45].

As shown in Table 4.2, there are 17 different locations where the A354 Grade BD hot-dipped galvanized bolts and rods were used. Above, Figures 4.13 to 4.15 show the fasteners on their locations, with the number of the location on the figure corresponding to those in Table 4.2 (#1 to #17).

After the failure of the A354 Grade BD rods at Pier E2 (Location #1), the question arose of what should be done to analyze **the risk at all other locations** containing this type of hot-dip galvanized bolts. According to TBPOC official report, to analyze the risk for hydrogen embrittlement (see section 4.1.1) **several tests were done**: i) Test I was an *in-situ hardness test* on all accessible A354 BD rods/bolts; ii) Test II was a *laboratory test* on a number of samples or spare rods in order to determine *hardness (Rockwell), toughness and chemical composition*; iii) Test III was a laboratory test of full-size rods extracted from Pier E2 bearings and shear keys, until their failure *to determine hardness, toughness, mechanical properties and chemical composition*; iv) Test IV was an *accelerated stress corrosion test* with samples from highly tensioned areas (70% specified minimum ultimate tensile strength) usually called *Townsend test*; v) Test V was a *laboratory test of reduced size specimens* to measure the resistance of the material to SCC.

The samples were selected and collected from some of the 17 locations containing A354 BD bolts and rods (Table 4.2). Nevertheless, according to the Official Report issued by TBPOC, bolts and rods at locations 5, 6 and 10 were not tested at all; at location 11 only Test III was done; at locations 9, 15, 16, 17 only Test I and II were done and location 13 only Test I, II, V were done. Moreover, many of the locations had only few samples tested in comparison to their total number, which means they might not be fully representative. Therefore, **the results cannot give a fully global guarantee** about the safety of all A354 BD locations on the SAS span.

Tests I, II and III were completed on June 21, 2013 and the results verified the mechanical properties of the rods according to the TBPOC. Results for Tests IV and V were not documented at the TBPOC official report, since they took longer to be completed. For Test IV (Townsend test), the plan is to use the 2013 new replacement anchor rods to build the KI_{SCC}-HRC curve. Results from Test IV *will create the graphical curve per Townsend's research based on the ASTM A354 BD rods* to input on the properties of the SAS Bridge A354BD (Figure 6.16). ***Rods that are to the right of the Townsend's curve are considered susceptible to SCC*, according to TBPOC.** Fig. 4.17 presents a KI_{SCC}-HRC curve from Townsend study, with the bottom curve typical of galvanized steel.

To facilitate the understanding of the abovementioned graphs, KI (or K) is the stress intensity and varies according to the stress σ or the pretension levels in the rods, whereas KI_{SCC} is the fracture toughness, a material property, like yield strength, that is unaffected by stress. It should be highlighted that this distinction is not properly done in TBPOC official report.

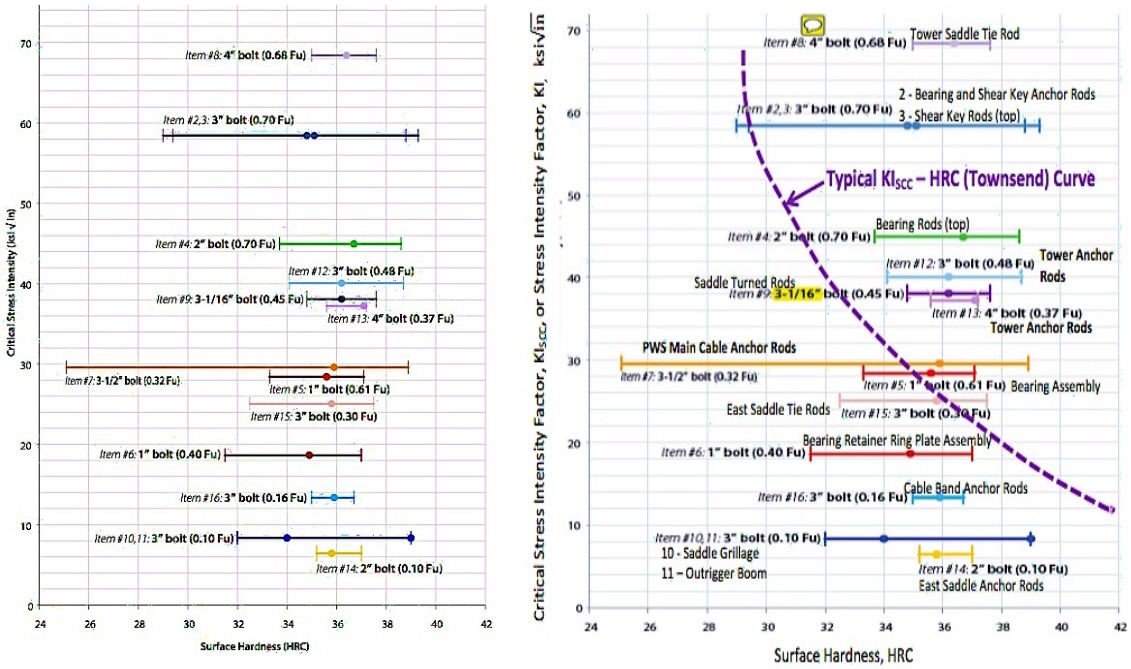

Fig. 4.16. –TBPOC KI-HRC graph from testing (left) and the same overlapped with a typical KI_{SCC}-HRC curve [45; 44].

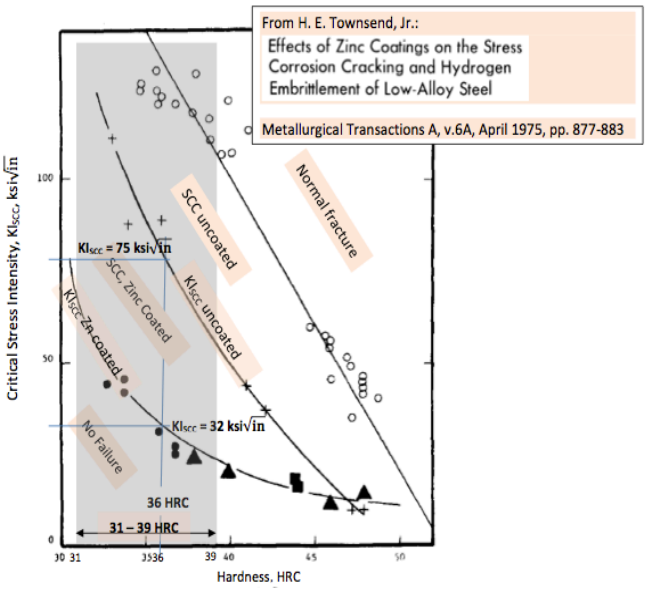

Fig. 4.17. –KI_{SCC}-HRC curve from Townsend study [44].

However, the experts Chung and Thomas state that ***the Townsend Test is not what TBPOC wants the public to believe***. It cannot solve all the problems of "long-term stress corrosion cracking", but only determine KI_{SCC} or σ_{SCC} for the particular specimens tested. It might be useful to determine a threshold stress for avoiding SCC (EHE) combined with more data. But, KI_{SCC} should not be used to predict during service the SCC phenomenon and its timing. One of the reasons accelerated tests such as Townsend cannot be completely successful in simulating the actual environmental corrosion is that the phenomenon may vary from years to decades, because it has many factors involved [43]. Furthermore, these authors state that the TBPOC-Caltrans testing rigs are probably *one of a kind*, since testing using 3in diameter full-size rods has never been performed. Besides being expensive, for most threaded fasteners the ASTM F1624 for small specimens can do almost everything as the Townsend KI_{SCC} testing. The exception would be on anchor rods from two locations: PWS anchorage (#7) and the Tower base (#12, #13). The special metallurgical conditions of these rods can bring problems not foreseen by TBPOC and will be discussed later [44].

As far as Hydrogen embrittlement is concerned, by the time the Official Report was issued, the TBPOC committee considered that since the remaining 2018 bolts/rods have not failed so far (from 91 to 1429 days since tensioning) and HE is a *time-dependent phenomenon*, these bolts/rods have *low risk of hydrogen embrittlement.* Moreover, facing the testing results (I, II, III), the Committee concluded the other bolts/rods have *low risk of near-term hydrogen embrittlement failures because the rods exhibit better metallurgical uniformity and improved toughness as compared to the failed 2008 rods. In regard to longer-term stress corrosion cracking, there are a number of rods that exhibit surface hardness that is in excess of 35HRC, a point at which there is increased risk of stress corrosion cracking under sustained high tension. However, based on the tests these rods also exhibit better metallurgical uniformity and improved toughness. Further, many of the remaining rods are not subject to high sustained tension levels or are located in dehumidified or sealed areas that provided additional corrosion protection* [45]. The Committee also stated *that it is safe to open the new East Span after replacing the capacity lost by the failed 2008 rods. It is unnecessary to replace any of the remaining rods (Items #2 through #17) before the bridge opening since the risk of near-term hydrogen*

embrittlement has passed, and especially in light of the safety imperative of moving traffic off the seismically deficient existing East Span Bridge. ***While some rods are highly susceptible to longer-term stress corrosion cracking, ample evidence exists that none are at high risk of near-term fracture.***

First of all, the fact that time should not be considered a validation of safety or even a distinguishing factor between types of HE as already been discussed previously. Secondly, the team of experts Chung and Thomas disregard the low Notch toughness as a cause of susceptibility to HE and even more to the failure at Pier E2, since there is no metallurgical evidence of it. Indeed, the authors present examples of high toughness materials that are HE susceptible, as well as the opinion of other experts supporting the fact that high toughness alone will not protect high strength bolts from stress corrosion cracking (EHE). Moreover, it should be highlighted that only 5 out of the 17 locations are dehumidified (Tables 4.2 and 4.3).

According to TBPOC, after analyzing the data and gathering findings and conclusions, in case of susceptibility to SCC if tension and exposure to corrosion can be reduced, 2 options were proposed: reduce tension or improve corrosion protection, including dehumidification. If these measures cannot be applied, replacement before bridge opening is suggested. The Committee resolutions are shown in Table 4.3 for the rods/bolts at all locations enumerated on Table 4.2 (17 in total) [45].

Table 4.3. – Rod-by-rod resolution according to TBPOC Committee [45].

	Construction		Maintenance		
Location	**Replace Before opening**	**Replace After opening**	**Reduce Tension**	**Increase dehumidification**	**Accept and Monitor**
Pier E2	#1 (Replace by steel saddle retrofit)	#2 #3 #4	-	-	#5 #6
Anchorage	-	-	-	#7*	-
Top of Tower	-	#11	#8* ; #9*	-	#10
Bottom of Tower	-	-	#12* ; #13*	-	-
East Saddle	-	-	-	-	#14 ; #15
East Cable	-	-	-	-	#16
Pier W2	-	-	-	-	#17

* Already dehumidified locations.

Furthermore, TBPOC asked for the FHWA review of their official report, such as of the findings, decisions and other test data. The FHWA was in full agreement with the official report, with no recommendations for error correction, test data or its interpretations validation. Moreover, the decision

for the replacement of the 740 rods from 2010 was backed by FHWA with the additional suggestion of their Greg Assessment Tool *to determine vulnerability to HE or SCC*. This way, the authors Chung and Thomas, not only criticize the lack of justification for the replacement of all the rods, but also point out a *serious problem in the application of this FHWA Tool for high strength steel anchor rods.* The authors go further and recommend no decisions related to the disposition of the ASTM A354 BD rods be done based on the FHWA Greg Assessment Tool [43].

4.1.2 CABLE

As far as the A354 Grade BD rods are concerned, the authors Chung and Thomas believe the TBPOC report left **serious questions unanswered, relating to the specific metallurgical conditions of the main cable anchor rods**. As a matter of fact, these anchor rods are ***facture-critical***, which means their failure can cause the collapse of the entire structure. Therefore, they issued a supplementary report, specifically for the problems at both the main cable and tower base anchor rods [44].

These main cable anchor rods are located inside the splay chamber at East side Deck anchorage (Location #7) and can be named PWS (parallel wire strand). There are 274 of them in total, 217 of them with rolled threads and 55 with cut threads. Their initial tensioning level is 30% of the minimum specified ultimate tensile strength (Table 4.2). The TBPOC resolution for this A354 BD location was dehumidification (Table 4.3), but Chung and Thomas recommend the splay chamber be made air tight and not only water tight as recommended by TBPOC.

The threads were executed with cold rolling of steel bars (previously heat treated to high hardness, such as 38 HRC), which altered the microstructure of the surface layer (0,1-0,15in surface) and increased its hardness. This alteration together with the high hardness of the fastener has been unknown to effects on the HE susceptibility. Therefore, the authors believe the KI_{SCC} values for the rolled threads rods of PWS may be very different from rods at other locations and recommend that the KI_{SCC} be obtained specifically for these PWS rods. Indeed, if all locations could be represented by a single KI_{SCC} curve that might as well be taken from previous studies and literature. This specific curve would either support the current resolution for dehumidification or the need for further evaluation. The PSW anchor rods with cold rolled threads might be more susceptible to HE than any of the other 740 rods the TBPOC advised to replace.

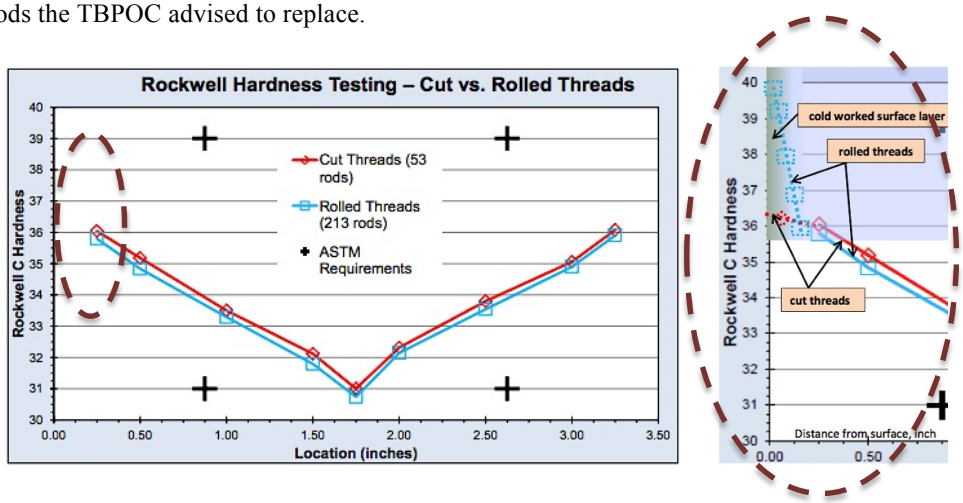

Fig. 4.18. –Comparison of HRC for cut and rolled threads and the scenario at the surface for cut and rolled threads, respectively [48; 44].

Figure 4.18 shows one of the test result presented by TBPOC. The image to the left is a test plot of the Rockwell hardness and might mislead to the conclusion that cut and rolled threads have the same hardness. Nevertheless, the most important piece of information is missing, which is the surface hardness (0,25in to surface). Indeed, Figure 4.18 also contains a typical plot of cut and rolled thread surface hardness (image at the right), showing how differently can the HRC hardness be in both cases. As discussed before, the cold rolling process alters the microstructure at the surface and hardens it further. Since it is known that the higher the hardness, the higher the HE susceptibility, the cold rolled thread rods might be more susceptible to HE. But this effect is still unknown, as there are *no laboratory test or field performance data on the HE cracking susceptibility of anchor rods with cold rolled threads.*

Furthermore, for the Test IV (Townsend) performed by Caltrans, 4 samples of rods from location #7 were used. These samples comprised 2 cut threads and 2 rolled threads, which were probably randomly chose (no concern so far about the hardness surface study of rolled threads). Also, the saddle tie rods at Location #8 have cold rolled threads and only one sample was used for Test IV.

Therefore, Chung and Thomas go further and state that *the main purpose and benefits of the (above) Townsend KI_{SCC} test rig should have been to determine the KI_{SCC} or (σ_{SCC}) for the PWS anchor rods with cold rolled threads.* For cut threads with adequate metallurgical conditions, a Townsend curve (KI_{SCC} – HRC) can be estimated by previous studies and literature [44].

4.1.3 TOWER

4.1.3.1 Top Saddle

Rolled threaded A354 BD rods were previously discussed in Chapter 4.1.2 (Cable). Nevertheless, there are other locations where this type of rods exists, such as the 4in-diameter (100mm) saddle tie rods (#8). However, instead of presenting high hardness at the rod surface, these tie rods have M-shaped hardness distribution [48]. This distribution can be due to insufficient tempering, causing higher residual stresses and, consequently contribute to a higher HE susceptibility.

These effects are equally present at Locations #12 and #13 and will be explained with more detail in the following chapter (see section 4.1.3.2).

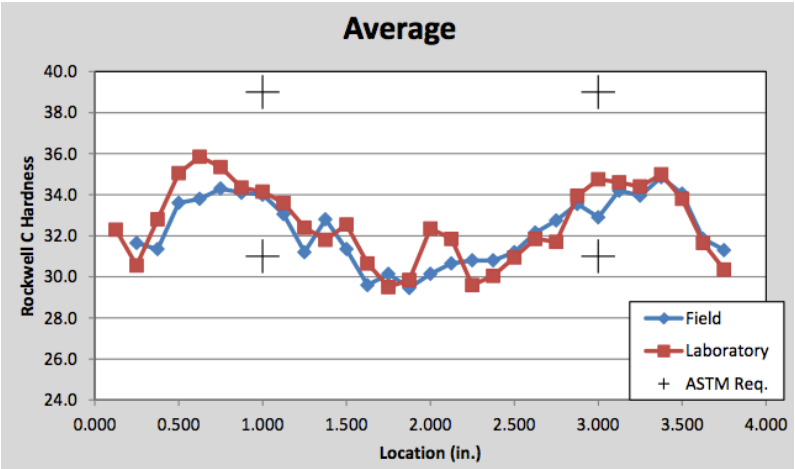

Fig. 4.19. –Average Rockwell hardness distribution for location #18, respectively [48].

4.1.3.2. Base

At the base of the tower 3 and 4-inch (75 and 100mm) A354 BD anchor rods are used to secure it to the foundation. According to Table 4.2, these rods corresponds to location #12 and #13, which means Anchor rods Type 1 and 2. There are 388 Type 1 anchor rods with 3in diameter and 36 Type 2 anchor rods with 4in diameter. According to the TBPOC testing results for this location [48], both Type 1 and 2 rods have M-shaped hardness distribution across their cross section (Figure 4.20). The M-shaped distribution implies the maximum hardness (40 HRC, for instance) occurs around 1/2in from the surface of the rod. The typical distribution of properly heat-treated rods is V-shaped, which means the lowest hardness occurs inside the rod core (Figure 4.18). Therefore, this might be due to insufficient tempering of these rods that can lead to higher residual stress, once these did not get properly reduced after hardening. Despite these relevant facts, the official TBPOC report does not address them. Chung and Thomas even state that (TBPOC-Caltrans) need to provide a metallurgical explanation as to why the tower base anchor rods have M-shaped hardness distribution curves and what their effects on HE susceptibility might be [44]. This because the tensile stresses that cause SCC (or EHE) include the residual stresses and therefore, its effect should not be ignored.

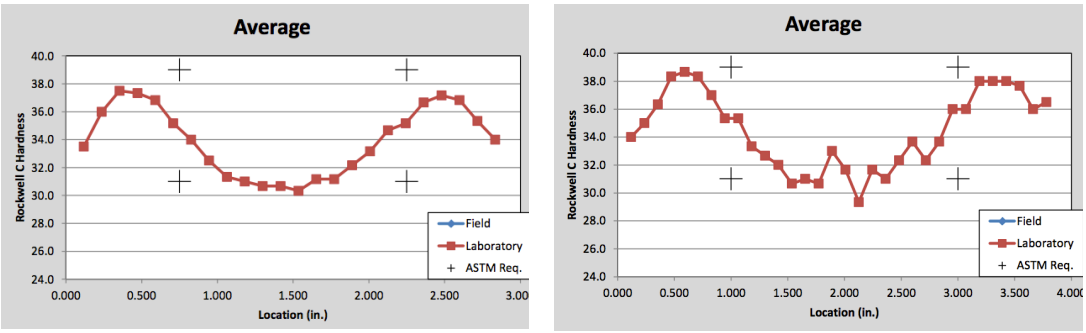

Fig. 4.20. –Average Rockwell hardness distribution for locations #12 and #13, respectively [48].

This peculiar effects all together make these anchor rod locations unsuitable for using KI_{SCC} data from literature, small sample testing or testing from other SAS span locations.

It should also be highlighted that the resolution given by TBPOC for these locations #12 and #13 was the reduction of tension. Nevertheless, the initial tension at these anchor rods was already low: 48% and 37%, respectively. For all the abovementioned factors, this decision should be reevaluated because it might not be enough to prevent these bolts from HE. The decision has to take into consideration the critical location of these rods: like the PWS anchor rods, their failure might imply the failure of the entire SAS span.

Moreover, there are other construction issues related to the tower base connection. Indeed, on a May 29, 2013 TBPOC briefing it was revealed that inspectors had found imperfections at electroslag welds at the tower base, on a process that had been enduring for 9 months. However, engineers were mapping these welds that needed to be removed and replaced by quality weld material. These welds have to ensure the 1500-year seismic demand capacities [49].

4.1.3.3. Composite piles

Furthermore, the tower piles were the center of a controversy between Caltrans and Sacramento Bee newspaper after the investigation of the newspaper into inspection and construction diaries revealed poor quality concrete used in the piles of the main tower.

Kiewit-FCI-Manson joint venture was responsible for the 177$ million foundation contract. Among the findings, Pile 3 and 8 out of 13 piles have *suspect and inadequately tested concrete.* Indeed, for Pile 3 the sonic-wave test revealed a 19-foot section that had not hardened to the required strength when tested and that was not retested. Experts were contacted at the time of the investigation and the way the testing program was conducted and the results was said to raise serious issues with respect to the quality of the concrete. Indeed, the absence of sonic data for Pile 8 and the fact the location of the concrete problem in Pile 3 (towards the top) is where the most significant loads during an earthquake are. Nevertheless, a deep-foundation expert stated that the pile foundations for that structure are highly redundant because a structural defect in one or two of them would not really be a *game changer*.

4.1.4. SUPERSTRUCTURE

4.1.4.1. Steel Orthotropic Deck

Zhenhua Heavy Industries in Shangai fabricated the segments of the steel orthotropic deck. These enormous segments are **linked by welded connections**. The problem was that when the segments arrived at the Bay Area and were put in place on the west side of the Self-anchored span, the sections did not fit each other properly. The sections lined up properly when laid on the factory floor in China, however once they arrived and were bolted together for use in the span they no longer fit in the same way. This phenomenon was explained by Ted Hall (consultant working on the project) as a *very simple mistake*. The method used in China to assemble the steel sections did not account for their behavior when suspended on the bridge and subjected to their own self-weight for instance. Some of the misalignment is of 6mm (half the thickness of the steel plate to be joined). Caltrans rules forbid bridge decks from being joined together if they are off by more than approximately 3mm, because of the increased stress that is created in the welds at the joint. Brian Maroney (Caltrans chief engineer on the project) said that the builders could use a less strict standard (AASHTO) instead of the state of California guidelines.

Moreover, hundreds of Chinese fabricator's welds on the steel sections were cracked and had to be repaired. Nevertheless, the welds used to link the several sections together were made on-site at the Bay Bridge by the US contractor. For the former, the issue was not the welds themselves, but the role they played in linking the misaligned sections of the span. As far as this problem is concerned, several experts expressed the opinion that Caltrans decision to accept the nonstandard connections could undermine a key feature of the self-anchored span – its ability to open to traffic soon after a major seismic event (lifeline structure). Moreover, Professor Bob Bea said that *this span is not robust to begin with* and that one *can't predict exactly how the bridge could fail, but with this issue there is a high likelihood of trouble in its ability to serve as a lifeline structure.* He goes further and says this connection issue shows the bridge has been built to the edge of safety margins and that *all of these decisions lead to an erosion of your margin of quality, a factor of safety.* In Professor Bea's opinion what they have done is *rationalized the acceptance of excessive fatigue damage at these locations* which for a lifeline bridge is a maintenance nightmare. Also, Professor Abolhassan Astaneh noted that bridge builders have kept at the welded connections the steel backing bars that are normally used only temporarily to keep molten metal from falling through during welding. The bars are angled to account

for height differences between deck sections. The Professor also states these backup bars being left in place on Southern California steel structures contributed to cracks and failures during the 1994 Northridge earthquake.

Also, Marwan Nader the lead engineer designer of the new East span of the Bay Bridge said the welds used to hold the steel deck sections that do not fit properly are vulnerable to fatigue damage in a major earthquake. Moreover, welds on almost half the eastbound deck and a quarter of the westbound deck have most likely to have excessive stresses that do not match Caltrans standards. Checking these welded areas as the years go by will prove difficult since the steel backing bars were left in place under the welds. Nevertheless, Brian Maroney responded that some damage is inevitable and manageable in a major earthquake and that it would not have long-term effects on the bridge's ability to carry traffic. Moreover, Caltrans considers the risk of cracking remote and that the choice for nonstandard welding had to be balanced between cost and potential complications of trying to repair the misaligned sections [50; 51].

An official briefing report from the TBPOC refers problems with the welds quality. In 2008 there were cracks found in the welds of the deck plates in China, but according to the TBPOC more testing was performed and the cracks were repaired. Also, between 2008 and 2010 *field welding of deck segments in the Bay was not achieving required tolerances for planar alignment* and more repairs were made [49].

Besides the welding issues, **water leaks were found inside** the steel orthotropic deck. These leaks were identified first on the four guardrails (two on each deck) of the new self-anchored span. Testing indicates the system designed to keep rainwater from seeping inside the guardrails is failing and contributing to hundreds of leaks that could put the bridge at risk of corrosion. Indeed, more than 900 leaks have been identified during recent storms. For this issue, Brian Maroney said that the bridge was designed to be water-resistant not watertight. After more testing was performed, the 1st test showed that when the water was poured against service-access panels on the guardrails, it soon dripped into the hollow guardrail and gathered at the bottom. After pooling at the bottom, water went through the bolt holes were the guardrails are connected to the steel orthotropic deck. At one location not tested for leaks, the inspectors removed one of the access panels and found no waterproof caulking had been applied as required by contract. The lack of caulking allows the water to seep inside the road guardrail and leak into the deck. In a second location, leaks occurred inside the steel orthotropic deck after an hour. At another location tested, storm conditions were created with wind and water. With this condition, small droplets of water made their way through the base of the guardrail after 5 minutes [53]. Original construction plans defined the guardrails laid in a continuous line of caulk, but with Caltrans permission the contractor American Bridge/Fluor decided instead to lay the guardrails on top of the steel and apply the caulk along the outside [52]. Nevertheless, after the water is inside the guardrails it leaks into the steel orthotropic deck through the holes drilled in the deck top plate for bolt connection. The guardrails at the SAS span are made of steel, while on all other locations they are made of concrete. This measure was used to decrease the weight applied to the structure. See Fig. 4.21 with the official project drawing of the connection between deck and guardrail. The caulking is evidently not stopping the water from infiltrating through the bolted connection holes, as it was supposed to be.

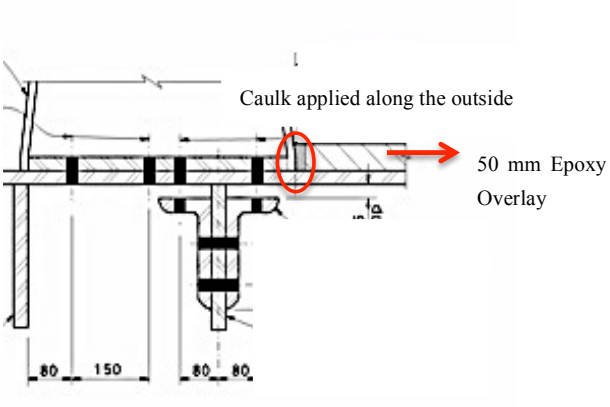

Fig. 4.21 – Connection between guardrail and steel orthotropic deck top plate *[Ref.: Caltrans drawings 638/1204].*

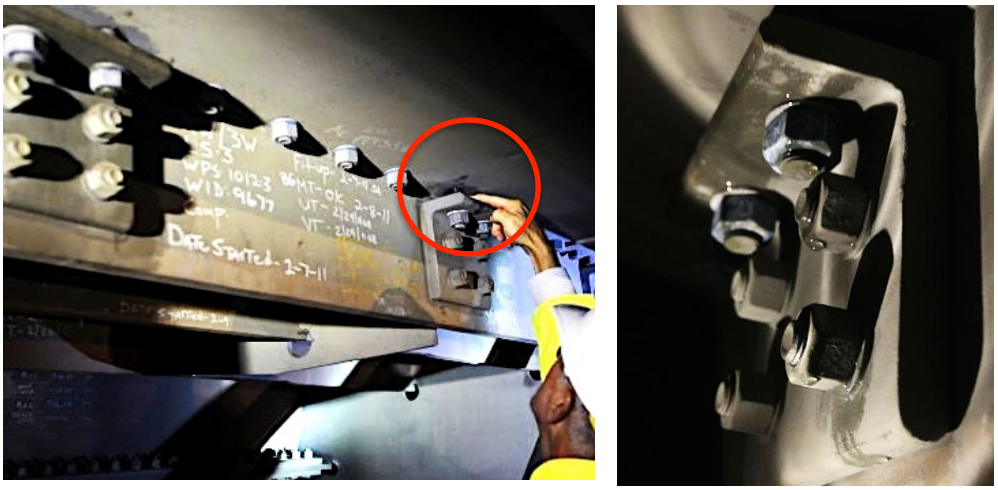

Fig. 4.22. –Water leak inside the deck on the guardrail bolted connection [52].

Moreover, during a guided tour inside the deck signs of corrosion were photographed, such as patches of brown sludge and white powdery residues that had formed where the water was visibly leaking.

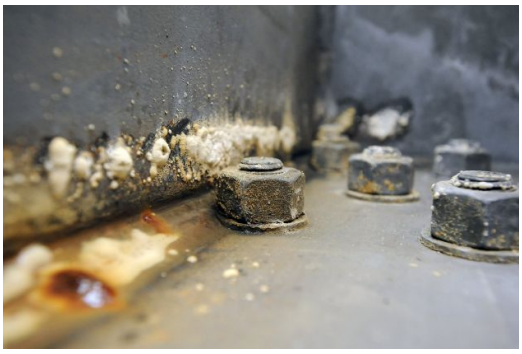

Fig. 4.23 –Corrosion signs inside the deck [52].

Experts note that the white powder can be a result of the failure of zinc-based coating that protects the steel and if that is the case, the brown sludge is probably corrosion of the steel structure itself. For this to be certain, testing would need to be performed [52].

Another issue with the deck occurred at the **Bike path connection**. According to an official TBPOC report, while removing divider rails to make electrical and shimming modifications, it was observed that some bolts connecting the rails to the deck had been sheared. The cause was most likely by *thermal movement of the deck.* The bolted connection was restrained from thermal expansion/contraction due to an oversized weld of architectural bolts caps to the base plate. To solve the problem, all divider panel bolts were removed, railings modified with larger slotted bolt holes in the base plate and bolt caps were eliminated. It was estimated that 10% of over 2000 divider bolts had this problem.

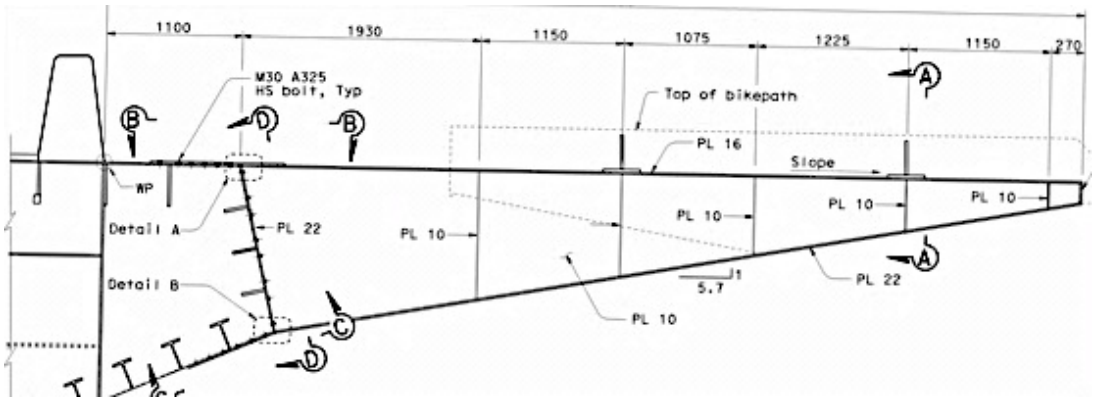

Fig. 4.24 –Connection between bike path and steel orthotropic deck [*Ref.: Caltrans drawings 826/1204].*

4.1.4.2. Skyway

The East Bay Bridge is comprised not only by the self-anchored span, but also by the precast pre-tensioned segmental concrete skyway structure. These precast concrete segments are completed with post-tension prestress tendons to avoid cracking. According to the study of official inspection records [54] from the construction site of the new East SAS span of the Bay Bridge, Caltrans inspectors found water leaking through damaged vents that led into tendon ducts. During past few decades, prestressing is commonly used and so the tendon corrosion is a well-known phenomenon. For that reason, there are federal and state rules intended to ensure that salt water or moist air cannot enter tendon ducts. In addiction, the construction contract requires grouting of ducts within 10 days of the tendon installation or 30 days if the builder blows a rust-inhibiting powder into the ducts.

Nevertheless, according to a November 2004 inspection diary many of the tendons found ungrouted and exposed to water had been installed around 2 months before. Indeed, the inspector states (…) *I noticed that the top of the grout injection/vent hoses were not sealed against the rain (...). Inspected all the hoses and found many instances where it was obvious that rain water was already in the ducts with the prestressed tendons. (...) I duct taped over the tops of the tubes myself for one hour.* Six months later, the same inspector (Rubalcaba) would report damaged grout vents along a 1/3 of mile of the bridge roadway.

After many months, the problem was recognized and vents had been leaking over a considerable length of the bridge. First, 18 tendons inside ducts were inspected by means of a borescope (camera in flexible tube). The worst cases were left ungrouted for nearly 14 months and showed signs of rust and formation of pits. Some strands were removed, tested and deemed as *moderately* corroded by Caltrans experts. In the end, Caltrans examined 1600 out of 5600 tendons, which was said to be 80% of the ungrouted (still accessible) tendons inside ducts.

Professor Sagués stated in a assessment for Caltrans that *uncertainty remains* because direct inspection was not possible in most tendons of the Eastbound bridge (2 parallel road decks). This inspection was not possible because most of the Eastbound ducts had been grouted by the time the problem was identified. However, Caltrans decided those would not be in worst state than the ones tested for the Westbound, since they were grouted earlier.

One of the causes for the long delays in grouting was that grout migrated between ducts through leaks at joints of concrete segments. Leaking grout ended up blocking adjacent ducts and preventing other tendons from installation. This way, in each skyway section, tendons for all adjacent ducts had to be installed and tensioned before any could be grouted (lead to long delays).

Furthermore, Thomas Janssen (Kiewit Corp. builder spokesman) stated that the company protected the tendons with Vapor Phase Inhibitor Powder. But records show the company applied the inhibitor in only one in four ducts. Moreover, the bridge concrete segments contain ducts for additional tendons [54].

These corrosion issues at the tendons represent not only lack of quality, but also possible difficulty for the East Bay Bridge to behave as a lifeline structure in case of a major seismic event.

After this discovery, an official report from the TBPOC committee states that the leaking of the grout between ducts is the main cause for delays. Also, it is recognized that rain water entered the vents and partially filled the prestressing ducts with tendons causing some steel corrosion. The committee states that after additional inspection and lab testing, the steel was *within tolerance for successful use* [49].

4.1.5. WEST SIDE (W2)

Due to the self-anchored system, the West side had to include a very rigid connection, as well as a uplift of the concrete columns due to the asymmetry between spans. To avoid damage to the concrete columns, a tie-down system was designed. The tie-down cable system does not include A354 BD bolts, but only Grade BC ones. Once again the suspension bridge system implies a complex and maybe problematic solution, due to an uncommon force distribution. On a TBPOC report about construction challenges, the deck connection between SAS suspension bridge and Yerba Buena was referred as an issue. The Yerba Buena transition concrete deck was a few centimeters higher than the SAS bridge deck. This added elevation was due to over pulling of imbedded pre-stress tendons. After considering several options, a steel ballast was decided to solve the situation [49]. Nevertheless, it increases the mass of the structure and seismic response.

5
FINITE-ELEMENT MODELS

5.1 INTRODUCTION

After a detailed study of the East Bay Bridge structure, a 3D finite-element model is used to analyze in detail the response of the structure due to exterior loads and displacements. The model was developed mostly by University of California Berkeley's Professor Astaneh and his students and researchers, using SAP2000 software and intends to replicate the existing structure as best as possible. The author studied the model geometry, elements definition and properties, materials, boundary conditions, nonlinear behavior, loading and the assumptions/simplifications made, in order to check and make necessary changes or improvements. Although there are more powerful finite element software available, SAP2000 proves to have adequate accuracy and computational effort for this study. Further studies can eventually use ANSYS for local models and greater accuracy.

One of the main purposes of the present study is to compare the behavior of two different systems: self-anchored suspension bridge (SAS) and ground-anchored suspension bridge (GAS). Therefore, the existing Self-anchored model will undergo changes related to its restraints, in order to behave as if the cable is externally anchored. Firstly, the original geometry will remain mostly unaltered, so that a reasonable comparison between models can be made and allow further comparative conclusions about their advantages and disadvantages. Afterwards, the author developed two different Ground-anchored models from the study of previous results (iterative designing process). In the end, the author develops three different Ground-Anchored models.

For these models, the prestressing forces at the suspenders will not be introduced. These *target forces* are obtained from the Gravity analysis (iteratively) for the load combination and intend to invert the effect of the loads on the deformed shape of the deck. For the purpose of this study, the initial deformed shape of the deck is of interest, since it allows the comparative study between different systems. For the next phase of design, it would be necessary to introduce this prestress on the suspenders. Nevertheless, these suspenders' forces influence the nonlinear analysis results.

Furthermore, a 3D model is necessary because the *interaction between the response in the orthogonal bridge directions and the variation of axial loads in column bents throughout the analysis are captured more accurately* [55] and only this way we can correctly evaluate the capacity and ductility.

5.2 GROUND MOTION AND MULTIPLE-SUPPORT EXCITATIONS

The vibrations initially obtained for seismic design of structures are *rock motions*. With them it is possible to calculate the maximum seismic forces on the structure and design it accordingly. Movements in the earthquake faults cause these vibrations, which travel through the bedrock layer. Depending on the structure's relative location and historical, geotechnical site data, there can be developed different rock motions. When these rock motions propagate through other soil layers, they become *ground motions* and there is a difference between them. *Ground motions caused by the same rock motions will vary due to soil conditions.* That is the reason why, for a long crossing like East Bay Bridge, there are different ground motions for different supports. Moreover, for designers it poses a challenge that rock motion frequencies from future earthquakes cannot be anticipated. This way, it is assumed that rock motions are strong over a broad range of frequencies (even if its not realistic). There are two methods to estimate the major rock motion for a structure: Maximum Credible Event (MCE), used by Caltrans *in the past* and Safety evaluation earthquake (SEE). The MCE is the largest earthquake that a fault can origin, without considering how often it may occur (return period). For the East Bay Bridge SAS project, Caltrans used a SEE, which is an earthquake that generates the largest motions expected to occur in 1500 years (return period). For the East Bay Bridge span, since it has a 150-year service life, it means a 10% probability of occurrence [56].

A Seismic Ground Motion Ad Hoc Committee helped with the ground motions criteria for this project. As a matter of fact, they recommended the probabilistic approach for defining the Bay Bridge Safety Evaluation earthquake (SEE). This committee had four members: Professor Bruce Bolt, Dr. Norman Abrahamson, Dr. Richard Borcherdt and Dr. Joseph Penzien. For the definition of ground motion, the **dominant sources are San Andreas (M=7.8) and Hayward (M=7.0) faults**, due to their high activity and proximity to the structure. Nevertheless, some other active faults were taken into consideration for the hazard analysis, such as San Gregorio, Rogers Creek or Calaveras. **Six sets of multi-support ground motions (3 for San Andreas and 3 for Hayward fault) were developed for a SEE** and used to do structural analysis, since the character of the motions is very different from one support to the other. The Ad Hoc Committee recommended that the initial time histories should be **based on empirical recordings** and not synthetic recording, when adequate empirical data is available. Moreover, since the Bridge is a **long-period structure it becomes *essential* to characterize long-period motion.** For that purpose, **rock motion attenuation relations** including strong motion records from recent earthquakes such as the 1989 Loma Prieta, the 1994 Northridge and the 1996 Kobe were used [57].

The bridge is designed to provide full service almost immediately after a Safety Evaluation Earthquake, as well as suffer repairable[10] damage. The bridge is also designed to provide full service immediately after a Functional evaluation earthquake and with minor[11] damage to the structure.

A report by the Army Corps of Engineers (ACOE) concluded that *the performance of the replacement bridge during a Maximum Credible Earthquake cannot be determined. The bridge has not been evaluated or designed for a MCE event, which is larger than the SEE event.*

The 30 percent type-selection design phase was based on a set of ground motions and ARS design criteria developed for the retrofit of the existing East Bay Bridge (by the Office of Structural

[10] Repairable damage: can be repaired with low risk of losing its function, such as yielding of reinforcement, spalling of concrete cover and limited yielding of structural steel.

[11] Minor damage: elastic performance with some less relevant inelastic performance, such as narrow cracking in concrete, no apparent permanent deformations, and damage to expansion joints.

Foundation of Caltrans). To include new data, a join venture between Fugro and Earth Mechanics elaborated a ground motions report for the design of the San Francisco-Oakland Bay Bridge replacement. It included new ground motions and ARS (acceleration response spectrum) criteria and was divided in two phases: i) provide *ARS criteria to allow initial design and sizing of the components by response spectrum approach;* ii) provide *multi-support input motion for dynamic response analysis*, in order to final check the structure. For these abovementioned goals, some other tasks were performed:

- Probabilistic seismic hazard analysis (define target rock motion design spectra);

- Generation of spectrum-compatible reference rock motions from actual earthquake records;

- Generation of coherency function compatible rock motions for SAS span and skyway;

- Studies on site response analysis to understand wave propagation phenomenon and compute depth-varying free-field motions;

- Development of ARS criteria using representative soil profiles;

- Development of multiple-support free-field and kinematic motion arising from soil-pile interaction to be used in time-history analysis [57].

For the SAP2000 model used in the present study, the nonlinear time history analysis was performed for only one of the 6 sets of ground motions that were used to design the structure. The selected ground-motion That set of Ground motions includes longitudinal, transverse and vertical records. Also, as it was referred before, the soil conditions vary along the longitudinal axis of the bridge and multiple-support excitation is considered. That way, there are also longitudinal, transverse and vertical ground motions for soil conditions at Pier E2. The foundations at Pier W2 and T1 are founded on the bedrock. Fig. 5.1 and 5.2 display the referred ground-motion displacements as function of time.

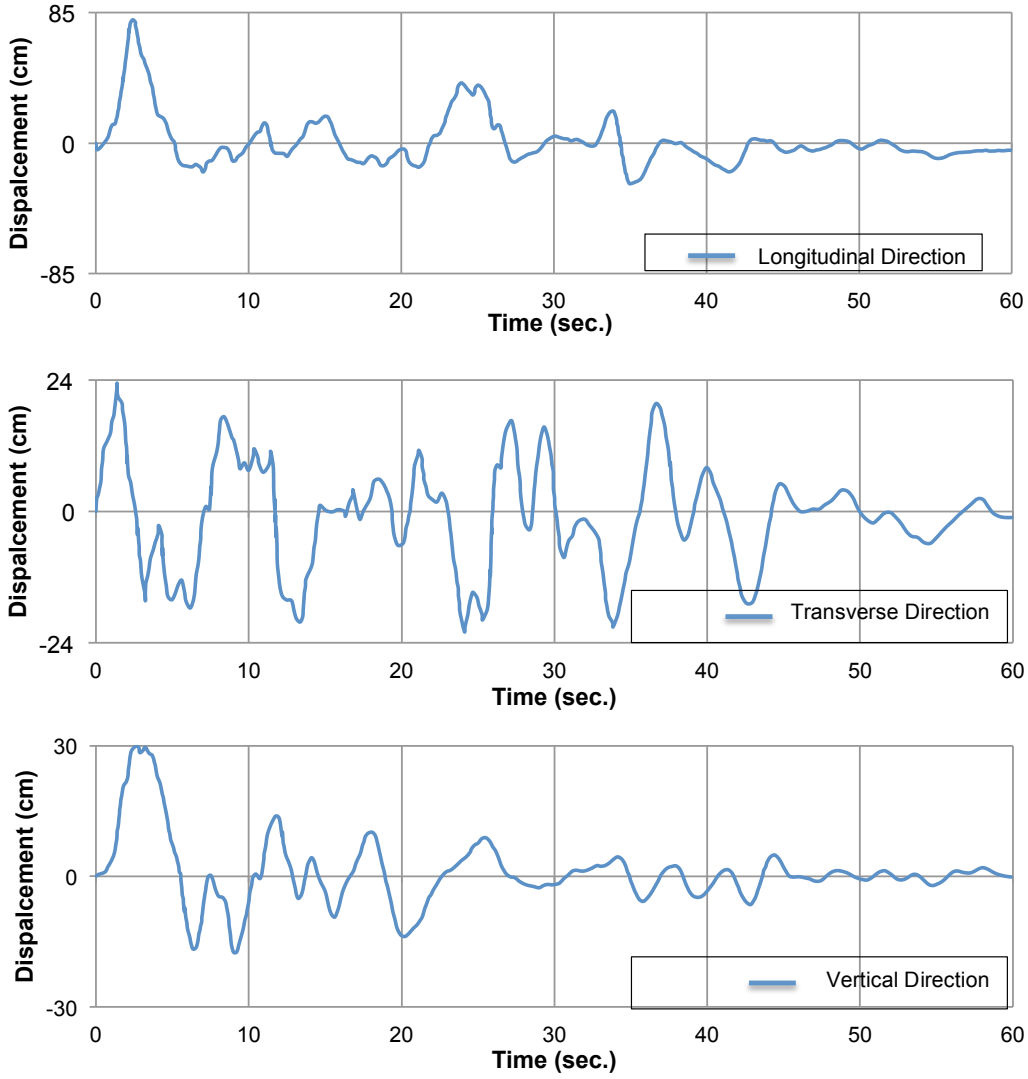

Fig. 5.1 – Set 1 of Ground motions from Caltrans (Rock motions for T1 and W2 foundations) *[57]*.

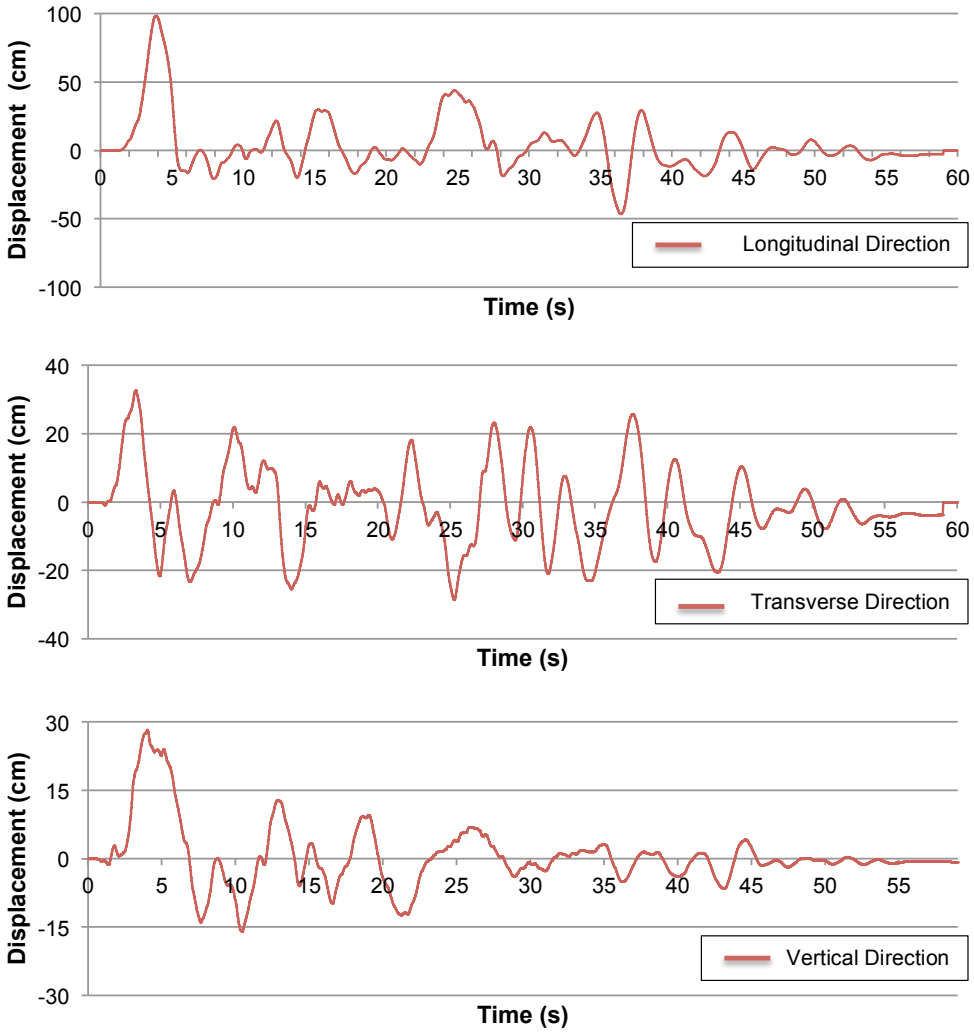

Fig. 5.2 –Soil motions from Caltrans for Pier E2 foundation *[57]*.

5.3 CALTRANS MODEL FOR SAS

The software used for modeling the bridge by the design team was ADINA. Their global model of the self-anchored suspension bridge is illustrated in Figure 5.3. Besides the modeling of the SAS span, it includes boundary frames representing the skyway and the YB transition structure. This model uses only nonlinear truss and beam elements and it is largely inelastic. The deck is modeled with two parallel beam elements representing the axial, bending and torsional properties of the suspended deck structure. For the connection with the suspenders, stiff beam elements extend from the edge of the bridge deck. These elements represent the deck stiffness for vertical deformations, but are rigid for transverse deformations. The suspenders were modeled using truss elements (axial only), in order to allow them to go slack during time history analysis (large displacement formulation).

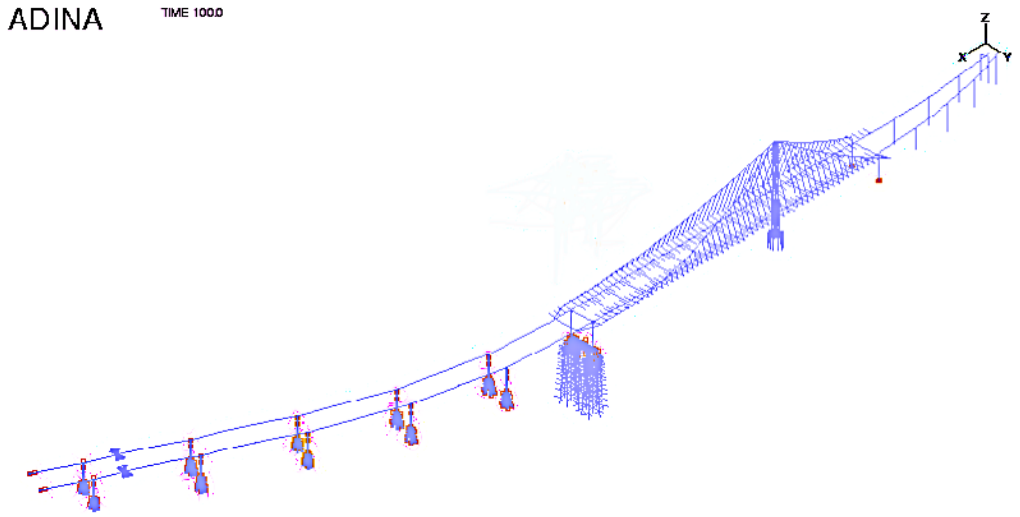

Fig. 5.3 – ADINA global model of the bridge [7].

An initial strain was applied when the model was built, in order to represent the dead load stress in the main cables and suspenders. Also, the tower shafts were modeled with nonlinear beam elements and the shear links with inelastic moment-curvature beam elements. The yield moment of these links was set to obtain the desired plastic shear capacity of the links (the rotation of the beam plastic hinges serves as a measure of the shear deformation of the links).

For the piles on the tower foundation, nonlinear beam elements (pile cap to bedrock) were used. The ground motion was applied directly to the bottom of the piles assuming that they are fixed to the bedrock. The mass of the foundation was lumped at a node at the center of gravity of the pile cap. For the east and west piers nonlinear beam elements were used. The west pier was also considered as fixed to rock and the ground motions were also applied to the bottom of the pier.

For the east piles two models were considered: hybrid model and a detailed model (Figure 5.4). The hybrid model had beam elements from pile cap to mud-line. Below mud-line each pile had 12 degree of freedom for stiffness and damping matrices. These matrices were used in a local coordinate system at each pile, oriented along the pile axis, so that battering of the piles was rigorously modeled. The mass of the foundation was lumped at a node at the center of gravity of the pile cap. The detailed model comprised of nonlinear beam elements from pile cap to the bottom of the pile. Each pile had nonlinear p-y and t-z springs along its length.

The ground motion applied to the hybrid model was not in the mud-line, but the motion at the firm soil layer below the Young Bay mud. Since the structure has relatively large piles, this is assumed to be the input of the structure instead of the mud-line motion.

The ground motion for the detailed model was varying with depth and applied to p-y and t-z springs.

Furthermore, this global model included the first frame of the skyway structure as a boundary frame. This model accounted for the nonlinear behavior of the skyway piers and made use of the hybrid model to model the foundations. For connecting the main span to the skyway and the YB transition structures only the transverse and vertical directions were considered (they are free to move independently in the longitudinal direction).

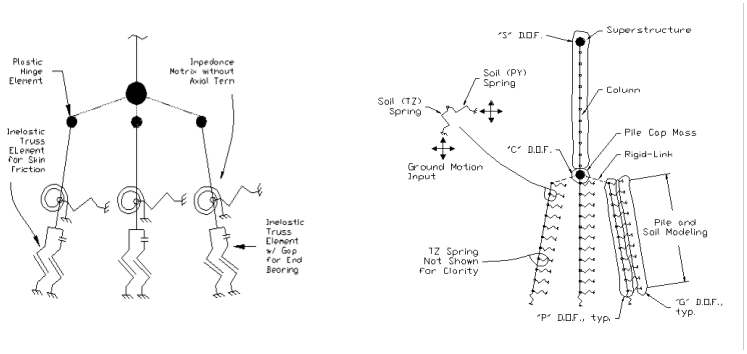

Fig. 5.4 – Hybrid and detailed models of the East piles [7].

Seismic analysis was implemented on the abovementioned model, using three different types: i) time history analysis on the global model; ii) pushover analysis and iii) local detailed analysis.

Time history analysis was the main analysis for reasons such as the fact that different bridge foundation conditions that subject them to different ground motion excitations. West Pier W2 and tower foundations are embedded in the rock, while the east Pier E2 foundation is in deep soil. The ground motions in these supports are completely different in character and intensity, which resulted in applying different time histories of ground displacement at these supports.

Also, a large displacement analysis and nonlinear material were used in order to capture the true behavior of the bridge (geometric stiffness of the bridge, P-delta effects, slacking of suspenders, plastic hinges in piers and tower links). Furthermore, the model was built in a single step (instantaneous gravity application). Time history analyses were done as restart analyses from the dead load state; pushover analysis was mainly used to evaluate ductility of critical elements and to establish failure mode sequence. Local detailed analysis was used to establish local strain/stress demands and to evaluate the modeling used in the global model [7].

5.4 SELF-ANCHORED MODEL

As mentioned previously, the geometry, sections and materials, boundary conditions and nonlinearities were checked and necessary changes or improvements were made, according to Caltrans official project drawings. All that information about the model is included in this report. Also, the author was responsible for changing the entire steel orthotropic deck plate's thicknesses and bending stiffness along the length, in order to improve the model accuracy. The deck accuracy alters the weight and mass of the structure and impacts the analysis. Professor Astaneh's PhD student Cindy Qian had developed the tower model. It is a very complex system comprised of 4 separate shafts with vertical stiffeners and plate thickness that vary along the height, as well as diaphragms and shear links. The results reveal it is a suitable enough replica for this study, but nevertheless deeper research needs to be done specifically for the tower.

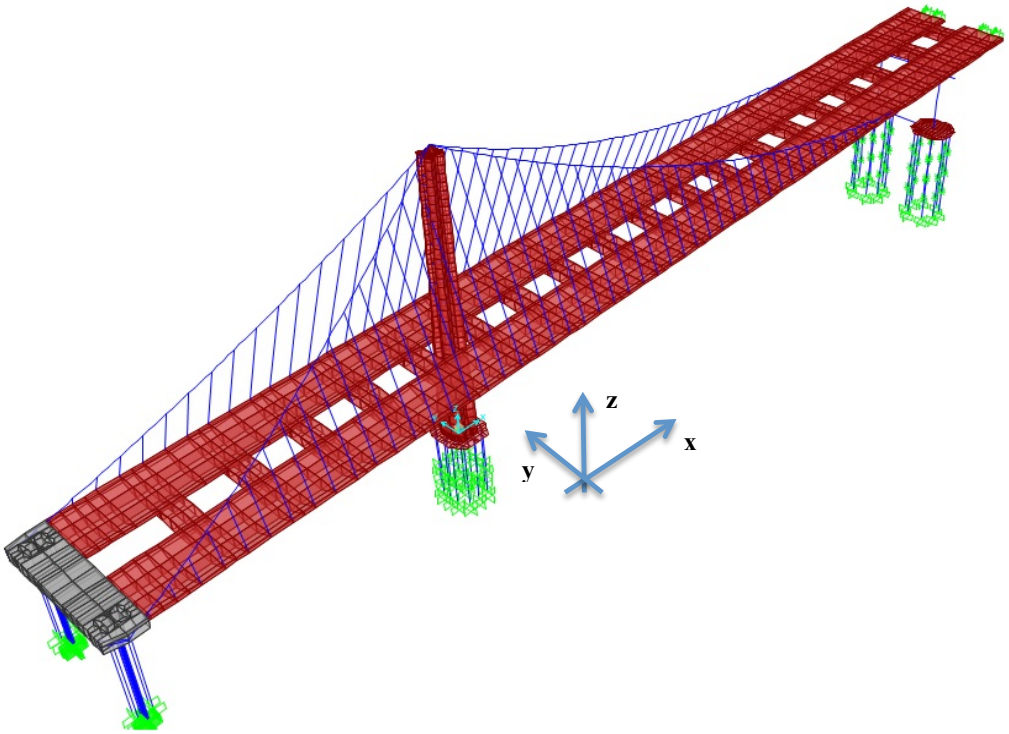

Fig. 5.5 – SAP2000 model of the SAS span used in this study.

5.4.1 ELEMENTS

Table 5.1 – **West Side and Cable elements** and properties at the SAP2000 model for the Self-anchored span *[Ref.: Caltrans official project drawings (1204)].*

Location	Cross section				Properties
	Section label	Element Type	Type	Material	
West side (W2)	W2-Column-Section	Frame	Reinforced Concrete column	Concrete (fc'=55MPa)	Cross section Area= 10,821 m^2 I33=9,7344 m^4 I22=9,1665 m^4 (See Fig.4.6)
	W2-Tie-down Cable	Frame	14 Steel cable	ASTM A416	Area of each= 0,0108 m^2
	W2-Cap-Beam	Solid	Prestressed concrete cap beam	Concrete (fc'=60MPa)	-
	W2-Pier-Cap-Slab			Concrete (fc'=55MPa)	-

Location	Cross section				Properties
	Section label	**Element Type**	**Type**	**Material**	
Cable	CABLES-Main-Frame	Frame	Main cable strands	FrameMain Cable	D= 0,78m D= 0,14m D=0,18m Reduction of Torsional Constant= Reduction Moment of Inertia axis 2 and 3 (x0,10)
	CABLES-Suspenders-Type1		Cable suspenders	FrameSuspenders	
	CABLES-Suspenders-Type2		12 Cable suspenders close to the Tower	FrameSuspenders	

Table 5.2 – **East Side** elements and properties at the SAP2000 model for the Self-anchored span *[Ref.: Caltrans official project drawings 625/1204]*.

Location	Cross Section				Properties
	Section label	**Element Type**	**Type**	**Material**	
East side (E2)	E2-Pier-Column	Frame	4 Reinforced concrete columns	Concrete fc'=35MPa	Cross section Area= 37,737 m^2 I33=61,519 m^4 I22=55,183 m^4
	E2-Bearing-TOP		4 Bearings	SC Gr345	(3,5x2,9)m Height from CR: 0,75m
	E2-Bearing-BOTTOM		4 Bearings	SC Gr550	(2,92x2)m Height from CR: 0,995m
	E2-Pier-Cap-Rigid-Beam		Connector	A615Gr50	-
	E2-Shr-Key-Top		4 Shear Keys	SC Gr550	(3,6x3,4)m Height from CR: 0,75m
	E2-Shr-Key-Bottom		4 Shear Keys	SC Gr550	(2,78x2,78) Height from CR: 0,995m

Location	Cross Section				Properties
	Section label	**Element Type**	**Type**	**Material**	
East side (E2)	E2-Pile-cap-Rigid Beam		Connector	A615Gr50	-
	E2-Cap beam-frame		Reinforced concrete beam	Concrete fc'=55MPa	(6x3,93)m Length=60,6m I33=70,74 m^4 I22=30,35 m^4
	E2-Pile cap connection beam		Reinforced concrete beam	Concrete fc'=35MPa	(5,7x11,75)m Length= 16,7m I33=181,33 m^4 I22=770,56 m^4
	E2-Pile Cap	Shell (thick)	Concrete cap at base	Concrete fc'=35MPa	Thickness (Membrane)=5,7m (Bending)=5,7m
	E2-Pile	Frame	Concrete Column	Concrete fc'=25MPa	Outer D=2,5m Steel casing thickness= 0,085m Vertical reinforcement= 36 bars (A=0,0026 m^2)
	Spring-East-End	Link	Connection between SAS and Skyway (L=10m)	Mass=Weight=0,001 kN Rotational Inertia 1,2,3 = 0,001m^4 - Free for U1 Direction - Direction R2, R3 Fixed - Direction U2 and U3 with Stiffness Matrix Damping uncoupled	

The connection between the SAS span and the skyway was modeled using a Link element (Fig. 5.8). This element allows displacements along the longitudinal direction, but requires a stiffness matrix for transverse and vertical directions. The force method is used to find flexibility matrix and, consequently the stiffness matrix.

A unit force (KN) is applied on the location and the displacement is obtained (mm):

$$F = \begin{bmatrix} 0{,}0223 & 0{,}0042 \\ 0{,}0042 & 0{,}0170 \end{bmatrix} \text{ (mm/kN)} \quad \Rightarrow \quad K = F^{-1} = \begin{bmatrix} 47{,}03 & -11{,}62 \\ -11{,}62 & 61{,}69 \end{bmatrix} \text{ (kN/mm)}$$

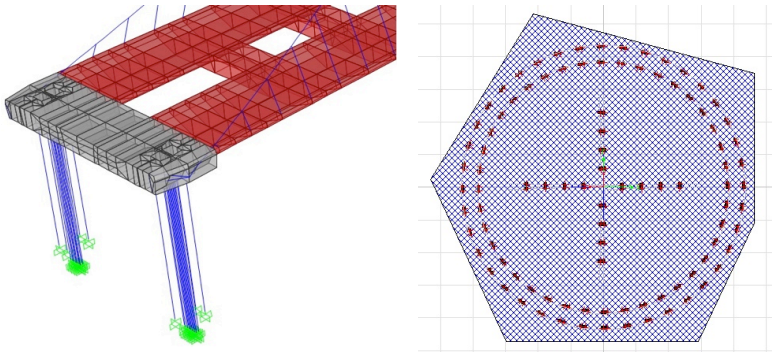

Fig.5.6 – 3D view of the West side and cross section of one W2 column

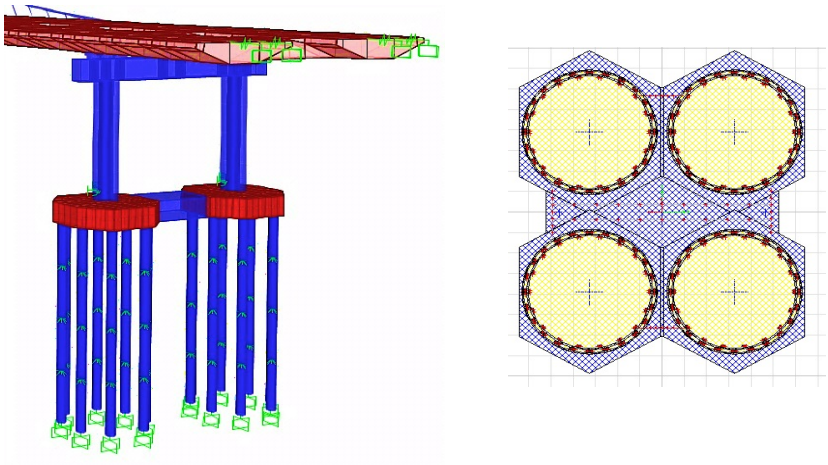

Fig. 5.7 – 3D view of the East side and cross section of E2 pier

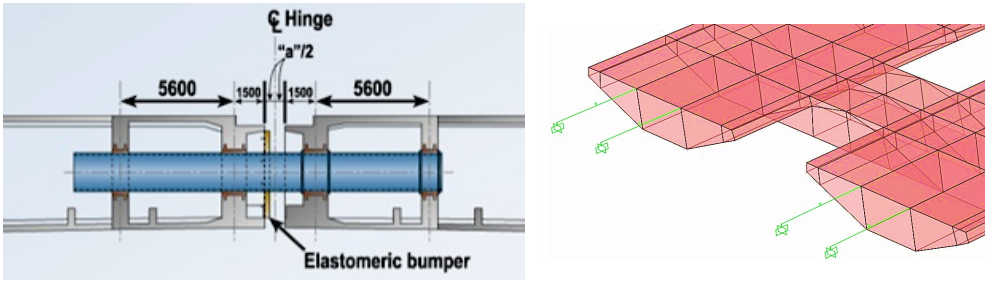

Fig. 5.8 – Hinge at the transition to Skyway and spring modeling at SAP2000.

The tower consists of its piles, pile cap, anchor rods, shaft plates, diaphragms, shear links, grillage and cable saddle. These elements are included in the model and will be enumerated in Tables 5.3 to 5.5. As discussed before, its plates have additional axial and bending stiffness due to the existing stiffeners along its height. Therefore, modifiers were added to represent these additional properties. Also, since Plates B, C and D (see Fig. 5.10) have the same thickness, they were given the same properties in the model. Plate A and Plate E were modeled separately. The variation of properties along the height of the tower was simplified and only considered a single variation in the plate's properties at z= 33m (considered Lower and Higher plates only). For a more accurate representation, more variations of properties along the height should be introduced. Nevertheless, the tower shafts are expected to remain elastic during analysis and so these simplifications seems reasonable.

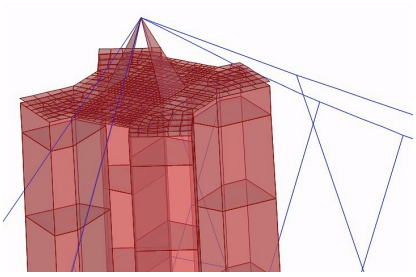

Fig. 5.9 – Tower top saddle on the SAP2000 model.

Table 5.3 – **Tower elements properties** at the SAP2000 model for the Self-anchored span *[Ref.: Caltrans official project drawings (1204)].*

Location	Cross Section				Properties
	Section label	**Element Type**	**Type**	**Material**	
TOWER (Saddle)	SADDLE-Bott-PL	Shell (thick)		SADDLE PL	Thickness Membrane/Bending= 0,12m
	SADDLE-Grillage-PL			SADDLE PL	Thickness Membrane/Bending= 0,10m
	SADDLE-Anchor-Bolts	Frame	Anchor rods connect the grillage to saddle	SADDLE ANCHOR	Length= 0,22m D1 = 0,08m D2= 0,10m D3=0,12m
	SADDLE-Rigid-PL	Shell (thick)	Saddle (top of the tower)	A992Fy50	Thickness Membrane/Bending= 1,00m Stiffness modifiers (x100)

Table 5.4 – **Tower plate's properties** at the SAP2000 model for the Self-anchored span *[Ref.: Caltrans official project drawings (1204)].*

Location	Cross Section				Properties
	Section label	**Element Type**	**Type**	**Material**	
TOWER (Plates)	TOWER-PL-**A** - Lower	Shell (Thin)	Tower shafts plate (z=3,125 to z=33)	A992Fy50	Thickness = 0,07m Modifiers: M11 and M22 (x88,7) V13 and V23 (x1,6)
	TOWER-PL-**A** - Higher	Shell 40(Thin)	Tower shafts plate (z=33 to z=152,38)		Thickness = 0,09m Modifiers: M11 and M22 (x47,5) V13 and V23 (x1,47)
	Tower-PL-**E** - Lower	Shell (Thin)	Tower shafts plate (z=3,125 to z=33)		Thickness = 0,06m Modifiers: M11 and M22 (x56,7) V13 and V23 (x1,311)
	TOWER-PL-**E** – Higher	Shell (Thin)	Tower shafts plate (z=33 to z=152,38)		Thickness = 0,075m Modifiers: M11 and M22 (x40) V13 and V23 (x1,33)
	TOWER-PL-**B/C/D** - Lower	Shell (Thin)	Tower shafts plate (z=3,125 to z=33)		Thickness = 0,075m Modifiers: M11 and M22 (x135) V13 and V23 (x1,45)
	TOWER-PL-**B/C/D** – Higher	Shell (Thin)	Tower shafts plate (z=33 to z=152,38)		Thickness = 0,06m Modifiers: M11 and M22 (x104) V13 and V23 (x1,5)

Location	Cross Section				Properties
	Section label	**Element Type**	**Type**	**Material**	
TOWER (Plates)	TOWER-Base-Shr-6- PL	Shell (Thin)	Longitudinal and Inside base shear plates (z=3,125 to z=13)	A992Fy50	Thickness Membrane/Bending= 0,06m Modifiers: M11 and M22 (x104) V13 and V23 (x1,5)
	TOWER-Base-Shr-8-PL	Shell (Thin)	Transverse base shear plates (z=3,125 to z=13)		Thickness Membrane/Bending= 0,08m Modifiers: M11 and M22 (x50)
	TOWER-Diaphragms	Shell (Thick)	Diaphragms inside tower shafts (along entire height)		Thickness Membrane/Bending= 0,075m

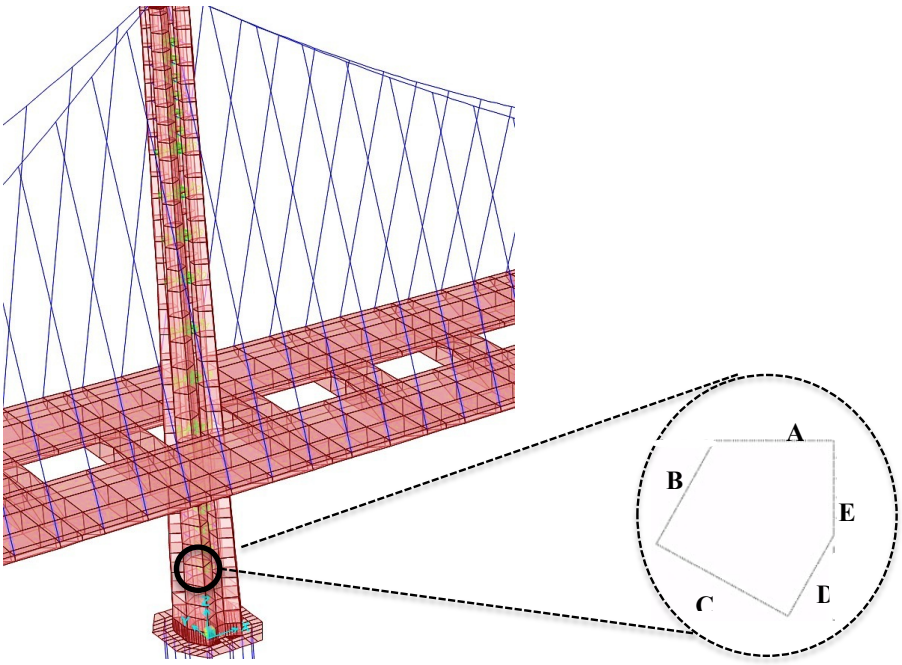

Fig. 5.10 – Tower with detail of 1 of 4 tower shafts with plate labeling as in SAP2000 model.

Table 5.5 – **Tower shear link and bracing's properties** at the SAP2000 model for the Self-anchored span *[Ref.: Caltrans official project drawings (1204)].*

Location		Cross Section				Properties (m)
		Section label	Element	Type	Material	
TOWER	(Struts and bracings)	TOWER-Transv-Strut-Middle (STRUT 1)	Frame	Transverse strut mid-height of Tower	A992Fy50	tf=0,045; tw=0,028 hf=0,60; hw=0,86
		TOWER-Transv-Strut-Top-Bott (STRUT 2)		Transverse strut at bottom and top of Tower		tf=0,045; tw=0,016 hf=0,475; hw=0,86
		TOWER-Longitud-Strut (STRUT 3A&B)		Longitudinal strut for all the height		tf=0,045; tw=0,028 hf=0,475; hw=0,86
		TOWER-Cross-Bracings	Frame	Bracing between tower shafts		Rectangular cross section: 0,35x0,035

Table 5.6 – **Tower elements and properties** at the SAP2000 model for the Self-anchored span *[Ref.: Caltrans official project drawings].*

Location		Cross Section			Properties
		Section label	Element Type	Material	
TOWER	(Base and Foundations)	AROD-Type A; A* AROD-Type C AROD-Type E* AROD-Type G	Frame (Orthotropic)	AROD-Type A; A*; C; E*; G	Diameter = 0,16m
		AROD-Type B	0,125-meter Anchor rods at the base of the tower (Base plate)	AROD-Type B	Diameter = 0,18m
		AROD-Type D; D*; D** AROD-Type J AROD-Type M AROD-Type N AROD-Type O		AROD-Type D; D*; D**; J; M; N; O	Diameter = 0,10m

Location	Cross Section			Properties
	Section label	Element Type	Material	
	AROD-Type E AROD-Type H AROD-Type I AROD-Type K	Frame (Orthotropic) 0,125-meter Anchor rods at the base of the tower	AROD-Type E; H; I; K	Diameter = 0,14m
	AROD-Type F AROD-Type L	(Base plate)	AROD-Type F; L	Diameter = 0,08m

Table 5.7 – **Tower elements and properties** at the SAP2000 model for the Self-anchored span *[Ref.: Caltrans official project drawings].*

Location		Cross Section				Properties
		Section label	Element Type	Type	Material	
TOWER	(Base and Foundations)	TOWER-Pile-Cap	Shell (thick)	Concrete cap at base	Concrete (fc'=35MPa)	Thickness Membrane/Bending= 6,65m
		TOWER-Pile-Cap-Rigid-Pile	Frame	Piles inside the pile cap at the base of tower	A992Fy50	Circular Cross Section (D=3m) Length= 6,65m Stiffness modifiers (x1000)
		TOWER-Piles	Frame	Concrete Column with steel casing	Concrete (fc'=35MPa)	Outer D=2,5m Inner D=2,31m Steel casing thickness= 0,095m Vertical reinforcement = 36 bars (A=0,0026 m^2)

For the steel orthotropic deck plates, properties such as thickness and stiffeners were analyzed along the full length of the superstructure. The properties variation along the length was then included in the model. Table 5.8 contains the plate thicknesses and their equivalent thickness on the model. The equivalent thicknesses were introduced, in order to increase the axial capacity due to presence of the stiffeners.

Table 5.8 – **Steel orthotropic deck** plate's properties at the SAP2000 model for the Self-anchored span [*Ref.: Caltrans official project drawings 625/1204].*

	Plate thickness / Equivalent thickness (considering stiffeners) [mm]							
Deck panel numeration and X Coordinates	**10 to 14**	**14 to 30**	**30 to 112**	**112 to 115**	**115 to 118**	**118 to 120**	**120 to 122**	**122 to End**
SAP shell labels	-171 to -140 m	-140 to -40 m	-40 to 250 m	250 to 260 m	260 to 280 m	280 to 300 m	300 to 320 m	320 to 435 m
(1) DECK-Top-interior	20/ 35,5	14/ 29,5	14/ 29,5	20/ 35,5	20/ 35,5	20/ 35,5	20/ 35,5	20/ 35,5
(2) DECK-Top-Edge-Outside	20/ 32,8	20/ 32,8	20/ 32,8	20/ 32,8	20/ 32,8	20/ 32,8	20/ 32,8	20/ 32,8
(3) DECK-Side-Outside	20/ 25,5	25/ 31,4	28/ 38,6	18/ 24	18/ 24	18 /18	18 /18	18 /18
(4) DECK-Bott-Sloped-Edge-Outside	18/ 30,9	18/ 30,9	18/ 30,9	16/ 26,5	16/ 28,9	18/ 30,9	18/ 30,9	18/ 30,9
(5) DECK-Bott-Sloped-Outside	20/ 30,5	22/ 34,7	18/ 30,5	20/ 32,5	22/ 34,7	25/ 38,5	22/ 32,5	30/ 40,4
(6) DECK-Bott-Flat	35/ 60,7	20/ 32,6	20/ 32,6	28/ 41,8	35/ 48,5	60/ 76,4	35/ 48,5	22/ 35,2
(7) DECK-Bott-Sloped-Inside	20/ 30,4	16/ 26,5	16/ 26,5	16/ 26,5	25/37,7	25/ 32,4	22/ 32,4	16/ 26,5
(8) DECK-Bott-Sloped-Edge-Inside	18/ 30,9	16/ 26,5	16/ 26,5	16/ 26,5	18/29,5	18/ 29,5	18/ 30,9	16/ 26,5
(9) DECK-Side-Inside	20/ 25,2	18/ 23,2	18/ 22,4	18/ 24	18/ 24	18/ 24	18/ 24	18/ 24
(10) DECK-Top-Edge-Inside	20/ 29,4							

On Annex A5.1 there is a complementary table with the intermediate calculations for the deck plates.

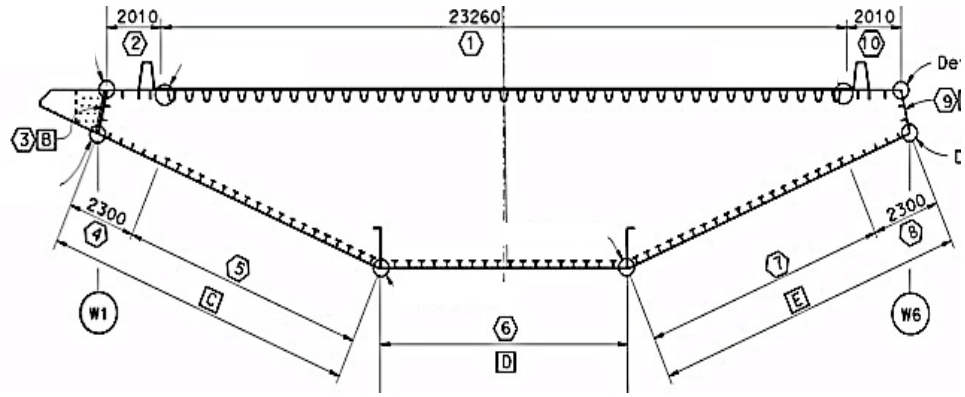

Fig. 5.12 – Typical section of the Deck ("W" Line) with plate numeration *[Ref.: Caltrans official project drawings 614/1204].*

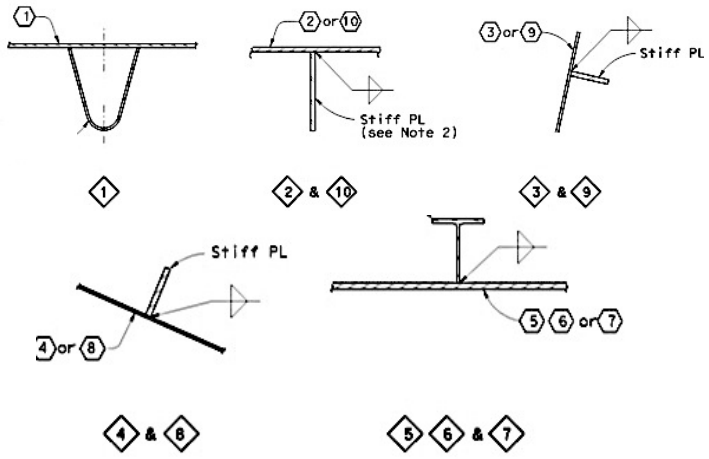

Fig. 5.13 – Stiffeners type for typical section of the Deck ("W" Line) [Ref.: Caltrans official project drawings 627/1204].

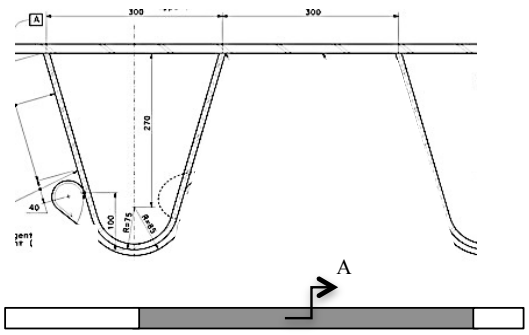

Fig. 5.14 – Equivalent thickness of the steel orthotropic deck plate without ribs *[Ref.: Caltrans and author drawings].*

Also, bending modifiers for local axes 1 and 2 (longitudinal and transverse) were included, in order to properly represent the bending stiffness due to the stiffeners and real plate thickness. On local axis 1 (longitudinal), the bending modifier (M11) decreases the stiffness. Since we are considering an equivalent thickness for the axial capacity that is larger, M11 is needed to reduce the bending capacity of that plate to the level of the actual existing thickness (smaller). The stiffener contribution to bending is neglected on this direction. On local axis 2 (transverse), the bending modifier (M22) increases the stiffness. The stiffeners increase the bending stiffness of deck plates in the longitudinal direction. This was achieved with a quotient between the Moment of inertia of the actual plate with stiffeners and the Moment of inertia of the equivalent thickness plate only (used in SAP model). See Annex A5.1 for M11 and M22 values and intermediate calculations.

$$m11 = I_{actual} / I_{equiv} = t_{actual}^3 / t_{equiv}^3 < 1 \quad (1)$$

$$m22 = (I_{stiff}) / (I_{equiv\ plate}) > 1 \quad (2)$$

Table 5.9 – **Steel orthotropic deck** diaphragms and cross beams at the SAP2000 model for the Self-anchored span [*Ref.: Caltrans official project drawings 646-705/1204].*

		Equivalent thickness (considering stiffeners) [mm]	
	Location	**8 to 115** (-171 m to 280 m)	**118-End** (East Transition: 280 to 435 m)
SAP shell Labels	DECK-Trans-Diaph-Edge	16 mm	-
	DECK-Trans-Diaph-Middle	10 mm	-
	DECK-Trans-Diaph	-	14 mm
	DECK-Longit-Diaph	23 mm	
	CROSSBEAM - Vertical-Side	21 mm	
	CROSSBEAM -Vertical-Middle	19 mm	
	CROSSBEAM -Horiz-Top	33 mm	
	CROSSBEAM -Horiz-Bottom	17 mm	

All the abovementioned segments of the steel orthotropic deck were modeled as shell elements (thin) and their material had a yield stress of 50ksi (344,7 MPa). The author's change in the deck along its length represents a 5% weight increase compared to the previous model weight of deck plates. Furthermore, it allows for a better accuracy of stresses and displacements on the deck.

5.4.2 MATERIAL PROPERTIES

Table 5.10 – **Materials** at SAP2000 model.

	Label	Properties
West Side (W2)	Concrete **(fc'=55MPa)**	Specified compressive concrete strength= 55MPa Weight per unit volume= 25,134 KN E= 24855 MPa G= 10356 MPa
	ASTM416	Steel; Hysteresis type: Kinematic; Parametric simple stress-strain curve Strain at onset of strain hardening= 0,015m Strain at rupture= 0,17m Minimum Yield Stress (Fy)= 1861,6 MPa Weight per unit volume= 82,361KN E= 200 GPa G= 76,9 GPa
	Non-linear Isotropic Concrete **(fc'=60MPa)**	Specified compressive concrete strength= 60MPa Hysteresis type: Takeda; Parametric Mander stress-strain curve Weight per unit volume= 25,134 KN E= 24855 MPa G= 10356 MPa
Cable	**FrameMainCable**	Steel; Isotropic; Hysteresis type: Kinematic; User defined stress-strain curve (no compression) 1) Strain= -6,75e^-15 m; Stress= -2,7e^-6 KPa 2) Strain and Stress=0 3) Strain= 6,751 mm; Stress= 1350 MPa Minimum Yield Stress (Fy)= 1350 MPa Weight per unit volume= 76,97KN E=200GPa; G=76,9 GPa
	FrameSuspenders	Steel; Isotropic; Hysteresis type: Kinematic; User defined stress-strain curve (no compression) 1) Strain= -9,79e^-15 m; Stress= -6,9e^-7 KPa 2) Strain and Stress=0 3) Strain= 9,79 mm; Stress= 1350 MPa Minimum Yield Stress (Fy)= 1350 MPa Weight per unit volume= 76,97KN E=137,9 GPa; G=53,04 GPa
Deck		A992Fy50

	Label	Properties
East Side (E2)	Concrete **(fc'=35MPa)**	Specified compressive concrete strength= 35MPa Hysteresis type: Takeda; Parametric Mander stress-strain curve Weight per unit volume= 25,134 KN E= 24855 MPa G= 10356 MPa
	SC Gr345	Same characteristics as A992Fy50 steel (below)
	Concrete **(fc'=25MPa)**	Specified compressive concrete strength= 25MPa Hysteresis type: Takeda; Parametric Mander stress-strain curve Weight per unit volume= 25,134 KN E= 24855 MPa G= 10356 MPa
Tower	**Steel A992Fy50**	Actual weight per unit of volume: 490 lb/ft^3 In the model, it was used a 7% additional weight for the A992Fy 50 steel (525 lb/ft^3) to include non-structural elements, connections such as bolts, plates, welds, lighting systems etc. This affects the Tower and the Deck where this material is used. Hysteresis type: Kinematic; Parametric simple strain-stress curve. Strain at onset of strain hardening= 0,015m Strain at rupture= 0,17m Minimum Yield Stress (Fy)= 345 MPa Weight per unit volume= 82,361KN E= 200 GPa G= 76,9 GPa
	SADDLE ANCHOR	Steel; Isotropic; Hysteresis type: Takeda; User defined stress-strain curve (High compression and elastic behavior of steel for tension) 1) Strain= -0,1 m; Stress= -723,95MPa 2) Strain= -3,62 mm; Stress= -723,95MPa 3) Strain and Stress=0 4) Strain= 2,97 mm; Stress= 594,7 MPa 5) Strain= 15,9 mm; Stress= 723,95 MPa Weight per unit volume= 76,97KN E= 200 GPa G= 76,9 GPa
	SADDLE PL	Same characteristics as A992Fy50 steel (below)
	A-ROD (all types)	Hysteresis type: Takeda User defined stress-strain curve 5 points Weight per unit volume= 76,97KN E= 4544MPa G=1748GPa

For AROD type, since the rods have 5,5 m of length in reality, but only 0,125m on the SAP model an equivalent modulus of elasticity was calculated:

$$E' = 29000*0,125/5,5 = 659ksi = 4544\ MPa.$$

Table 5.11 – **Restraints and releases** assigned for SAS model.

Location		Restraints						Releases					
		U1	U2	U3	R1	R2	R3	P	V2	V3	M2	M3	T
West Side	W2 to YBI approach	Connection between W2 cap beam and YBI approach structure are inexistent, since the effects of this approach structure on the massive W2 cap beam are minor.											
	W2 column base	✓	✓	✓	✓	✓	✓	-	-	-	-	-	-
	W2 column top	Body Constraint (U1, U2, U3, R1, R2, R3) between top of Pier W2 and Cap beam slab.											
	Tie-down cable base	✓	✓	✓	-	-	-	-	-	-	-	-	-
East Side	Shr-Key-TOP	Body Constraint (U1, U2, U3, R1, R2, R3) between top SK and Deck bottom plates											
	Shr-Key-BOTT	-	-	-	-	-	-	✓	✓	-	✓	✓	✓
	Bearing-TOP	Body Constraint (U1, U2, U3, R1, R2, R3) between top Bearing and Deck bottom plates											
	Bearing-BOTT	-	-	-	-	-	-	-	-	-	-	✓	-
	Piles z=-15m	✓	✓	-	-	-	-	-	-	-	-	-	-
	Piles z=-30m	✓	✓	-	-	-	-	-	-	-	-	-	-
	Piles z=-45m	✓	✓	-	-	-	-	-	-	-	-	-	-
	Piles z=-60m	✓	✓	✓	-	-	-	-	-	-	-	-	-
	E2 to Skyway	Springs were used to represent the 4 hinges that only have longitudinal movement.											

	Location	Restraints						Releases					
		U1	U2	U3	R1	R2	R3	P	V2	V3	M2	M3	T
Tower	Cross Bracings	-	-	-	-	-	-	-	-	-	-	✓	-
	Piles z=-19m	✓	✓	✓	✓	✓	✓	-	-	-	-	-	-
	Piles z=-34m	✓	✓	✓	✓	✓	✓	-	-	-	-	-	-
Cable	Type 1 and Type 2 Suspenders	-	-	-	-	-	-	-	-	-			-
		-	-	-	-	-	-	-	-	-			-

OBS: Axis 1, 2 and 3 are local and correspond to Longitudinal Axis (x) is Direction 1; Transverse Axis (y) is Direction 2; Vertical Axis (z) is Direction 3 for each element.

OBS 2: All the coordinates related to z are related to the center of the pile cap (average sea level).

OBS 3: Bottom is considered fixed since it is embedded in rock.

As referred before on Chapter 3, the Shear Keys allow all movements, but restrain transverse displacements and the Bearings allow rotation on the longitudinal direction.

There are also body constraints assigned in the model to certain nodes. The purpose is to make two elements move as a rigid body (same displacements and rotation). These constraints were assigned at the East side between the shear keys/bearings and deck bottom plates and between the rigid beams and the piles. Also, they were assigned at the Tower base connecting the pile cap with rigid beam and beginning of the tower piles. Furthermore, on the West side these constraints were used between the cap beam solid element and the shell deck; on the connection of the main cable to the solid cap beam and between the slab on top of the piers and the cap beam.

For the east column piles, the soil conditions are unfavorable[12]. Due to the varying soil conditions, it was assumed that the piles can only have displacements on the longitudinal direction of the bridge and so the rollers restrain only displacements on local axis 1 and 2 (vertical and transverse). This way, the 1st roller was used at the beginning of the mudline (after water level) approximately at z=-15m (under sea level). The 2nd roller is at z=-30m (under sea level) where the soil varies from a soft layer of Fat Clay (Soil undrained shear strength =50KPa) to a stiffer layer of Fat Clay (150KPa). The 3rd roller is located at z=-45m (under sea level) where approximately the layer changes to a stiffer one (200KPa). The total length of the piles is 60m on the SAP model, which seemed an adequate representation of the reality since the soil conditions do not change much from z=-60 to z=-100m. At the bottom (z=-60m), it was considered a pinned connection (were there can still be rotation, but no displacements).

The tower is located at +58m on the global coordinate system of the bridge and the soil conditions at that location are better compared to the East pier ones. The center of the tower pile cap is considered

[12] Caltrans official Project drawings (pg. 105, 107 and 108/118) contain boring tests results for the East piles location.

the average sea level. The piles were considered to be 30-meter deep in the SAP model. That seemed adequate since at 30m under the sea level the soil conditions are already very similar to the ones at the 60m bottom (soil undrained shear strength=160 compared to the 190KPa at the bottom). Since the first mudline below water is considered to start around z=-19m (under sea level, from the center of pile cap), the first restraints are at that level and are fixed. Also, at the bottom (z=-34m under sea level) there is a fixed restrain. This restrains all displacements and rotations. These approximation of the reality seemed adequate, since the soil conditions vary from 120 to 170 KPa of Soil undrained shear strength from mudline to 15m below, which are considered to be very stiff soils.

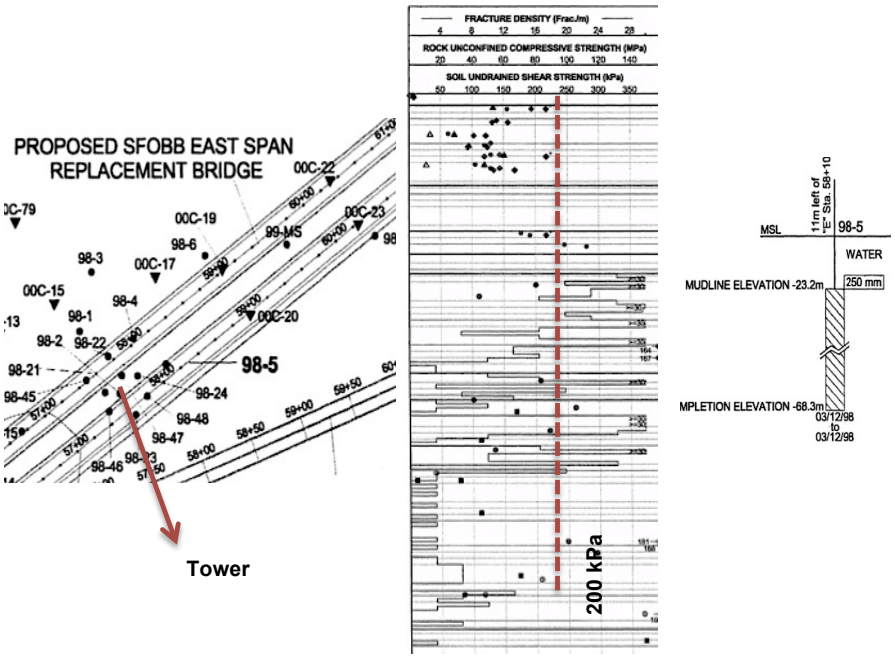

Fig. 5.16 – Results of boring test at Tower location with undrained soil shear strength until 60-meter deep *[Ref.: Caltrans official project drawings (pg. 100/118].*

5.5 GROUND-ANCHORED MODEL WITH CABLE DISCONNECTED

To simulate a ground-anchored suspension bridge, the cable should not have any connection to the deck itself. Furthermore, the original SAS configuration was kept, in order to analyze the impact of a simple change such as the anchorage being hold to the ground. That way, the ends of the cable were disconnected from the deck and west end cap beam and pinned (translations restrained). Although the cable length was not continued as in a real ground-anchorage, that does not influence the output results.

For the GAS model, the Modal analysis will also be performed for the first 200 modes. Graph 5.1 presents the Cumulative Mass Participation Ratio, which shows 100% of longitudinal and transverse participation and 80% of vertical participation after the first 200 modes.

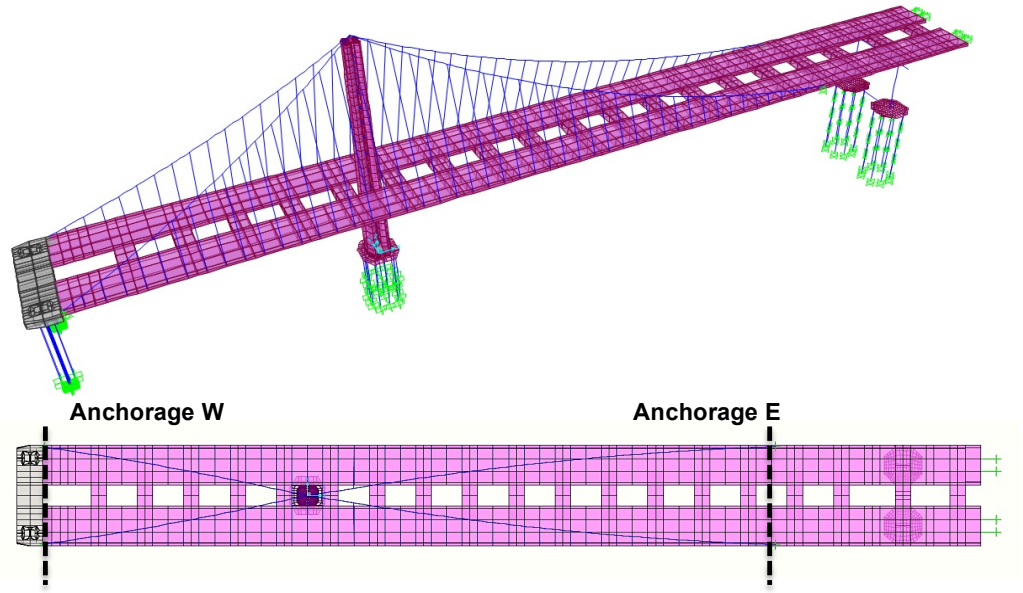

Fig. 5.17 – SAP2000 ground-anchored model views

5.6 GROUND-ANCHORED MODEL REDESIGNED

More changes need to be performed on the original SAS model, in order to obtain a more realistic ground-anchored suspension bridge design. This is mainly because a typical ground-anchored bridge system would not need some elements that are necessary for the SAS system. Those elements are for instance, the rigid cap beam element on the West side for the looped anchorage and connection to YBI; the heavy columns and tied-down system for Pier W2 and the deck cantilevers to east and west of Pier E2. This redesigned is merely an academic exercise.

Therefore, the following changes were made:

1) Remove rigid cap beam on the West side, only necessary in case of a deck anchorage;
2) Extra cross beam on the West side at coordinate X=-165m to connect last segments of both roadways;
3) Replacement of W2 columns and tie-down system by Pier E2 previous cap beam and column section (replicate Pier E2 geometry on the West Side);
4) The connection between deck and piers will be done with the same shear key/bearing system, but the bearings being replaced by *rockers*. These rockers only restrain the vertical direction (axial force) and are free on the longitudinal direction. The Shear keys will keep their previous releases and restrain of the transverse direction. Also, all body constraints are kept except the ones between shear keys/bearings and deck at Pier E2.
5) The cable on the East span has its configuration changed in order to suspend the entire deck until Pier E2;
6) Cable is disconnected from the deck and pinned at its extremities.

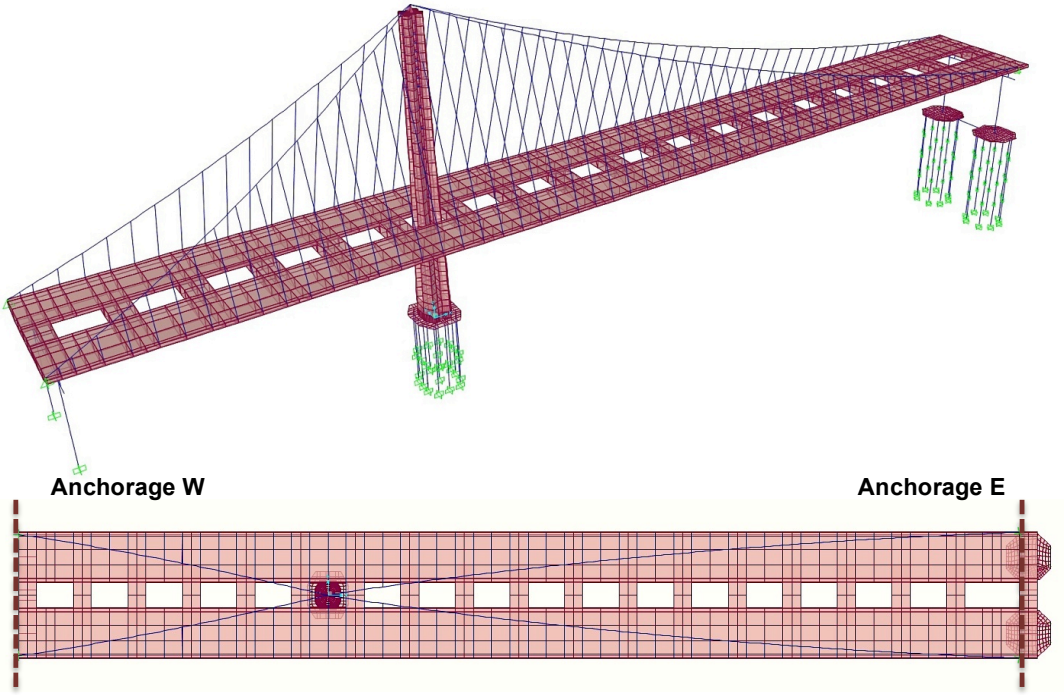

Fig. 5.18 – SAP2000 redesigned ground-anchored model views.

5.7 SYMMETRIC REDESIGNED GROUND-ANCHORED MODEL

With the results of the previous redesigned GAS model (see Chapter 6 and 7), some conclusions were withdrawn. The previous redesigned model is not an optimized Ground-anchored model (see section 5.6), due to the asymmetry of the spans and the subsequent cable sag on the East side. Therefore, a new design was attempted and the following changes were performed to the previous redesigned GAS:

1) Symmetric spans with tower in the middle. These spans have now 280m each, while before they had 170+385m.
2) Pier E2 and W2 were kept, but their connection to the deck is now pinned for both sides. The four bearings have the moment in transverse direction released and the four shear keys restrain only the transverse shear. There were assigned body constraints between the top of bearings/shear keys and the deck shell plates nodes;
3) The new main cable configuration had to be defined, in order to optimize the forces installed. The cable parabolic equation used and the cable coordinates are presented in Annex A5.2;
4) There are only 18 crossbeams for the new design.

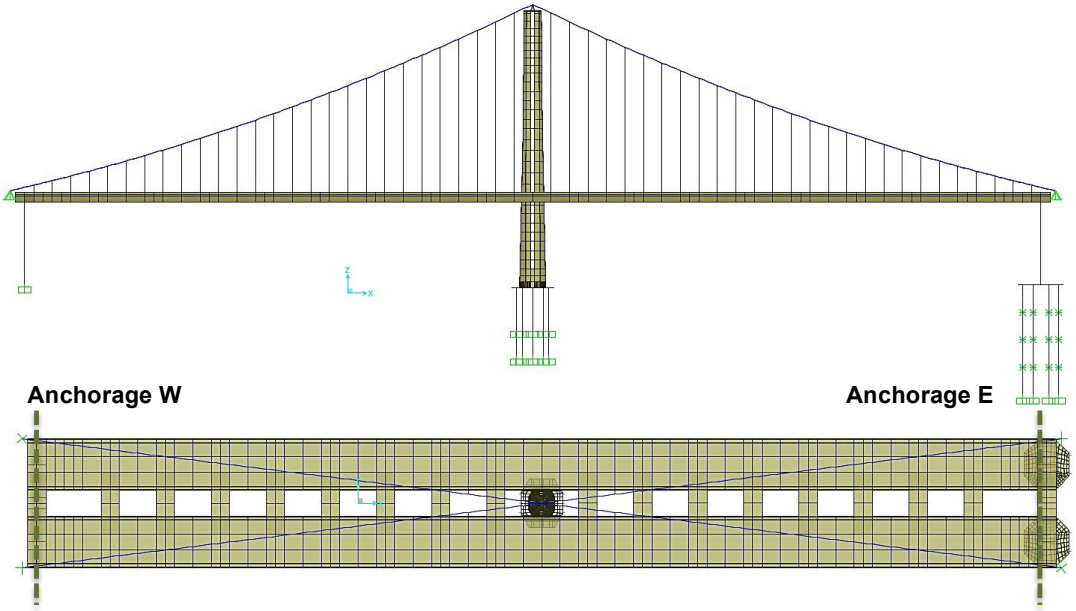

Fig. 5.19 – SAP2000 symmetric design of ground-anchored bridge.

An analysis of this initial symmetric model clarified its behavior and some further modifications were performed on the structure. Consequently, the new symmetric design final model had the following changes:

1) The same section was assigned for all the suspenders: Type 1 with a cross section area of 0,015$m^{2.}$ There is no need for stiffer suspenders near the tower on the symmetric design;
2) The four suspenders connected directly to the top of the tower were removed on both sides;
3) The deck and tower plates' thickness was now reduced, approximately according to the stresses of the initial analysis. Consequently a reduction of 30% was applied at all these locations. The exceptions were the deck mid spans (X=20m to X=80m) where there was applied a 50% reduction to all the plates except the top ones. Indeed, the top plates thickness should not be reduced at all, due to the applied live load on them. Nevertheless, since the equivalent thickness is an approximation considering the stiffeners (ribs, plates), this reduction is really being applied to these stiffeners and not to the steel plate.

5.8 ANALYSIS

The first analysis to be performed is a nonlinear Static analysis for Dead and Live loads. This gravity analysis is performed for all models and its results are presented on Chapter 6. This is one of the most relevant analysis for comparison between models and to understanding the behavior of the overall structural systems.

Also, Modal analysis results will be presented for all three GAS models. After a Modal analysis of the GAS models, a dynamic analysis will also be presented for the two optimized models: GAS with only cable disconnected and symmetric GAS design. For Dynamic analysis, the new East Bay Bridge is qualified as an Important bridge (critical lifeline that needs to provide almost immediate transportation capacity after a SEE event) but it also has a very complex and irregular geometry. Therefore, according to Caltrans criteria, a nonlinear time-history analysis should be performed.

5.8.1 GRAVITY (NONLINEAR STATIC)

It will be performed including loads such as self-weight, non-structural elements weight (overlay, guard Rail and counterweight) and Live loads. More importantly, this analysis includes PDelta and Large displacements effects. For suspension bridges analysis, the P-Delta effects are essential for the stiffness since the lateral stiffness of cable is due mostly to tension (very flexible element when unstressed). Nevertheless, this nonlinear analysis (P-Delta) should also be performed for the entire structure when the Tower or deck compressions are a concern. When the load acting on a structure is small and causes relatively small deformations, the load-deformation relation can be considered linear for that structure. This allows forming equilibrium equations based on the original undeformed geometry. On the other hand, if both of them have large values, then their relation becomes nonlinear. This nonlinear behavior in a suspension bridge structure can be due to the following main aspects: i) P-Delta effects; ii) Large displacements effects; iii) Material nonlinearity. The first effect is due to large stresses (either forces or moments) existing in the structure, which make the equilibrium equations for undeformed and deformed state differ considerably even if deformations are small. As a consequence, there are impacts on transverse bending and shear behavior: tensile forces cause the elements to resist transverse deformation (stiffens them) and compression forces cause the opposite effect for shear and bending behavior. The Large Displacements effect considers the equilibrium equations in the deformed state of the structure. For that purpose, large displacements and rotations are included, but strains are considered reduced. Therefore, if the position or orientation of an element changes, its effect upon the structure is accounted for.

This analysis is of the utmost importance for the comparison between the Self-anchored and Ground-anchored model. On Chapter 5 there will presented plots of results such as longitudinal and transverse displacements at the top and bottom of the Tower, Pier E2 and Pier W2, as well as in Deck. Furthermore, an analysis of stresses is even more relevant and plots will be presented for the Deck. Also, forces such as axial in main cable/suspenders or longitudinal moment and axial in pier columns and piles are also presented.

5.8.2 MODAL

The dynamic characteristics of a structure are represented by its modal analysis. The mode shapes and their periods/frequencies are based on the mass and stiffness properties of the structure. These modal results (periods) are then parameters for response spectrum and time-history analysis. For this analysis, both Ritz and Eigen vectors can be used for the algorithm calculation. Eigen vectors determine the undamped elastic mode shapes, while Ritz vectors finds modes that are excited by a particular loading. Ritz can provide a good basis when used for time-history analysis that is based on superposition. The SAP standard convergence tolerance of 1E-04 was used.

Modal analysis is important to verify the behavior of the model and to eliminate possible modeling mistakes. To optimize the analysis time, a decision related to the number of modes that are relevant to the analysis is essential. For that, the Mass Participation Ratio of the modes should be analyzed. Graph 1 to 3 show the cumulative Mass participating ratio curve for longitudinal, transverse and vertical modes of vibration as a function of each vibration mode. From the graph below we can conclude that after the first 200 modes already 100% of the longitudinal and transverse modes of vibration of the structure are being included. Nevertheless, vertical modes of vibration have a smaller contribution to the initial modes because their contribution grows slowly in each mode. Stiffness contributing on the longitudinal and transverse directions of the bridge are smaller (bending of tower and deck, e.g), while stiffness contributing for the vertical direction is higher (Axial stiffness of piers, tower, cable e.g).

Therefore, only after a high number of modes the contribution of vertical modes is total. A minimum of 90% of MPRatio on longitudinal and transverse directions is recommended [58] for the choosing of degrees of freedom and n.ºmodes. A 60% minimum MPR for the vertical vibration modes was considered adequate as well. Therefore, only the first 200 modes were included in the calculations.

However, as shown in Graph 5.3, for the symmetric GAS model only after 250 modes a 60% cumulative mass participation ratio is included. Therefore, 300 modes were considered for this last model, in order to include 80% MPR like in previous models.

Chapter 6 will present the Modal analysis results for all three Ground-Anchored models.

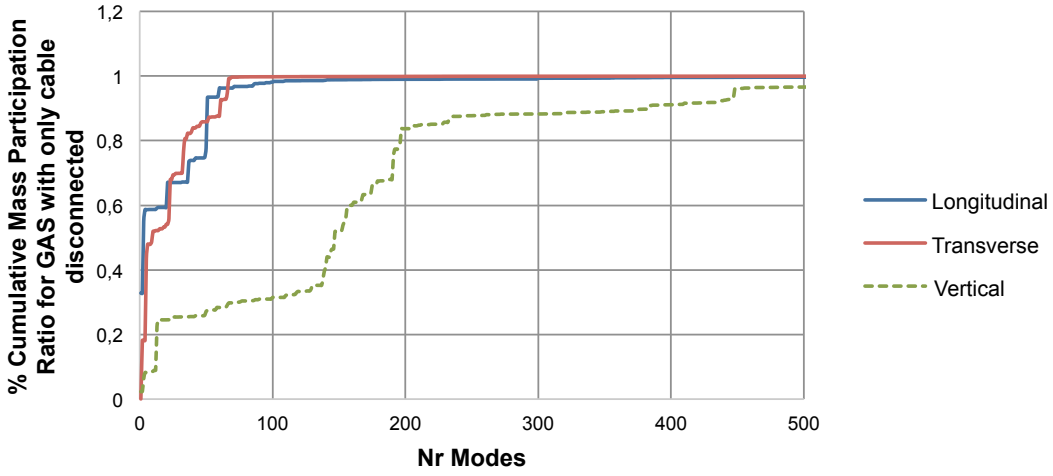

Graph 5.1 – % Cumulative Mass participation ratio for each mode for GAS model with cable disconnected.

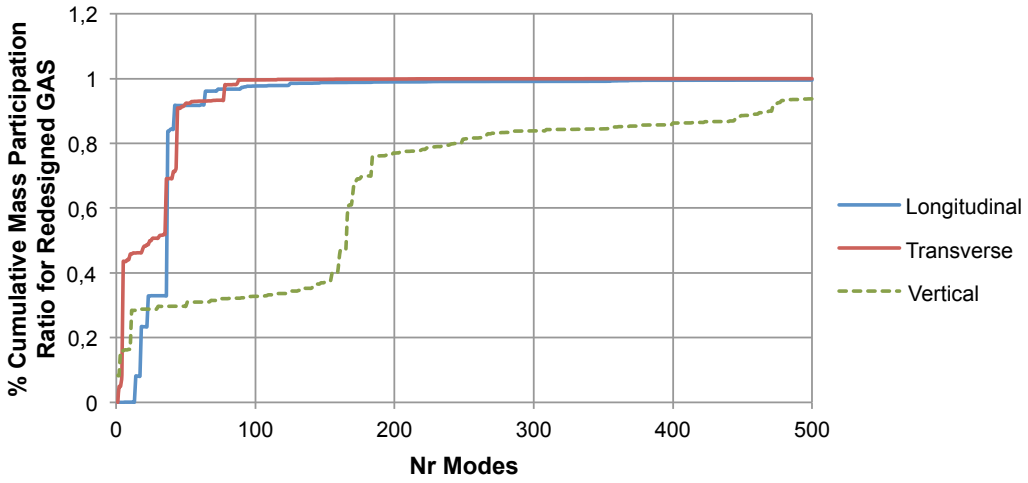

Graph 5.2 – % Cumulative Mass participation ratio for each mode for redesigned GAS model.

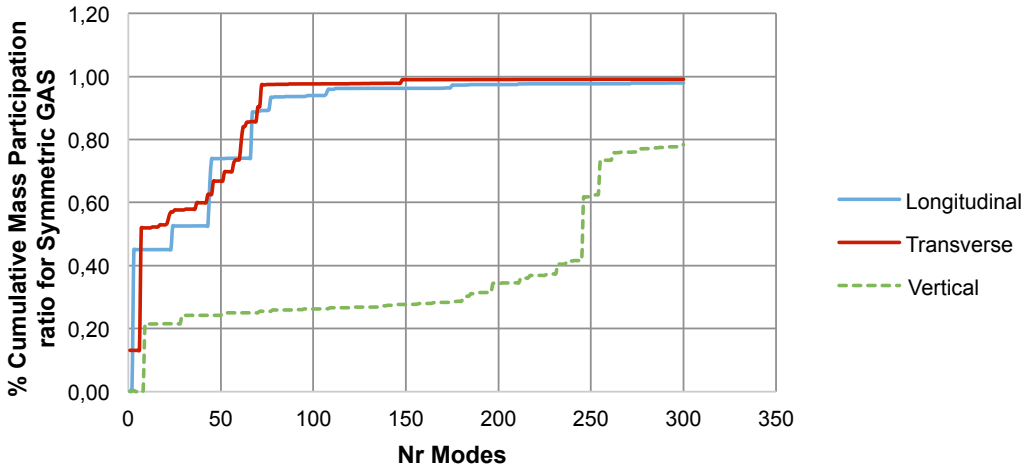

Graph 5.3 – % Cumulative Mass participation ratio for each mode for new symmetric GAS design.

5.8.3 NONLINEAR TIME-HISTORY

Time-History analysis consists on a step-by-step analysis of the response of a structure to a specific loading that varies with time and it may be a linear or nonlinear analysis. The loading does not consist of externally applied loads, but of foundation displacement or ground motion acceleration. When the structure deforms due to the ground-motion, inertial forces are created in the structure and internal forces in the elements. Since a given seismic motion can excite higher modes of the bridge and neglect higher modes of the bridge system, it can eventually introduce a significant error in the dynamic analysis results. For that, Graphs 1 to 3 were generated with SAP2000 and the number of modes to include was evaluated. The main disadvantages of the NL time-history are the high computational effort and the amount of output information generated. A FNA (Fast nonlinear analysis) is a modal solution of the equation of motion, that only accounts for nonlinear behavior in Link elements and ignores geometric or material nonlinearities everywhere else. The most accurate method to obtain the seismic demand is Direct Integration, but it is too computationally complex and time consuming.

Nevertheless, since the main goal in this study is to allow a comparison between two systems (self and ground anchored) and both of them will be subject to the same method of study, the FNA analysis was deemed adequate.

Some results for the Nonlinear Time-History analysis are presented on Chapter 6, for the optimized Ground-anchored suspension bridge models (GAS only with cable disconnected and symmetric GAS models).

5.9 LOAD CASES AND FUNCTIONS

According to AASHTO there are several Load combinations that can be used. For this study, there are going to be used two of the combinations also used for the SAS bridge official Design Criteria [58; 59]. Combination I relates to the normal vehicular use of the bridge without wind and Combination VII including earthquakes.

Combination I is used for Gravity and Modal analysis and Combination VII for Seismic analysis (Nonlinear Time-History). All dead loads have a factor of 1.0. For Dynamic analysis (Seismic), Live load is not included in the model.

Table 5.12 – Load Combination [58; 59].

Load Combination	Calculation
I	γ*βd*DL + 1,67*(L+I) + 1.0*(CF+B+SF) + βe*E + 0,77*PS
VII	1.0*DL + 1.0*(B+SF) + βe*E + 1.0*PS + 1.0*EQ

OBS.1: γ*βd factor is taken as 1.0 for suspension bridges whenever it controls the design.

OBS.2: CF (Centrifugal force), B (Buoyancy), SF (Stream flow pressure) and PS (Prestress). These forces are all considered zero in this study.

5.9.1 DEAD LOAD

The self-weight of the elements is automatically considered by the program (self-weigh multiplier x1). Also, some additional loads need to be considered such as the overlay, the counterweight/ bike lane and the guardrails. For these last 3 loads, tables 5.13 to 5.15 provide the calculations and values used to represent them in the SAP model. The overlay (asphalt) load was considered uniform and acting over the three deck top plates containing the road lanes. The counterweight and guardrail loads act on the top edge plates of the deck and were applied as joint loads.

Table 5.13 – **Dead load for counterweight/bike lane**

Counterweight and Bike lane				
		Quantities		
	Trapezoidal Cross section Length/Heights (ft)	7,239	6,93	0,984
	Area Cross Section (ft^2)	28,64		
	Normal weight of concrete w/ reinforcement	2480 kg/m^3	0,1546 $kips/ft^3$	
	Total weight of Cross section (kips/ft)	**4,3**		
Joints	**Type 1**: influence length = 5m = **16,4ft**	**69 kips**		
	Type 2: influence length = 7,5m = **24,6 ft**	**103 kips**		
	Type 3: influence length = 10m = **32,8 ft**	**138 kips**		

OBS1: Weights of materials from pg. 423/1204 of Caltrans official project drawings.

Table 5.14 – Dead load for Overlay.

	Epoxy AC overlay	
Weight of Epoxy AC Overlay	2365 kg/m3	0,147 $kips/ft^3$
Thickness of Epoxy Layer	50 mm	0,164 ft
Uniform area loading	**0,024 $kips/ft^2$**	

Table 5.15 – Dead load for Guard Rails.

Guard rails (outside plate and diaphragms)			
Thickness of Bent Plate	12 mm	0,03936 ft	
Area of Bent Plate (ft^2)	0,27		
3 side lenght of Rail Guard Bent plate (ft)	Top= 1,00	Height =2,82	Bottom= 1,75
Thickness of Diaphragm	12 mm	0,03936 ft	
Spacing between diaphragms	900 mm	2,952 ft	
Volume of diaphragm (ft^3)	0,153		
Volume of Bent Plate (ft^3)	0,78		
Assumed weight Guard Rail ($kips/ft^3$)	0,5		
Total weight (for @ 900mm) (kips)	**0,465**		
Joints	**Type 1**: influence length = 5m = **16,4ft**	**7,6 kips**	
	Type 2: influence length = 7,5m = **24,6 ft**	**11,5 kips**	
	Type 3: influence length = 10m = **32,8 ft**	**15,5 kips**	

The guardrail loads are considered on the edge of the lane width, four locations in total (inside and outside of both decks). The counterweight load is only considered on the outside of both decks (two locations in total). Fig. 5.20 shows a portion of the deck with the guardrails and counterweight joint loading (non-structural elements).

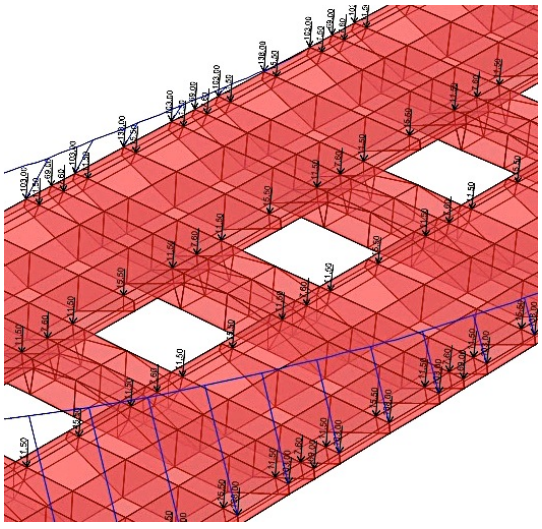

Fig. 5.20 – Non-structural elements loading in SAP2000 models.

5.9.2 LIVE LOAD

According to AASHTO (American Association of State and Highway Transportation Officials) and the Design Criteria for the SAS Bay Bridge span there are considered 6 lanes. The width of the top interior plates in the model is approximately 76 ft.

$$\text{Lane} = \text{INT}(w/12ft) = 76/12 = 6,(3) \approx 6 \text{ lanes} \quad (5.1)$$

Considering a truck type of HS 20-44, it specifies a uniform loading of 640 lb/ft^2 per lane. Therefore, for the 6 road lanes the total uniform load is 3840 lb/ft.

$$L = 3840 / 76 = 50 \text{ lb/ft}^2 \quad (5.2)$$

Therefore, the uniform load on the top interior plates is 42 lb/ft^2. According to Table 5.15, the load combination I has a factor of 1,67 for Live Load.

$$L = 1,67 * 50 = \mathbf{84 \text{ lb/ft}^2 = 0,084 \text{ kips/ft}^2} \quad (5.3)$$

Since the goal is to maximize the response for the main span and there is no connection between the tower and deck, there are 2 possible distributions of forces that could be used. Distribution A considers uniform Live load for both spans L1 and L2 (maximize Moment on top of Pier E2) and Distribution B considers only uniform Live load at span L1 (maximize bending moment in main span). See Fig. 5.21 with span numeration. For the present study distribution B was used, in order to maximize the stresses at the main span.

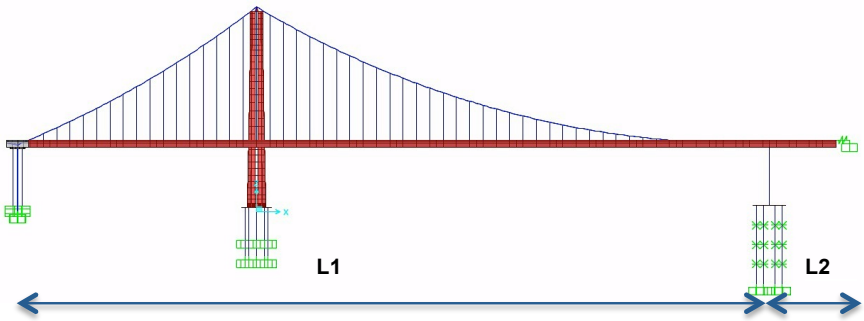

Fig. 5.21 – XZ view of SAS model with span division.

For concentrated loads, AASHTO recommends 18 kips for maximum Moment and 26 kips for maximum Shear. Since the bending moment is much higher for this span than the shear forces, 18 kips are going to be applied at the critical section of the main span (x=+180m). In order to have the most detrimental effect, this concentrated load is going to be applied symmetrically at the inside edge of road lanes (2 locations, one at each roadway).

$$1,67 * 18 = \mathbf{30 \text{ kips}} \quad (5.4)$$

5.9.3 P-DELTA

The load case was defined as Nonlinear Static and considering the effect of Dead (self-weight, overlay, guardrails) and Live loads on the structure: Also, Large Displacements Geometric

Nonlinearity was considered, since the bridge is expected to undergo large deformations (translations and rotations on SAP only, strains are assumed to be small for each element). On this case, the equilibrium equations have to be written for the deformed geometry. Cable element modeled as a frame should always be divided into smaller elements, in order to keep strains and relative rotations values low within each element.

The results for this P-Delta load case are used afterwards for other Load cases analysis, which start with the P-Delta results as initial conditions.

5.9.4. MODAL

The Modal analysis is linear and takes the stiffness from the PDelta Load case as initial conditions, in order to ensure the cables are in tension. Moreover, Eigen vectors method is used to determine the undamped free-vibration mode shapes and frequencies of the system. As discussed previously on section 5.8, the maximum number of modes considered necessary was 200 for both GAS with only cable disconnected and redesigned GAS and 300 modes for the symmetric GAS.

5.9.5. NL TIME HISTORY

The ground motion functions used for this analysis are shown in Fig. 5.1 and 5.2. For those multi-support excitations, load patterns were created for each direction (total of 6). Afterwards, the restraints were selected (W2 and T1 separately from E2, which as different foundation conditions) are assigned a unitary displacement for each direction for the load patterns. Afterwards, the ground-motion functions are going to scale the unitary displacements in each direction. The method used is Modal Nonlinear (FNA). For this modal method a damping of 3-5% is the usual value for reinforced concrete bridges [55]. Chopra also states that for welded steel under working stress (no more than half of yield point) the recommended damping value is between 2 and 3% [61]. Also EC8-part 2 [60] recommends 2% of damping for welded steel elements. Since the entire deck and tower of the Self-anchored span are comprised of welded steel plates, it seemed a reasonable assumption to consider **2% damping coefficient** constant for all modes.

The time-history functions have 59s of duration, which implies 1180 output steps of 0,05s size each. The initial conditions will be at the end of a nonlinear modal history load case (Gravity). This Nonlinear (FNA) load case was defined as a function (RAMPTH) for the Dead Load addition to the system that takes 50s to fully achieve 100% Dead load contribution and lasts 100s in total. This allows a slow input of the Dead load to the system. If these conditions are not considered before the Time-history calculation, the instantaneous input of Dead load may alter the dynamic response itself. Also, mode shapes from the Modal Load Case will be used for the non-linear time-history analysis.

6
ANALYSIS RESULTS

6.1 STATIC GRAVITY ANALYSIS

This Chapter includes plots of the models developed, in order to allow further comparison and conclusions. The conclusions and study of these results will briefly be presented on Chapter 7. The main goal of this analysis is a comparison of deformed shape and stresses for the imposed Dead and Live loads. No prestress forces were introduced in the suspenders, as discussed before. These suspenders' forces intend to annul the effects of the loading on the deformed shape of the deck and would influence the analysis.

6.1.1 SAS MODEL

6.1.1.1 Stresses

After running the *PDelta* Load Case (see Chapter 5), the deck deformed vertically as expected. Since the West side has a stiffer connection with an almost rigid cap beam, the deformation on this side is relatively low. In contrast, on the East side, the connection to the deck is only pinned, which results in fairly large rotation and deformation of the deck elements. The longitudinal stresses on the Deck top and bottom faces can be seen on Fig. 6.1 and 6.2. The material of the orthotropic deck plates is Grade 50 steel. Its minimum yield stress is 345 MPa or 50ksi.

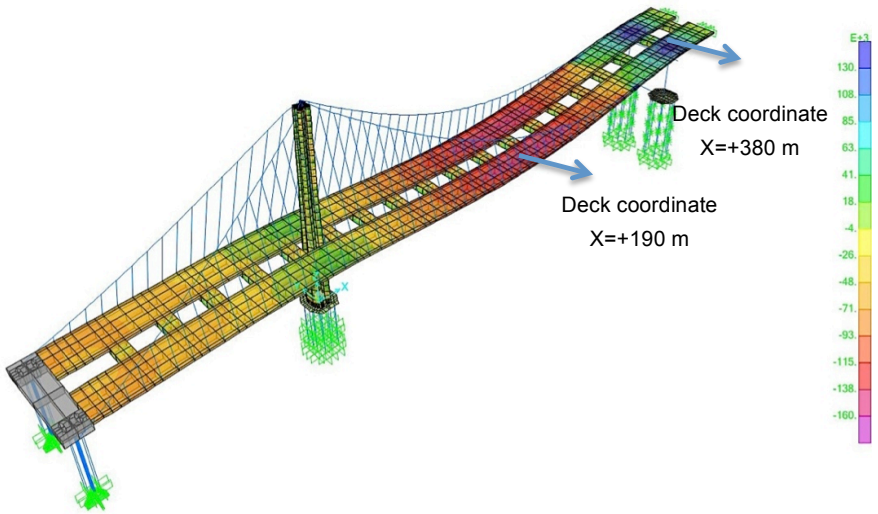

Fig.6.1 – Longitudinal stresses on the **top plates of the SAS bridge deck** for Gravity Analysis.

More specifically, the maximum compressive and tensile longitudinal stresses for top plates are -165 MPa or -23,9ksi (X=+190m) and 140 MPa or 20,3ksi (X=+380m). Comparatively to the yield point, the demand/capacity ratio is 48% and 41%, respectively.

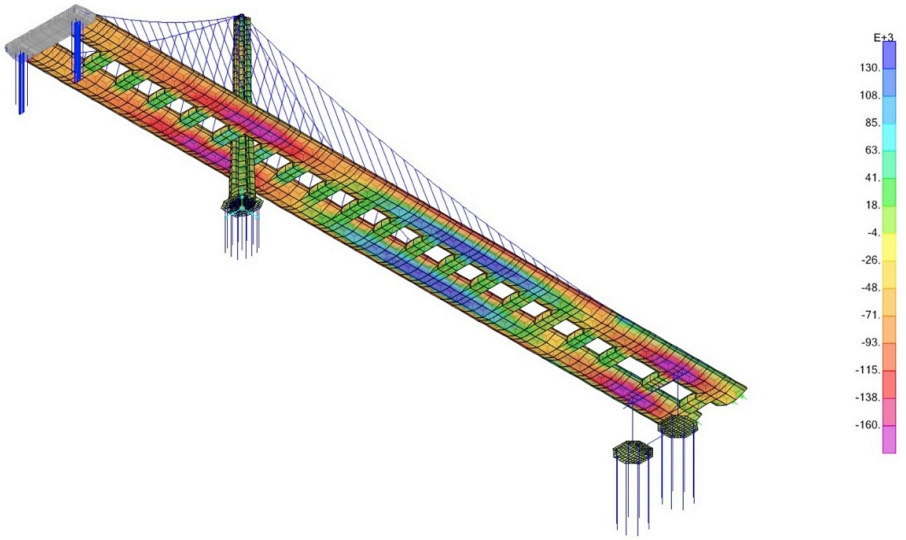

Fig.6.2 – Longitudinal stresses on the **bottom plates of the SAS bridge deck** for Gravity analysis.

For bottom plates, the maximum compressive and tensile longitudinal stresses are -192 MPa or -27,8ksi (X=0m) and 126 MPa or 18,3ksi (X=+210m). Comparatively to the yield point, the demand/capacity ratio is 56% and 37%, respectively.

These stresses are more than half below the yielding point.

6.1.1.2 Forces

The axial force at the cables is enumerated at Table 6.1 as well as their Demand/Capacity ratio. The forces at Pier W2, Pier E2, Piles and East end of SAS bridge are shown in table 6.2.

Table 6.1 – **Axial Force** at the cables for Gravity analysis

	Location	Axial Force [kN / kips]	Capacity	Demand/ Capacity Ratio
Main Cable	Top of Tower saddle (East Side)	190420 / 42806	Area main cable=0,4778 m^2 Minimum Yield Stress=1350 MPa **Capacity= 645080 kN** (145014 kips)	**30%**
	East anchorage Working Point	156300 / 35136		**24%**
	Top of Tower saddle (West Side)	200400 / 45050		**31%**
	West anchorage Working Point	171400 / 38531		**27%**

	Location	Axial Force [kN / kips]	Capacity	Demand/ Capacity Ratio
Suspenders	At the Tower	12090 / 2718	Area=0,025 m^2 Minimum Yield Stress=1350 MPa **Capacity= 33750 kN** (7587 kips)	**36%**
	2nd from the Tower (West - East)	3620 – 3500 / 814 - 787		**11%**
	Anchorage (West - East)	2600 – 2500 / 584,5 - 562	Area=0,015 m^2 Minimum Yield Stress=1350 MPa **Capacity= 20782 kN** (4672 kips)	**12%**

Table 6.2 – **Forces** at the Piers and piles for SAS Gravity analysis

	Location	Axial Force [kN / kips]			D/C Ratio	M 2-2 [kN.m/ kips.in]		D/C Ratio
Pier W2	West columns Top	-8360 / -1879	**Axial Capacity =** 115300 kN (tension)	= -486500 kN (compression)	≈ 0	32800 / 290292	**Bending Capacity =** 150000 kN.m	22%
	West columns Bottom	-19800 / -4451			4%	-31000 / -274362		21%
	East columns Top	≈ 0			≈ 0	32800 / 290292		22%
	East columns Bottom	-11400 / -2563			2%	-31000 / -274362		21%
Pier E2	Top Pier	-78000 / -17534	**Axial Capacity =** 308900 kN (tension)	-1114300 kN (comp)	7%	-60000 / -318614	**Bending Capacity =** 636850 kN.m	9%
	Bottom Pier	-109650 / -24649			10%	-332300 / -2940980		52%

	Location	Axial Force [kN / kips]		D/C Ratio	M 2-2 [kN.m/ kips.in]		D/C Ratio
Tower Piles	Eastern edge Pile Top	-56900 / -12791	**Axial Capacity =** 38700 kN (tension) -120700 kN (comp)	47%	925 / 8187	**Bending Capacity =** 40200kN.m	≈ 0
	Eastern edge Pile 1st fixed support	-58650 / -13184		48,5%	-1800 / -15931		5%
E2 Piles	Eastern edge Pile Top	-16550 / -3720		14%	5600 / 49562		14%
	Eastern edge Pile 1st roller support	-18500 / -4159		15%	-5900 / -52217		15%
	Eastern edge Pile 2nd roller support	-20800 / -4676		17%	1500 / 13276		4%
E2 End Spring Reactions (fixed restraint)		N = ≈ 0		V = -7700 kN / -1731 kips		M 2-2 = -77000 kN.m / 681479 kips.in	

It is relevant to plot the Pier W2 and E2 columns combined capacity with the results of the static load case. As it can be observed in Graph 6.1 and 6.2, the Gravity loading creates very small combined forces at the piers top and bottom when compared with the piers capacity.

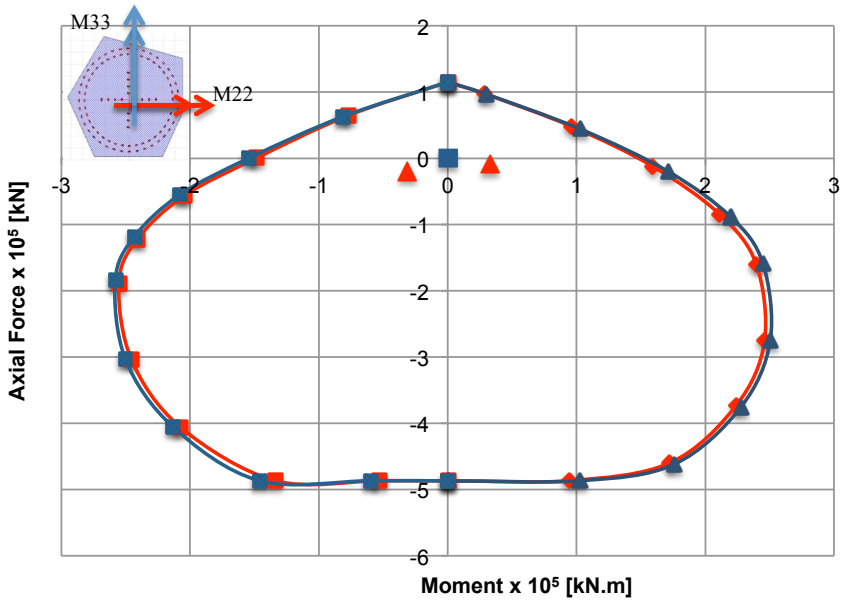

Graph 6.1 – Interaction curve P-M for W2 columns with Gravity analysis maximum results.

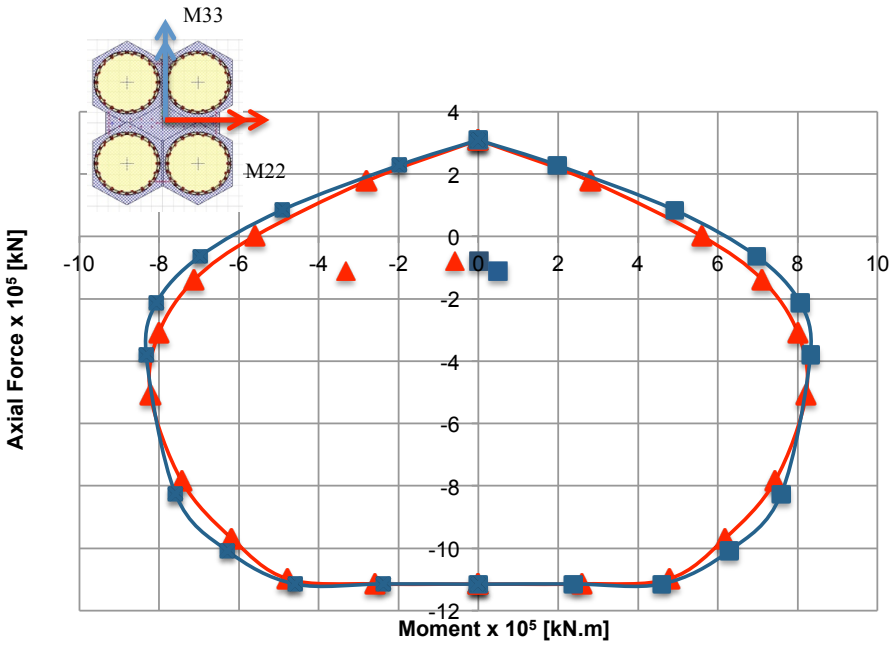

Graph 6.2 – Interaction curve P-M for E2 piers with Gravity analysis maximum results.

6.1.1.3 Displacements

We can conclude that the absolute maximum vertical displacement occurs approximately at the mid-point of the main span and that the vertical displacements on the back span are very reduced when compared to the main span. This is due to the rigid cap beam on the West side, which restrains very much the displacements on the back span of the deck. The color scale bar for vertical displacements is from 0,35 to -4,20m. The longitudinal displacements diagram has a color scale bar of 0,66 to -0,77m.

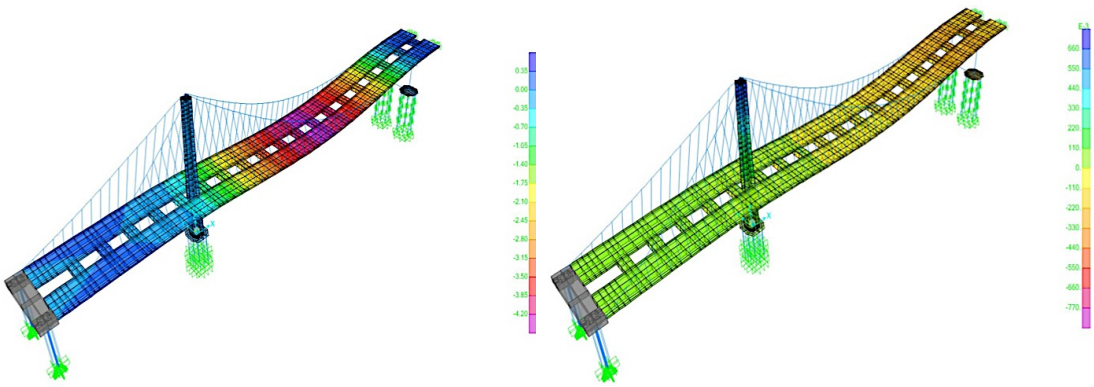

Fig.6.6 – Vertical and longitudinal displacements for SAS bridge for Gravity Analysis, respectively

Table 6.3 – **Vertical and longitudinal displacements** for Gravity analysis

Location		Vertical displacements (Z axis)		Longitudinal Displacements (X axis)	
		[m]	[in]	[m]	[in]
Deck	X= - 85m (mid back span)	+0,077	+3,03	+0,055	+2,17
	X=0m (at Tower)	-0,59	-23,2	-0,052	-2,05
	X= 180m (max displac)	**-4,213**	-165,9	-0,195	-7,68
	X= 190m (mid main span)	-4,211	-165,78	+0,207	+8,15
	X= 425m (East cantilever)	+0,165	+6,50	+0,300	+11,8
Tower	Top of Tower Z=156m	-0,113	-4,45	**+0,62**	+24,4
	Tower at deck level Z=53m	-0,039	-1,54	≈ 0	

The total length of the span is 556m from W2 cap beam to top of the Pier E2, since there is no connection between the deck and the tower. The ratio of the maximum vertical displacement over the total length is 0,8%.

6.1.2 GAS MODEL WITH CABLE DISCONNECTED

6.1.2.1 Stresses

The scale for Fig. 6.7 is the same as in previous plots (-160 MPa to 130 MPa), but the gradient changes considerably when compared to the plot in Fig. 6.1 for the SAS model.

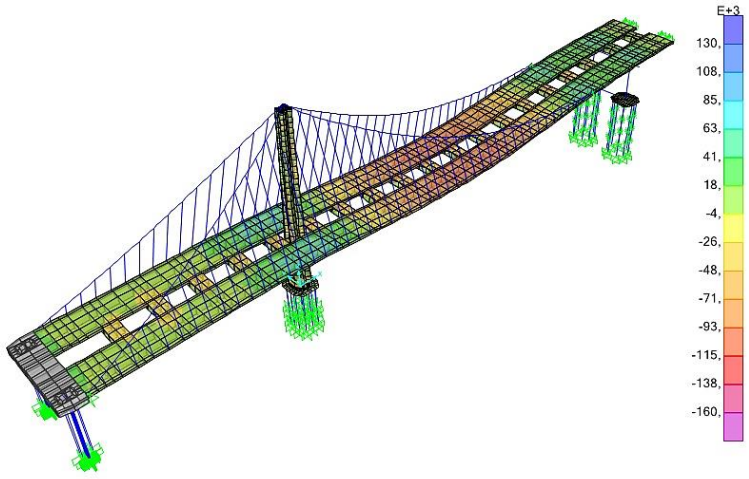

Fig.6.7 – Longitudinal stresses on the **top plates of the GAS bridge deck** for Gravity Analysis

More specifically, the maximum compressive and tensile longitudinal stresses for top plates are -84 MPa or -12,2ksi (X=+190m) and +61 MPa or 8,8ksi (X= 0m). The demand/capacity ratio is 24% and 18%, respectively. For top plates in the middle of the main span (x=190m), a 50% reduction is registered.

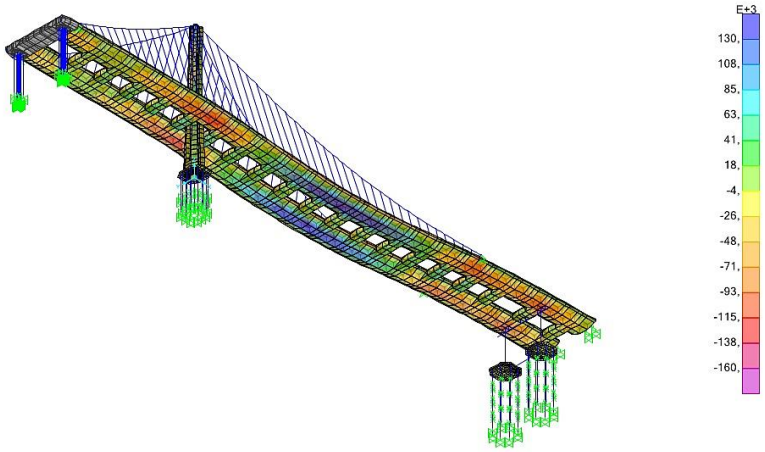

Fig.6.8 – Longitudinal stresses on the **bottom plates of the GAS bridge deck** for Gravity Analysis

For bottom plates, the maximum compressive and tensile longitudinal stresses are -115 MPa or -16,7ksi (X=+385m) and +133,5 MPa or 19,4ksi (X=+150m). The demand/capacity ratio is 34% and 39%, respectively. For bottom plates in the middle of the main span (x=210m), a 20% reduction is registered. These reductions in stresses are expected, since in the ground-anchored bridge model the main cable is no longer introducing compressive forces into the deck.

6.1.2.2 Forces

The axial force in the main cable for this GAS model has an 18% overall reduction when compared to the SAS model values.

Table 6.4 – **Axial Force** at the cables for Gravity analysis for GAS model.

	Location	Axial Force [kN / kips]	Capacity	Demand/ Capacity Ratio
Main Cable	Top of Tower saddle (East Side)	160150 / 38081	Area main cable=0,4778 m^2 Minimum Yield Stress=1350 MPa **Capacity= 645080 kN** (145014 kips)	**25%**
	East anchorage Working Point	132000 / 31472		**21%**
	Top of Tower saddle (West Side)	170400 / 40486,5		**26%**
	West anchorage Working Point	144000 / 34372		**22%**

	Location	Axial Force [kN / kips]	Capacity	Demand/ Capacity Ratio
Suspenders	At the Tower	15300 / 3158,4	Area=0,025 m^2 Minimum Yield Stress=1350 MPa **Capacity=33750 kN** (7587 kips)	**45%**
	X= +20m (West - East)	3550–3300 / 809 - 753		**10%**
	X= +50m	2220 / 500	Area=0,015 m^2 Minimum Yield Stress=1350 MPa **Capacity= 20782 kN** (4672 kips)	**11%**

Table 6.5 – **Forces** at the Piers and piles for Gravity analysis for GAS model.

	Location	Axial Force [kN / kips]		D/C Ratio	M 2-2 [kN.m/ kips.in]		D/C Ratio
Pier W2	West columns Top	-5200 / -1169	**Axial Capacity =** 115300 kN (tension) = -486500 kN (compression)	≈ 0	-3800 / -33631	**Bending Capacity =** 150000 kN.m	**2,5%**
	West columns Bottom	-16600 / -3732		4%	-4900 / -43721		**3%**
	East columns Top	-39100 / -8790		8%	3800 / 33631		**2,5%**
	East columns Bottom	-50500 / -11352		10%	4900 / 43721		**3%**
Pier E2	Top Pier	-52000 / -11690	**Axial Capacity =** 308900 kN (tension) -1114300 kN	5%	930 / 8231	**Bending Capacity =** 590000 kN.m	≈ 0
	Bottom Pier	-84000 / -18883		8%	6000 / 53102		≈ 0

	Location	Axial Force [kN / kips]		D/C Ratio	M 2-2 [kN.m/ kips.in]		D/C Ratio
Tower Piles	Eastern edge Pile Top	-50300 / -11307	**Axial Capacity =** 38700 kN (tension) -120700 kN (comp)	42%	730 / 6461	**Bending Capacity =** 40200kN.m	**2%**
	Eastern edge Pile 1st fixed support	-52000 / -11690		43%	-1350 / -11948		**3,5%**
E2 Piles	Eastern edge Pile Top	-21800 / -4901		18%	-63 / -558		≈ 0
	Eastern edge Pile 1st roller support	-23700 / -5328		20%	85 / 752		≈ 0
	Eastern edge Pile 2nd roller support	-26200 / -5890		22%	-20 / -177		≈ 0
	E2 End Spring Reactions (fixed restraint)	N = 0		V = -710 kN / -160 kips		M= 7100 kN.m / 62838 kips.in	

6.1.2.3 Displacements

The scale of the vertical displacement plot varies from 0 to -2,6 m. The maximum vertical displacement in the main span of this GAS model is approximately -2,66m. The scale for the longitudinal displacement varies from 0,48 to -0,56 m. The longitudinal displacement at the top of the tower is 0,464 m. The vertical displacement for this GAS model has a 40% decrease when compared to the previous SAS Bay Bridge model, since also the forces and stresses are considerably reduced. Nevertheless, the suspenders' *target forces* were not considered for this comparison.

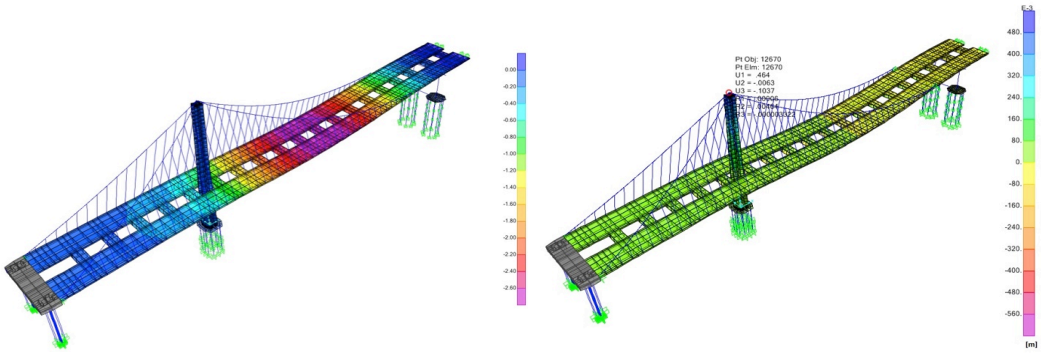

Fig.6.9 – Vertical and longitudinal displacements for GAS bridge for Gravity Analysis, respectively.

Table 6.6 – **Vertical and longitudinal displacements** for Gravity analysis

	Location	Vertical displacements (Z axis)		Longitudinal Displacements (X axis)	
		[m]	[in]	[m]	[in]
Deck	X= - 85m (mid back span)	-0,169	-6,65	+0,028	+1,10
	X=0m (at Tower)	-0,66	-25,98	-0,049	-1,93
	X= 160m (max displac)	**-2,736**	-107,7	-0,008	-0,3
	X= 190m (mid main span)	-2,577	-101,5	+0,014	+0,55
	X= 425m (East cantilever)	+0,015	+0,60	-0,011	-0,43
Tower	Top of Tower z=156m	-0,10	-3,94	**+0,423**	+16,65
	Tower at deck level Z=53m	-0,035	-1,38	≈ 0	

The total length of the span is 556m from W2 cap beam to top of the Pier E2, since there is no connection between the deck and the tower. The ratio of the maximum vertical displacement over the total length is 0,5 %.

6.1.3 REDESIGNED GROUND-ANCHORED MODEL

6.1.3.1 Stresses

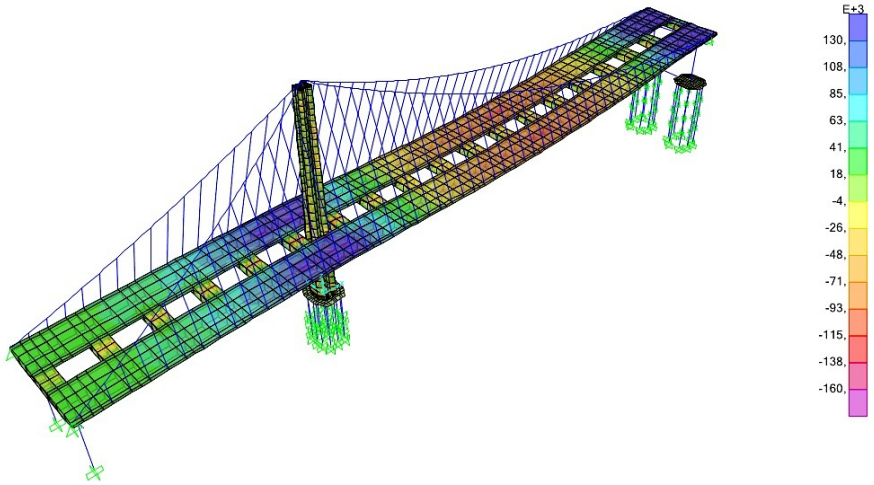

Fig.6.10 – Longitudinal stresses on the **top plates of the redesigned GAS bridge deck** for Gravity Analysis.

The maximum compressive and tensile longitudinal stresses for top plates are -95,5 MPa or -13,8ksi (X=+180m), +152 kPa or 22ksi (X= 0m) and +315 MPa or 45,7ksi (X=380m). The demand/capacity ratios are 28%, 44% and 90%, respectively. For top plates in the middle of the main

span (x=+180m), a 40% reduction is achieved when compared with the SAS model. Nevertheless, the stresses at top of Pier E2 reach too high levels.

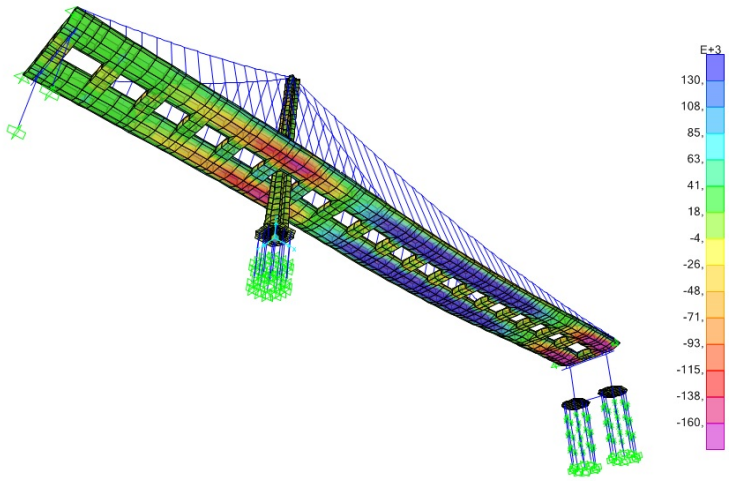

Fig.6.11 – Longitudinal stresses on the **bottom plates of the redesigned GAS bridge deck** for Gravity Analysis

For bottom plates, the maximum compressive and tensile longitudinal stresses are -162 MPa or -23,5ksi (X=0m) and 258 MPa or 37,4ksi (X=+180m). The demand/capacity ratio is 47% and 75%, respectively.

6.1.3.2 Forces

The axial forces in the main cable for this redesigned GAS model are very similar when compared to the SAS model values and have a 15% increase when compared to the previous GAS model.

Table 6.7 – **Axial Force** at the cables for Gravity analysis for redesigned GAS model.

	Location	Axial Force [kN / kips]	Capacity	Demand/ Capacity Ratio
Main Cable	Top of Tower saddle (East Side)	177400 / 39880	Area main cable=0,4778 m^2 Minimum Yield Stress=1350 MPa **Capacity= 645080 kN** (145014 kips)	**28%**
	East anchorage Working Point	154000 / 34619		**24%**
	Top of Tower saddle (West Side)	200200 / 45005		**31%**
	West anchorage Working Point	168900 / 37969		**26%**

	Location	Axial Force [kN / kips]	Capacity	Demand/ Capacity Ratio
Suspenders	At the Tower	23000 / 5170	Area=0,025 m^2 Minimum Yield Stress=1350 MPa	**68%**
	X= +20 m (West - East)	10150 – 9150 2282-2057	**Capacity= 33750 kN** (7587 kips)	**30%**
	X= +50m	1300 / 292	Area=0,015 m^2 Minimum Yield Stress=1350 MPa **Capacity = 20782 kN** (4672 kips)	**6%**

Table 6.8 – **Forces** at the Piers and piles for Gravity analysis for GAS model.

	Location	Axial Force [kN / kips]		D/C Ratio	M 2-2 [kN.m/ kips.in]		D/C Ratio
Pier W2	Top Pier	-25000 / -5620	**Axial Capacity =** 308900 kN (tension) = -1114300 kN (compression)	2%	1000 / 8850	**Bending Capacity =** 590000 kN.m	≈ 0
	Bottom Pier	-59500 / -13376		5%	25260 / 223560		**4%**
Pier E2	Top Pier	-60000 / -13488		5%	≈ 0		≈ 0
	Bottom Pier	-91300 / -20524		8%	-700 / -6195		≈ 0

	Location	Axial Force [kN / kips]		D/C Ratio	M 2-2 [kN.m/ kips.in]		D/C Ratio
Tower Piles	Eastern edge Pile Top	-55200 / -12409	**Axial Capacity =** 38700 kN (tension) -120700 kN (comp)	46%	650 / 6461	**Bending Capacity =** 40200kN.m	**2%**
	Eastern edge Pile 1st fixed support	-56900 / -12791		47%	-1430 / -12656		**4%**
E2 Piles	Eastern edge Pile Top	-21200 / -4766		18%	≈ 0		≈ 0
	Eastern edge Pile 1st roller support	-23000 / -5170		19%			
	Eastern edge Pile 2nd roller support	-25400 / -5710		21%			

6.1.3.3 Displacements

The scale of the vertical displacement plot varies from 0 to -5,2m. The maximum vertical displacement in the main span is 5,5m. The scale for the longitudinal displacement varies from 0,56 to -1,26 m. The longitudinal displacement at the top of the tower is 0,464 m. The vertical displacement for this GAS model corresponds to a 25% increase when compared to the previous SAS model and a 50% increase compared to the previous GAS model.

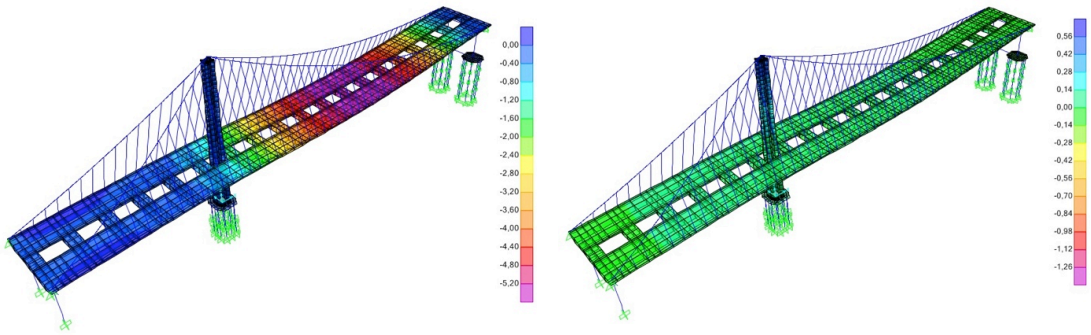

Fig.6.12 – Vertical and longitudinal displacements for redesigned GAS bridge for Gravity Analysis, respectively

Table 6.9 – **Vertical and longitudinal displacements** for Gravity analysis

	Location	Vertical displacements (Z axis)		Longitudinal Displacements (X axis)	
		[m]	[in]	[m]	[in]
Deck	X= - 85m (mid back span)	-0,02	-0,79	+0,015	+0,59
	X=0m (at Tower)	-0,96	-37,8	+0,086	+3,39
	X= 170m (max displac)	**-5,50**	-216,5	-0,019	-0,748
	X= 190m (mid main span)	-5,45	-214,6	≈ 0	
Tower	Top of Tower z=156m	-0,11	-4,33	**+0,524**	+20,6
	Tower at deck level Z=53m	-0,035	-1,38	≈ 0	

The total length of the span is 556m from W2 pier to E2 pier, since there is no connection between the deck and the tower. The ratio of the maximum vertical displacement over the total length is 1%.

6.1.4 SYMMETRIC GROUND-ANCHORED MODEL

After observing the behavior of the SAS and the two GAS models discussed in previous sections, it was clear that having the unequal spans in the SAS Bay Bridge is the cause of the inefficiency of the design. Consequently, a symmetric design was created and analyzed. Moreover, as discussed before, this symmetric GAS model underwent some improvements, based on a first analysis. The conclusions withdrawn from that initial analysis are discussed in Chapter 7. The following results are for the improved design, without suspender cables connected directly to the tower, with uniform suspender cross-section and lighter deck and tower elements. Again, like in the previous models the suspenders were not prestressed during this comparative study. Nevertheless, on Chapter 7 these prestressing forces will be discussed for this symmetric model.

6.1.4.1 Stresses

The maximum compressive and tensile longitudinal stresses for top plates are -84,5 MPa or -12,3ksi (X=+130m), +100 MPa or 14,5ksi (X= 0m) and +190E MPa or 27,6ksi (X=±280m). The demand/capacity ratios are 25%, 29% and 55% respectively. For top plates in the middle of the main span (x=180m) and near the tower (x=0), a 45% reduction and a 31% increase are observed when compared to the original SAS model, respectively.

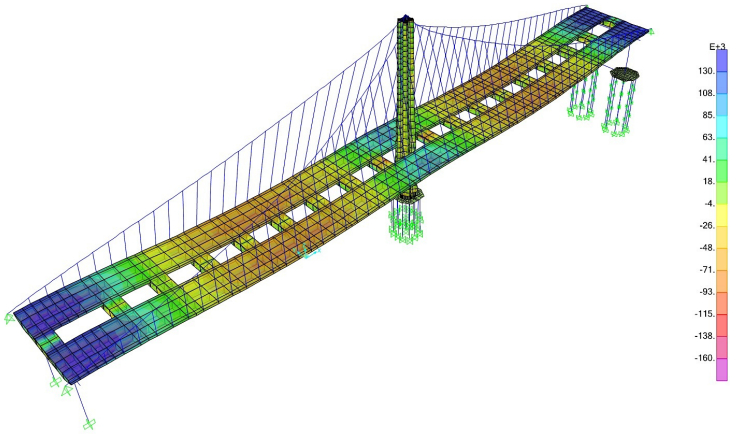

Fig.6.13 – Longitudinal stresses on the **top plates of the symmetric GAS bridge deck** for Gravity Analysis.

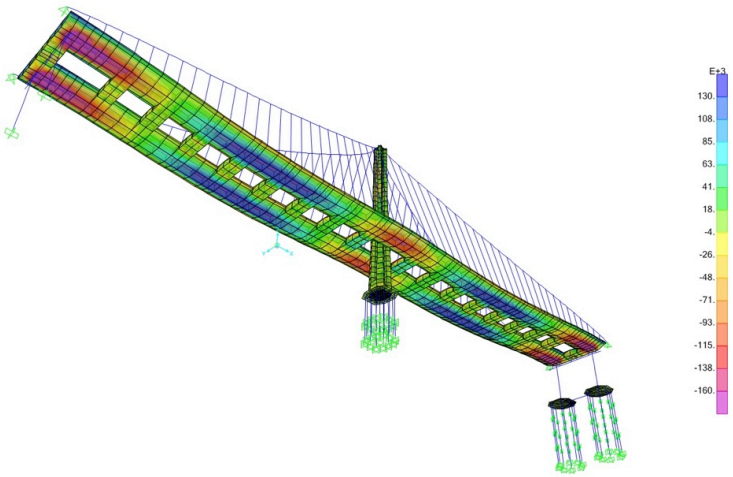

Fig. 6.14 – Longitudinal stresses on the **bottom plates of the symmetric GAS bridge deck** for Gravity Analysis.

For bottom plates, the maximum compressive and tensile longitudinal stresses are -140E+03kPa or -20,3ksi (X=0m), -270E+03kPa or -39ksi (X=±280m) and +161,5E+03kPa or 23,4ksi (X=±130m). The demand/capacity ratio is 41%, 78% and 47%, respectively.

6.1.4.2 Forces

The axial force in the main cable for this symmetric redesigned GAS model has a 30% decrease when compared to the original SAS and a 25% decrease when compared with the other GAS models discussed earlier.

Table 6.10 – **Axial Force** at the cables for Gravity analysis for symmetric GAS model.

	Location	Axial Force [kN / kips]	Capacity	Demand/ Capacity Ratio
Main Cable	Top of Tower saddle	137000 / 30798	Area main cable=0,4778 m^2 Minimum Yield Stress=1350 MPa	**21%**
	Anchorage	115500 / 25964	**Capacity= 645080 kN** (145014 kips)	**18%**
Suspenders	X=+10m	14800 / 3327	Area=0,015 m^2 Minimum Yield Stress=1350 MPa	**71%**
	X=+100 m	900 / 202	**Capacity = 20782 kN** (4672 kips)	**4%**

Table 6.11 – **Forces** at the Piers and piles for Gravity analysis for symmetric GAS model.

	Location	Axial Force [kN / kips]		D/C Ratio	M 2-2 [kN.m/ kips.in]		D/C Ratio
Pier W2	Top Pier	-93500 / -21019	**Axial Capacity =** 308900 kN (tension) = -1114300 kN (compression)	8%	- 3700/ -32746	**Bending Capacity =** 590000 kN.m	≈ 0
	Bottom Pier	-125600 / -28235		11%	1500/ -13276		
Pier E2	Top Pier	-2000 / -500		≈ 0	3500 / 30976		
	Bottom Pier	-30000 / -6744		3%	-1000 / -8850.4		

	Location	Axial Force [kN / kips]		D/C Ratio	M 2-2 [kN.m/ kips.in]	D/C Ratio
Tower Piles	Eastern edge Pile Top	-33300 / -7486	Axial Capacity = 38700 kN (tension) -120700 kN (comp)	27%	≈ 0	≈ 0
	Eastern edge Pile 1st fixed support	-35000 / -7868		29%		
E2 Piles	Eastern edge Pile Top	-15600 / -3507		13%		
	Eastern edge Pile 1st roller support	-17300 / -3889		14%		
	Eastern edge Pile 2nd roller support	-19500 / -4384		16%		

Bending Capacity = 40200kN.m

6.1.4.3 Displacements

The scale of the vertical displacement plot varies from 0 to -2,6m. The maximum vertical displacement in the main span was -2,7m. Since this GAS model is symmetric, the longitudinal displacements are almost non-existent and can be ignored. The vertical displacement for this GAS model has a 40% decrease when compared to the original SAS and a 50% decrease compared to the redesigned GAS discussed earlier (subchapter 6.1.3). The -2,7m vertical displacement is nevertheless very similar to the maximum displacement measured at the GAS model created only by disconnecting the cable from the deck on the SAS.

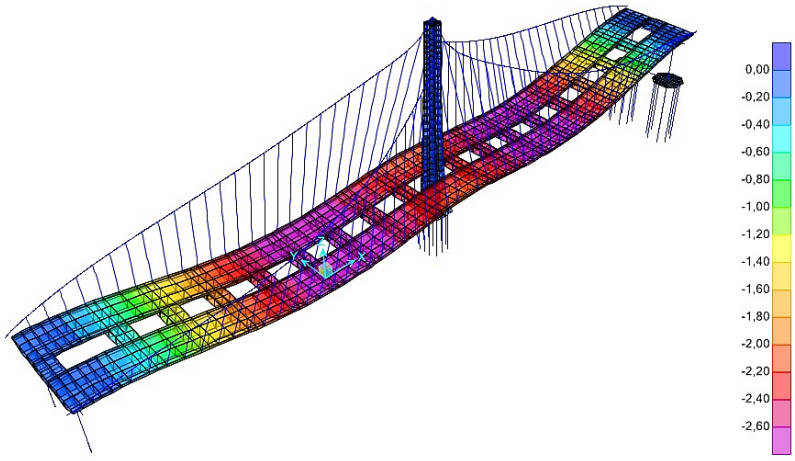

Fig.6.15 – Vertical displacements for symmetric GAS bridge for Gravity Analysis.

Table 6.12 – **Vertical and longitudinal displacements** for Gravity analysis

	Location	Vertical displacements (Z axis)		Longitudinal Displacements (X axis)	
		[m]	[in]	[m]	[in]
Deck	X=0m (at Tower)	-2,13	-83.85	+0,0037	+0.14
	X= ±100m (max displac)	**-2,78**	-107,7	-0,019	-0,74
	X= ±140 m (mid span)	-2,65	-104.3	+0,007	-0.27
	X= ±280 m (Piers top)	-0,0054	-0.21	-0,004	-0.16
Tower	Top of Tower z=156m	-0,097	-3.8	+0,003	+0.12
	Tower at deck level Z=53m	-0,271	-10.7	-0,0011	-0.04

The total length of the span for this symmetric GAS design is 560m from Pier W2 to Pier E2, since there is no connection between the deck and the tower. The ratio of the maximum vertical displacement over the total length is 0,5 %.

6.2 MODAL ANALYSIS

In this report, the first six mode shapes and properties are presented. The six higher modes by themselves represent 50% of Cumulative Mass Participation Ratio in Longitudinal and Transverse directions.

The Modal Analysis will be presented for the Ground-anchored models.

6.2.1 GAS MODEL WITH CABLE DISCONNECTED

As far as modal analysis is concerned, Mode 13 brings 13% of the mass participation for the vertical direction and Mode 201 bring 8% of mass participation each (for a cumulative ratio of 79%). The transverse direction is almost fully mobilized after mode 59 (99% Cumulative mass participation ratio) and the longitudinal direction after mode 224 (98,5% Cumulative mass participation ratio).

Annex A 6.1 presents the Mass Participation ratio for the most relevant ones out of the first 200 modes.

Mode 1 – **T= 4,18 s**; Lateral and Torsional movement

Mass Participation Ratio: UX≈ 0; **UY=0,22**; UZ≈ 0; **RX= 0,359**; RY≈ 0; RZ=0,017

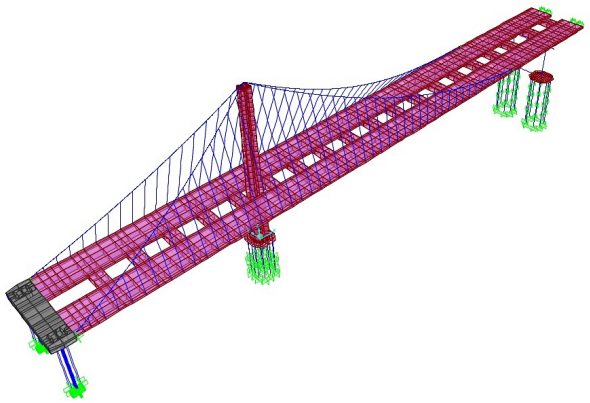

Fig. 6.16 – 3D view of 1st mode for GAS model

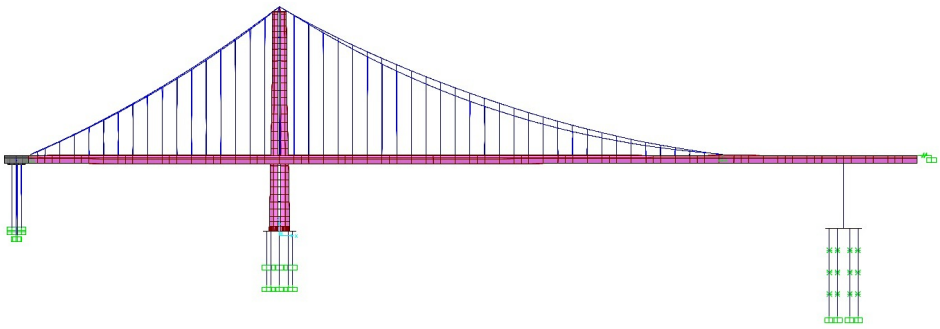

Fig. 6.17 – XZ view of 1st mode for GAS model

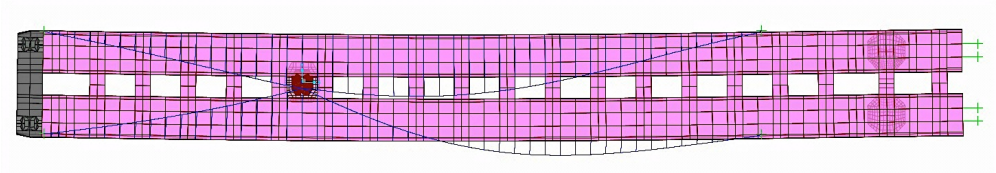

Fig. 6.18 – XY view of 1st mode for GAS model

Mode 2 – T= 4,02 s; Vertical movement of deck

Mass Participation Ratio: UX= 0,0118; UY≈ 0; **UZ=0,05**; RX≈ 0; **RY= 0,024**; RZ≈ 0

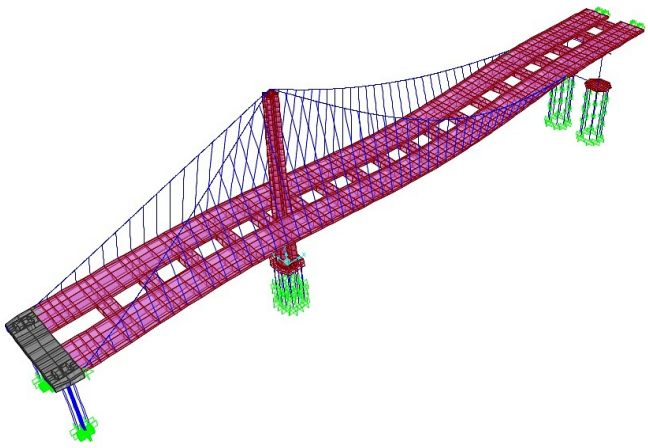

Fig. 6.19 – 3D view of 2nd mode for GAS model

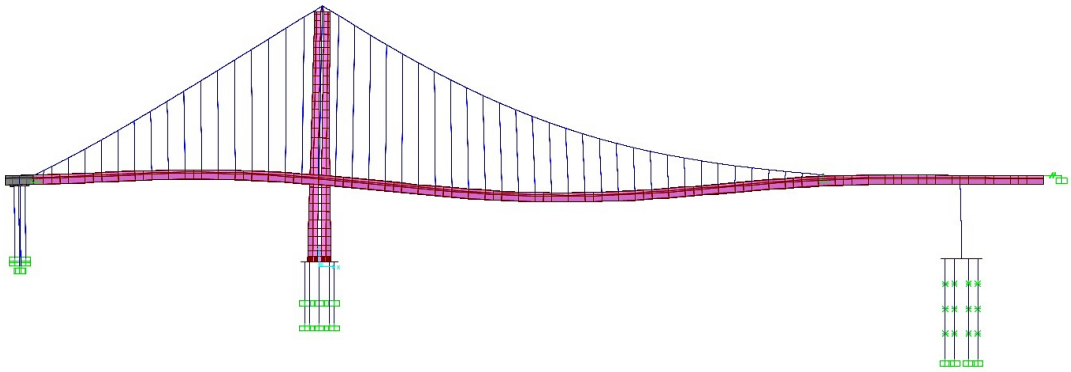

Fig. 6.20 – XZ view of 2nd mode for GAS model

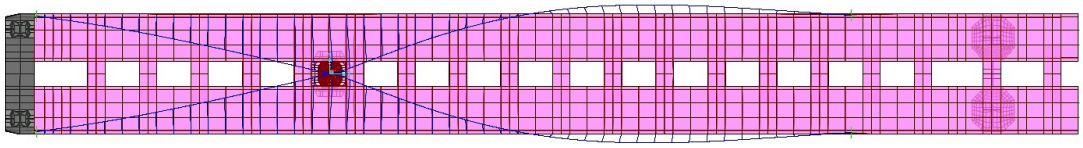

Fig. 6.21 – XY view of 2nd mode for GAS model

Mode 3 – T= 3,87 s; Vertical movement

Mass Participation Ratio: UX=0,008; UY≈ 0; **UZ= 0,018**; RX≈ 0; RY=0,009; RZ≈ 0

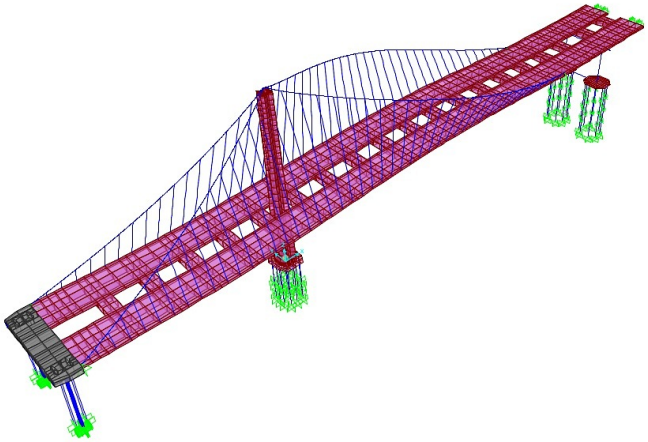

Fig. 6.22- 3D view of 3rd mode for GAS model

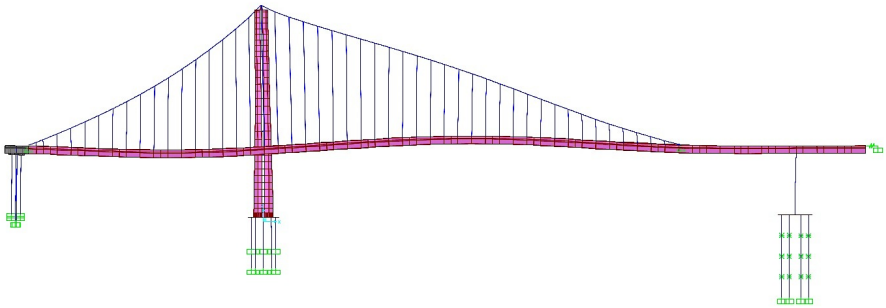

Fig. 6.23 – XZ view of 3rd mode for GAS model

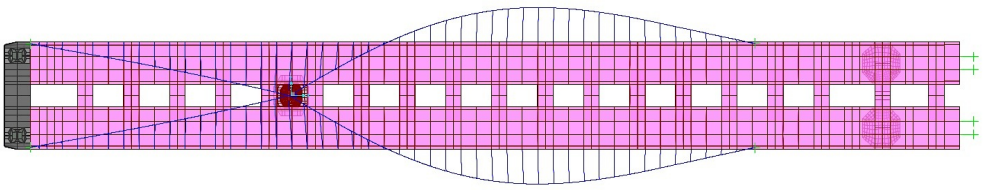

Fig. 6.24 – XY view of 3rd mode for GAS model

Mode 4 – T= 3,6s; Transverse and torsional movement of deck

Mass Participation Ratio: UX=0,0017; **UY=0,23**; UZ≈ 0; **RX=0,115**; RY≈ 0; RZ=0,012

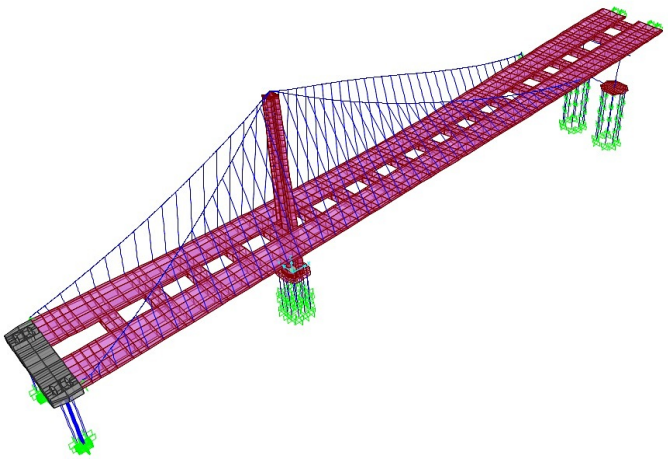

Fig. 6.25– 3D view of 4th mode for GAS model

Fig. 6.26 – XZ view of 4th mode for GAS model

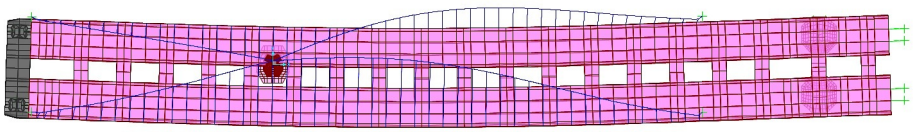

Fig. 6.27 – XY view of 4th mode for GAS model

Mode 5 – T= 3,5s; Longitudinal movement of piers

Mass Participation Ratio: **UX=0,55**; UY≈ 0; UZ=0,009; RX≈ 0 ; RY=0,027; RZ≈ 0

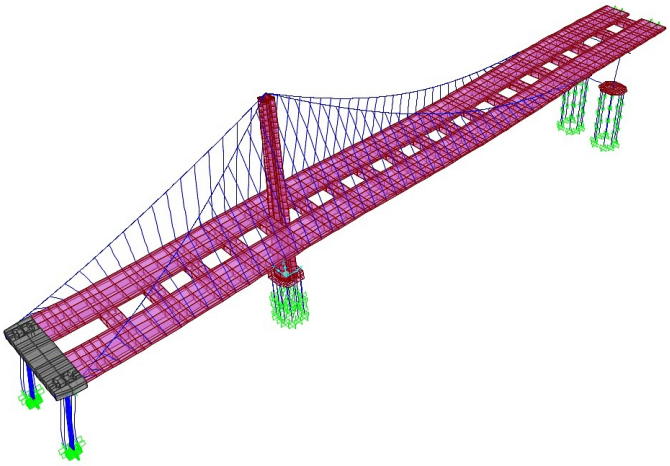

Fig. 6.28 – 3D view of 5th mode for GAS model

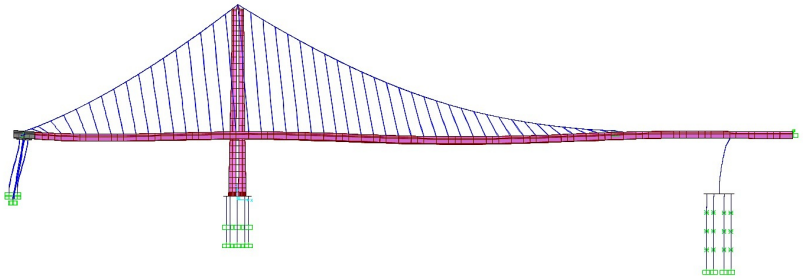

Fig. 6.29 – XZ view of 5th mode for GAS model

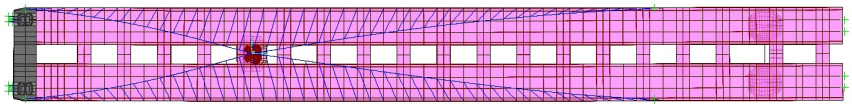

Fig. 6.30 – XY view of 5th mode for GAS model

Mode 6 – T= 3,04s; Transverse movement of tower and torsion of deck

Mass Participation Ratio: UX≈ 0; **UY=0,05**; UZ≈ 0; **RX=0,23**; RY≈ 0; RZ=0,019

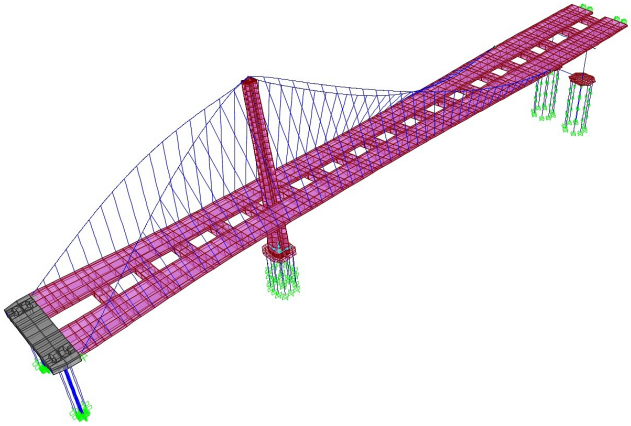

Fig.6.31 – 3D view of 6th mode for GAS model

Fig. 6.32 – XZ view of 6th mode for GAS model

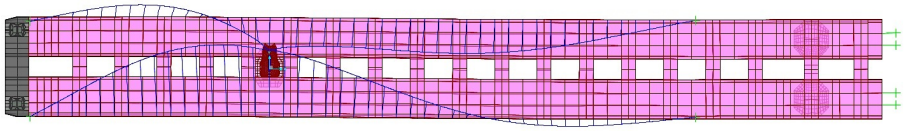

Fig. 6.33 – XZ view of 6th mode for GAS model

6.2.2 REDESIGNED GAS MODEL

Mode 13 brings 12,5% of mass participation for the vertical direction and Mode 152 brings more 8% of mass participation (for a cumulative ratio of 46%). The transverse direction is almost fully mobilized after mode 66 (99,5% Cumulative mass participation ratio) and the longitudinal direction after mode 148 (98,5% Cumulative mass participation ratio).

Annex A 6.2 presents the Mass Participation ratio for the first 200 modes.

Mode 1 – T= 4,9 s; Longitudinal displacement of piers and deck

Mass Participation Ratio: **UX= 0,40**; UY≈ 0; UZ≈ 0; RX≈ 0; **RY=0,01**; RZ≈ 0

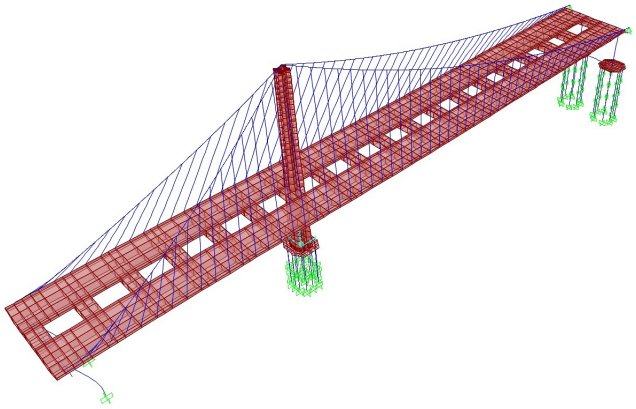

Fig. 6.34 – 3D view of 1st mode for redesigned GAS model

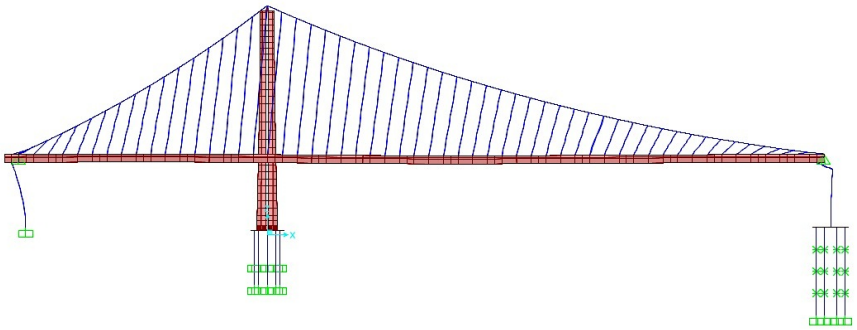

Fig. 6.35 – XZ view of 1st mode for redesigned GAS model

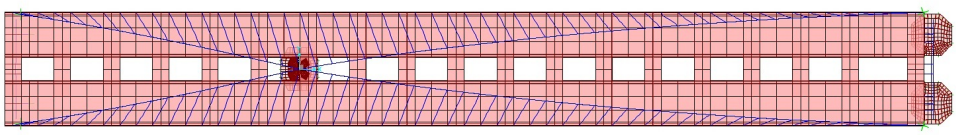

Fig. 6.36 – XY view of 1st mode for redesigned GAS model

Mode 2 – T= 4,77 s; Vertical movement of deck

Mass Participation Ratio: UX≈ 0; UY≈ 0; **UZ= 0,093**; RX≈ 0; **RY=0,045**; RZ≈ 0

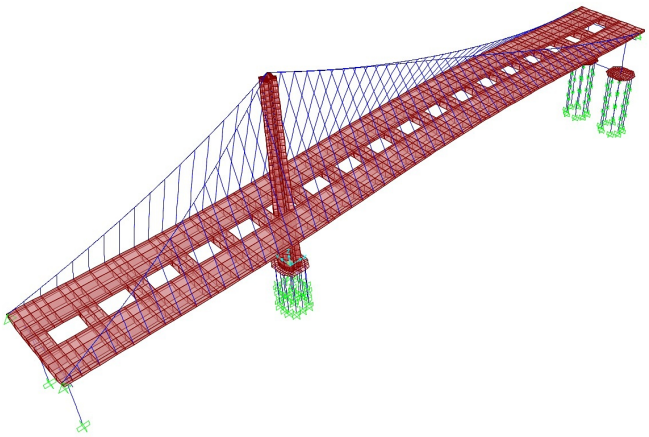

Fig. 6.37 – 3D view of 2nd mode for redesigned GAS model

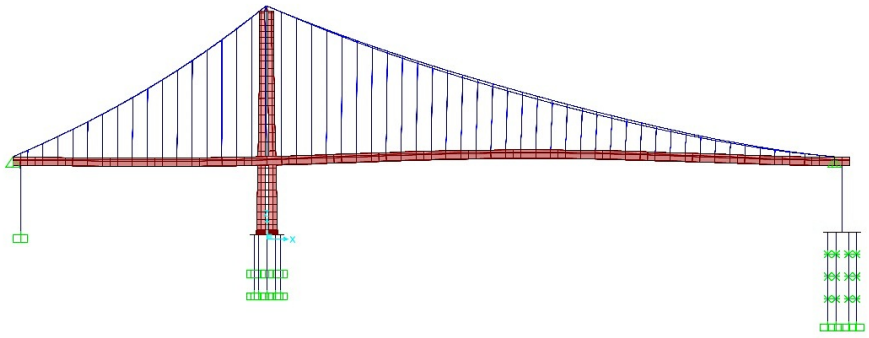

Fig. 6.38 –XZ view of 2'ª mode for redesigned GAS model

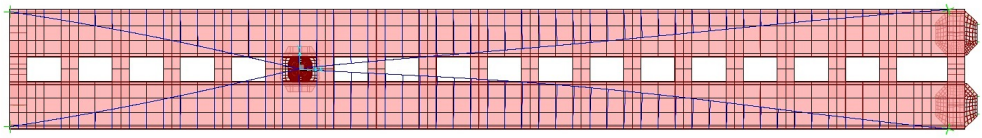

Fig. 6.39 – XY view of 2'ª mode for redesigned GAS model

Mode 3 – T= 4,75 s; Transverse and torsional movement

Mass Participation Ratio: UX≈ 0; **UY=0,076**; UZ≈ 0; **RX=0,20**; RY≈ 0; RZ=0,022

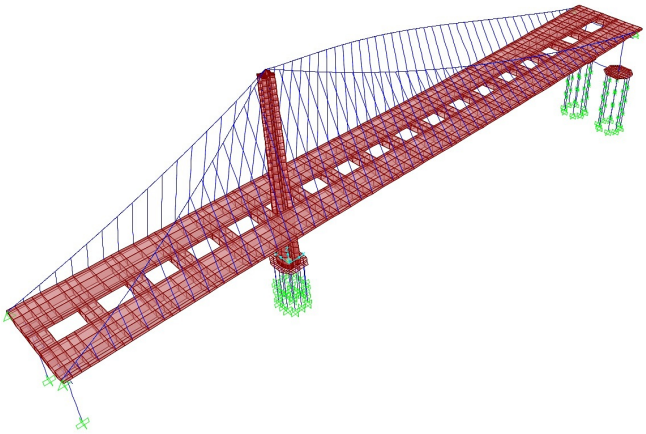

Fig. 6.40 – 3D view of 3rd mode for redesigned GAS model

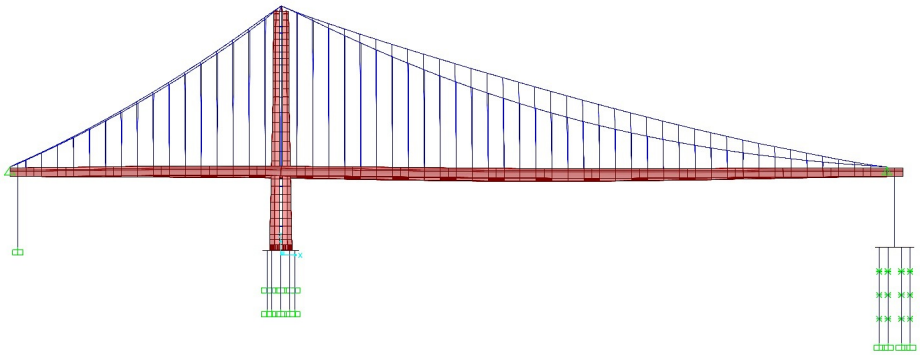

Fig. 6.41 – XZ view of 3rd mode for redesigned GAS model

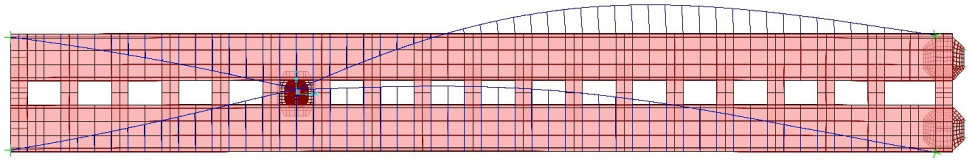

Fig. 6.42 – XY view of 3rd mode for redesigned GAS model

Mode 4 – T= 4,57 s; Vertical movement of deck

Mass Participation Ratio: UX≈ 0; UY≈ 0; **UZ= 0,071**; RX≈ 0; **RY=0,04**; RZ≈ 0

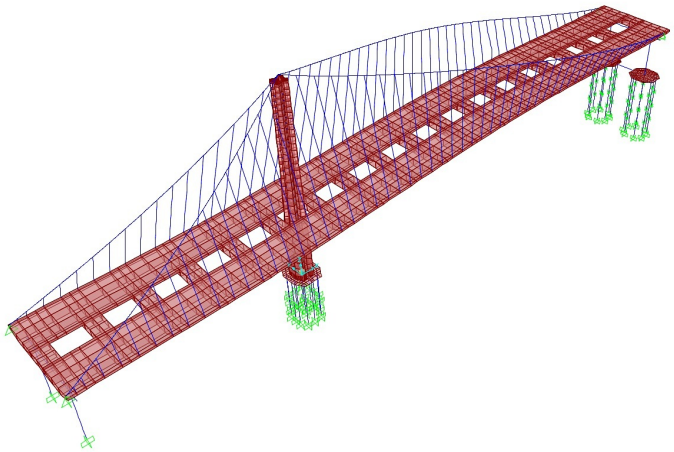

Fig. 6.43 – 3D view of 4th mode for redesigned GAS model

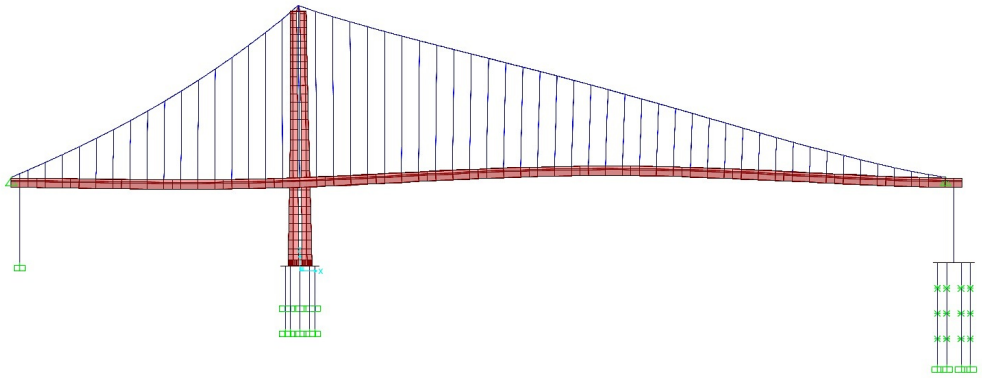

Fig. 6.44– XZ view of 4th mode for redesigned GAS model

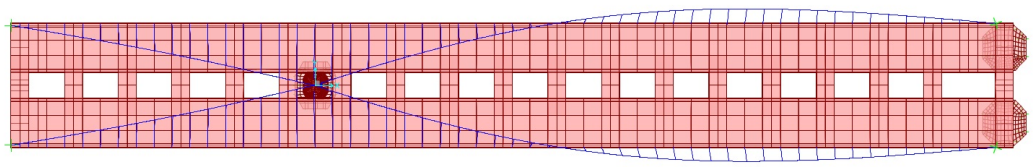

Fig. 6.45 – XY view of 4th mode for redesigned GAS model

Mode 5 – T= 3,36 s; Lateral and torsional movement of deck

Mass Participation Ratio: UX≈ 0; **UY= 0,47**; UZ≈ 0; **RX=0,36**; RY≈ 0; RZ=0,09

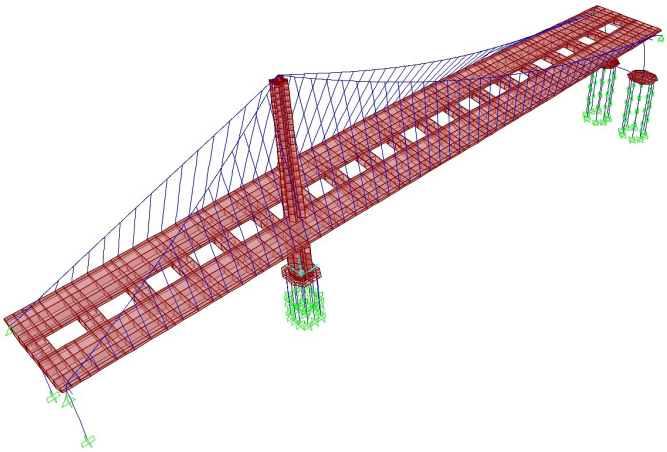

Fig. 6.46 – 3D view of 5th mode for redesigned GAS model

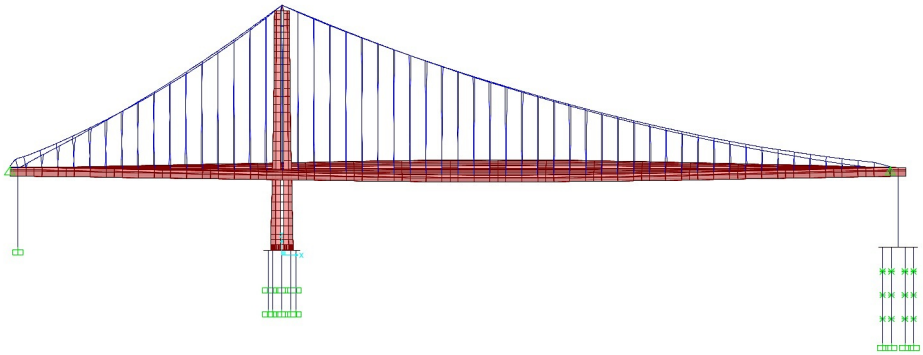

Fig. 6.47 – XZ view of 5th mode for redesigned GAS model

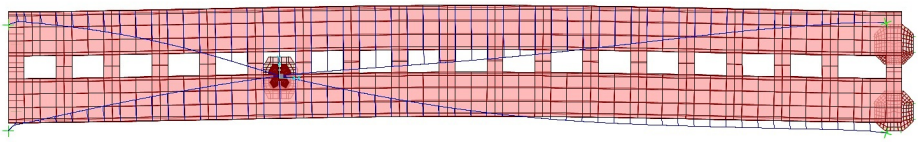

Fig. 6.48 – XY view of 5th mode for redesigned GAS model

Mode 6 – T= 3,17 s; Transverse and torsional movement of deck

Mass Participation Ratio: UX≈ 0; **UY= 0,036**; UZ≈ 0; **RX=0,27**; RY≈ 0; RZ=0,007

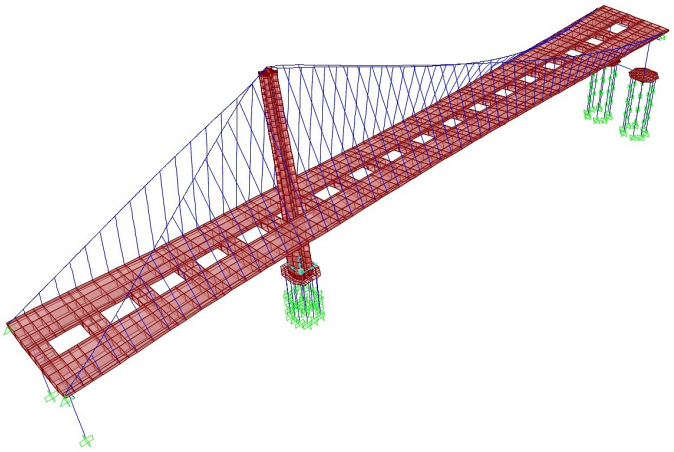

Fig. 6.49 – 3D view of 6th mode for redesigned GAS model

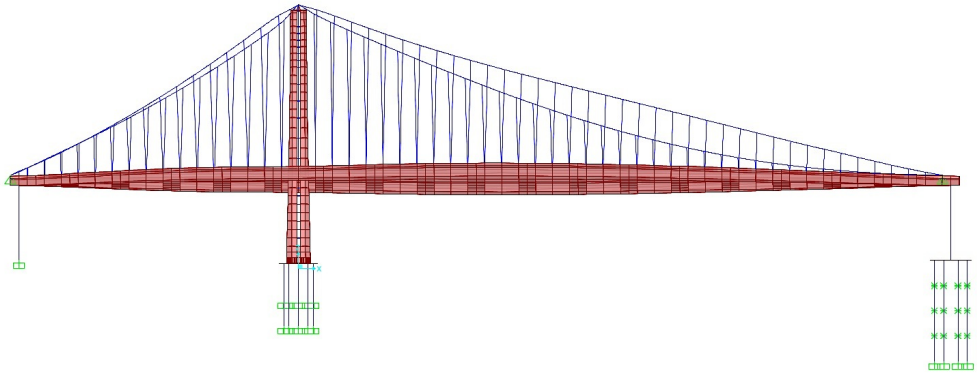

Fig. 6.50 – XZ view of 6th mode for redesigned GAS model

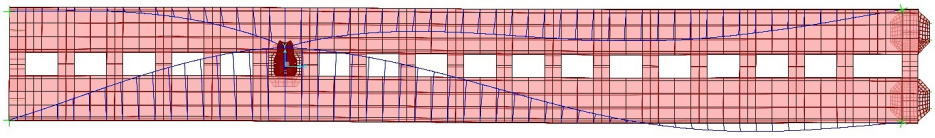

Fig. 6.51 – XY view of 6th mode for redesigned GAS model

6.2.3 SYMMETRIC GAS MODEL

Mode 9 brings 21% of mass participation for the vertical direction and Mode 246 brings more 20% of mass participation (for a cumulative ratio of 62%). The transverse direction is almost fully mobilized after mode 148 (99% Cumulative mass participation ratio) and the longitudinal direction after mode 211 (97,6% Cumulative mass participation ratio).

Annex A 6.3 presents the Mass Participation ratio for the most relevant of the first 300 modes.

Mode 1 – T= 5,02 s; Transverse and torsional movement

Mass Participation Ratio: UX≈ 0; **UY=0,134**; UZ≈ 0; **RX=0,47**; RY≈ 0; RZ=0,018

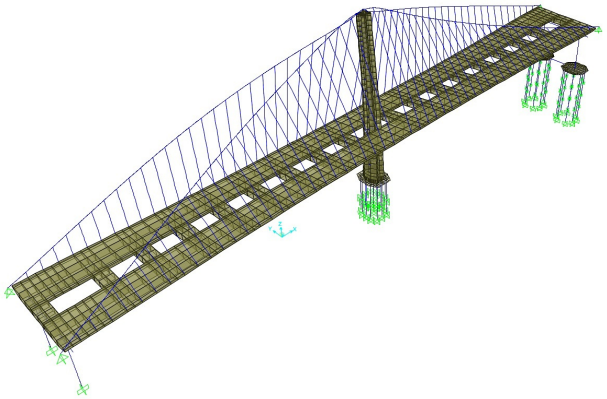

Fig. 6.52 – 3D view of 1st mode for symmetric GAS model

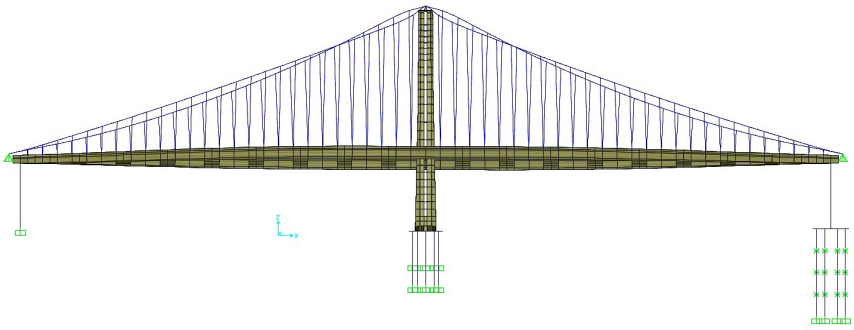

Fig. 6.53 – XZ view of 1st mode for symmetric GAS model

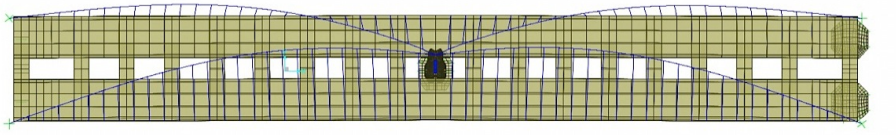

Fig. 6.54 – XY view of 1st mode for symmetric GAS model

Mode 2 – T= 4,78 s; Longitudinal movement

Mass Participation Ratio: **UX=0,341**; UY≈ 0; UZ≈ 0; RX≈ 0; **RY=0,034**; RZ≈ 0

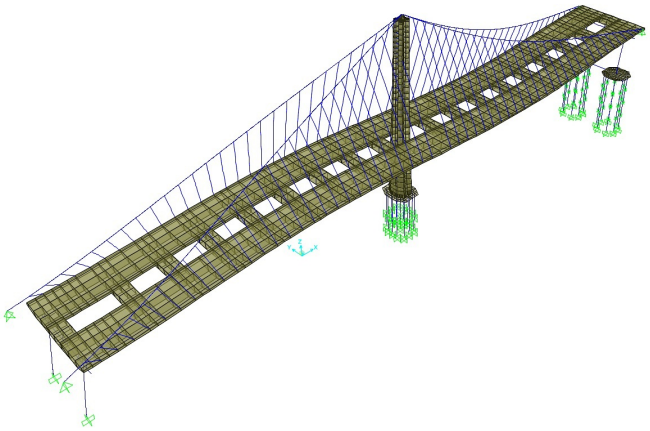

Fig. 6.55 – 3D view of 2nd mode for symmetric GAS model

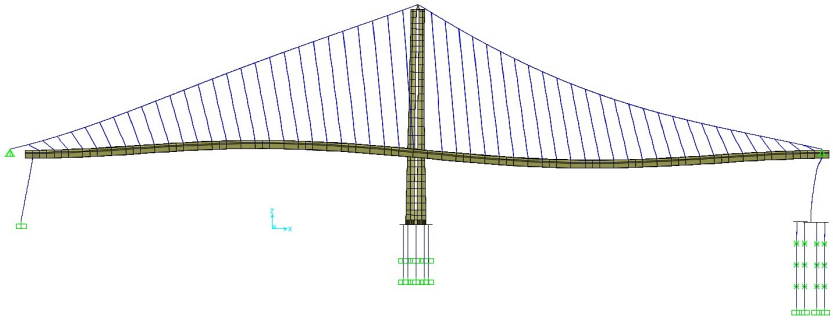

Fig. 6.56 – XZ view of 2nd mode for symmetric GAS model

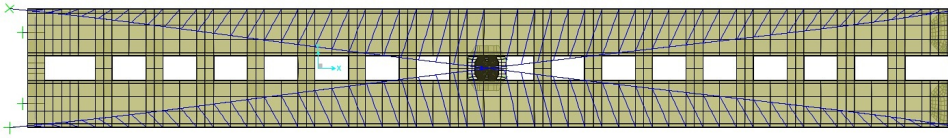

Fig. 6.57 – XY view of 2nd mode for symmetric GAS model

Mode 3 – T= 4,71 s; Longitudinal movement

Mass Participation Ratio: **UX=0,112**; UY≈ 0; UZ≈ 0; RX≈ 0; **RY=0,0138**; RZ≈ 0

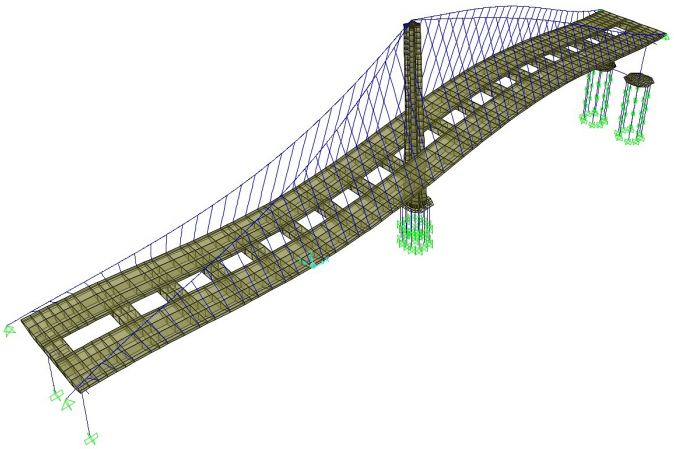

Fig. 6.58 – 3D view of 3rd mode for symmetric GAS model

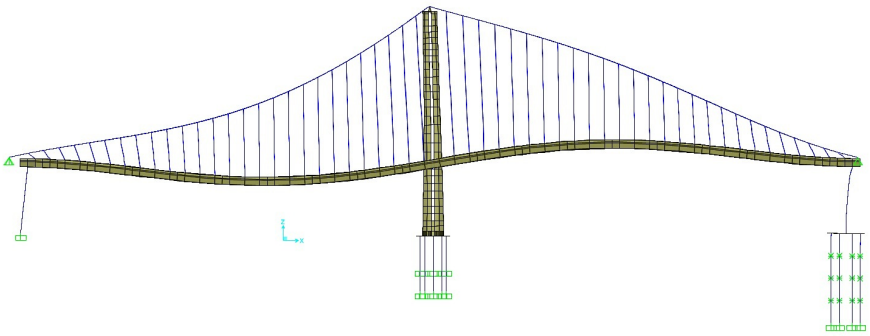

Fig. 6.59 – XZ view of 3rd mode for symmetric GAS model

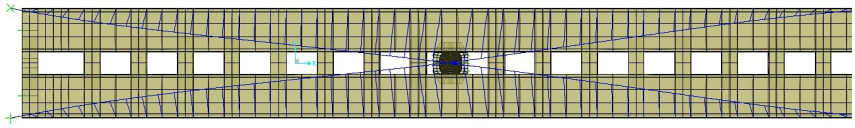

Fig. 6.60 – XY view of 3rd mode for symmetric GAS model

Mode shape 4, 5 and 6 are very similar and will not be displayed. They represent cable mode shapes (vertical, vertical and torsional, respectively). They have very small mass participation. Instead, Mode shape 7, 8 and 9 will be displayed, since they provide an important contribution to the transverse and vertical modes.

Mode 7 – T= 3,9 s; Transverse movement

Mass Participation Ratio: UX≈ 0; **UY= 0,388**; UZ≈ 0; **RX=0,285**; RY≈ 0; **RZ=0,047**

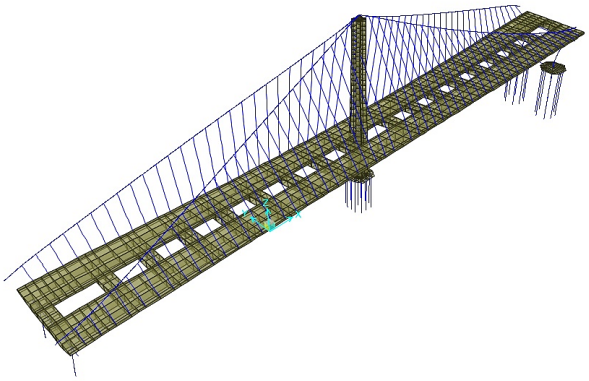

Fig. 6.64 – 3D view of 7th mode for symmetric GAS model

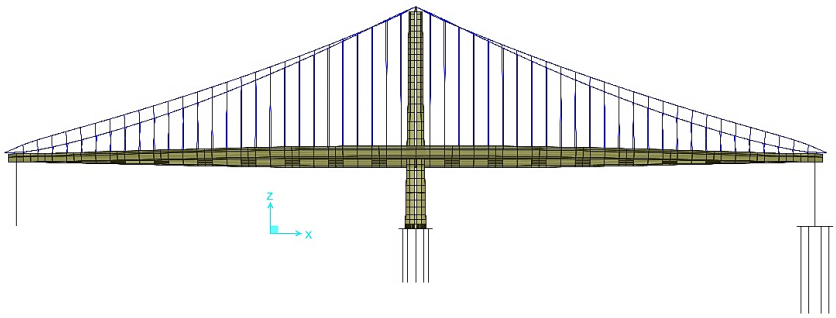

Fig. 6.65 – XZ view of 7th mode for symmetric GAS model

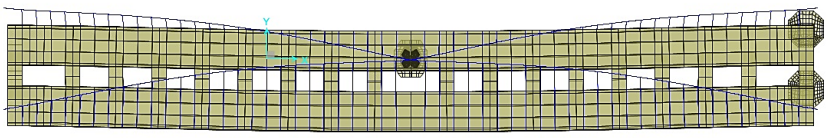

Fig. 6.66 – XY view of 7th mode for symmetric GAS model

Mode 8 – T= 3,58 s; Torsional movement

Mass Participation Ratio: UX≈ 0; UY≈ 0; UZ≈ 0; **RX=0,035**; RY≈ 0; RZ≈ 0

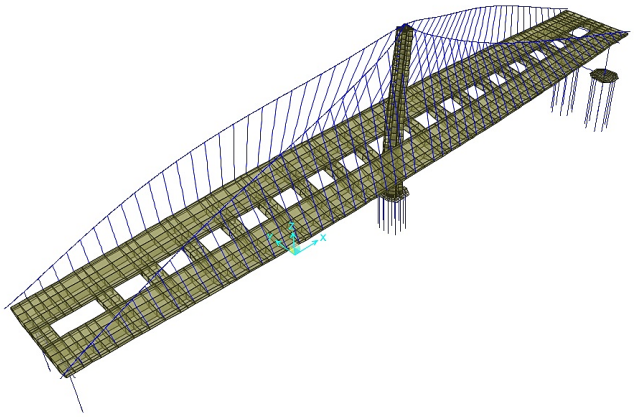

Fig. 6.67 – 3D view of 8th mode for symmetric GAS model

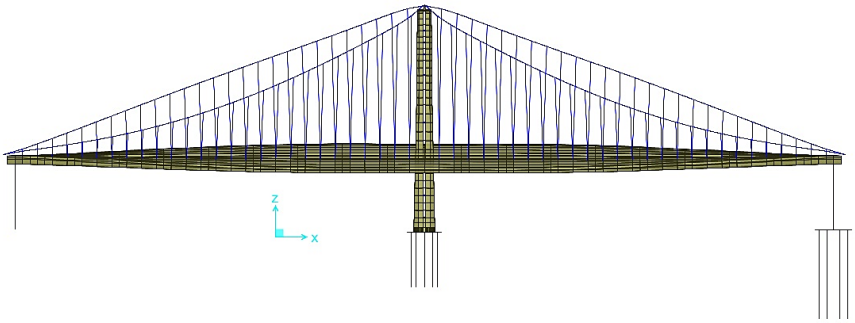

Fig. 6.68 – XZ view of 8th mode for symmetric GAS model

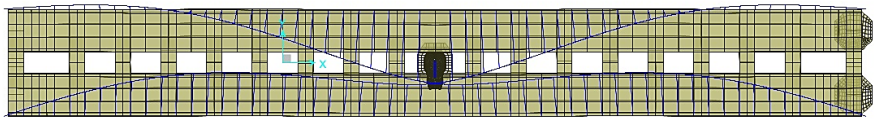

Fig. 6.69 – XY view of 8th mode for symmetric GAS model

Mode 9 – T= 3,3 s; Vertical movement

Mass Participation Ratio: UX≈ 0; UY≈ 0; **UZ=0,214**; RX≈ 0; **RY=0,027**; RZ≈ 0

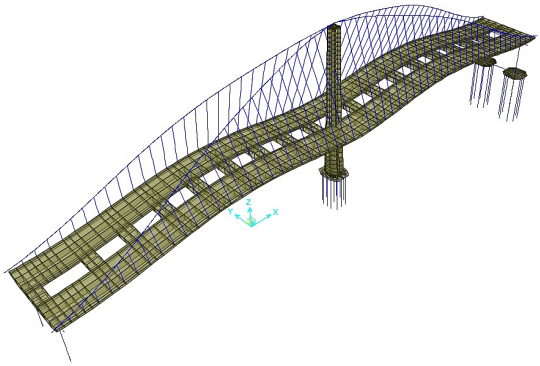

Fig. 6.70 – 3D view of 9th mode for symmetric GAS model

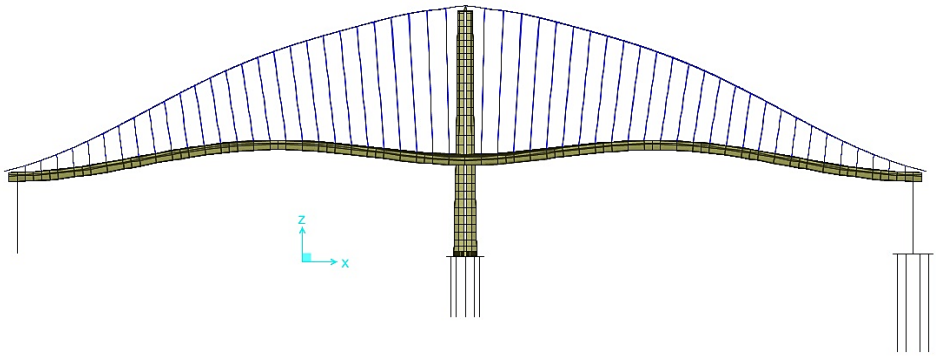

Fig. 6.71 – XZ view of 9th mode for symmetric GAS model

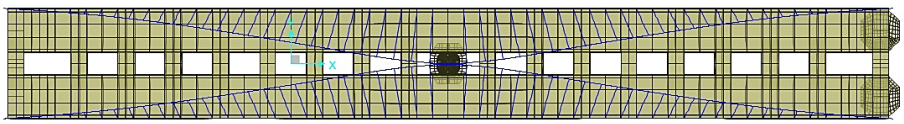

Fig. 6.72 – XY view of 9th mode for symmetric GAS model

6.3 TIME-HISTORY ANALYSIS

As it has been discussed before, for Gravity and Modal analysis the models were studied on an initial state of design that does not include target force iteration for the suspender cables. This prestressing force is introduced during the construction process and alters the deformed shape due to gravity loads, as well as the dynamic response of the structure. Moreover, on the inelastic locations (where yielding occurs), plastic hinges were not introduced as nonlinear links for any of the models. Nevertheless, a FNA analysis (Fast Nonlinear) was performed on 3 of the models under dead load and for the set of ground-motion presented in Chapter 5. This analysis would need the abovementioned prestressing introduced to be representative of the real response of the structure. However, its elastic response allows some more understanding on the differences among various systems. Also, only one out of 6 sets of ground-motion were used, which alone does not represent the real response of the structure.

Furthermore, the 2nd redesigned Ground-anchored (GAS) model will not be studied for Dynamic analysis. Indeed, as discussed before and further explained in Chapter 7, this redesigned model has too high stresses and displacements (see section 6.1.3) and was used mainly as a case study for a design improvement. It is not an optimized design for a ground-anchored suspension bridge.

The main span deck displacements were plotted below with the same scale, in order to make the comparison easier. The deck top plates stresses on the main span were also plotted as a function of time.

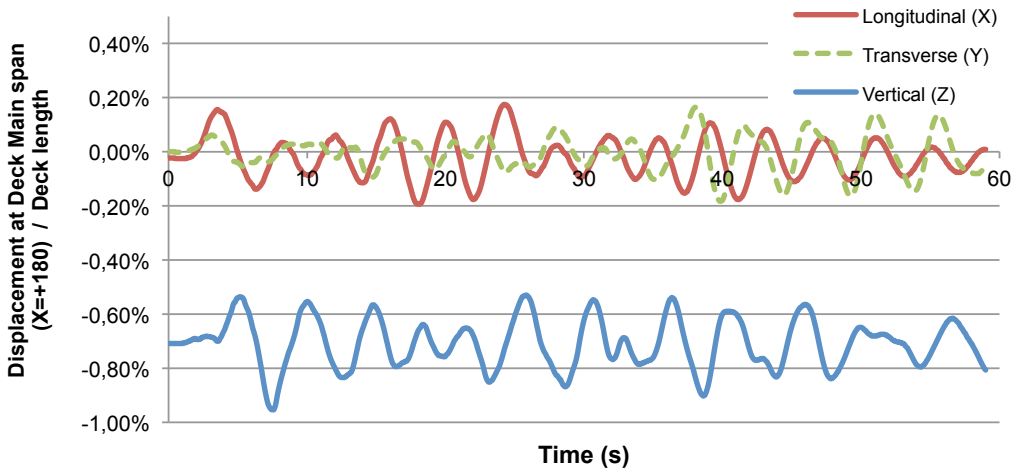

Graph 6.3 – Displacement of main span as function of time for **SAS model.**

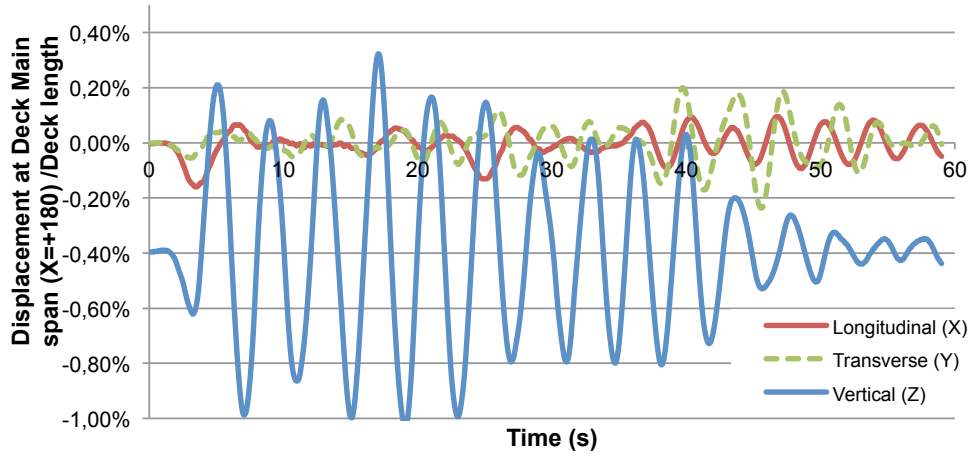

Graph 6.4 – Displacement of main span as function of time for **GAS with only cable disconnected.**

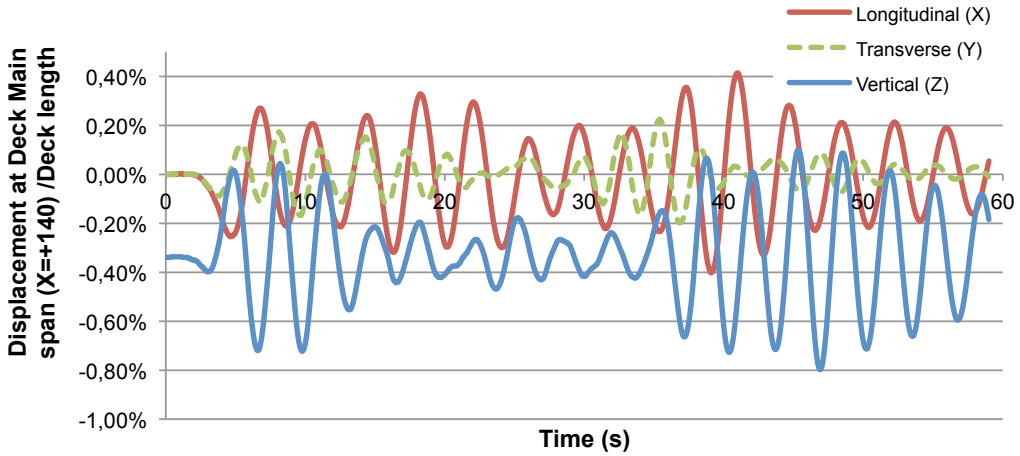

Graph 6.5 – Displacement of main span as function of time for **symmetric GAS.**

The longitudinal and transverse displacements do not have major differences. On the contrary, the average vertical displacement for the ground-motion input is approximately -0,7%, -0,4% and -0,4% for SAS, GAS with only cable disconnected and symmetric GAS, respectively.

Although the SAS model presented higher absolute values for vertical displacement, those values vary between 0,6% and 1% of the total span's length (Δmax=0,4%). On the other hand, the GAS model with cable disconnected varies from +0,3% to -1,0% of the total span's length (Δmax=1,3%) and the symmetric GAS model varies from 0 to -0,7% (Δmax=0,7%). Therefore, the GAS models main span deck has smaller displacements during the input ground-motion when compared with SAS results, but larger variation.

This might be related to the fact that the Ground-anchored system has ground-motion displacement input directly to the main cable through the earth-anchorages, while the Self-anchored system has ground motions applied mainly through the foundation piles.

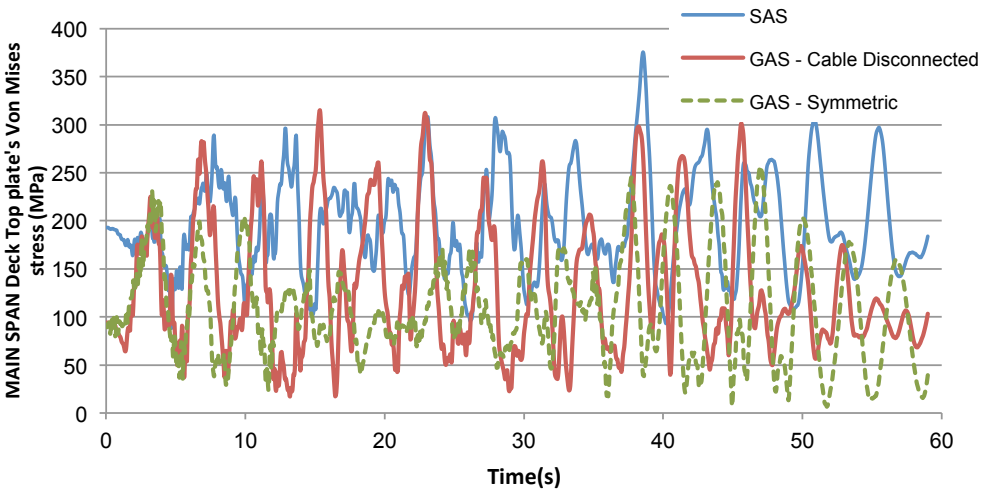

Graph 6.6 – Main span von Mises stress at deck top plates for three models.

Observing the graph above, the von Mises stresses at the deck top plates for the mid-span are generally larger for SAS than others. Nevertheless, the GAS model with cable disconnected also has relatively higher stresses and a larger stress variation.

These maximum von Mises stress values are not representative of the real response and reach the yield level. This is not the accurate response value as it was mentioned previously.

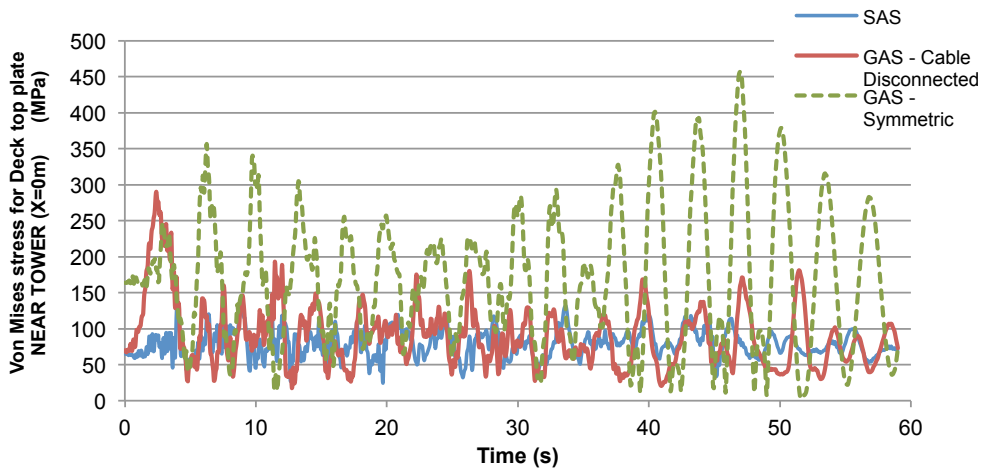

Graph 6.7– Deck (X=0m) von Mises stress for three models.

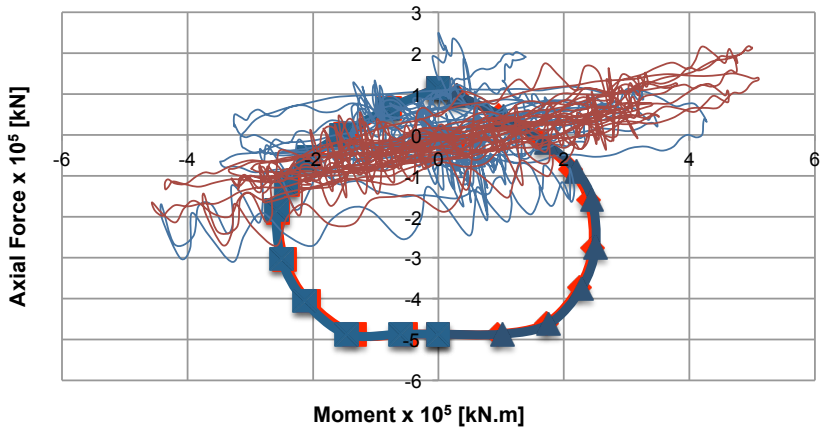

Graph 6.8 – SAS and GAS with cable disconnected P-M(longitudinal) for time-history at **Top of Pier W2.**

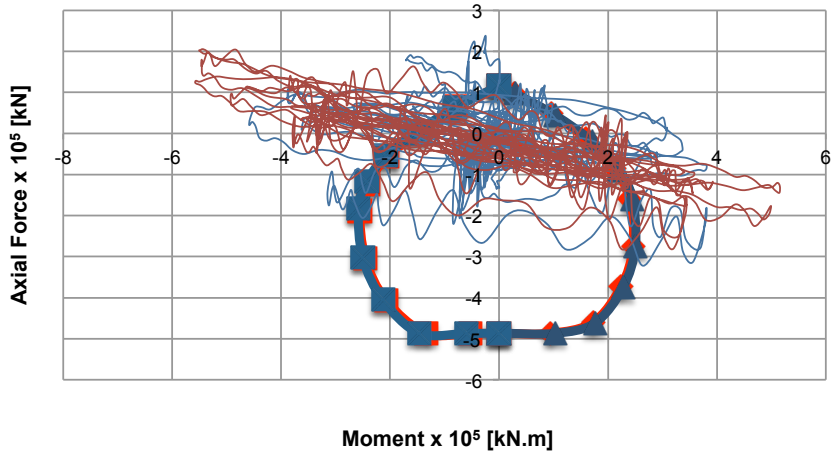

Graph 6.9 – SAS and GAS with cable disconnected P-M(longitudinal) for time-history at **Bottom of Pier W2.**

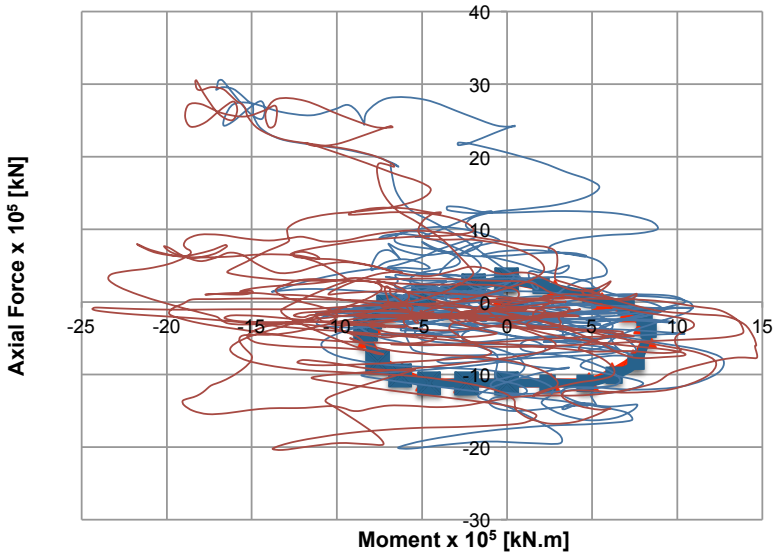

Graph 6.10 – SAS and GAS with cable disconnected P-M(longitudinal) for time-history at **Bottom of Pier E2.**

For both SAS and GAS with "only cable disconnected" models, the W2 pier axial-bending moment response was plotted against its capacity, as well as the bottom of Pier E2. For the top and bottom of Pier W2 and bottom of Pier E2, the response exceeds the capacity (Graph 8 to 10). This means a plastic hinge is formed and a nonlinear link should be introduced in the model at these locations, to simulate increased ductility. The pier response for both models is very similar, since from one model to the other the piers were kept and only the main cable was altered. So, although for Gravity analysis the forces at the piers are much reduced for the GAS model, the seismic response remained similar for SAS and GAS with only cable disconnected.

7
COMPARISON AND CONCLUSIONS

7.1 STATIC GRAVITY ANALYSIS

After the results plotted in Chapter 6, it is important to compare and make conclusions on the models developed. For this gravity analysis, all models were subject to the same loading (see Chapter 5). Fig. 7.1 to 7.4 summarize the most important results for the models.

For the **SAS model**, there is a rigid connection between deck and capbeam on Pier W2 side and a pinned connection on the Pier E2. The bridge behaves like a 'fixed-pinned beam' in compression and with elastic springs along its length (suspenders). The compression force introduced into the deck by the main cable through the deck anchorages reduces the stiffness of the deck. So when compared with the **GAS model with cable disconnected** from the deck, it presents a bigger negative **displacement** (downwards) on the main span.

As far as the **deck plates' stresses** are concerned, the most important analysis is for the top plates because the deck anchorages were simplified and assumed connected to the deck at the top. For the GAS model with cable disconnected, the top plates longitudinal stress gets reduced to half at the main span and Pier E2. For the back span there is a reduction of 5 times for the top plate longitudinal stresses. For the deck plates at the tower location, the tension stresses double their value for the GAS model. Since there is no more compression acting on the deck top plates, the compression stresses are reduced and the tension stresses become larger.

For the SAS and GAS models, when comparing **Pier W2 and Pier E2 bending moments**, they are greatly reduced. Indeed, Pier W2 columns have 10 times less bending moments for the GAS when compared to the initial SAS model, since the cable is not attached to the rigid capbeam anymore. The Pier E2 bending moments are almost inexistent in gravity analysis of GAS models. In GAS bridge not only the deck is not receiving compression force from the cable, but also the cantilever to the east of Pier E2 (49-meter long) is equilibrated by the cantilever to the west of Pier E2 (35-meter long). The anchorage forces are not transmitted to the deck on the GAS model, but to the ground.

To further evaluate the differences in gravity analysis between the original SAS model and GAS model with cable disconnected the Von Mises stresses for the deck top plates were ploted (Fig. 7.1 and 7.2). This stress combines the existing stresses in all directions and gives a maximum magnitude of stress that can be compared to the yield stress.

$$\sigma^2 = \frac{1}{2}[(\sigma_{11}^2 - \sigma_{22}^2)^2 + (\sigma_{22}^2 - \sigma_{33}^2)^2 + (\sigma_{11}^2 - \sigma_{33}^2)^2 + 6 * (\sigma_{23}^2 + \sigma_{31}^2 + \sigma_{12}^2)] \quad (7.1)$$

The von Mises stresses in GAS show a considerable difference for main span and top of Pier E2, as expected. Nevertheless, on the deck near the tower the maximum stresses occur for the GAS model with "only cable disconnected". It was mentioned previously that after removing the compression force applied to the deck, in general the compression stresses decrease whereas the tension stresses increase their value. For this reason, on the ground-anchored model the tension stresses in the deck near the tower register higher values and in all other locations show a stress decrease when compared to the self-anchored model.

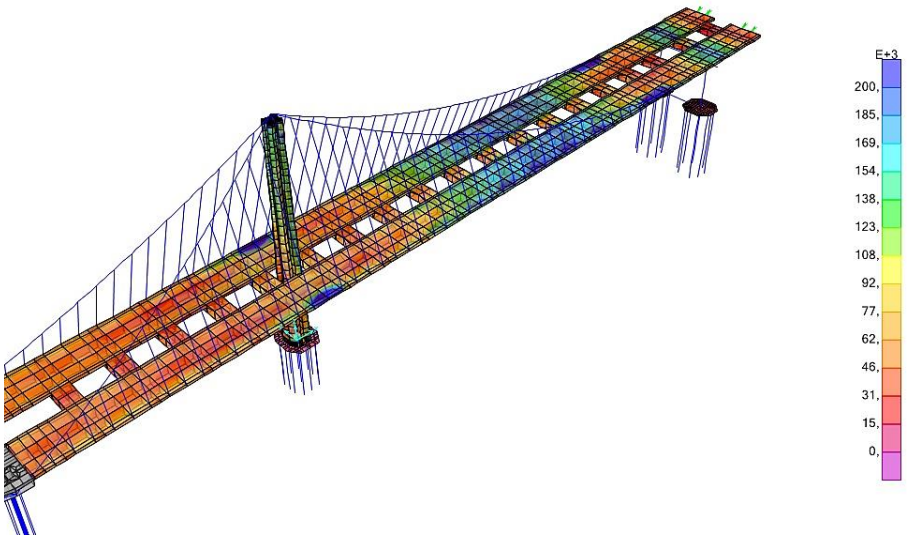

Fig.7.1 – **Von Mises stresses** on top deck plates of Original SAS model for Gravity analysis.

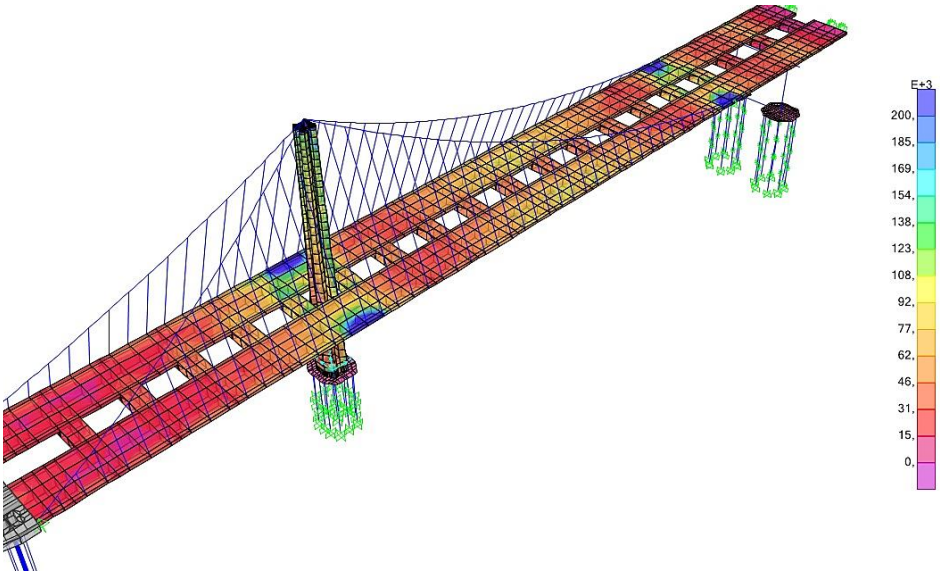

Fig.7.2 – **Von Mises stresses** on top deck plates of GAS model with cable disconnected for Gravity analysis.

The analysis of this Ground-anchored model shows that the forces and stresses are reduced considerably in ground-anchored bridges. In the next GAS model, some other changes will be made to increase efficiency further. First, the rigid connection between W2 and deck is no longer necessary in GAS bridge, as well as the heavy W2 columns and tiedown cable system. Also in GAS model, the connection on the East side is changed to a *roller connection*, since there is no more compression in the deck that was the reason for restrain in the longitudinal direction. Also, the expansion joint with the skyway deck was moved to top of the Pier E2, which means there is no need for a cantilever on the west side of Pier E2 and the sag of the main cable is also altered. This way, a redesigned GAS model was analyzed (see Chapter 5 and 6.1.3).

The **redesigned GAS** model behaved like a 'pinned-roller beam' with only downwards vertical displacements on the deck. Actually, it presents a larger vertical negative **displacement** at the main span, but a reduction of the top **deck plate longitudinal stress** when compared with SAS (-165 MPa to -95 MPa). Since the sag of the East side main cable was now reduced, the tension at the main cable registered a 10% increase when compared to the GAS model with cable disconnected only. Also, the vertical force at the suspenders was 40% smaller for the redesigned GAS model on the main span (x=+30 to x=+180m). All these facts combined make the vertical displacement larger for this redesigned GAS model. Moreover, even if there is a reduction of the longitudinal stresses on the main span, the tensile stresses on top of E2 and near the Tower locations increased to unbearable levels. Indeed, at top of Pier E2 the stresses increase 225% when compared to the SAS model. This happens after removing the cantilevers on both sides of Pier E2 and after changing the sag of the cable, since there is no more force equilibrium and also the cable reaches Pier E2 with a very horizontal tangent configuration that has reduced vertical component. For the back span, on the redesigned GAS model the deck top plate longitudinal stress is 3 times higher than on the SAS.

For both GAS models, when comparing **Pier E2 bending moment**, it is greatly reduced. Indeed, since it is a *rocker connection* and it does not restrain the longitudinal movement, the longitudinal bending moment is almost zero. Pier W2 is not comprised of 4 columns as in previous models, but has only a single column with the same cross section as Pier E2. That way, before the moment at the bottom was 4*5000=20000 kN.m and for the redesigned GAS model it is 25000 kN.m. This increase is small and not significant. Therefore, it can be concluded that the Pier forces and bending moments are very similar for both GAS models.

This redesigned GAS model is not an optimized design, as it was mentioned before.

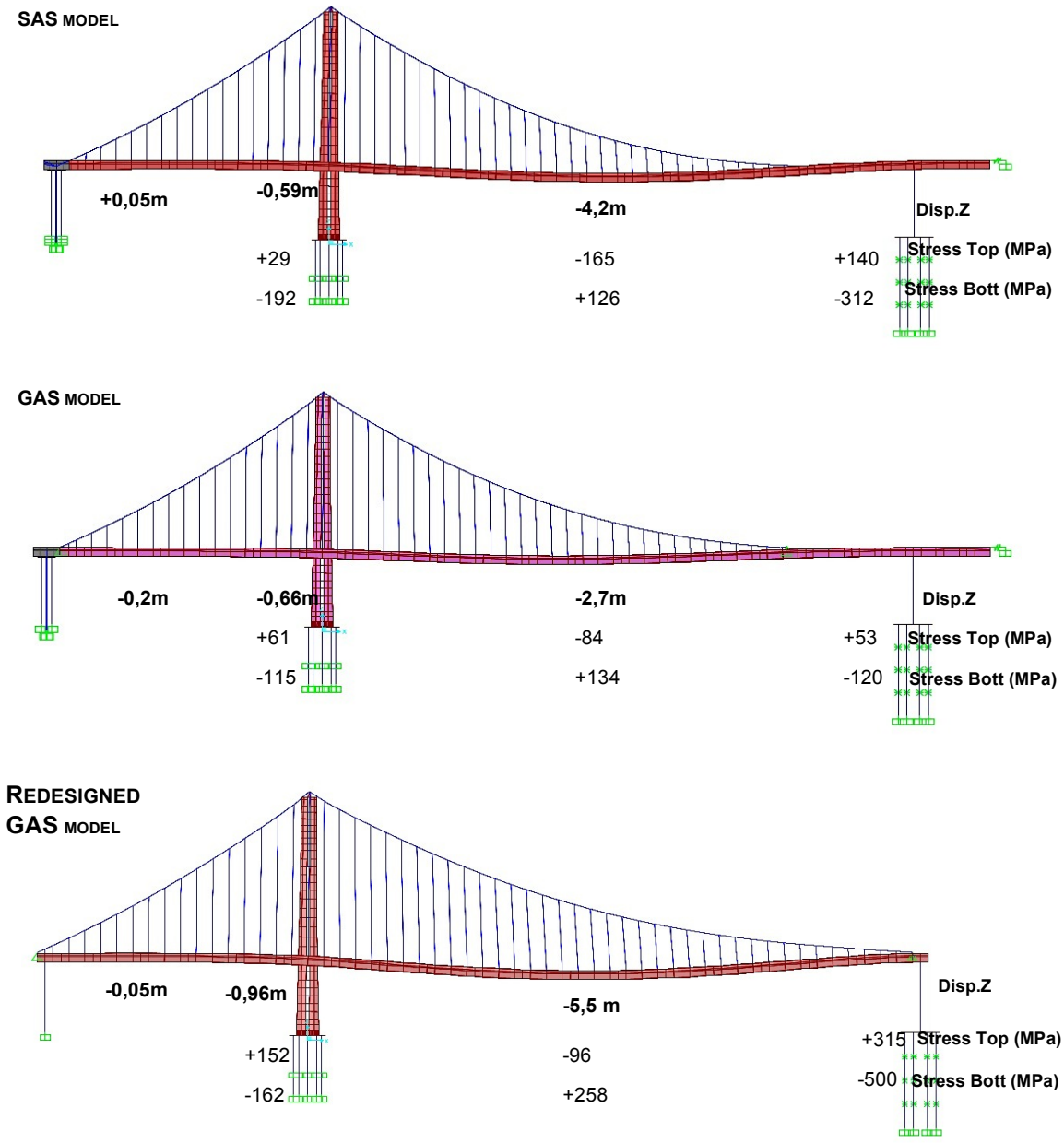

Fig.7.3 – **Deck's displacement and stresses** comparison between the 3 models for Gravity analysis.

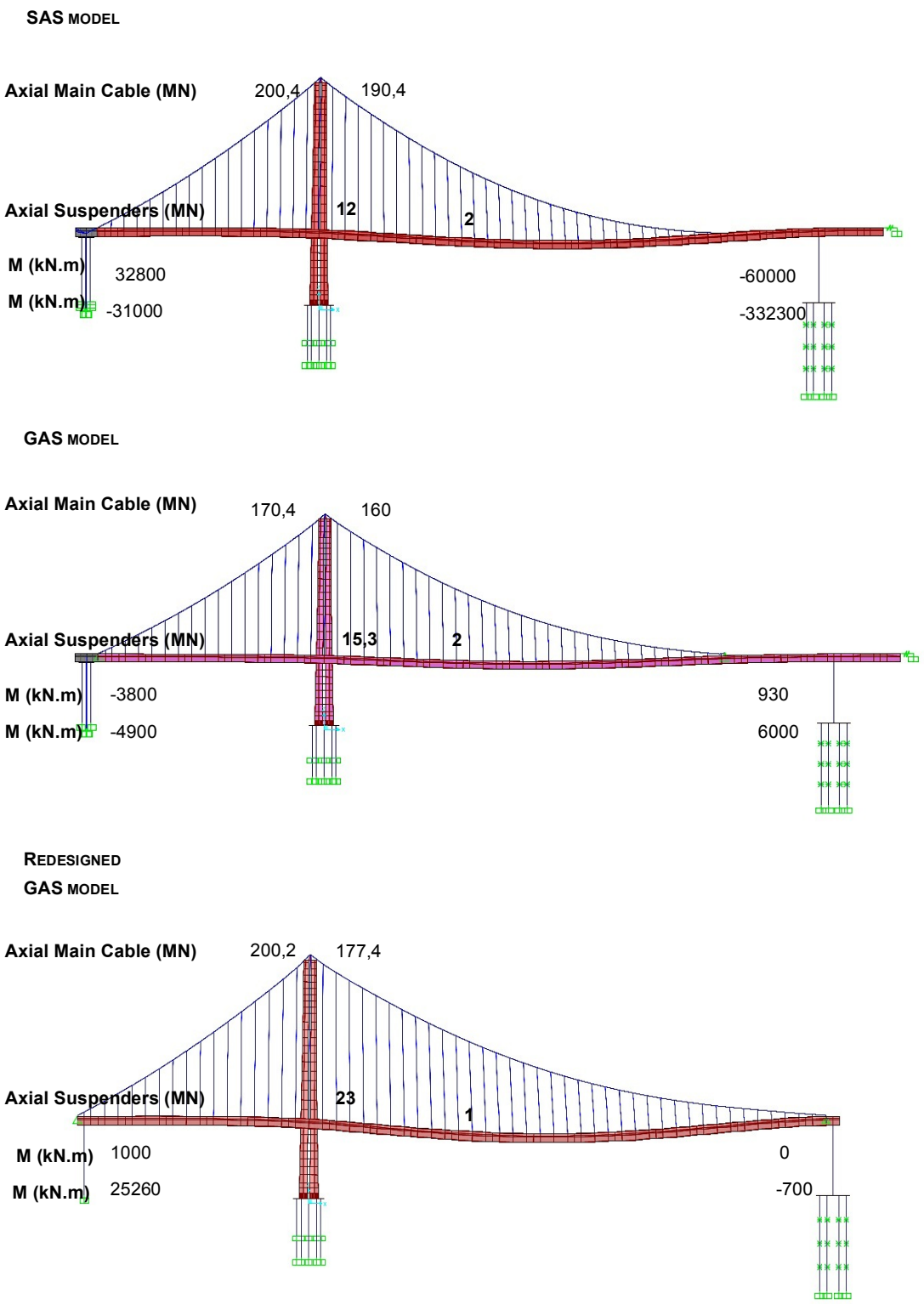

Fig.7.4 – **Forces** comparison between the 3 models for Gravity analysis.

The abovementioned redesigned GAS model presented very large stresses in the deck and the two suspenders connected directly to the tower. Indeed, the asymmetric single-tower configuration is not favorable for a typical ground-anchored suspension bridge and the attempts to keep the original geometry faced some issues. This GAS design attempt will not be further discussed.

Therefore, a new hypothetical design was attempted, more adequate to a conventional suspension bridge. Since the span asymmetry was causing stress distribution issues, the location of the tower was moved to the middle of the span. Furthermore, the deck spans were changed to a length of 280m each. The main purpose of this change was to improve the cable configuration, in order to suspend all the segments and still avoid too much horizontal tangent at the ends. A 1st analysis of this model was performed, as it is shown in Figure 7.5.

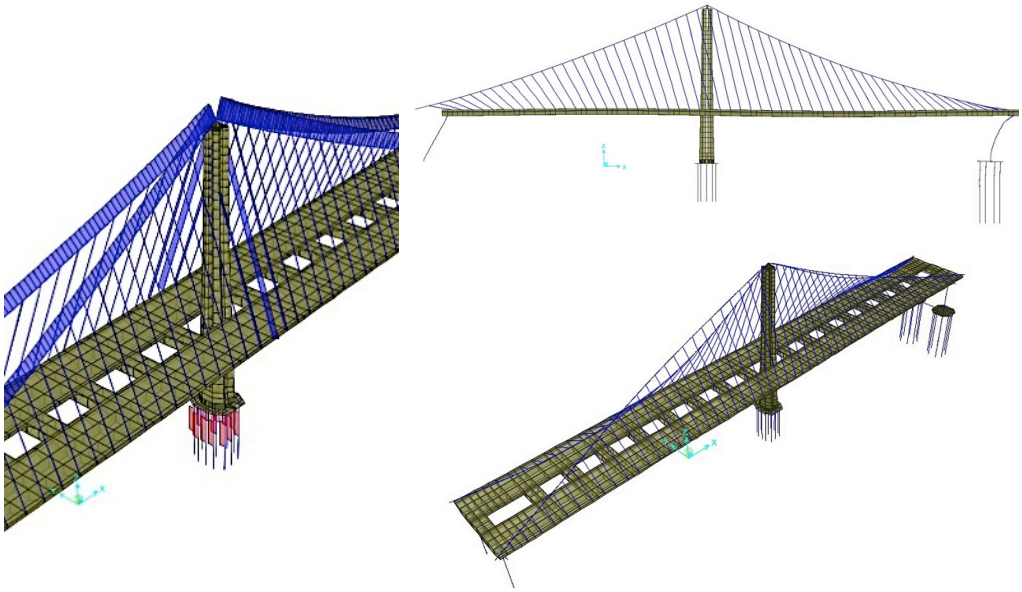

Fig.7.5 – 1st Gravity and Modal analysis results for **symmetric GAS model**

Besides the excessively high axial force registered in the two center suspenders connected to the tower and the high deck plates stresses near the tower, this model showed a 1st mode shape with only longitudinal movement of the piers and without bending of the deck. Also, the 2nd to 5th modes were cable mode shapes, where only the cable participates.

Firstly, the suspender cables near the tower have a stiffer section (Type 2, see Chapter 5) and also the 2 suspenders connected directly to the tower act like "pin connections" instead of elastic springs. On a symmetric design, these 2 suspenders are not necessary and should be removed. Removing these 2 suspenders will redistribute the axial force to the other suspender cables all connected to the main cable. Besides that, the cross section should be equal for all suspenders, since there are no more asymmetries. The type 1 cable section (smaller diameter) was selected, because the force in the all the other suspenders is fairly reduced.

Secondly, the mode shapes indicate that the deck and tower elements are too heavy for the structure. Indeed, the piers and cables dominate the first modes shapes (Fig.7.5). Therefore, a 30% thickness

reduction was applied to all deck and tower plates, with the exception of the mid span (X=20 to X=80m) that had a 50% reduction to decrease the maximum vertical displacement in the deck.

After these improvements, the new results were shown in chapters 6.1.4 and 6.2.4. On the present chapter, Figure 7.6 summarizes those results.

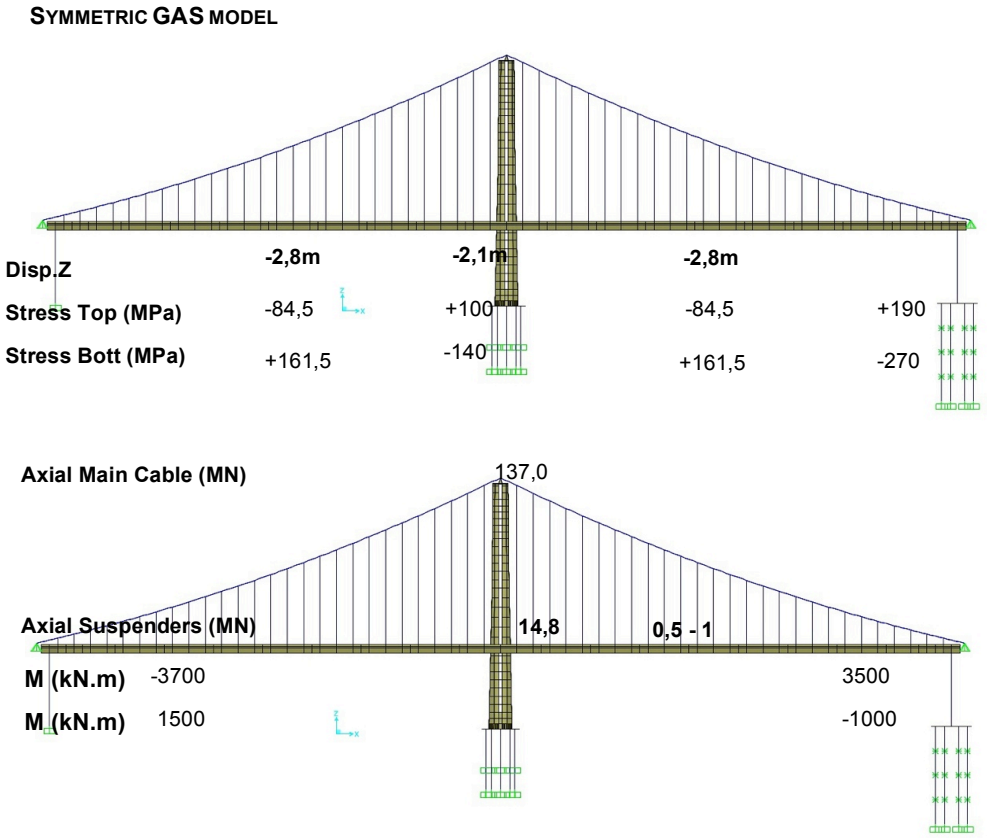

Fig.7.6 – **Deck's displacement and stresses and forces** for the Symmetric GAS model for Gravity analysis.

The **deformed shape** of the new symmetric design is entirely downward, with four inflection points. Its behavior can be compared to a simply supported beam with elastic springs along its length.

Besides being a more redundant design, it also evens the **stresses at top and bottom deck plates**. Indeed, between the mid span and near the tower deck plates, the tensile stresses have an average of (-85+100)/2 = 7,5 MPa. While for the SAS model, between the plates near the tower and the main span the average stresses are (29-165)/2 = -68 MPa. This variation influences the inflection point and is related to the difference between positive and negative displacements.

When compared with the GAS model with cable disconnected only (see chapters 5.5, 6.1.2 and 6.2.2), it actually increases the deck stresses near the tower 3,5 times and keeps the same stresses at the main

span. The average of stresses for the GAS model with "cable disconnected only" is of (61-84)/2= -8,5 MPa, very similar to the variation between deck and main span for the Symmetric GAS.

As far as **cable forces** are concerned, in the symmetric GAS model the main cable force is reduced 20% when compared with the GAS model with "cable disconnected only" and 40% when compared to the SAS model. Moreover, the suspenders axial force is also reduced for this model. This cable tension decrease is related to the smaller sag for the Symmetric GAS design (see Annex A.5.3). For the pier bending moment, this hypothetical symmetric GAS design has 17 times less longitudinal moment at the piers than the SAS model. That is expected, due to the symmetry of the new design. Also, the bending moment is small even when compared to the Redesigned GAS model, which has a "pinned-roller" connection instead of a "pinned-pinned" connection.

After studying the 4 models for Live and Dead load as defined in Chapter 5.9, it can be concluded the GAS with cable disconnected and the symmetric GAS models (2nd and 4th models) show a more uniform behavior and a significant reduction of longitudinal stresses in the main span, as well as in the piers (W2 and E2) for Gravity analysis when compared to the SAS design.

It can also be concluded that the asymmetric spans cause relatively large stresses in the deck and pier and cable forces, either for self-anchored or ground-anchored suspension design.

Nevertheless, the new symmetric GAS model changes the longitudinal tower foundations' position to deeper soil, which would be harder to construct.

Last but not the least, after studying the deformed shape under live and dead for the new symmetric design, the next design step would be to iterate the cable prestressing forces in the suspender cables (as it was done in the existing SAS Bay Bridge, see Chapter 3.10). This external force introduced in the suspenders cables is intended to uplift the deck in order to reverse the deformed shape caused by the gravity loading and, consequently return its deformed shape to almost undeformed configuration.

7.2 MODAL ANALYSIS

Comparing both GAS models, the **redesigned GAS** has a higher fundamental period of vibration (T=4,9s) than the GAS with cable disconnected only (T=4,18s). For the redesigned model, the mass stays approximately the same, the rigid connection between the deck and W2 becomes a pin connection and a roller connects the deck to Pier E2. Therefore, the deck is more flexible to move, which means it has smaller stiffness (k) and smaller angular velocity (w). Therefore, the frequency is smaller and the fundamental period is higher for the redesigned GAS model. The correlation between natural frequency, mass and stiffness of the structure is:

$$w = \sqrt{k/m} \qquad (7.1)$$

$$w = 2\pi f = \frac{2\pi}{T} \qquad (7.2)$$

The GAS redesigned model has a longitudinal movement of the piers as first mode shape. This increased pier flexibility is due to the removal of the rigid connection between deck-capbeam at Pier W2 and using a pinned connection instead, as well as using a roller connection at Pier E2.

On the other hand, the GAS with cable disconnected has lateral torsional movement as first mode shape. Also, only the 5th mode shape represents longitudinal movement of piers for GAS with "only cable disconnected".

The **new symmetric design** modal analysis reveals a fundamental period of 5,0s. The redesigned GAS model has 4,9s, which is a very similar fundamental vibration period. For the new symmetric GAS design, the mass was reduced roughly 30% in total (same as plate thickness reduction). If only the mass had been altered, that would reduce the period when compared with the redesigned GAS (T=4,9s). But also the different design alters the stiffness of the structure. Since the fundamental period is almost the same and the mass is reduced by 30%, one can conclude the symmetric GAS design has approximately only 70% of the redesigned GAS design stiffness.

Comparing the symmetric GAS (T=5s) fundamental period with the GAS with cable disconnected only (T=4,18s), the symmetric design is more flexible as expected.

BIBLIOGRAPHY

[1] McCallen, D.B., Astaneh-Asl, A. *Seismic Response of Steel Suspension Bridge*, 1996/Nov/1, Second U.S. Seminar on the Seismic Design, Evaluation and Retrofit of Steel Bridges, San Francisco, CA.

[2] McCallen, D., Astaneh-Asl, A., Larsen, S. *Seismic Studies of the San Francisco Oakland Bay Bridge*. 12th World Conference on Earthquake Engineering, 2000, New Zealand.

[3] Astaneh-Asl, A., *Seismic Evaluation and Retrofit of Long Span Bridges.* 11th World Conference on Earthquake Engineering, 1996, paper nr. 2020.

[4] Ochsendorf, J. and Billington, D. *Self-anchored Suspension Bridges.* Journal Bridge Engineering, 1999, pp. 151-156, vol.4, American Society of Civil Engineers.

[5] van Goolen, D. *Self-Anchored Suspension Bridges*. Master of Science, Delft University of Technology, 2006.

[6] Zhang, Z., Teng, Q.-J., Qiu, W.-L., *Recent concrete, self-anchored suspension bridges in China.* Bridge Engineering 159, 2006/Dec, pp. 169-177, issue B34, Institution of Civil Engineers.

[7] Nader, M., Maroney, B., Manzanarez, R., *Seismic Design Strategy of the new East Bay Bridge Suspension Span*. 12th World Conference on Earthquake Engineering , 2000, New Zealand.

[8] Sun, J., Manzanarez, R., Nader, M., *Design of Looping Cable Anchorage System of the New San Francisco-Oakland Bay Bridge.* Journal Bridge Engineering, 2002/Dec, pp. 315-324, vol.7, American Society of Civil Engineers.

[9] Manzanarez, R., Nader et al, *Design of the New San Francisco-Oakland Bay Bridge*. Advanced Technology in Structural Engineering, 2000, pp. 1-12, ASCE.

[10] http://www.sfweekly.com/2004-03-17/news/a-bridge-too-weak/full/, 10 March 2014.

[11] Sun, J., Manzanarez, R., Nader, M., *Suspension Cable Design of the New San Francisco-Oakland Bay Bridge.* Journal Bridge Engineering, 2004/Feb, pp. 101-106, vol.9, American Society of Civil Engineers.

[12] Knox, H., Sun, J., Manzanarez, R., Nader, M., *Discussion of "Suspension Cable Design of the New San Francisco-Oakland Bay Bridge"*. Journal of Bridge Engineering (ASCE), 2005, pp. 365.

[13] McDaniel, C, Seible, F. *Influence of Inelastic Tower Links on Cable-Supported Bridge Response.* Journal Bridge Engineering, 2005/May, pp. 272-280, vol.10, American Society of Civil Engineers.

[14] McDaniel, C., Uang, C.-M., Seible, F., *Cyclic testing of suspension tower shear links of the San Francisco-Oakland Bay Bridge.* Department of Civil Engineering, University of California San Diego, 2002/July.

[15] Nader, M., Maroney, B., *One-of-a-Kind Design.* Structure Magazine, 2007/Oct.

[16] Gao, Y., Yuan, W., Zhou, M., Cao, X. *Seismic Analysis and Design optimization of a Self-Anchored Suspension Bridge*. Technical Council on Lifeline Earthquake Engineering Conference (TCLEE), 2009, Oakland, California, pp. 1-12, American Society of Civil Engineers (ASCE).

[17] Li, T.-F., Zhang, Z., Shi, L. *Influences of Pile-Soil-Structure Interaction on Seismic Response of Self-Anchored Suspension Bridge. Electronic Journal of Geotechnical Engineering*, 2009, vol.14, Bund. J.

[18] Mu, Y., Zhang, Z., Chen, J., Miao, F. *Seismic Responses Analysis of a Self-Anchored Cable-Stayed Suspension Bridge*. International Conference on Transportation Engineering, 2009, pp. 1692-1698, American Society of Civil Engineers (ASCE).

[19] Jiang, M., Qiu, W., Yu, B. *Research on Seismic Response Reduction of Self-anchored Suspension Bridge.* Computational Structural Engineering, 2009, pp. 209-216, vol.5, Springer Science+Bussiness Media B.V.

[20] Nie, J., Tao, M., Fan, J. *Research on Cable Anchorage Systems for Self-Anchored Suspension Bridges with Steel Box Girders.* Journal Bridge Engineering, 2011/Sep, pp. 633-643, vol.5, American Society of Civil Engineers.

[21] Nie, J., Zhou, M., Wang, Y., Fan, J., Tao, M. *Cable Anchorage System Modelling Methods for Self-Anchored Suspension Bridges with Steel Box Girders.* Journal Bridge Engineering, 2014/Feb, pp. 172-185, vol.2, American Society of Civil Engineers.

[22] Lianzhen, Z., Tianliang, C. *Dynamic Characteristics and Seismic Response Analysis of Self-anchored Suspension Bridge.* Advanced Engineering Forum, 2012/Jul/26, pp. 183-188, vol.5, Trans Tech Publications.

[23] Qiu, W.-L., Kou, C.-H., Kao, C.-S., Ma, S.-W., Yang, J. *Study on the Seismic Behavior of Self-Anchored Suspension Bridges*. Journal of Marine Science and Technology, 2012, pp.384-391, vol.20.

[24] Lu, P., Chen, J., Zhong, J. and Lu, P., J. *Optimization Analysis Model of Self-Anchored Suspension Bridge*. Mathematical problems in engineering, 2014, pp.384-391, vol.20, Hindawi Publishing Corporation.

[25] Yuanming, L., Hui, T., Shaorui, W., Wenlong, W., Zhixiang, Z., *Dynamic Characteristics Analysis of Large Self-anchored Suspension Bridge,* Modern Applied Science, 2014, vol.8, Canadian center of Science and Education.

[26] Gimsing, N., *Cable supported bridges.* Jonh Wiley&Sons, Denmark, 1983.

[27] Chen, W.-F., Duan L., Earthquake Damage on Bridges. In *Bridge Engineering Handbook,* CRC Press, 2000.

[28] http://baybridgeinfo.org/projects/sas, 16 February 2014.

[29] http://www.dot.ca.gov/dist4/sfobb/PurposeandNeed.html (Purpose and need for the project), 31 March 2014.

[30] www.dot.ca.gov/hq/esc/construction/br_contractor_outreach/Mar2013/CIDH_Piles.pdf, 20 March 2014.

[31] https://www.youtube.com/watch?v=wJeyD_67YMo, 21 March 2014.

[32] Chen, W.-F., Duan L., Orthotropic Bridge Decks. In *Bridge Engineering Handbook,* CRC Press, 2000.

[33] Chen, W.-F., Duan L., Towers. In *Bridge Engineering Handbook,* CRC Press, 2000.

[34] http://www.shutoko.co.jp/english/technology/planningconstruction/, 15 April 2014.

[35] www.shutoko.jp/fun/lightup/rainbowbridge, 15 April 2014.

[36] Ishihara, K., *Liquefaction of Subsurface Soils during earthquakes.* Journal of Disaster Research, 2006, pp. 245-261, vol.1 n.º2.

[37] Yasuda, S., Ishikawa, K., Hagiya, S., *Remarkable liquefaction-induced damages along Tokyo Bay during the 2011 Tohoku-Pacific Ocean earthquake in Japan.* 15WCEE, 2012, Lisbon.

[38] Ishihara, K., *Liquefaction in Tokyo Bay and Kanto regions in the 2011 great East Japan earthquake.* Proceedings of the International Symposium on Engineering Lessons Learned from the 2011 Great East Japan Earthquake, 2012/March, Tokyo, Japan.

[39] http://www.shutoko.jp/fun/lightup/rainbowbridge/outline/

[40] Wang, Q. *et al, Caisson Foundation design for offshore Anchorage.* Advanced Materials Research, 2011/Oct, pg. 1491-1493, vol. 368-373.

[41]http://www.canadianconsultingengineer.com/awards/pdfs/2012/B7_SanFranciscoOaklandBayBridge.pdf, 15 June 2014.

[42] http://bata.mtc.ca.gov/pdfs/monthly/September2012.pdf, 15 June 2015.

[43] Chung, Y., Thomas, L., *High Strength Steel Anchor rod problems on the new Bay Bridge (Revision 1)*, 2013/Nov/12.

[44] Chung, Y., Thomas, L., *Main concerns about anchor rods on the new Bay Bridge*, 2013/Nov/29.

[45] Heminger, S., Dougherty, M., Boutros, A. (TBPOC), *Report on the A354 Grade BD High-strength steel Rods on the new East span of the San Francisco-Oakland bay Bridge with Findings and Decisions*, 2013/Jul/8.

[46] http://www.portlandbolt.com/, 5 May 2014.

[47] http://baybridgeinfo.org/sites/default/files/pdf/Saddles-Operational-PR.pdf, 5 May 2014.

[48] http://www.mtc.ca.gov/projects/bay_bridge/A354/Appendix_E_Rod_Project_Binders/E17.pdf, 5 May 2014.

[49] http://baybridgeinfo.org/sites/default/files/pdf/Briefing%20on%20Bay%20Bridge%20Bolts%20-%20May%2029%20Final.pdf, 6 May 2014.

[50]http://www.sfgate.com/bayarea/article/Bay-Bridge-designer-warned-Caltrans-in-2010-of-5264109.php#photo-5859751, 6 May 2014.

[51]http://www.sfgate.com/default/article/Caltrans-was-warned-Bay-Bridge-welds-could-crack-5398312.php#page-2, 6 May 2014.

[52]http://www.sfgate.com/bayarea/article/Bay-Bridge-Hundreds-of-leaks-possible-corrosion-5222501.php#page-1, 10 May 2014.

[53]http://www.sfgate.com/bayarea/article/Bay-Bridge-s-new-problem-leaks-5217783.php#page-2, 10 May 2014.

[54] http://www.sacbee.com/2013/05/18/5431401/corrosion-plagues-new-bay-bridge.html, 10 May 2014.

[55] Aviram A., Mackie K., Stojadinović B., *Guidelines for Nonlinear Analysis of Bridge Structures in California.* Pacific Earthquake Research Center (PEER), 2008/Aug, Berkeley.

[56] http://www.dot.ca.gov/dist4/sfobb/appendixK.html (Seismic Design), 31March 2014.

[57] *Ground Motion Report for San Francisco-Oakland Bay Bridge-East span Seismic Safety Project*, Prepared by Fugro, Earth Mechanics, Prepared for California Department of Transportation, 2001/Mar, Sacramento.

[58] Caltrans, *Seismic Design Criteria*. 2004/Feb.

[59] T.Y. Lin International/Moffatt&Nichol Engineers, *San Francisco-Oakland Bay Bridge East Span Seismic Safety Project: Design Criteria*. Caltrans/Division of Structures, 2001/Mar.

[60] Eurocode 8-Part 2: *Design of structures for earthquake resistance-Bridges.*

[61] Chopra, A., *Dynamics of Structures*. Prentice Hall, New Jersey, 1995.

APPENDIX A.2.1.

N.º	Name/Location		Year	Span (m)		Deck (m)				Main cable			Towers		Foundations System
				Main span	Side span	Width	Depth	System	Type	sag/ span	Type	Type/ Interval	Structural	Bottom	
1	**Wrsowicer**	Germany	1870	22,8	11,4	?	?	?	Continuous truss	?	?	?	?	?	?
2	**Muhlenthor**	Germany	1899	41,8	19,6	?	1,3	Slab on girders	Continuous warren truss	1/7,4	Steel encased	vertical/2,8	rocker	hinged at base	?
3	**Napageld**	Austria	1910	35,9	20,9	?	1,71	Slab on girders	Continuous truss	1/9	rivited	?	rocker	?	?
4	**Cologne-Deutz**	Germany	1915	185	92	27,5	3,2	Slab on girders	Continuous plate girder	1/8,6	eye-bar plates	vertical/11	rocker	hinged at supports	?
5	**Seventh street**	USA	1926	134,7	67,4	11,6	2,8	Slab on girders	Continuous girder	1/8,1	eye-bar plates	vertical/6,7	One fixed one movable	?	?
6	**Ninth Street**	USA	1926	125	65,5	11,6	2,7	Slab on girders	continuous girder	1/8,1	eye-bar plates	vertical/6,5	one fixed one movable	?	?
7	**Admiral Scheer**	Germany	1927	96	36,8	?	2,2	Slab on girders	Continuous plate girder	1/9	eye-bar plates	vertical/4,6	rocker	hinged at base	?
8	**Sixth Street**	USA	1928	131,1	65,5	11,6	2,7	Slab on girders	Continuous girder	1/8,1	eye-bar plates	vertical/6,5	one fixed one movable	?	?
9	**Kiyosu**	Japan	1928	91,5	45,8	25,8	2,6	Slab on girders	Three-hinged girder	1/7,1	eye-bar plates	vertical/4,5	rocker	hinged at base	?
10	**Hipólito Irigoyen**	Argentina	1928	150	60	8,8		?	2 Continuous steel Girder	?	locked-coil strands	vertical/5			
11	**Cologne-Mulheim**	Germany	1929	315	91	22	6	Slab on girders	Three-hinged girder	1/9,1	prestressed locked wire strands	vertical/ 11,3	rocker	hinged at base	?
12	**Little Niangua**	USA	1933	68,4	34	6	0,85	?	two-hinged I-girder	1/9	prestressed wire strands	vertical/3,8	fixed	?	?
13	**King Alexander I**	Serbia	1934	261	75	21	4,3	Slab on 2 girders	cantilever plate girder	1/9,3	prestressed locked wire strands	vertical/?	rocker	?	?
14	**Krefeld-Uerdingen**	Germany	1935	250	125	19	6,3		continuous warren truss	1/8,2	eye-bar plates	eye-bar plates/12,5	?	hinged at base	?

N.º	Name/Location		Year	Span (m)				Deck (m)		Main cable		Towers			Foundations System
				Main span	Side span	Width	Depth	System	Type	sag/ span	Type	Type/ Interval	Structural	Bottom	
15	**Chelsea Thames River**	England	1937	107	53	19	2,7	Concrete slab on girders	continuous plate I-girder	1/8,8	locked-coil strands	vertical/4,8	rocker	hinged at base	Mass concrete spread foundations
16	**Reichsbrücke**	Austria	1937	241	48	26	1,4	Slab on girders	Plate girder	?	eye-bar plates	vertical/?	?	?	?
17	**Hutsonville**	USA	1939	106,7	45,7	6,1	?	?	two-hinged I-girder	?	prestressed wire strands	vertical/7,6	?	fixed	?
20	**Duisburg**	Germany	1955	285,5	128,4	24	3,9	?	2 continuous box girders	1/9,2	prestressed wire strands	vertical/13	?	hinged at base	?
21	**Merelbeke**	Belgium	1960	100	46	22	1,9	?	continuous prestressed concrete box	1/11, 1	prestressed wire strands	vertical/5	?	?	?
22	**Konohana**	Japan	1990	300	120	26,5	3,17		Continuous box girder	1/6	parallel wire strands	inclined/10	?	fixed at base	?
23	**Yeong Jong Bridge**	Korea	2000	300	125	35	12	Orthotropic (upper deck) Girders (lower deck)	Double deck Stiffening truss	1/5	parallel wire strands	vertical spatial/ 12,5	Diamond-shape	fixed at base	Pneumatic Caisson method
24	**Golden Bay**	China	2000	60	24	12,5	1	Concrete girder	two longitudinal concrete edge beams	1/8	high strength steel wires	vertical/3	?	?	?
25	**WanXin Bridge**	China	2004	160	70	41	2,5	Cast-in situ Concrete box girder	Concrete box girder with precast cantilever beams	1/6	IWR type Steel ropes	vertical/5	?	?	?
26	**Kanne**	Belgium	2005	96,2	14,6	21,3	0,9	Slab on girders	Continuous I-girder	1/8	parallel wire strands	vertical/ 3,7	?	fixed at base	?
27	**PingSheng Bridge**	China	2006	350	-	78	?	Orthotropic	Steel box girder	?	4 main cables	vertical/?	?	?	?
28	**Sanchaji Bridge**	China	2006	328	132	35	3,6	Orthotropic	Steel box girder	1/5 (main span)	Pefabricated parallel wire strands	vertical/9	?	?	Drilled pile groups
29	**Tiaoyue Bridge**	China	2006	134,44	38,74	9	?	?	Steel box girder	?	?	3-dimensional shape	Inclined	?	Piles

B

N.º	Name/Location		Year	Span (m)		Deck (m)					Main cable		Towers		Foundations System
				Main span	Side span	Width	Depth	System	Type	sag/ span	Type	Type/ Interval	Structural	Bottom	
30	**Jianshe Bridge (Zhuanghe River)**	China	2007	100	41,6	28,6	2,17	Concrete girder	Concrete solid edge girder	1/5,2	parallel high-strength galvanized steel-wires	inclined/?	?	?	?
31	**Sorok**	Korea	2007	250	110	15,7	?	Orthotropic	Steel box girder	?	?	vertical/?	A-frame	?	?
32	**Jinzhou Strait Bridge**	China	2008	400	130	23,5	3	Orthotropic	Steel box girder	?	High-strength galvanized steel wire	vertical/?	?	?	Bored piles
33	**Jiangdong Bridge**	China	2008	260	83	47	?	Orthotropic ?	Steel box girder	?	?	spatial/?	?	?	?
34	**Qingfeng Bridge (Ningbo River)**	China	2008	280	?	?	?	?	Steel and concrete hybrid girder	?	?	vertical/6	?	?	
35	**Liede Bridge**	China	2008	219/167?	47	?	?	?	Steel box girder?	?	?	vertical spatial/13	?	?	?
36	**Great Loire River Bridge**	France	2008	200	?	25	1,8	Slab on girders	Girders	?	?	?	?	?	?
37	**Gushan Bridge**	China	2010	235	150		?	?	Steel box girder			spatial			
38	**Jiaozhou Bay Bridge (Qingdao-Huangdao)**	China	2011	260/190	80	47	3,6	Orthotropic (parallel decks)	Continuous steel box girder	1/12,5 1/18	prestressed wire strands	vertical/12	?	fixed at base	Piles
39	**Taohuayu (THY) Bridge**	China	2012	406	160	35,44	3,118	Orthotropic	Steel box girder	?	?	vertical/16	?	?	Piles
40	**Shengyang Gaokan Hunhe River Bridge**	China	2012	180/180	48	42,5	4	?	Steel box girder	single tower	?	vertical/?	?	?	?
41	**New East bay Bridge**	USA	2013	385	180	35	5,5	Orthotropic (parallel decks)	Continuous box girder	Single tower	parallel wire strands	spatial/10	?	fixed at base	Piles
42	**Luozhou Bridge**	China	2013	372	85	43	?	?	?	1/6,64	galvanized steel wires	?	?	?	Reinforced concrete piles

C

APPENDIX A 3.1. – E2 piles

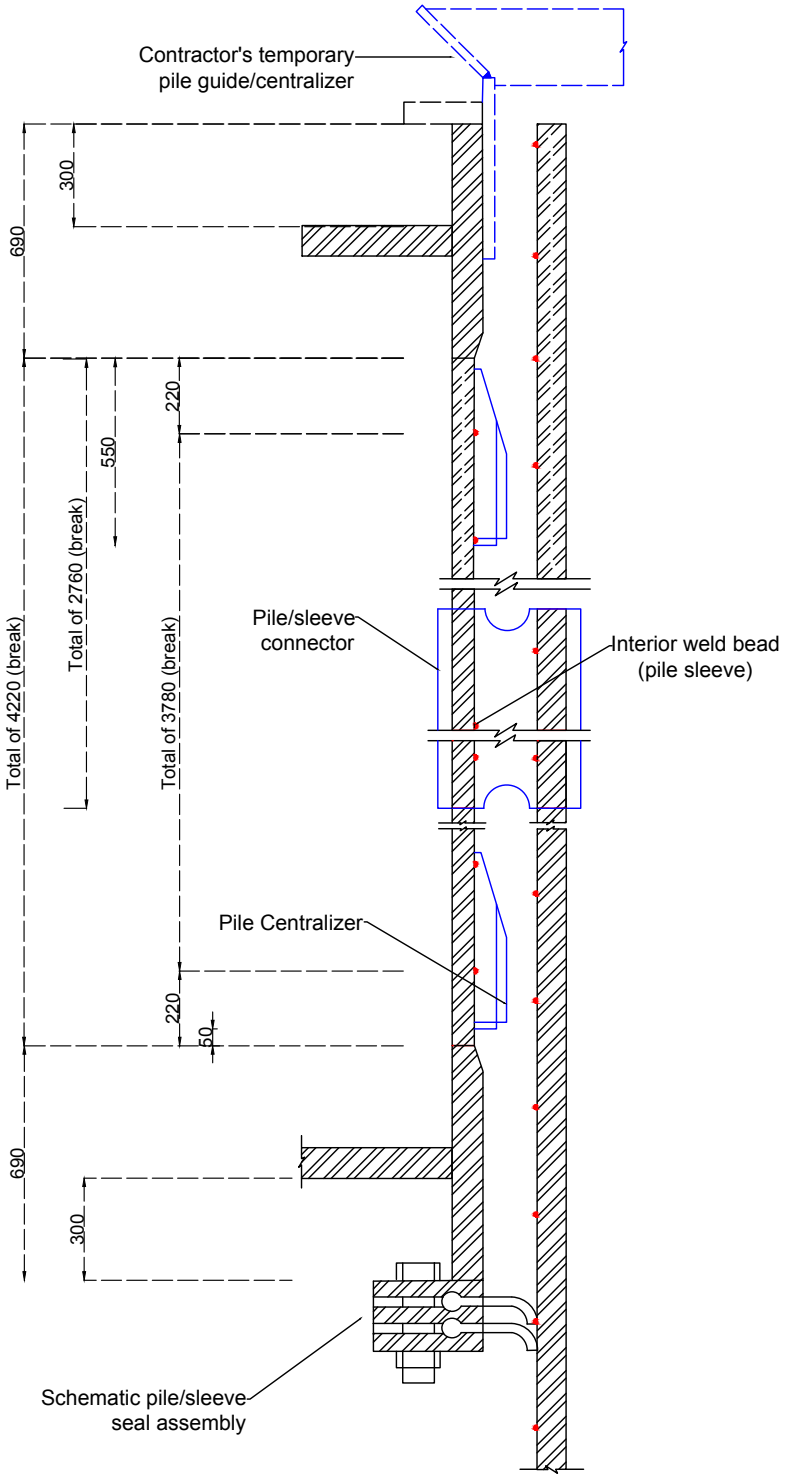

Section D-D
1:20 (mm)

D

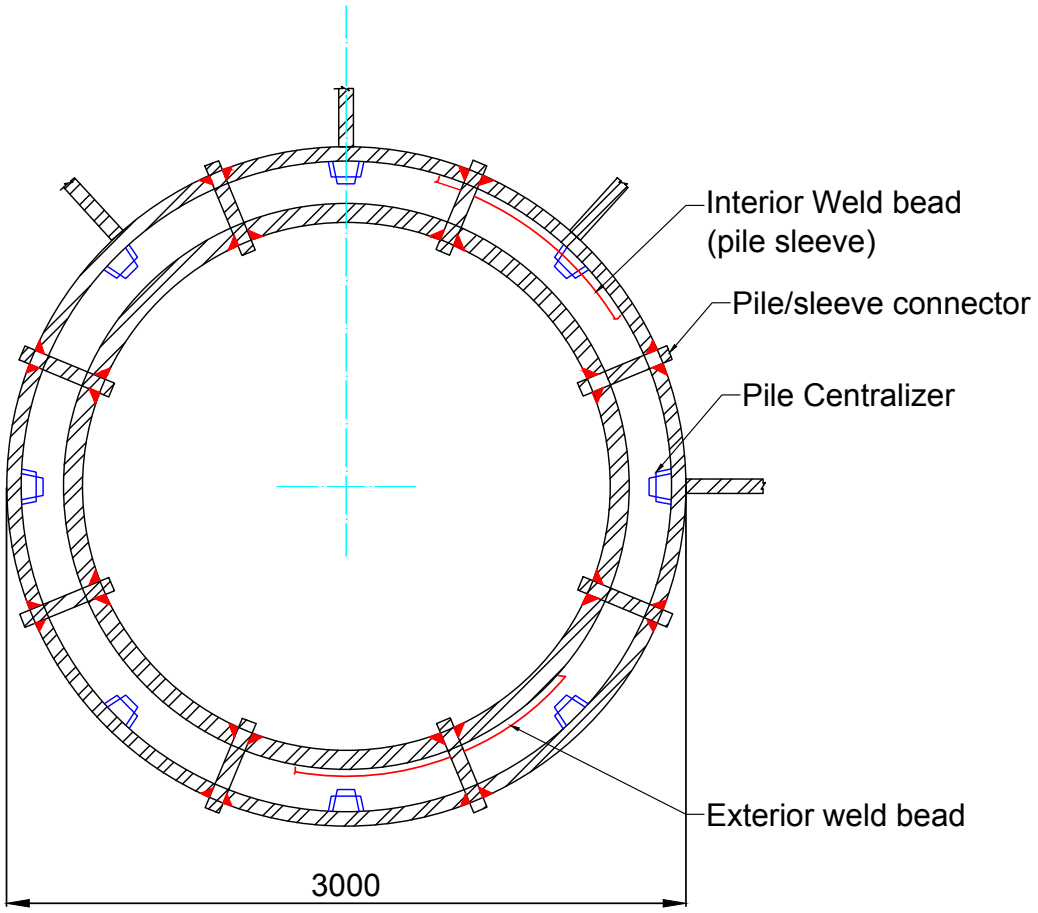

Section E-E
1:30 (mm)

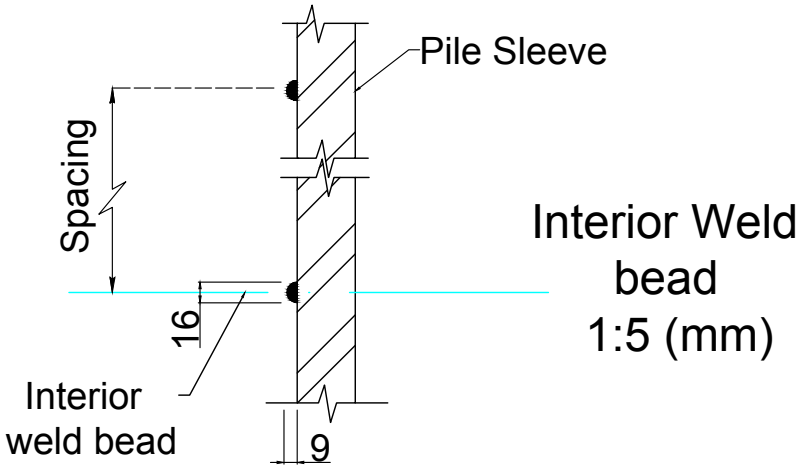

E

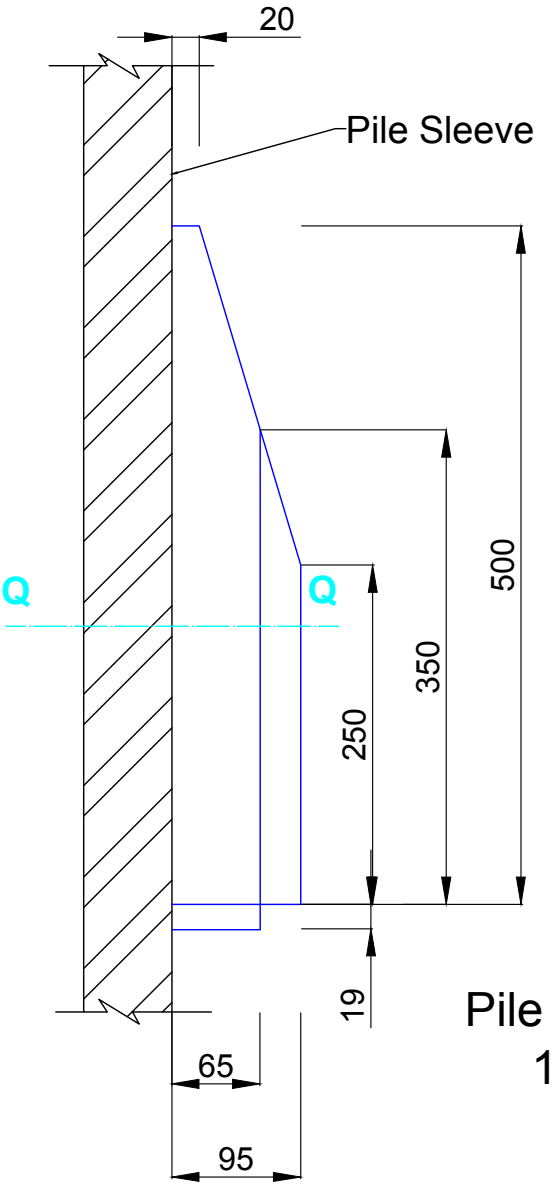

Pile Centralizer
1:5 (mm)

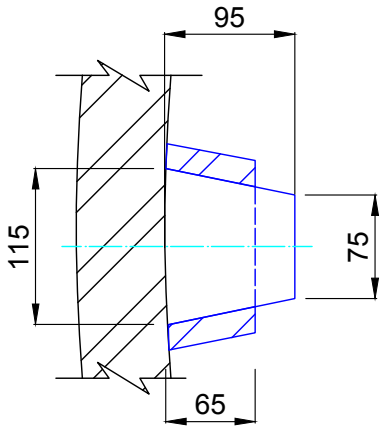

Section Q-Q
1:5 (mm)

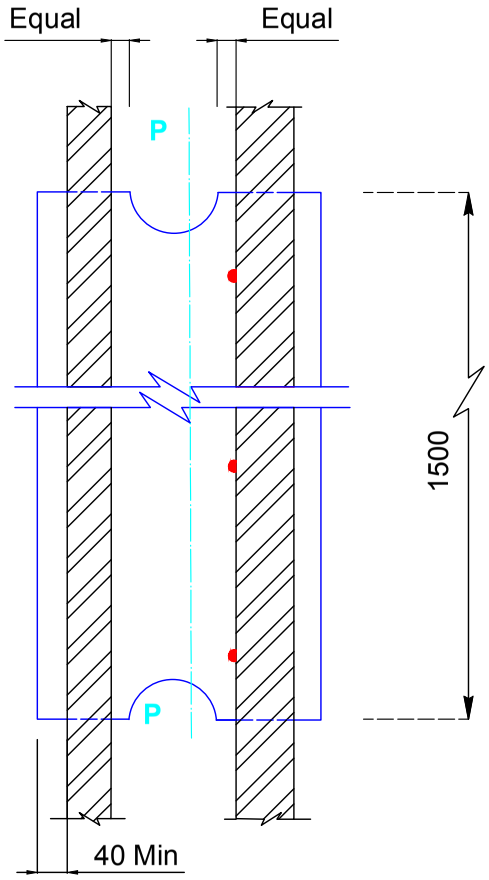

Pile/sleeve
connector
1:10 (mm)

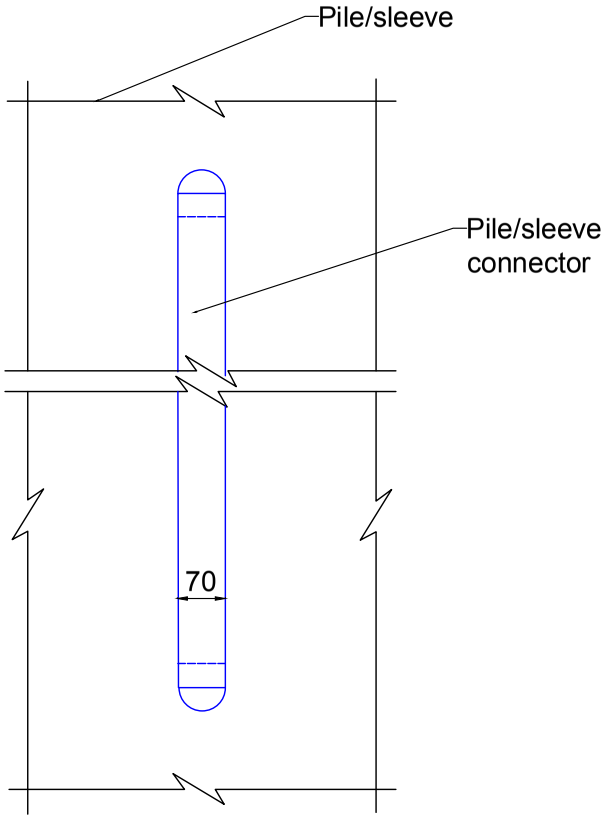

Section P-P
1:10 (mm)

G

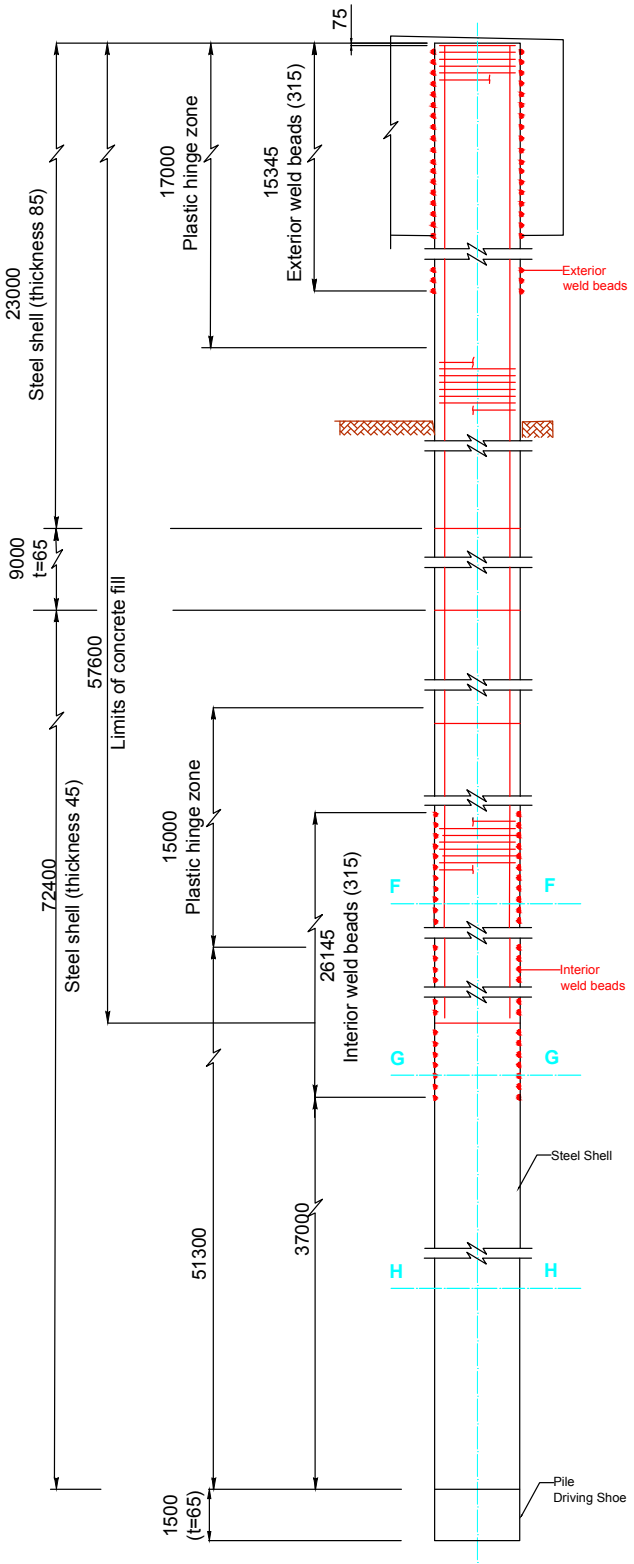

2500 DIA CISS Concrete Piling
No scale

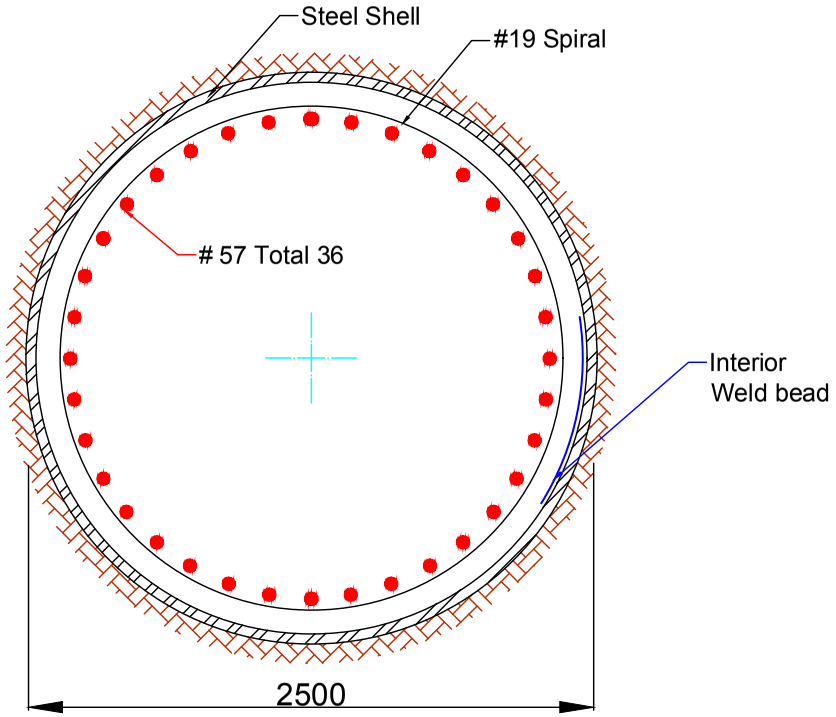

Section F-F
1:30 (mm)

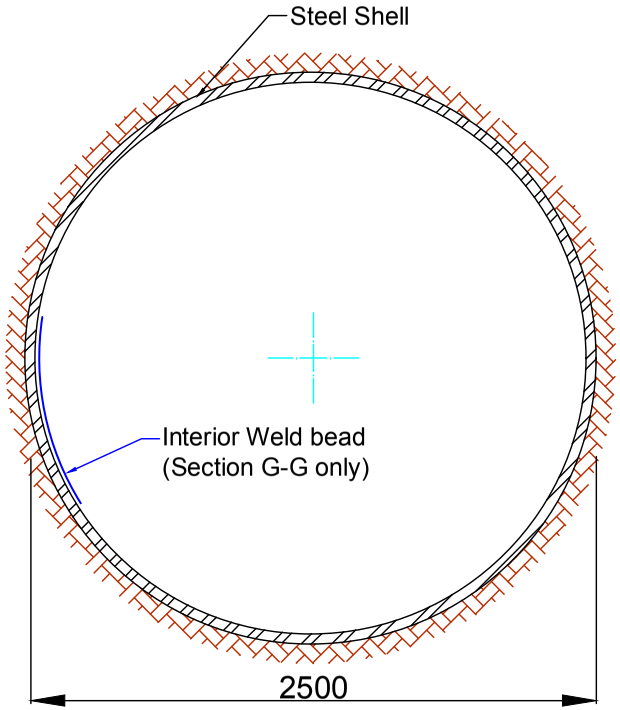

Section G-G
and H-H
1:30 (mm)

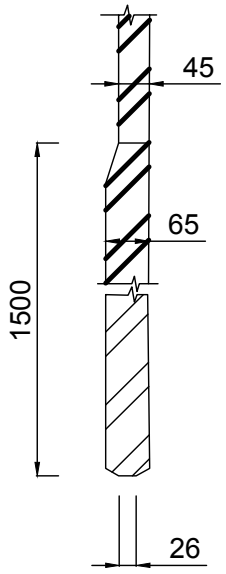

Pile Driving Shoe
1:10 (mm)

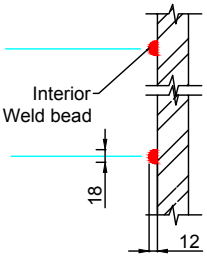

Interior weld bead
1:10 (mm)

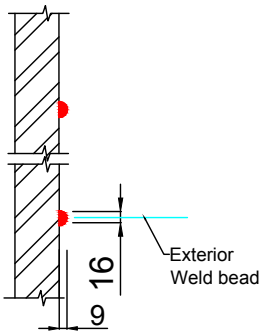

Exterior weld bead
1:10 (mm)

APPENDIX A3.3. – SAS SPAN ELEVATION AND PLAN

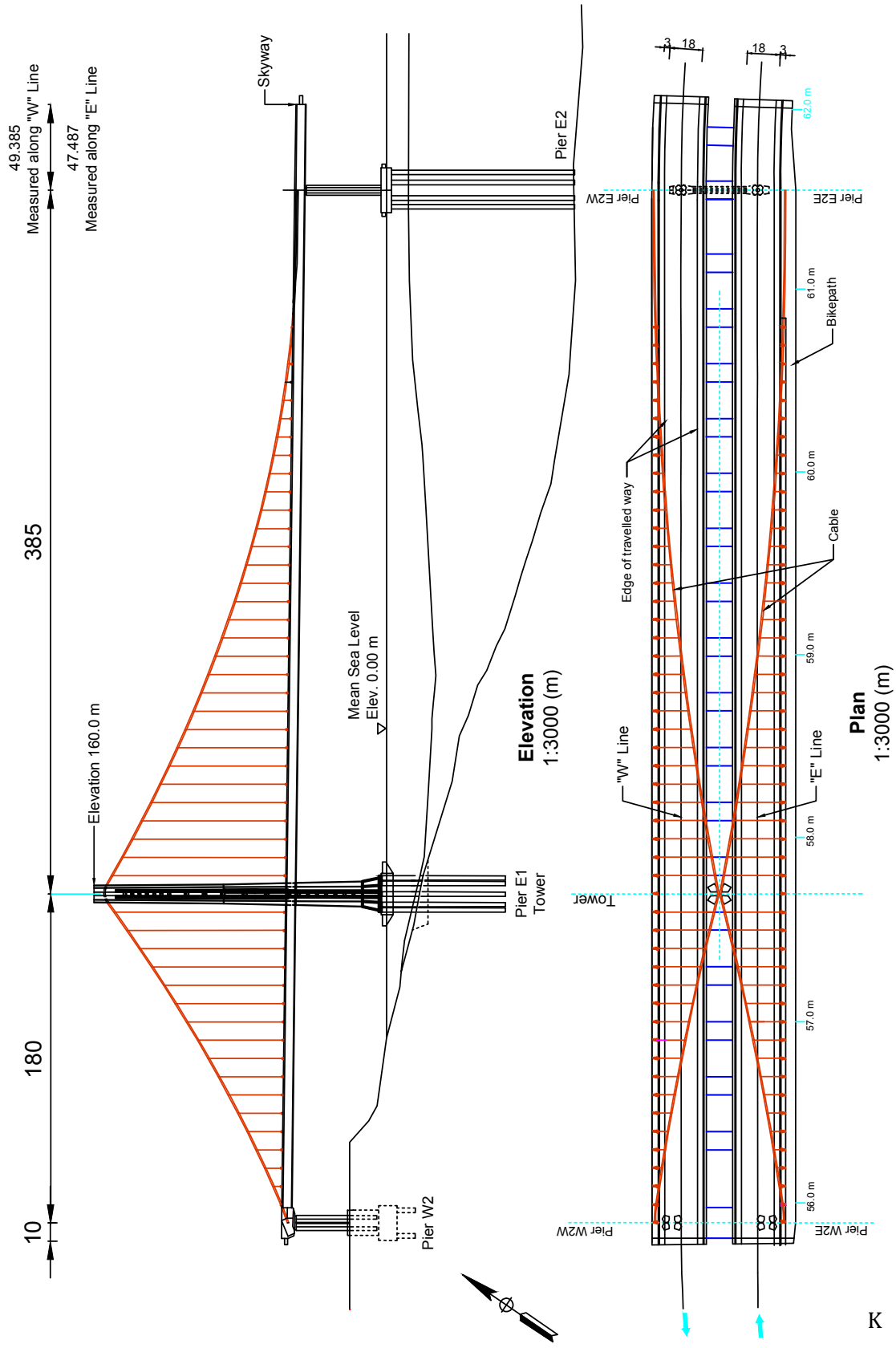

APPENDIX A3.4 - Deck section

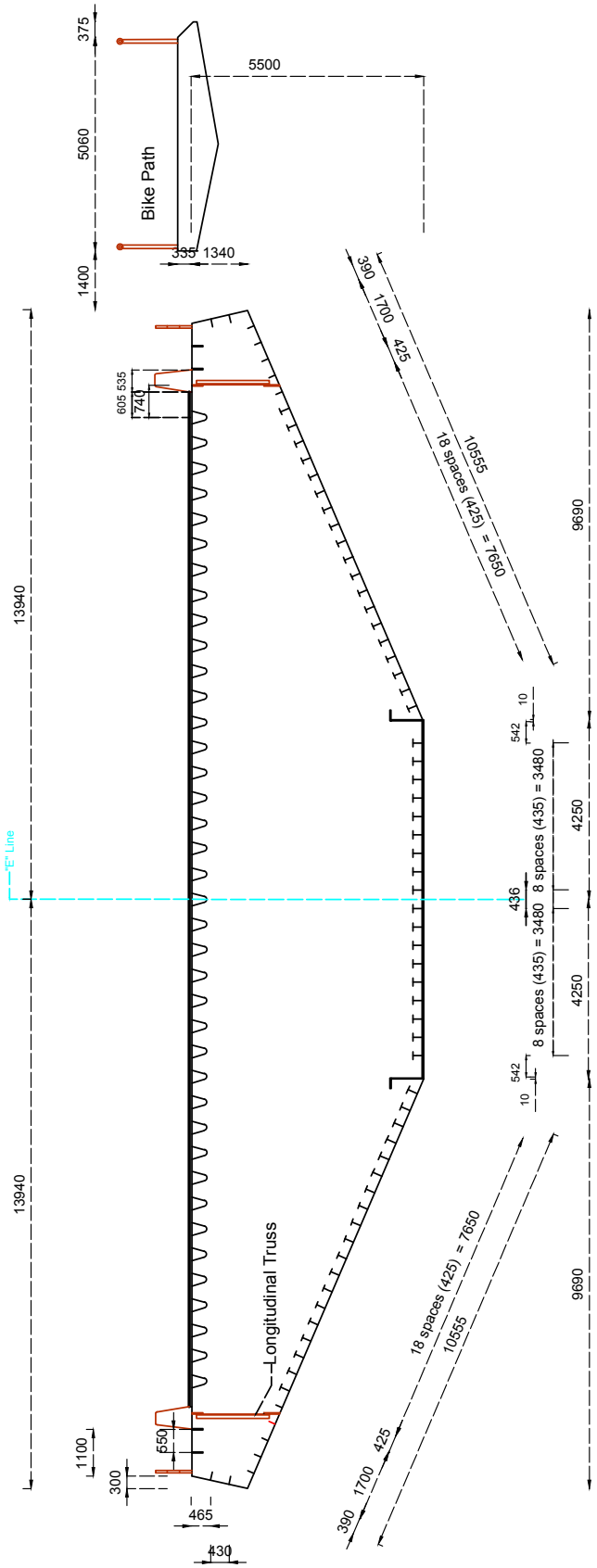

"E" Line
Section Type 1A
1:150

L

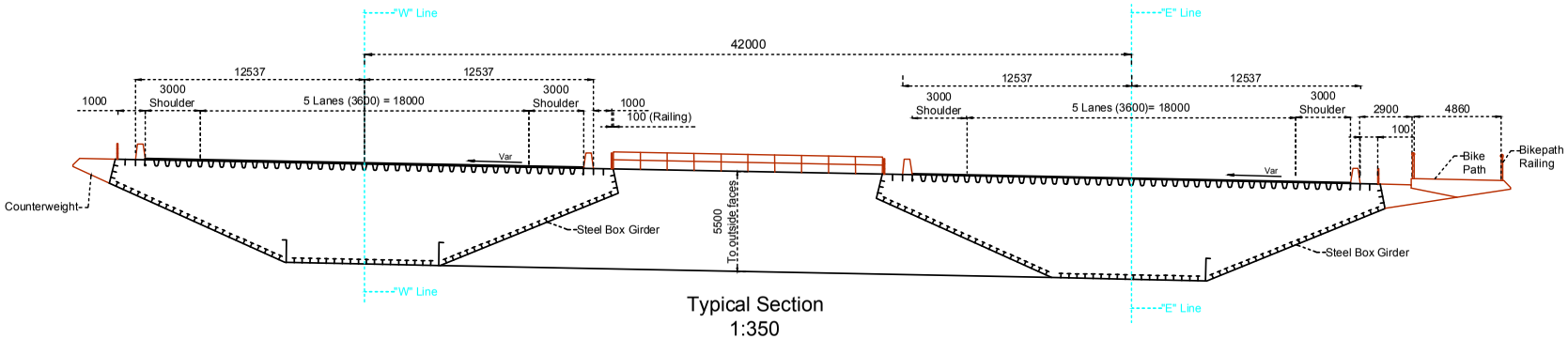

Typical Section
1:350

M

APPENDIX A3.5 - Tower

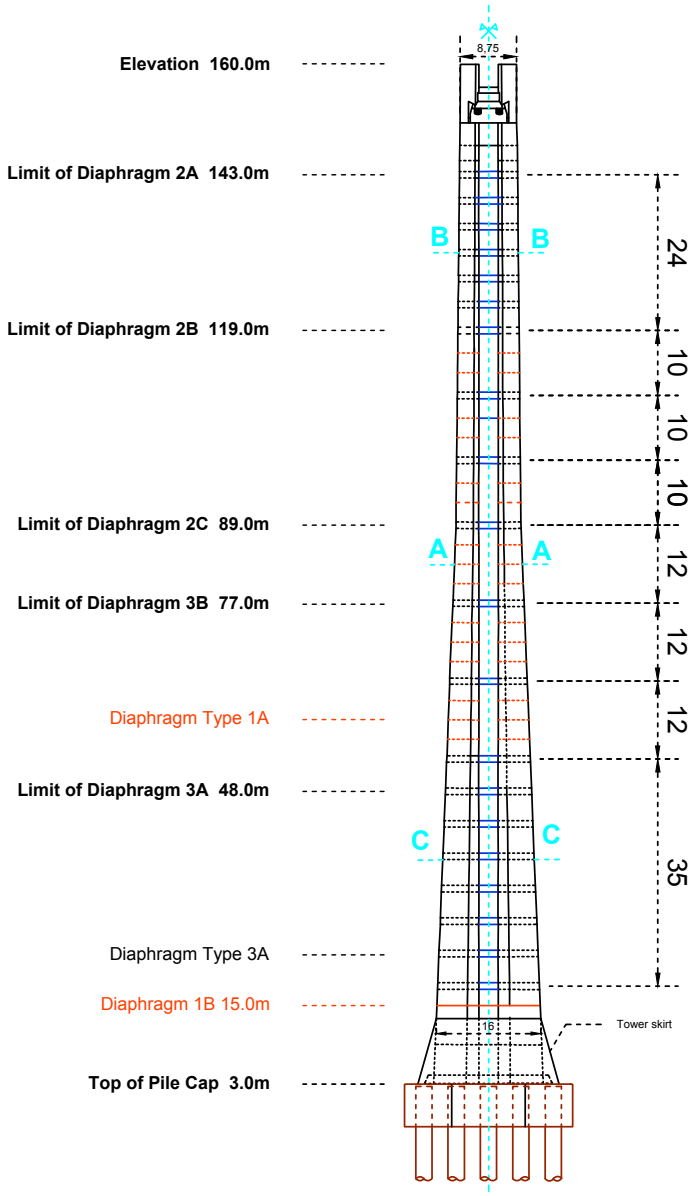

Tower Diaphragm Layout
1:1000 (m)

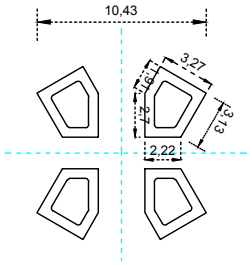

Typical Diaphragm 1 (A or B)
Section A-A
1:400 (m)

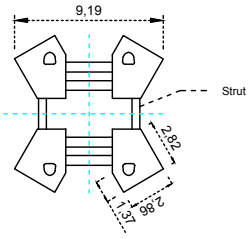

Typical Diaphragm 2 (A, B or C)
Section B-B
1:400 (m)

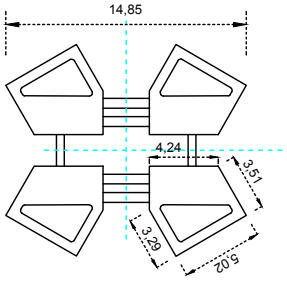

Typical Diaphragm 3 (A or B)
Section C-C
1:400 (m)

N

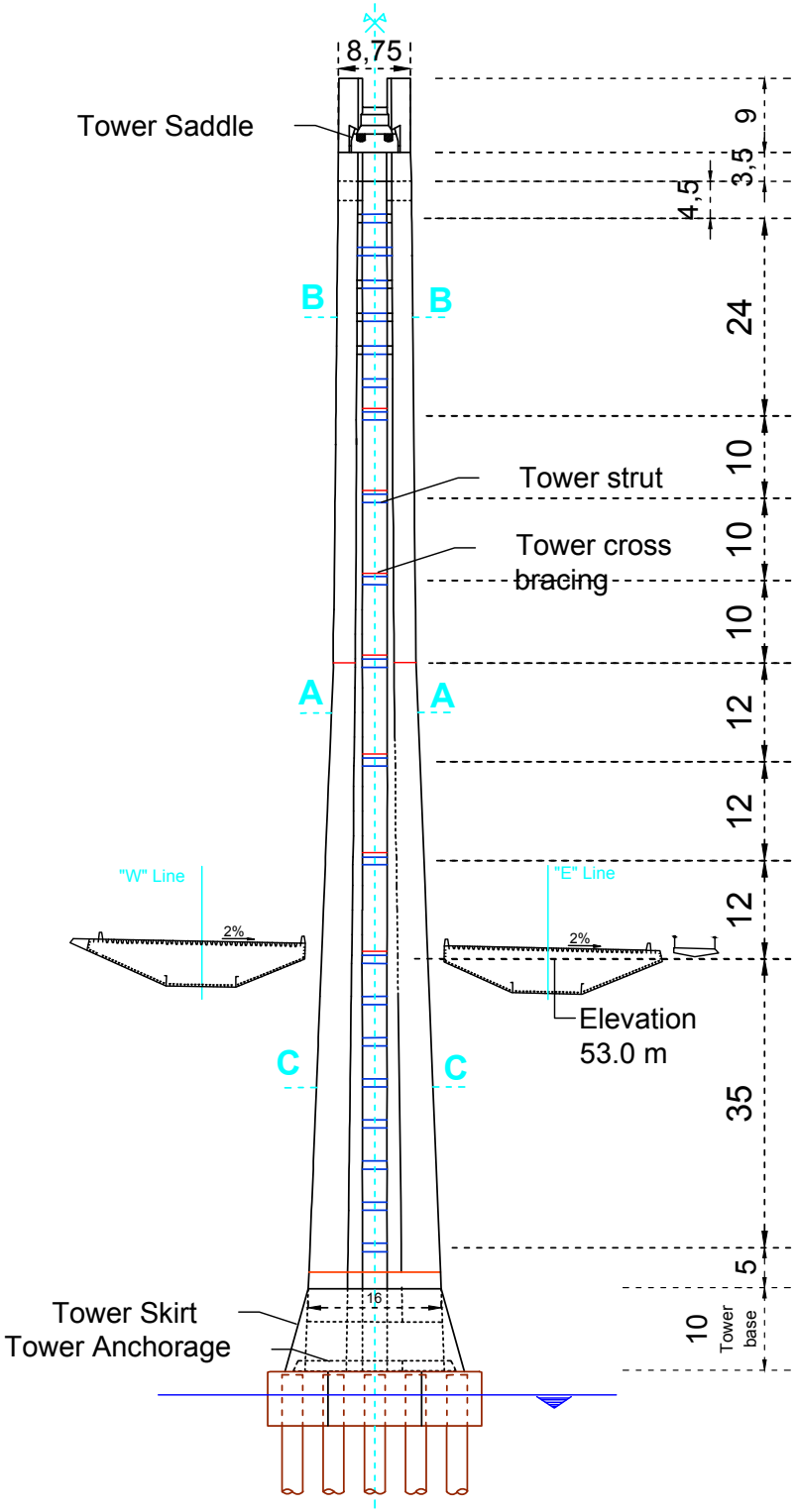

Transverse Elevation looking-east
1:1000 (m)

APPENDIX A 5.1 – DECK PLATE'S EQUIVALENT THICKNESS AND BENDING MODIFIERS USED IN THE SAP MODEL WITH INTERMEDIATE CALCULATIONS

Plate	Panels	Area x1 Plate [m^2]	Area x1 Stiff [m^2]	G (x1 stiff) [m]	Inertia (x1 stiff) [m^4]	N.º stiff	Area w/ stiff [m^2]	M11	Inertia (PL equiv)	G (PL+ stiff) [m]	d (PL) [m]	d' (Stiff) [m]	Inertia actual PL+stiff [m^2]	M22
1	10-14, 112-End	0,012	0,00932	0,105	1,5688E-04	1	0,02132	0,178	2,24E-06	0,060	0,050	0,065	2,26E-04	100,9
	14-112	0,0084	0,00932	0,105	1,5688E-04		0,01772	0,107	1,29E-06	0,066	0,059	0,053	2,12E-04	164,8
2	10-End	0,03	0,00963	0,1575	6,0658E-05	2	0,04925	0,226	4,41E-06	0,068	0,058	0,090	3,77E-04	85,57
3	10-14	0,02746	0,0036	-	-	2	0,03466	1	-	-	-	-	-	1
	14-30	0,03433	0,0044	-	-		0,04313	1	-	-	-	-	-	1
	30-112	0,03844	0,00728	-	-		0,05300	1	-	-	-	-	-	1
	112-118	0,02471	0,0040	-	-		0,03200	1	-	-	-	-	-	1
	118-End	0,02471	0		-		0,02471	1	-	-	-	-	-	1
4	10-112	0,0306	0,0044	0,118	1,4667E-05	5	0,05260	0,197	4,18E-06	0,055	0,046	0,063	2,26E-04	54,123
	112-115	0,0272	0,0036	0,106	9,7200E-06		0,04520	0,310	2,64E-06	0,047	0,039	0,059	1,53E-04	58,114
	115-End	0,0272	0,0044	0,116	1,4667E-05		0,04920	0,216	3,83E-06	0,056	0,048	0,060	2,16E-04	56,413
5	10-14	0,0085	0,0044	0,13	1,7747E-05	1	0,01290	0,282	1,00E-06	0,051	0,041	0,079	5,98E-05	59,490
	14-30	0,00935	0,00541	0,1322	9,0747E-05		0,01476	0,254	1,48E-06	0,056	0,045	0,077	1,42E-04	95,627
	30-112	0,00765	0,00541	0,1322	9,0747E-05		0,01306	0,206	1,00E-06	0,060	0,051	0,072	1,39E-04	138,42
	112-115	0,0085	0,00541	0,1322	9,0747E-05		0,01391	0,233	1,22E-06	0,058	0,048	0,075	1,40E-04	115,51

P

Plate	Panels	Area x1 Plate [m^2]	Area x1 Stiff [m^2]	G (x1 stiff) [m]	Inertia (x1 stiff) [m^4]	N.º stiff	Area w/ stiff [m^2]	M11	Inertia (PL equiv)	G (PL+ stiff) [m]	d (PL) [m]	d' (Stiff) [m]	Inertia actual PL+stiff [m^2]	M22
5 (cont)	115-118	0,00935	0,00541	0,1322	9,0747E-05		0,01476	0,254	1,48E-06	0,056	0,045	0,077	1,42E-04	95,627
	118-120	0,01063	0,00575	0,140	2,5348E-05	1	0,01638	0,273	2,02E-06	0,057	0,045	0,083	8,66E-05	42,824
	120-122	0,00935	0,0044	0,122	1,4667E-05		0,01375	0,310	1,22E-06	0,047	0,036	0,076	5,19E-05	42,695
	122-End	0,01275	0,0044	0,130	1,4667E-05		0,01715	0,411	2,34E-06	0,045	0,030	0,086	5,89E-05	25,214
6	10-14	0,01523	0,0112	0,195	9,5577E-05		0,02644	0,192	8,11E-06	0,093	0,075	0,1023	3,00E-04	37,058
	14-112	0,0087	0,00549	0,1322	9,0747E-05		0,01419	0,231	1,26E-06	0,057	0,047	0,075	1,41E-04	112,16
	112-115	0,01218	0,006	0,1656	1,3417E-04		0,01818	0,301	2,59E-06	0,064	0,050	0,1016	2,27E-04	87,870
	115-118	0,01523	0,006	0,1656	1,3417E-04	1	0,02122	0,376	4,04E-06	0,059	0,042	0,1062	2,30E-04	56,938
	118-120	0,0261	0,00714	0,1875	3,4545E-05		0,03324	0,484	1,62E-06	0,054	0,024	0,1335	1,71E-04	10,578
	120-122	0,01523	0,00575	0,150	2,5348E-05		0,02098	0,376	4,14E-06	0,0511	0,034	0,0989	1,00E-04	24,262
	122-End	0,00957	0,00575	0,150	2,5348E-05		0,01532	0,244	1,58E-06	0,0434	0,032	0,1066	1,08E-04	68,453
7	10-14	0,0085	0,0044	0,120	1,4667E-05		0,01290	0,285	9,95E-07	0,048	0,038	0,0725	5,00E-05	50,281
	14-115	0,0068	0,00446	0,107	5,2836E-05		0,01126	0,220	6,59E-07	0,047	0,039	0,0598	7,94E-05	120,47
	115-118	0,01063	0,00541	0,1322	9,0747E-05	1	0,01604	0,292	1,90E-06	0,053	0,040	0,0793	1,43E-04	75,198
	118-122	0,00935	0,0044	0,122	1,4667E-05		0,01375	0,313	1,22E-06	0,047	0,036	0,0755	5,19E-05	42,695
	122-End	0,0068	0,0044	0,106	9,7200E-06		0,01120	0,220	6,59E-07	0,042	0,034	0,1066	5,64E-05	85,546

Q

Plate	Panels	Area x1 Plate [m^2]	Area x1 Stiff [m^2]	G (x1 stiff)	Inertia (x1 stiff) [m^4]	N.º stiff	Area w/ stiff [m^2]	M11	Inertia (PL equiv)	G (PL+ stiff) [m]	d (PL) [m]	d' (Stiff) [m]	Inertia actual PL+stiff [m^2]	M22
	10-14	0,0306	0,0044	0,118	1,4667E-05		0,05260	0,198	4,18E-06	0,055	0,046	0,0634	2,26E-04	54,123
	14-115	0,0272	0,0036	0,106	9,7200E-06		0,04520	0,220	2,64E-06	0,047	0,039	0,0590	1,53E-04	58,114
8	115-120	0,0306	0,0040	0,1105	1,1608E-05	5	0,05000	0,227	3,64E-06	0,050	0,041	0,0610	1,85E-04	50,807
	120-122	0,0306	0,0044	0,118	1,4667E-05		0,05260	0,198	4,18E-06	0,055	0,046	0,0634	2,26E-04	54,123
	122-End	0,0272	0,0036	0,116	9,7200E-06		0,04520	0,220	2,64E-06	0,047	0,039	0,0690	1,76E-04	66,850
	10-14	0,02786	0,0036	-	-		0,03506	1	-	-	-	-	-	1
	14-30	0,02507	0,0036	-	-		0,03227	1	-	-	-	-	-	1
9	30-112	0,02507	0,00306	-	-	2	0,03119	1	-	-	-	-	-	1
	112-End	0,02507	0,0040	-	-		0,03300	1	-	-	-	-	-	1
10	10-End	0,03000	0,00705	0,1375	3,2445E-05	2	0,04410	0,315	3,18E-06	0,051	0,041	0,0867	2,22E-04	69,83

R

APPENDIX A5.2 – PARABOLIC CABLE EQUATION AND COORDINATES FOR SYMMETRIC REDESIGNED GAS MODEL

$$z = ax^2 + bx = c$$

Conditions: $x = 0 \quad z = 1{,}5$; $x = 180 \quad z = 56$; $x = 280 \quad z = 101{,}4$ $\leftrightarrow$ $\boldsymbol{z = 0{,}00045675x^2 + 0{,}228896x + 1{,}5}$

$$y = dx + e$$

Conditions: $x = 0 \quad y = 34{,}64$; $x = 280 \quad y = 0$ $\leftrightarrow$ $\boldsymbol{y = 0{,}1237x - 34{,}64}$

X (m)	Main cable coordinates	
	Z (m)	Y (m)
0	1.50	-34.64
10	3.83	-33.40
20	6.26	-32.17
30	8.78	-30.93
40	11.39	-29.69
50	14.09	-28.45
60	16.88	-27.22
70	19.76	-25.98
80	22.73	-24.74
90	25.80	-23.51
100	28.96	-22.27
110	32.21	-21.03
120	35.54	-19.79
130	38.98	-18.56
140	42.50	-17.32
150	46.11	-16.08
160	49.82	-14.85
170	53.61	-13.61
180	57.50	-12.37
190	61.48	-11.13
200	65.55	-9.90
210	69.71	-8.66
220	73.96	-7.42
230	78.31	-6.19
240	82.74	-4.95
250	87.27	-3.71
260	91.89	-2.47
270	96.60	-1.24
280	101.40	0.00

Obs.: Z coordinates assumed 0 at the deck level and Y coordinates assumed 0 at the Tower (middle of deck) and ±34,64 at the outside edge of deck.

APPENDIX A6.1 – RELEVANT VIBRATION MODES MASS PARTICIPATION RATIO FOR GAS MODEL WITH CABLE DISCONNECTED

Mode nr.º	Period (s)	UX	UY	UZ	RX	RY	RZ
1	4,9070	0,4017	2,40E-08	1,44E-04	5,84E-08	1,03E-02	2,67E-08
2	4,7668	3,38E-04	2,47E-04	0,0927	6,50E-04	4,54E-02	7,40E-05
3	4,7505	7,15E-07	0,0758	0,0004	0,2010	1,90E-04	2,22E-02
4	4,5710	1,70E-04	0,0000	0,0710	1,40E-05	3,80E-02	1,38E-06
5	3,3565	3,57E-09	0,4686	9,25E-08	0,3549	1,45E-08	0,0879
6	3,1725	1,59E-08	3,56E-02	1,23E-06	0,2705	1,82E-07	7,18E-03
7	2,8784	2,50E-05	5,67E-09	2,38E-03	1,17E-06	2,20E-02	6,15E-07
8	2,6213	5,12E-06	3,75E-07	1,80E-05	1,45E-06	6,70E-05	4,75E-07
9	2,5952	4,74E-12	4,59E-03	2,15E-08	1,12E-02	8,16E-08	2,10E-03
10	2,4949	3,58E-06	3,50E-06	2,28E-03	1,10E-05	5,60E-05	2,30E-05
11	2,4463	6,13E-08	3,12E-03	4,05E-07	9,81E-03	1,42E-07	4,52E-02
12	2,2274	2,52E-08	5,00E-05	2,03E-07	5,51E-04	1,62E-10	0,3146
13	1,9905	7,30E-05	7,74E-08	0,1253	5,82E-08	8,30E-05	3,25E-07
14	1,9068	2,26E-08	2,87E-03	1,40E-05	8,65E-03	1,02E-08	6,60E-05
15	1,8381	0,1344	3,63E-10	4,82E-06	6,94E-10	2,32E-03	1,96E-11
23	1,3149	0,0969	4,38E-07	1,60E-05	2,61E-07	2,55E-03	4,61E-08
41	0,7478	0,0749	2,74E-07	2,33E-06	1,25E-07	1,88E-04	1,20E-06
60	0,5133	0,2025	2,01E-08	3,26E-09	4,66E-09	5,00E-05	6,40E-10
65	0,4854	1,37E-04	0,1909	2,55E-06	1,94E-03	5,16E-06	0,4356
152	0,2390	8,64E-06	1,61E-07	0,0798	1,28E-09	0,1447	5,57E-10
186	0,2008	1,43E-04	1,11E-07	0,0505	2,88E-07	2,23E-02	2,99E-09
198	0,1931	5,30E-05	3,53E-08	0,0195	3,59E-06	0,0614	3,61E-08
203	0,1898	6,94E-08	6,17E-07	0,0558	8,24E-07	0,1102	1,27E-06
Σ TOTAL		**0,9871**	**0,9986**	**0,6928**	**0,9259**	**0,7375**	**0,9978**

T

APPENDIX A6.2 – RELEVANT VIBRATION MODES MASS PARTICIPATION RATIO FOR REDESIGNED GAS MODEL

Mode nr.º	Period (s)	UX	UY	UZ	RX	RY	RZ
1	4,184	7,34E-07	0,2214	5,13E-07	0,3593	2,51E-07	1,74E-02
2	4,017	1,18E-02	3,79E-06	0,0508	5,93E-06	2,36E-02	3,92E-08
3	3,877	8,43E-03	8,67E-07	1,81E-02	1,04E-06	8,09E-03	1,39E-07
4	3,624	1,73E-05	0,2286	3,87E-08	0,1142	1,31E-06	7,75E-03
5	3,481	0,5533	1,28E-05	8,61E-03	7,25E-06	2,86E-02	1,52E-06
6	3,039	1,46E-07	4,95E-02	1,22E-06	0,2332	1,94E-07	1,97E-02
10	2,365	2,94E-08	2,25E-02	3,59E-06	6,16E-03	3,49E-07	0,2458
13	2,092	5,36E-03	2,05E-07	0,1268	8,96E-08	6,20E-04	2,61E-07
18	1,454	7,80E-04	0,0567	4,73E-03	3,07E-02	6,46E-03	0,1079
21	1,385	6,18E-06	0,0536	1,81E-05	4,75E-02	3,97E-05	1,88E-02
22	1,305	0,0756	9,76E-06	3,80E-04	7,32E-06	7,20E-04	1,58E-05
38	0,746	0,0594	5,05E-06	3,30E-05	5,10E-11	8,95E-05	3,68E-07
48	0,597	0,0858	7,35E-06	6,30E-04	1,21E-07	1,80E-04	1,61E-06
58	0,515	1,67E-03	0,0927	4,19E-03	1,23E-03	2,43E-02	0,2063
59	0,511	2,19E-03	0,0960	3,58E-03	7,20E-04	1,99E-02	0,2099
60	0,494	0,0649	4,53E-05	9,40E-04	1,08E-06	2,57E-03	2,00E-04
143	0,247	1,20E-04	2,77E-07	0,0595	1,50E-06	0,1018	1,31E-06
147	0,242	1,78E-03	2,90E-07	2,90E-02	1,60E-04	0,0587	1,76E-08
149	0,239	3,20E-04	8,55E-09	3,62E-02	3,15E-07	0,0850	1,42E-08
199	0,188	2,72E-05	2,22E-13	0,0651	9,89E-10	2,81E-02	7,77E-08
Σ TOTAL		**0,984**	**0,999**	**0,784**	**0,948**	**0,809**	**0,999**

U

APPENDIX A6.3 – RELEVANT VIBRATION MODES MASS PARTICIPATION RATIO FOR SYMMETRIC REDESIGNED GAS MODEL

Mode nr.º	Period (s)	UX	UY	UZ	RX	RY	RZ
1	5.026	1.02E-04	0.130954	3.99E-04	0.4681	4.51E-03	0.017867
3	4.708	0.437229	6.05E-04	2.71E-03	1.19E-03	0.004451	2.19E-04
7	3.903	1.34E-06	0.3883	4.76E-04	0.285167	3.13E-04	0.047031
8	3.585	1.95E-10	0.000231	0.000019	0.063492	4.97E-03	0.000031
9	3.296	2.10E-03	1.58E-04	0.213793	3.23E-03	0.026893	2.49E-05
24	1.245	0.074802	9.45E-05	1.53E-08	7.50E-06	0.002964	2.98E-04
44	0.726	0.130473	7.04E-04	4.98E-03	2.28E-05	0.000193	8.59E-04
45	0.717	0.082494	0.000093	9.66E-06	2.81E-04	0.000175	0.00003
57	0.600	8.21E-04	0.028313	1.69E-05	0.003152	6.14E-05	0.446002
61	0.540	4.95E-03	0.058017	1.38E-03	0.000421	1.63E-03	0.100225
62	0.540	0.000011	0.045004	3.09E-04	0.000316	6.22E-03	0.077737
67	0.518	0.146061	5.50E-03	7.78E-04	7.77E-05	0.000016	2.57E-03
70	0.493	0.003234	0.046988	6.60E-04	0.000347	4.36E-04	0.062136
72	0.487	0.001778	0.06957	1.96E-04	0.000565	4.42E-04	0.061531
246	0.184	8.64E-05	5.89E-03	0.201142	0.000021	0.204646	0.000026
255	0.181	2.93E-04	0.000092	0.108409	0.000582	0.112564	0.000364
Σ TOTAL		**0.977**	**0.991**	**0.734**	**0.892**	**0.538**	**0,968**